

Alma Mater Studiorum – Università di Bologna

Dottorato di ricerca in:

Ingegneria Chimica dell’Ambiente e della Sicurezza

XXVIII° ciclo

Titolo tesi:

***MEMBRANE CONTACTORS
FOR HIGH TEMPERATURE APPLICATIONS***

Candidato: Dr. *Felipe Varela Corredor*

Settore Concorsuale di afferenza:

09/D2 – SISTEMI, METODI E TECNOLOGIE DELL’INGEGNERIA CHIMICA E DI PROCESSO

Settore Scientifico disciplinare:

ING-IND/24 PRINCIPI DI INGEGNERIA CHIMICA

Relatore:

Prof. Ing. Serena Bandini

Coordinatore Dottorato:

Prof. Ing. Serena Bandini

Esame finale anno: 2016

***MEMBRANE CONTACTORS
FOR HIGH TEMPERATURE APPLICATIONS***

Abstract	III
Introduction	1
A: Membrane characterization	37
B: Design-construction of SGMD pilot plant and test with membrane modules.	127
Conclusions and perspectives	189

Abstract

With the reduction of the energetic emissions the consciousness that other kind of compound, especially the nitrogenous ones, were equally responsible of environmental problems like acidification phenomena or eutrophication, and that the sources of this were not mainly the energy production, made all the efforts put on the reduction of energy emission to be superfluous if the nitrogenous ones were not controlled.

In 2012 the United Nation Economic Commission for Europe (UNECE) proclaimed the need for more ambitious goals in terms of emissions reduction, registered in the Göteborg Protocol (UNECE 1999). Inside the protocol it is evident the particular concern for the reduction of ammonia emissions with specific guidance documents setting national nitrogen budgets (ECOSOC 2013) and a guidance document for preventing and decreasing ammonia emissions from agricultural sources (ECOSOC 2014) to relevant industrial sectors and transport.

For many industrial sectors the reduction of the emissions is not only a commitment but also the opportunity to decrease the foot print in the atmosphere and reduce the marginal cost due to the losses of potential raw materials. This is the case of the ammonia, whose emissions represent the loss of a completely reduced raw chemical, potentially usable in many industrial processes.

The ammonia capture did not represent a major challenge itself. As a weak base, ammonia is suitable to be absorbed by an aqueous phase, especially if the water phase is slightly acid. A phosphoric acid solution has revealed a magnificent acid to perform this task. As a triprotic acid can donate as much as three protons to the ammonia converting it to ammonium.

After the capture of ammonium, it is necessary to regenerate the ammonium phosphate (through the ammonia stripping) stream in order to be recirculated on the absorption process and to obtain a second stream reach of ammonia suitable to be used on a production process. The regeneration process is strongly endothermic the equilibrium constant is favored by the formation of ammonia only at temperatures above 130 °C.

To avoid reaching such temperatures a good solution to perform the regeneration of the ammonium phosphate salts and obtain a stream reach in ammonia is the stripping of the volatile reaction products (ammonia), avoiding the system to reach the equilibrium, and promoting the formation of further ammonia.

A successful operation requires a great interfacial area, to perform the stripping operation at the lower possible temperature. The membrane contactors (MC) are membrane systems with the biggest interfacial area per equipment volume. However, Membrane Contactors is still a technology under development and the membranes and membrane modules are not yet adequate to perform the operation at such temperature conditions, especially at an industrial scale level.

It is going to be evaluated the availability of the MC process, particularly the Sweeping Gas Membrane Distillation (SGMD), to perform the regeneration of ammonium dihydrogen phosphate (ADP) from diammonium phosphate (DAP) and the study of the main parameters to perform the scale up of the process to an industrial level. Making focus on the selection and characterization of suitable membranes for the process and the design-development of SGMD pilot plant and test for the evaluation of the operative parameters.

The main requirement for the MC technology application is bank on suitable membranes for the process. This must act as a barrier for one of the phases on contact and should enable the mass transport of volatile components. For operative reasons is preferable to hold back the aqueous phase, making the use of hydrophobic membranes imperative.

The hydrophobic membrane character of the membranes is a critical argument for the MC process and is one of the main drawback for the massive application of this technology. Many studies to evaluate the hydrophobic character have been performed and continues to be a trend topic on the MC scenario. However few studies have been done to evaluate the variation of the hydrophobicity with the temperature and none of them to evaluate the effect of temperature above the normal water boiling point.

Through the first part of the thesis a completely new method will be propose to evaluate the hydrophobic character and the variation of a method nowadays used, with the aim of evaluate the membrane hydrophobic character at temperatures never explored before. Moreover, a model base on specific data treatment will be proposed to predict the hydrophobic character and the wettability of the membranes in function of the temperature.

The characterization methods and the models proposed will allow the definition of the most suitable membrane for the process and clear temperature operative limit for the MC technology with this membrane.

The second part of this thesis will be focused in the construction of a bench scale pilot plant to perform SGMD tests and the study of the physical-chemical parameters for the process scale-up.

Through the understanding of the process chemistry, will be initially set up the main process parameters. Therefore is of great importance carry out a deep study of the physical-chemical equilibrium. The creation of an equilibrium model will allow to understand not only the thermodynamics of the problem but also the mass transfer and heat transfer phenomena.

From preliminary SGMD tests in the developed pilot plant, it might be possible to evaluate the feasibility of the stripping of reaction products from an endothermic equilibrium reaction. The idea is quantify the fluxes across the membrane, the separation of the volatile components, the effect of the operative conditions, the effect of the membranes on the chemical equilibrium and the different parameters that allow to evaluate the application of the MC technology to a particular process.

Introduction

Summary

1	Preamble	2
2	Membrane Contactors.....	5
2.1	Configuration.....	6
2.2	Membrane distillation (MD).....	7
2.2.1	Mass transport through the membrane	10
2.2.2	Heat Transfer.....	12
2.2.3	Mass transfer with chemical reaction.	14
2.3	Membrane modules.....	15
3	Process applications: Stripping and absorption with or without chemical reaction.	17
4	Ceramic membranes	22
5	List of Symbols.....	26
6	Bibliography.....	28

1 *Preamble*

The energy production, throughout the use of fossil fuels, has been the main source of air pollutants. The growing concern for air pollutions and its consequences such as global warming, green house effects, acidification phenomena, have developed a great interest for scientist and policy makers to overcome these problems. The reduction of the emissions of the main pollutants Carbon dioxide (CO₂), sulfur oxide (SO_x) and nitrous oxide (NO_x) has been the focus and the goal of many, putting their efforts on the creation of new techniques. Many policies and technologies have been applied and the reduction of the emissions and of these pollutants has decreased even though the emission points have increased.

With the reduction of the energetic emissions the consciousness that other kind of compound, especially the nitrogenous ones, were equally responsible of environmental problems like acidification phenomena or eutrophication, and that the sources of this were not mainly the energy production, made all the efforts put on the reduction of energy emission to be superfluous if the nitrogenous ones were not controlled.

In 2012 the United Nation Economic Commission for Europe (UNECE) proclaimed the need for more ambitious goals in terms of emissions reduction, registered in the Göteborg Protocol (UNECE 1999) setting new national emission ceilings, to be achieved by 2020 and beyond, for four pollutants: sulphur (SO₂), nitrogen oxides (NO_x), volatile organic compounds (VOCs) and ammonia (NH₃). Inside the protocol it is evident the particular concern for the reduction of ammonia emissions with specific guidance documents setting national nitrogen budgets (ECOSOC 2013) and a guidance document for preventing and decreasing ammonia emissions from agricultural sources (ECOSOC 2014) to relevant industrial sectors and transport.

For many industrial sectors the reduction of the emissions is not only a commitment but also the opportunity to decrease the foot print in the atmosphere and reduce the marginal cost due to the losses of potential raw materials. This is the case of the ammonia, whose emissions represent the loss of a completely reduced raw chemical, potentially usable in many industrial processes.

The achievement of the ambitious goals set by UNECE will require the best available techniques to keep emissions down. Therefore the challenge goes to the industry and to the academic world, responsible to propose a suitable methodology to overcome the environmental problematics and to accomplish the changes the industry needs in order to promote a sustainable development.

The ammonia capture did not represent a major challenge itself. As a weak base, ammonia is suitable to be absorbed by an aqueous phase, especially if the water phase is slightly acid. The absorption operation could be performed on many equipment's, depending on the possibilities of investment or the availability of this sort of equipment in the production place: regular scrubbers, plate towers, packed bed towers or even new technologies like membrane contactors.

A phosphoric acid solution has revealed a magnificent acid to perform this task. As a triprotic acid can donate as much as three protons to the ammonia converting it to ammonium. Forming the very stable (tampon) ammonium phosphate, actually, the equilibrium between its three different forms (ammonium dihydrogen phosphate-ADP, diammonium phosphate-DAP and Triammonium phosphate-TAP).

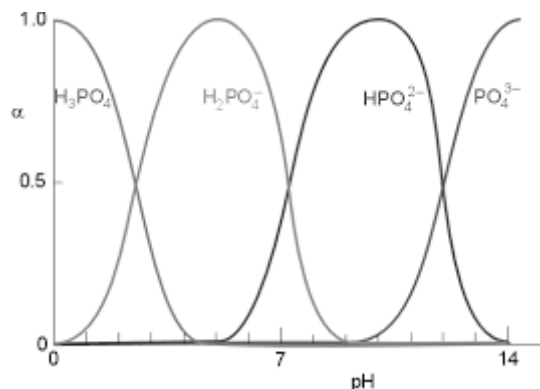
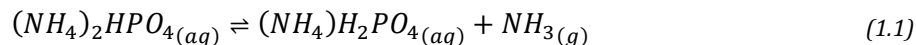


Figure 1.1 Effect of PH on the distribution of orthophosphate ions in solution. (Boyd 1982)

After the capture of ammonium, it is necessary to regenerate the ammonium phosphate (through the ammonia stripping) stream in order to be recirculated on the absorption process and to obtain a second stream reach of ammonia suitable to be used on a production process.

The most likely condition where the absorption-desorption process can take place is the equilibrium between ADP and DAP. Not only the pH conditions are softer but also the equilibrium conditions for the absorption and the regeneration process are less demanding in terms of equipment materials and process duty.

The chemical reaction we are considering is the one presented on equation (1.1). During the absorption the ammonium dihydrogen phosphate reacts with the gaseous ammonia to form the diammonium phosphate (everything on aqueous phase), that can liberate the ammonia during the regeneration phase.



The equilibrium constant for the reaction between DAP, ADP and ammonia is presented in function of the temperature on the Figure 1.2. It can be seen that the formation of DAP is favored on a big range of temperature and so the absorption of ammonia. On the contrary the regeneration process is strongly endothermic the equilibrium constant is favored by the formation of ammonia only at temperatures above 130 °C.

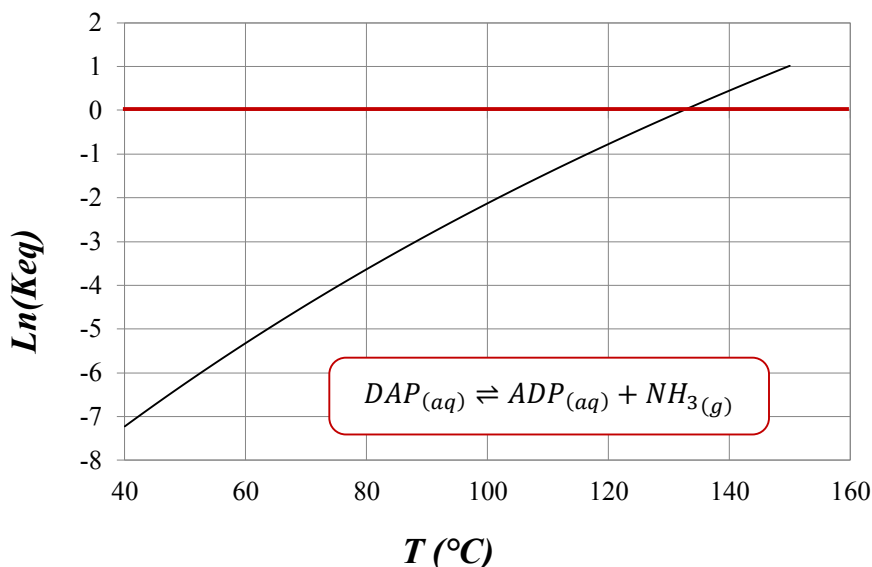


Figure 1.2 Equilibrium constant vs. Temperature for the reaction Between DAP-ADP and Ammonium

To avoid reaching such temperatures a good solution to perform the regeneration of the ammonium phosphate salts and obtain a stream reach in ammonia is the stripping of the volatile reaction products (ammonia), avoiding the system to reach the equilibrium, and promoting the formation of further ammonia.

A successful operation requires a great interfacial area, to perform the stripping operation at the lower possible temperature. The membrane contactors (MC) are membrane systems with the biggest interfacial area per equipment volume. They could perform the stripping of the reaction products with a content equipment volume and at lower operative conditions compared with the traditional systems. Particularly the operation known as Sweeping Gas Membrane Distillation (SGMD) seems to be the most indicated to perform such operation.

However, Membrane Contactors is still a technology under development and the membranes and membrane modules are not yet adequate to perform the operation at such temperature conditions, especially at an industrial scale level.

In this thesis it is going to be evaluated the availability of the Membrane Contactors process, particularly the SGMD, to perform the regeneration of DAP into ADP and the study of the main parameters to perform the scale up of the process to an industrial level.

2 Membrane Contactors

The concept of “Membrane Contactors” identifies the equipment where a semipermeable barrier is used to put in contact two phases (Liquid-Liquid or Gas-Liquid) and perform mass transport operations across it. In this case, the barrier is well defined by the membrane, the interfacial area (between the two involve phases) is constant and defined by the membrane morphological parameters. As a barrier the membrane avoids mixing or dispersion phenomena and so the interface remains constant. The separation process, usually characterized by the membrane selectivity and the driving force, in this case does not have the selectivity component, as the membrane does not show a particular selectivity for any component. Its function is only to separate the two phases. The transport across the membrane, from a phase to the other, occurs only by diffusion, the differences in the diffusivity coefficient and the driving force determine the transport phenomena.

In order to perform mass transport operations the membrane should overfill two main conditions. It has to be porous (pore size 1000 to 10 nm), in order to promote the diffusion transport across the membrane, and has to keep the phases well separated. The porosity condition imposes that the membrane cannot be a mechanical barrier, process conditions and the affinity of the membrane with the fluids are the parameters to be considered for the containment of the fluids. Usually hydrophobic or hydrophilic membranes are used depending on which fluid is desired to fill the pores, and a greater pressure of the non-wetting fluid is used to avoid the dispersion of the wetting fluid on it. Hydrophobic membranes are used to avoid wetting of polar liquids while hydrophilic membranes are used to avoid wetting of non-polar liquid or gases and their dispersion on the other phase.

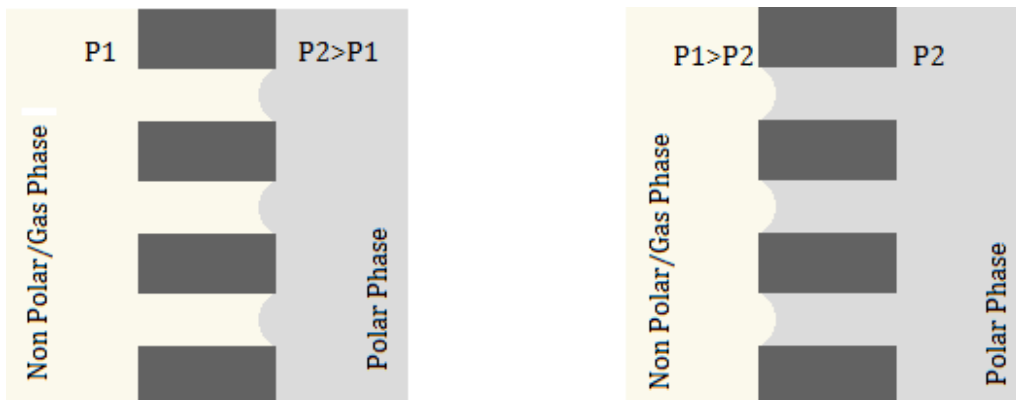


Figure 2.1 Interface of the non-wetting liquid and the wetting liquid for the hydrophobic membrane (left) and hydrophilic membrane (right)

In both cases, if a cylindrical pore is considered, the interface between fluids will be located at the edge of pore and the diffusion phenomena across the pore will consider the wetting fluid as the continuous phase.

Nevertheless, the lack of affinity of the membrane for the non-wetting liquid (hydrophobicity / hydrophilicity), is not a warranty for its containment. The non-wetting liquid could flood the membrane if the transmembrane pressure is higher than a critical value generally known as Pressure of Breakthrough. The breakthrough pressure for given membrane – fluid couple will depend on the membrane morphology (pore size distribution and tortuosity), the interfacial properties of the liquid and the fluid (interfacial tensions) and the mechanical equilibrium between phases. The condition where the membrane gets wet by the “non-wetting” fluid must be avoided in order to keep the contactor in function. This parameter will be widely discussed later in this thesis.

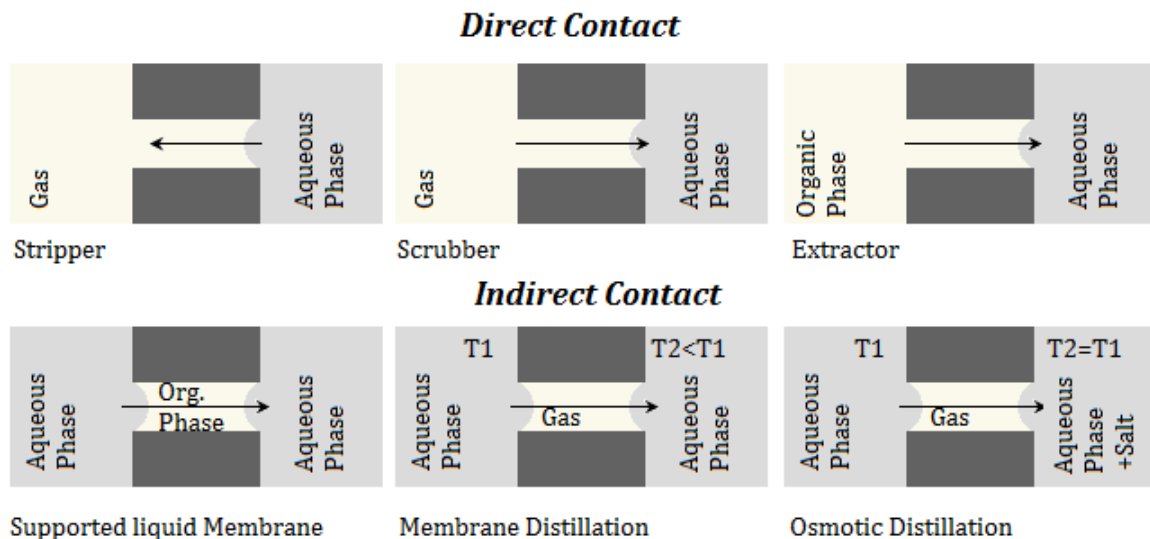


Figure 2.2 Configuration schemes for membrane contactors applications

The membranes configuration is wide, the desire of the location for the interfacial boundary should guide its selection. Generally the membranes can be divided between hydrophobic and hydrophilic, already described, and between symmetric and asymmetric. Symmetric membranes are those membranes whose pore diameter is mostly constant along the thickness while for asymmetric membranes it increases. For the asymmetric membranes the interface could be located within the pores instead of the mouth. The last configuration might mix the previous ones, known as composite membranes. The composite membranes are made of different layers, casting a hydrophobic layer over a hydrophilic or combining layers of different pore size. The selected configuration must fit the process fluids and should improve the performances of the mass transfer process.

2.1 Configuration

With membrane contactors many unit operations can be performed. The differences between the phases used and the process conditions will define the operation performed. Some of the

names reported for this operation copy the name of the traditional one, and could work as substitute, however complete new operations can be defined.

The phases can be in direct contact or in contact through a third phase inside the pores. In the first case, there are in contact immiscible phases. Traditional operations like Stripping, Scrubbing, distillation or liquid-liquid extraction can be perfectly performed. The interface will be created directly between the two fluids and so the equilibrium, the diffusion will come across the wetting fluid and the driving force will be the difference of concentration or partial pressure (if gases-vapors are involved). If the mass exchange should be performed between two miscible phases, the contact will come across a third phase immiscible with them and trapped in the membrane pores. In this case the interface will be in both edges of the pore, between the process fluids and the third phase. For each interface an equilibrium will be set. Operations like Supported Liquid Membrane, Air Gap Membrane Distillation, Osmotic Distillation or extractive distillation can be performed using this configuration.

2.2 *Membrane distillation (MD)*

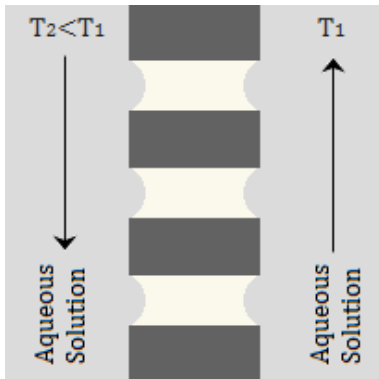
The concept of membrane distillation (MD) covers a number of operations where a heated volatile liquid phase is in contact with a low affinity macroporous membrane. In most cases the liquid phase is an aqueous phase and the membrane has a hydrophobic nature. The low affinity of the membrane with the aqueous phase prevents the liquid flooding and the transport of the liquid phase across the membrane. For instance, on the mouth of the membrane pores, it is located the liquid-vapor interface. Despite the impermeability of the membrane to liquid, the macroporous membrane is very permeable to vapor and gas, which are able to diffuse or convect across the membrane pores, if a driving force is applied to the system.

The first approach to the concept of membrane distillation could be traced back to the patent granted to Bodell in 1968, who proposed that the "Production of potable water is achieved wherein a membrane, impermeable to liquid water but permeable to water vapor allows for the passage of water vapor there through, but not impurities, into a gaseous medium from which potable water is recovered."

The vapor pressure of the components, on each side of the membrane, will act as the driving force. Volatile compounds on the liquid phase (feed side) evaporate and are transported to the other side (permeate side) of the membrane. On the permeate side the vapor could be condensed or removed of the system. In order to create the driving force and remove the vapor generated on the feed side, many methods have been proposed. Vapor can be condensed by another liquid in contact with the membrane or by a cold solid surface. Also it can be removed by a lower pressure on the permeate side (vacuum) or even swept by a transport gas. Depending on which method is used to create the driving force the process takes different names, well established by the academy and industry. The selection of each one of these methods depends of many variables; the product of interest is on the retentate or the permeate; the product should remain on vapor phase or liquid phase; the volatility of components is low;

the components in the system are thermally sensitive; the desirable concentration of the products and others.

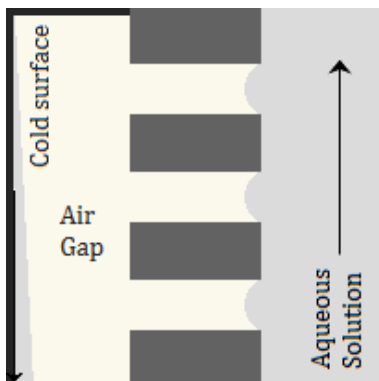
The four most common configurations of Membrane Distillation are:



Direct Contact Membrane Distillation (DCMD): a liquid phase is placed on both sides of the membrane. The differential vapor pressure is established by the different temperatures of each liquid phase. Higher temperatures are used to enhance the evaporation and low temperatures to promote the condensation.

This is the simplest of the configurations. Useful to concentrate nonvolatile components on aqueous phase present on the retentate. The volatile compounds that have passed through the membrane are condensed and diluted by a liquid phase. The direct contact of liquid phase on both sides of the membrane creates important heat losses.

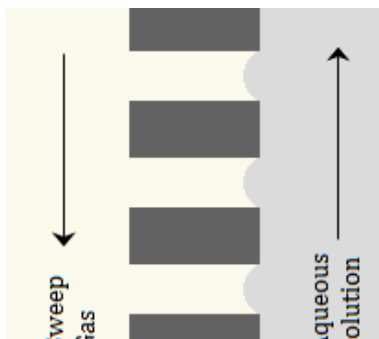
Figure 2.3 Direct Contact Membrane Distillation configuration



Air Gap Membrane Distillation (AGMD): the permeate side of the membrane is full of Gas where the vapor is transported, when the permeated vapor comes in contact with the cold surface the vapor gets condensated and the vapor pressure decreases.

A versatile configuration appropriate to concentrate non volatiles compounds on the retentate side or to concentrate condensable compounds on the permeate side It is characterized by low fluxes (lower driving forces). The heat losses are much lower than on DCMD (Bandini, Gostoli and Sarti 1992).

Figure 2.4 Air Gap Membrane Distillation configuration



Sweeping Gas Membrane Distillation (SGMD): The partial pressure of the volatiles decreases on the permeate side by a constant flow of gas that sweeps the permeate volatiles as soon as they pass through the membrane.

Suitable to remove volatile compounds from a liquid phase, greater fluxes than the previous configurations (only one phase equilibrium involved). The volatile compounds swept by the gas stream are highly diluted, further steps should be performed to recover the permeated products. The higher fluxes make the heat losses higher (mainly by latent heat).

Figure 2.5 Sweeping Gas Membrane Distillation configuration

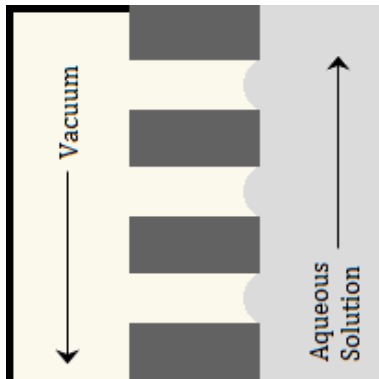


Figure 2.6 Vacuum Membrane distillation configuration

Vacuum Membrane Distillation (VMD): on the permeate side the partial pressure of the transported component is lower than the interface by the action of a vacuum pump. The vacuum action promotes the transport of volatile components across the membrane.

The volatile compounds (Sarti, Gostoli and Bandini 1993) passed through the membrane are removed by the vacuum action. The products on the permeate side are easily recuperated at high concentrations. The use of vacuum is convenient when the operation must be performed at low temperatures. The heat losses are negligible (Lawson and Lloyd 1997). The fluxes are lower than SGMD and the vacuum action made the operation more expensive (Bandini & Sarti, 1995,1997), (Mengual, Khayet and Godino 2004).

Membrane Distillation processes have some clear advantages over the traditional distillation process and over other well established membrane processes (pressure driven).

- The interfacial area is constant regardless the ratio of streams in contact.
- Phase mixing and the associated problems (emulsification, bobbling, flooding, unloading...) are not present in the operation.
- The phases are well separated independently of the density of these.
- The modularity of the technology made the process Scale-Up is linearly with the potentialities.
- High specific interfacial area.
- Lower operative conditions (Temperature – Pressure) for the same design requirements.
- Lower Hold-Up of solvent
- Possible use of alternative renewable energy sources.
- Polymeric modules reduce parts corrosion.
- Respect to reverse osmosis (RO) process, the concentration polarization effect is not a limitation. The permeate can arrive to higher concentrations.

Even though this technology presents many advantages, there are still some drawbacks and opportunities of development, where many of them are a matter of study.

- The operative temperature limit is not as wide as the traditional distillation. The materials of membranes, potting, and modules are the main limitation.
- The presence of the membrane presents an extra resistance for mass transport.
- The membranes are susceptible to fouling phenomena that decrease the mass transport performance.
- The materials of modules, potting and membranes are less resistant to extreme conditions of pH, pressure and temperature.

- The modules configurations to obtain high packing densities and good fluid dynamics gives high pressure drops.
- The wetting of the membrane is still an important matter that reduce mass transport and phase mixing.

2.2.1 Mass transport through the membrane

For a particular component driving force in MD is a partial pressure difference of that component across the membrane; the partial pressure difference can be promoted by a temperature difference across the membrane, or by vacuum or a sweep gas on the permeate side of the membrane. The transport will be proportional to the molar concentration difference across the membrane times a transport coefficient (K) (M. Khayet 2011).

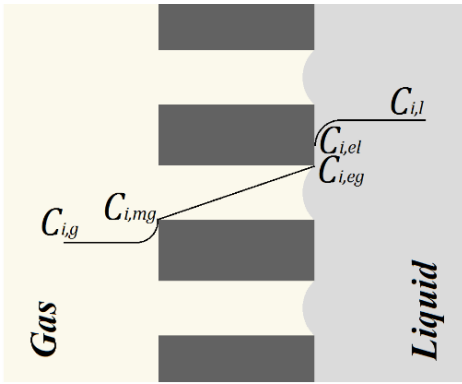


Figure 2.7 Concentration profile for the component i in the transport from the liquid phase to the gas phase

$$J_i = k_{i,g}(C_{i,l} - C_{i,el}) = k_{i,m}(C_{i,eg} - C_{i,mg}) = k_{i,l}(C_{i,mg} - C_{i,g}) \quad (2.1)$$

Generally the molar concentration on the gas phase is described by the partial pressure of the component. In case of non-ideal mixtures, the vapor-liquid equilibrium is described by the partial pressure of i (P_i) defined in terms of the vapor pressure of the pure component (P_i^0) and the activity of the component i (a_i). (Gostoli 1999)

$$P_i = P y_i = P_i^0 a_i = P_i^0 \gamma_i x_i \quad (2.2)$$

The pure component vapor pressure varies accordingly with the Clausius-Claperyron's equation where L is the latent Heat and R is the ideal gas constant:

$$\frac{dP_i^0}{dT} = \frac{P_i^0 L}{RT^2} \quad (2.3)$$

So even if the activity of the of the component is higher on the permeate side that the feed side the driving force is the total vapor pressure and the difference in temperature or the lower partial pressure on the permeate side make possible the transport across the membrane.

Regardless how the driving force is created the transport of the volatile component through the pores can be described by three different mechanisms. The presence of one or all of these transport mechanisms are related with the collisions between the molecules, and/or molecules with the membrane described by the Dusty Gas Model (DGM) (Alkudhiri, Darwish and Hilal 2012). Knudsen diffusion takes place when the pore size is small enough that the collisions between the molecules and the walls of the pore are more relevant than collisions between molecules. Molecular diffusion characterized by collisions of a diffusion molecule with other molecules moving under the influence of a concentration gradient and Viscous Flow (Poiseuille Flow) resulting from the transfer of momentum, where the molecules are driven by a pressure gradient.

Usually on MD processes the resistance due to the boundary layer is negligible, even though the total resistance to the mass transport can be explained using an electrical analogy where the different resistance can be added one to the other in series or parallel and form a total resistance to the mass transport. Figure 2.8 represents the most probable resistance present on MD process.

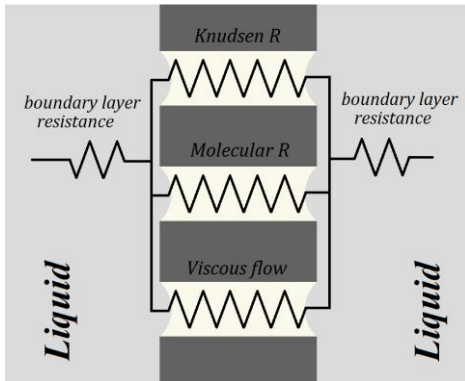


Figure 2.8 Mass transfer resistance in MD

The Knudsen number (Kn) can give an indication of the ruling transport mechanism, this is defined as the ratio between the mean free path and the characteristic length of the transport channel (pore size). The mean free path (λ), the average distance travelled by molecules between collisions can be calculated accordingly with kinetic theory of gases.

$$Kn = \frac{\lambda}{d_p} \quad (2.4)$$

$$\lambda = \frac{k_b T}{\sqrt{2} \pi P d_e^2} \quad (2.5)$$

For $Kn > 1$ the mean free path is comparable with the pore size and so the dominant mechanism is Knudsen diffusion. Khayet (Khayet, Velázquez and Mengual 2004) report a relation for calculation of the mass transport coefficient

$$C_{Kn} = \frac{2\pi}{3} \frac{1}{RT} \left(\frac{8RT}{\pi MW} \right)^{1/2} \frac{r^3}{\delta \chi} \quad (2.6)$$

If $Kn < 0.01$ the dominant mechanism is the molecular diffusion.

$$C_D = \frac{\pi PD r^2}{RT P_{gas} \delta \chi} \quad (2.7)$$

If the Knudsen number is between the two previous cases both the mechanisms are present on the transport phenomena, can be consider a transition region. The following expression was proposed also by Khayet et al.

$$C_C = \frac{\pi}{RT \delta \chi} \left[\left(\frac{2}{3} \left(\frac{8RT}{\pi MW} \right)^{1/2} r^3 \right)^{-1} + \left(\frac{PD}{P_{gas}} r^2 \right)^{-1} \right]^{-1} \quad (2.8)$$

However Poiseuille Flow should be considered as one of the mechanisms of mass transport for large pores as studied by (Zhongwei, Liying and Runyu 2003)

One of the first assumptions made when modelling the MD process is that kinetic effects at the vapor-liquid interface are negligible. In other words, that vapor and liquid are assumed to be in the equilibrium state corresponding to the temperature at the membrane surface and the pressure within the membrane pores.

2.2.2 Heat Transfer

In membrane distillation processes the heat transfer and the mass transport are strictly related. At the equilibrium the concentration of volatile components is defined by the temperature through the vapor pressure of the component. In the general case, the bulk temperature (T_h - T_c) is different to the temperature at the membrane (interface) due to a boundary layer resistance. The membrane offers an extra resistance creating a temperature profile. Indeed it is the temperature profile to rule the mass transport as the concentration is defined by the temperature.

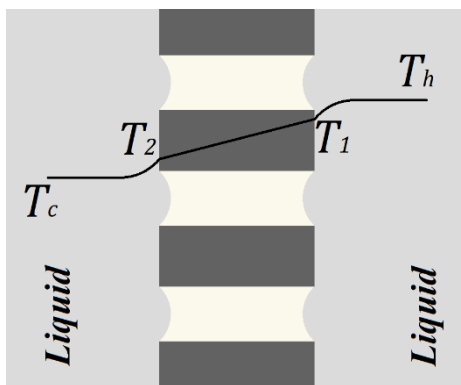


Figure 2.9 Membrane distillation temperature profile.

The heat transport is described in terms of the resistances due to the phase boundary layers and the membrane. The array of serials and parallels resistances defines the heat transport and the temperature profile, modifying the mass transport itself.

The boundary layers are the main drawbacks on the mass transport phenomena, and these create a concentration difference between the bulk temperature and the membrane surface one which limit the evaporation effect on the interface.

Across the membrane two heat transport phenomena can be verified. The conduction across the solid material (membrane), considers a heat loss to be minimized, as no mass transport is associated to this heat and the latent heat of vaporization directly related with the transport of vapor through the membranes pores and a direct function of the Knudsen, molecular and viscous mass transport coefficients.

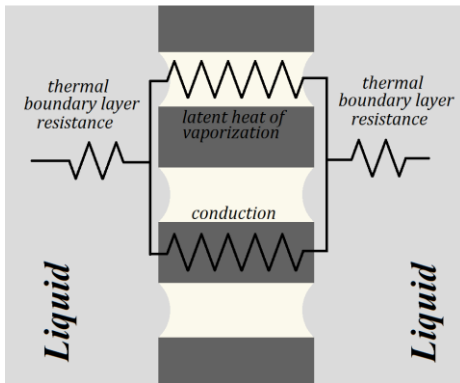


Figure 2.10 Heat transport resistances for DCMD.

The total heat flux (Q) the consequence of the overall resistance and the driving force can be divided in the three regions previously described. Heat transfer by convection in the hot boundary layer and the cold boundary layer.

$$Q_h = h_h(T_h - T_1) \quad (2.9)$$

$$Q_c = h_c(T_2 - T_c) \quad (2.10)$$

Heat transfer through the membrane by conduction, and vapor transport across the membrane or latent heat of vaporization (ΔH_v)

$$Q_m = h_m(T_1 - T_2) + J\Delta H_v \quad (2.11)$$

These three heat are equal one to the other at the steady state and can be on one overall heat transfer coefficient calculated through the electric analogy.

$$Q = U(T_h - T_c) \quad (2.12)$$

As the temperature on the membranes cannot be experimentally measured, the concept of Temperature Polarization Coefficient has been used to quantify the effect of heat transfer boundary layer to the total heat transfer resistance of the system. It is used to calculate the temperature of the membrane and so the interface temperature.

$$\psi = \frac{T_1 - T_2}{T_h - T_c} \quad (2.13)$$

The effect of temperature polarization is more or less important on certain MD configurations, for example on DCMD the falls between 0.4 and 0.7 for performant systems and can be near to one when the mass transfer operation is limited. For other configurations like VMD or AGMD the effect is reduced due to the absence of one boundary layer (Bandini and Sarti 1995).

Different values of ψ has been used empirically for various modules configurations in function of the fluid-dynamic regime the Nusselt number and the module geometry.

2.2.3 *Mass transfer with chemical reaction.*

The combined operation of chemical reaction with separation process is of particular interest for many industries. The possibility of stripping the products of an equilibrium reaction, with the direct consequence of increasing the production rate over the equilibrium limits; or to perform the capture of gaseous products on aqueous solutions over the solubility limits are just one of the advantages of this kind of operation. Even more the mass transfer operation itself comes enhanced by the presence of the chemical reaction.

As seen before on macroporous membranes, the transfer of a component from one phase to the other involves the transfer from the bulk of the phase to the membrane, through it and to the bulk of the other phase. The chemical reaction hypothetically takes place on the gas-liquid interface.

The transport of the component is expressed in terms of the driving force (the difference of chemical potential on membranes contactors is usually rule by the difference in concentration) and the resistance to transport K_{ov} . The film theory has been used to describe a resistance in series model for gas-liquid systems. Here, three serial resistance can be enumerated: the gas film resistance, the liquid film resistance and finally the resistance due to the transport through the membrane. (Khaisri, et al. 2011)

$$N''_i = K_{ov} \Delta C_i \quad (2.14)$$

$$K_{ov,i} = \left[\frac{1}{k_{g,i}} + \frac{1}{k_{m,i}} + \frac{H_{i,dms}}{Ek_{l,i}} \right]^{-1} \quad (2.15)$$

In the expressions above $H_{i,ad}$ is the dimensionless Henry constant for the component i . k_g , k_m and k_l are the mass transport coefficients in the gas, liquid. Finally E is the enhancement factor, which is included to account for the effect of the reaction. This is defined as the ratio of the absorption/desorption of a vapor/gas in the liquid on presence of the chemical reaction to the absorption/desorption rate in the absence of the reaction (when the same driving force is in action on both systems).

Practically the enhancement factor reduces the effect of the liquid boundary layer resistance increasing the driving force through the membrane transport.

$$E = \frac{N''_i \text{ with reaction}}{N''_i \text{ without reaction}} \quad (2.16)$$

The individual mass transfer coefficients and the enhancement factor can be theoretically calculated through correlation equations, provided by the literature, which depends on the operation conditions and the module configuration.

2.3 Membrane modules

Once the particular membrane has been selected for a particular application, the configuration on which these membranes are going to be arranged should be defined. The membranes array is known as module. This is the equipment volume where both phases are going to be in contact through the membrane area. A good module configuration can provide compactness, robustness and through the appropriate fluid-dynamic it might reduce pressure drops, enhance the mass transfer, imparting a positive impact to the process (Drioli, Ali and Macedonio 2015). As a result it will be reduced the thermal/concentration polarization, the fouling and the energy consumption. The high density packing, interface area and high mass transfer coefficient made the height of the transfer unit lower than conventional units design for the same operation.

A benefit of the membrane process is a straightforward scale-up because the available surface area between gas and liquid phase is known (Khaisri, et al. 2011). Assembling modules on series and parallels is a practical way to increase the capacity, reach a desired performance and control pressure drops, with the aim to avoid phase breaking through into the membrane pores.

Usual membrane modules configurations are:

Plate and frame: flat sheet membranes are arrayed together with spacers between two plates. The membranes in this configuration are easy to clean and replace. Though, the packing density is low compared with other modules configuration. This module configuration is used mainly on laboratory scale applications.

Shell and tubes:

Hollow fibers: the hollow fibers are tubes of diameters around the millimeter which are packed on bundles by thousands of them. The bundle is set inside a shell ensuring phase separation

through proper potting sealing. Accordingly with process requirements (density, viscosity, temperatures, reactivity) one of the phases flows through the tubes and the second on the shell side, parallel or perpendicular to the tubes if baffles are used. The high packing density gives this module configuration a great membrane area. However the fouling is more frequently as well as higher pressure drops. The compactness of the bundle made the substitution of single membranes impossible and cleaning process is more difficult than in other configurations.

Tubular membranes: this configuration is schematically equal to hollow fibers, but the tubes diameter is larger. For many application it is preferred as the packing density is higher than plates and frame but the drawbacks phenomena in hollow fibers are reduced.

Spiral wound membrane: a flat sheet membrane and the spacers are rolled around a perforated central collector tube. One of the phases flow in the axial direction of the modules, while the second flows radially to the center. The packing density on this configuration is high, but the flow pattern reduce the fouling effects and the pressure drops.

Each configuration has its own particularities which make it preferable for a certain process. The difference on the structure and flow pattern made necessary the use of exclusive equation to describe the mass transport.

3 ***Process applications: Stripping and absorption with or without chemical reaction.***

Membrane contactors and particularly the Gas-Liquid systems have gained a relevant importance due to their versatility to be applied on different process. Biological, food and pharmaceutical processes where the conditions might degrade the product or simply the necessity of a better performance, the reduction of the operative costs and environmental impact could be one of the reasons to apply this growing technology. Operations like absorption, stripping and distillation might be performed for gas separation, liquid separation, products concentration, purification among others.

Usually the membranes used are hydrophobic, as the mass transfer mechanism is limited when the pores are full with liquid. The polymeric membranes have been preferred due to their low cost of production (compared with coated ceramic membranes), their versatility for modules production, high packing factor and the existence of standard commercial products available on different materials for diverse applications.

With the purpose to evaluate the availability of performing the chemical regeneration of diammonium phosphate (DAP) into ammonium dihydrogen phosphate (ADP), it was evaluated among the bibliography the publications that presented similar applications or desired conditions. On Table 3.1 and Table 3.2 the main characteristics are reported of the processes where membranes contactors were used to perform stripping or absorption with or without chemical reaction. Of particular interest was the process temperature and pressure on gas and liquid phase.

Table 3.1 Stripping applications of membrane contactors process with or without chemical reaction.

<i>Application</i>	<i>Process</i>	<i>Membrane</i>	<i>Module</i>	<i>Operative conditions</i>	<i>Reference</i>
<i>CO₂ tripping from MEA by N₂</i>	<i>SGMD - Rx</i>	<i>PTFE hollow fibers (Markel Corp.)</i>	<i>Shell&tube prototype</i>	<i>T_L=90-100°C</i>	<i>(Khaisri, et al. 2011)</i>
<i>Water –Formic acid Separation</i>	<i>SGMD</i>	<i>PTFE TF200 (Gelman)</i>	<i>module prototype</i>	<i>ΔP=0.3bar ΔT=10-60°C</i>	<i>(García-Payo, et al. 2002)</i>
<i>Water – Isopropanol Separation by N₂</i>	<i>SGMD</i>	<i>PTFE hollow fibers (PORE-FLON)</i>	<i>Shell&tube prototype</i>	<i>T_G=10-25°C T_L=20-50°C</i>	<i>(Lee and Hong 2001)</i>
<i>Water – ammonia Separation by Air</i>	<i>SGMD</i>	<i>PTFE flat-sheet (Advantec MFS Inc.)</i>	<i>Flat module - prototype</i>	<i>T_G=T_{room} T_L=55- 65-75°C</i>	<i>(Xie, et al. 2009)</i>
<i>Water – ammonia separation by H₂SO₄ aq</i>	<i>SGMD - Rx</i>	<i>PP/PE hollow fibers</i>	<i>Liquicel module</i>	<i>T_G=T_L=20°C</i>	<i>(Ashrafizadeh and Khorasani 2010)</i>
<i>CO₂ Stripping from DEA by N₂</i>	<i>SGMD - Rx</i>	<i>PVDF self-made hollow fibers</i>	<i>Shell&tube prototype</i>	<i>T_L=80°C ΔP=0.2bar</i>	<i>(Naim, Ismail and Mansourizadeh 2012)</i>
<i>CO₂ Stripping from Water by N₂</i>	<i>SGMD - Rx</i>	<i>PVDF self-made hollow fibers</i>	<i>Shell&tube prototype</i>	<i>ΔP=0.3bar</i>	<i>(Mansourizadeh and Ismail 2011)</i>
<i>Gas Stripping from Water by Humid Air</i>	<i>SGMD</i>	<i>PTFE TF200 and TF450 flat sheet (Gelman)</i>	<i>Plate&frame – Filtron M.</i>	<i>T_G=10-30°C T_L=40-70°C</i>	<i>(Khayet, Godino and Mengual 2000)</i>
<i>Gas Stripping from Water by N₂</i>	<i>(SGMD-VMD)</i>	<i>(Celgard)</i>	<i>Shell&tube</i>	<i>T_{room}</i>	<i>(Sengupta, et al. 1998)</i>
<i>O₂ Stripping from Water by N₂</i>	<i>VMD</i>	<i>PP hollow fibers</i>	<i>Shell&tube (Hyflux)</i>	<i>T_{room} P_G=0.6 bar</i>	<i>(Peng, et al. 2008)</i>

<i>CO₂ absorption in MEA/TEA</i>	<i>Membrane Scrubber</i>	<i>PVDF self-made hollow fibers</i>	<i>Shell&tube</i>	<i>T_L =40°C T_G =80°C ΔP=0.1-0.3 bar</i>	<i>(Yeon, et al. 2005)</i>
<i>CO₂ stripping from DEA by N₂</i>	<i>SGMD - Rx</i>	<i>Grafted alumina self-made hollow fibers</i>	<i>Shell&tube prototype</i>	<i>T_L=80-90-100°C</i>	<i>(Koonaphapdeelert, Wu and Li 2009)</i>
<i>CO₂ stripping from Water by N₂</i>	<i>SGMD</i>	<i>Modified PVDF self-made hollow fibers</i>	<i>Shell&tube prototype</i>	<i>T_L=80-90°C ΔP=0,2bar P_L=0,5bar</i>	<i>(Rahbari-Sisakht, et al. 2014)</i>
<i>O₂ Stripping from da H₂O by N₂</i>	<i>SGMD</i>	<i>PP, hollow fibre, , Hoechst Celanese</i>	<i>Shell&tube</i>	<i>T_L=22°C</i>	<i>(Tai, et al. 1994)</i>
<i>CO₂ stripping from water by N₂</i>	<i>SGMD</i>	<i>Modified PVDF, self-made hollow</i>	<i>Shell&tube prototype</i>	-	<i>(Mansourizadeh and Pouranfard 2014)</i>
<i>CO₂ from aqueous MEA by N₂</i>	<i>SGMD</i>	<i>PTFE, hollow fiber</i>	<i>Shell&tube</i>	-	<i>(Ghadiri, Marjani and Shirazian 2013)</i>
<i>CO₂ from aqueous MEA by N₂</i>	<i>SGMD</i>	<i>Surface modified alumina hollow fibers</i>	<i>Shell&tube</i>	-	<i>(Koonaphapdeelert, Wu and Li 2009)</i>
<i>CO₂ from aqueous K₂CO₃</i>	<i>SGMD - Rx</i>	<i>PTFE and PES modified</i>	<i>Flat</i>	<i>T_L=60-100°C</i>	<i>(Simioni, Kentish and Stevens 2011)</i>

Table 3.2 Absorption applications of membrane contactors process with or without chemical reaction.

<i>Application</i>	<i>Process</i>	<i>Membrane</i>	<i>Module</i>	<i>Operative conditions</i>	<i>Reference</i>
<i>Absorption of CO₂ on MEA/DEA</i>	<i>Membrane Scrubber</i>	<i>PP hollow fibers</i>	<i>Shell&tube prototype</i>	<i>T_L: 15-35°C P_{L,in}=1.2-1.8bar</i>	<i>(Lü, Zheng and Cheng 2008)</i>

Absorption of CO ₂ on MEA/AMP	Membrane Scrubber	PP (Mitsubishi Rayon Ltd.) e PTFE (Sumitomo Electric) hollow fibers	Shell&tube prototype	-	(DeMontigny, Tontiwachwuthikul and Chakma 2006)
Absorption of CO ₂ and N ₂ O on Water	Membrane Scrubber	PP hollow fibers (Liquicel)	Liquicel Mini module	P _G : Patm T _G : 25-40°C	(Porcheron and Drozd 2009)
Absorption of CO ₂ on NaOH (aq)/DEA	Membrane Scrubber	PP hollow fibers	Hoechst Celanese Corp.	T _{room}	(Rangwala 1996)
Dehumidify Air by LiCl(aq)	Membrane Scrubber	PP (Membra-na GmbH) e PEI (ULTEM 1000, GE) hollow fibers	Prototype	ΔP=0.1-0.5 bar	(Albrecht, et al. 2005)
Absorption of CO ₂ on Air saturated Water	Membrane Scrubber	PP, hollow fibers Hoechst Celanese	Shell&tube	T _L = T _{room} P _G = P _{room} P _L > P _G	(Li, Tai and Teo 1994)
Absorption of CO ₂ on Water/NaOH (aq)/DEA	Membrane Scrubber	PP, hollow fiber	Shell&tubeHoechst Celanese Corp.	-	(Rangwala 1996)
Absorption of CO ₂ on MEA, DEA, TEA e PZ	Membrane Scrubber	PTFE, PP, PVDF	Shell&tube	-	(Favre and Svendsen 2012)
Absorption of CO ₂ on MEA	Membrane Scrubber	PP microporous hollow fiber membrane (Membrana Oxyphan); PDMS dense hollow fiber membrane (Silastic, Dow Corning)	Shell&tube	P = 1 bar; T = 313 K	(Bounaceur, et al. 2012)
Review absorption of gas on liquids MC	Membrane Scrubber	ePTFE, PVDF, PTFE, PSf, PAI, PEI, PP, PPO. hollow fibers	Shell&tube	review	(Yang, Mingchien and Cussler 1986)
Absorption of CO ₂ on MEA	Membrane Scrubber	PP e PTFE, hollow fibers	Shell&tube	P _{L,in} = 1.05bar T _L = 40°C	(Rode, et al. 2012)
Absorption of CO ₂ on MEA	Membrane Scrubber	Hidrophobized PP, hollow fiber by Cyclohexanone/MEK	Shell&tube	P=1atm, T=20°C	(Lv, et al. 2012)

From the many applications reported on literature, it is evident the interest for the absorption/desorption of carbon dioxide with/from organic solutions in order to reduce the emissions from combustion process. The process conditions reported are, mainly close to room temperature and on few cases the temperature arrives close to 100 °C. The modules are made hydrophobic polymeric membranes and the most used configuration is the shell and tubes modules, where their big packing factor, superior membrane area and the well-studied fluid-dynamics made the process more efficient and easy to study.

Until now there are no reports of similar processes for the concrete application or the desirable conditions.

4 Ceramic membranes

In recent years the use of ceramic membranes has gained the interest of the academics as well as the industry. The uses of ceramic membranes has spread numerous sectors as water treatment (Lee, Wu and Li 2015) including micro and ultra-filtration (clarifying fermentation broths, fruit or sugar cane juices and treatment of highly oily wastewaters) or even nano-filtration (Mazzoni, Orlandini and Bandini 2009). It is well-known the mechanical, thermal and chemical stability of ceramic membranes, leading to an extensive range of applications across many industries.

The drawback for the application of ceramic membranes on a large scale is their high capital cost, the lower packing factor, the higher thickness and fragility, compared with the polymeric membranes widely used on the water purification process. Nevertheless the application of ceramic membranes ensures the long operational life of the membranes (can be back washed, cleaned with harsh cleaning agents and sterilized at high temperatures, offering reliable performance over longer periods of time) and robustness of the process (TiO₂ can be used at pH values close to 0 and up to 14 Mallada & menendez, 2008).

Ceramic oxides, including alumina (γ -Al₂O₃ and α -Al₂O₃), zirconia (ZrO₂), titania (TiO₂), silica (SiO₂) and not oxides like silicon carbide (SiC), are the most commonly used materials for the fabrication of membranes. The ceramic materials show a natural hydrophilic character due to the presence of hydroxyl group on the surface. This has made the ceramic membranes not so popular for MD applications (the transport coefficient on a wet membrane is lower than on a dry membrane). The use of ceramic membranes on MD requires the modification of the membrane surface, using hydrophobic terminating materials. Reactive groups (methoxy, ethoxy, or active chlorine) must be used for the surface modification process (Kujawa, et al. 2013). The reaction of the reactive groups with the hydroxyl creates a stable covalent bond that forms a molecular layer of hydrophobic nature. The Figure 4.1 shows the general formula of Perfluoroalkylsilanes (PFAS), the most popular molecules to add a hydrophobic character to ceramic membranes. PFAS possessing such reactive grouping can effectively change the surface character of a material from hydrophilic to hydrophobic one. On Figure 4.2 can be seen the substitution process of the hydrophobic chain for the hydroxyl group.

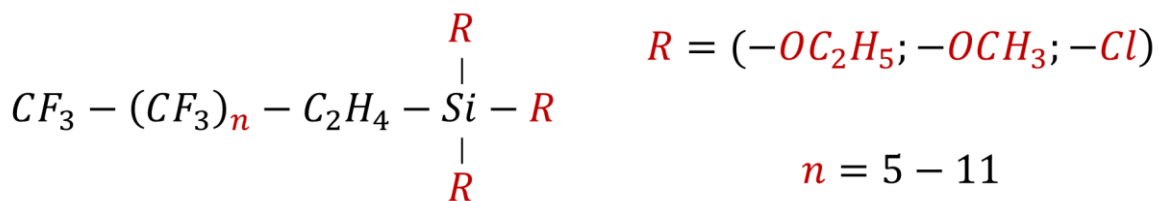


Figure 4.1 General Formula of PFAS and possible Oxyalkyl Groups – Radical

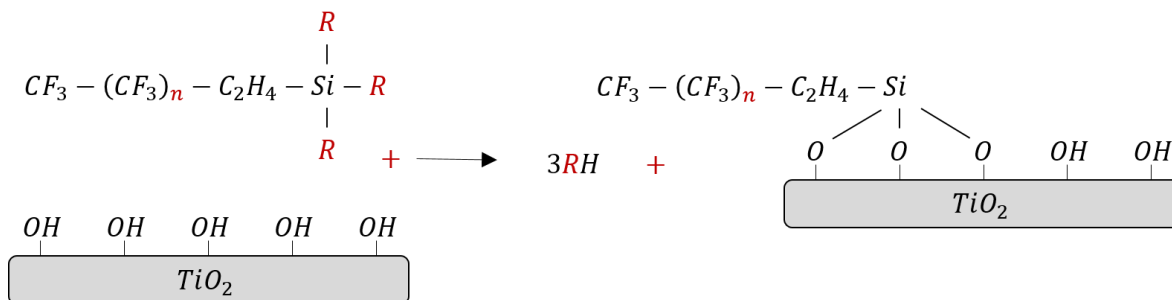


Figure 4.2 PFAS deposition on titania

The first studies for the surface modification on ceramic membranes was performed by Okubo & Inoue, 1989: they modified the silica surface with tetraethoxysilane (TEOS) in order to increase the selectivity in the separation of helium-oxygen. Later on, other authors have performed substitutions on ceramic membranes looking to increase the hydrophobic character. This is the case of Peterson et al, 1995, 1997 who modified the surface of zirconia and titania with phosphoric acid and alkylphosphoric acid obtaining a greater hydrophobicity. The modified membranes were used on tests of gas separation displaying higher permeability and selectivity for carbon dioxide separation.

Larbot's and Li's groups have performed the most extensive studies on the ceramic membranes modification (C. Picard, et al. 2004) (S. Krajewski, W. Kujawski, et al. 2006) (S. Krajewski, W. Kujawski, et al. 2004) (Kujawa, et al. 2013) (Larbot, et al. 2004) (Koonaphapdeelert and Li 2007) (Wei and Li 2009). The studies of both groups confirmed the use of PFAS for the modification of ceramic membrane surface throughout grafting process.

Generally the ceramic membranes grafted with PFAS were found to be thermally stable up to a temperature of 250 °C (studies conducted with Thermogravimetric analysis), the membrane properties were unchanged in contact with organic solvents and corrosive agents, the hydrophobic character was improved reaching contact angles between 100 and 140 ° depending on the grafting conditions (time, temperature, pressure, atmosphere and the concentration of the reactants) and the length of the PFAS chain (observing higher contact angles for longer chains) even if permeability was reduced.

On Table 4.1 is listed an overview of various modifications applied to ceramic membranes for MD applications

Table 4.1 overview of various modifications applied to ceramic membranes for MD applications. Table modified from the one published by (Drioli, Ali and Macedonio 2015)

<i>Base Material</i>	<i>Modifier</i>	<i>Attachment technique</i>	<i>Contact angle (°)</i>	<i>Comment</i>	<i>Ref.</i>
Porous alumina	Polydimethylsiloxane oil	Thermal grafting	–	No water permeation was observed	(Leger, Lira and Patero 1996)
Zirconia and KTiOPO ₄ based mesoporous membranes	Fluorinated silanes	Grafting through condensation reaction	140–150	No results for water are quoted	(C. Picard, et al. 2001)
γ -Alumina membrane	Different alcohols	Adsorption	–	Ethanol shows the strongest chemisorption	(Dafinov, García-Valls and Font 2002)
Mesoporous γ -alumina	Organochlorosilanes	Grafting via Soaking	–	Short chain organochlorosilanes are more effective	(C. Picard, et al. 2004)
Zirconia membranes	Fluoroalkylsilanes	Grafting via soaking	116–145		(Sah, et al. 2004)
Zirconia and alumina	Fluoroalkylsilane	Grafting via soaking	116–145	The flux is quite poor	(Larbot, et al. 2004)
Zirconia and alumina based	Fluorosilanes	Grafting via soaking	–	Flux is ~ 6 L/m ² h at feed temp. of 95 °C	(S. Krajewski, W. Kujawski, et al. 2006)
Zirconia alumina and alumino-silicate	Fluorodecyltriethoxysilane	Grafting via soaking	–	Flux is very low	(Gazagnes, et al. 2007)
Alumina HF	FAS solution	Grafting via soaking	100	No change in hydrophobicity after 96 h of operation	(Koonaphapdeelert and Li 2007)
Alumina Anodisc™	Various silanes	Grafting via soaking	141	Expected thermal losses are too high	(Lu, et al. 2009)
Alumina hollow fiber	Fluoroalkylsilane	Grafting via soaking	130	Obtained flux is comparable to that for polymeric membranes no results for long term performance	(Fang, et al. 2012)
Tubular and planar TiO ₂ ceramic membranes	Perfluoroalkylsilanes	Grafting via soaking	130–140	The flux obtained is quite low as compared to polymeric membranes	(Kujawa, et al. 2013)
Zirconia and alumina	Perfluoroalkylsilanes	Grafting via soaking	142-148	Thermally stable up to 230 °C	(S. Krajewski, W. Kujawski, et al. 2004)
Alumina	Perfluoroalkylsilanes	Grafting via soaking	141	LEP = 5.61 bar. Thermally stable up to 200 °C	(Hendren, Brant and Wiesner 2009)

The bibliographical study of ceramic membranes shows that these are an encouraging technology, which high temperature stability and high contact angle at room temperature, could allow an effective and safety operation at higher temperatures. Further studies should be performed to characterize the hydrophobicity of these membranes at higher temperatures.

5 List of Symbols

Symbol	Meaning
K_{eq}	Reaction equilibrium constant
T	Temperature
P	Pressure
J	Flux through the membrane of i
C_i	Molar concentration of i
P_i	Partial pressure of i
y_i	Vapor mole fraction of i
P_i^0	Vapor pressure of pure i
a_i	Activity of component i
γ_i	Activity coefficient
x_i	Liquid molar fraction of i
L	Latent heat of vaporization
R	Universal Gas Constant
Kn	Knudsen number
λ	Mean free path
d_p	Pore diameter
k_b	Boltzman constant
d_e	Molecule diameter
π	Pi number
MW	Molecular weight
r	Pore radius
δ	Pore length
χ	Pore tortuosity
D	Diffusion coefficient
C_{Kn}	Knudsen mass transport coefficient
C_D	Molecular diffusion mass transport coefficient
C_C	Transition region mass transport coefficient

P_{gas}	<i>Gas pressure within the membrane pore</i>
T_h	<i>Temperature hot fluid</i>
T_c	<i>Temperature cold fluid</i>
T_1	<i>Temperature membrane-hot</i>
T_2	<i>Temperature membrane-cold</i>
Q_h	<i>Heat flow</i>
h_h	<i>Heat transport convective coefficient hot fluid</i>
h_c	<i>Heat transport convective coefficient cold fluid</i>
h_m	<i>Heat transport conductive coefficient</i>
ΔH_v	<i>Enthalpy of vaporization</i>
U	<i>Overall heat transport coefficient</i>
ψ	<i>Temperature polarization coefficient</i>
N''_i	<i>Component i Molar flux</i>
K_{ov}	<i>Overall mass transport coefficient</i>
$k_{g,i}$	<i>Component i mass transport gas coefficient</i>
$k_{m,i}$	<i>Component i mass transport membrane coefficient</i>
$k_{l,i}$	<i>Component i mass transport liquid coefficient</i>
E	<i>Reaction Enhancement factor</i>
$H_{i,dms}$	<i>Dimensionless henry constan</i>

6 Bibliography

- Adamson, Arthur W. "Potential distortion model for contact angle and spreading. II. Temperature dependent effects." *Journal of Colloid And Interface Science* 44, no. 2 (1973): 273-281.
- Alami-Younssi, Saad, Carolin Kiefer, Andre Larbot, Michel Persin, and Jean Sarrazin. "Grafting γ alumina microporous membranes by organosilanes:: Characterisation by pervaporation." *Journal of Membrane Science* 143, no. 1-2 (1998): 27-36.
- Albrecht, W., Roland Hilke, K. Kneifel, Thomas F. Weigel, and Klaus Peinemann. "Selection of microporous hydrophobic membranes for use in gas/liquid contactors: An experimental approach." *Journal of Membrane Science* 263, no. 1-2 (2005): 66-76.
- Alkudhiri, Abdullah, Naif Darwish, and Nidal Hilal. "Membrane distillation: A comprehensive review." *Desalination* 287 (2012): 2-18.
- Ashrafizadeh, Seyed Nezameddin, and Z. Khorasani. "Ammonia removal from aqueous solutions using hollow-fiber membrane contactors." *Chemical Engineering Journal* 162, no. 1 (2010): 242-249.
- Bandini, Serena, A. Saavedra, and Giulio Cesare Sarti. "Vacuum membrane distillation: Experiments." *AIChE Journal* 43 (1997): 398-408.
- Bandini, Serena, and Giulio Cesare Sarti. "Heat and mass transport resistances in vacuum membrane distillation." *AIChE Journal* 45 (1995): 1422-1433.
- Bandini, Serena, Carlo Gostoli, and Giulio Cesare Sarti. "Separation efficiency in vacuum membrane distillation." *Journal of membrane science* 73 (1992): 217-229.
- Bernardin, John D, Issam A Mudawar, Christopher B Walsh, and Elias I Franses. "Contact angle temperature dependence for water droplets on practical aluminum surfaces." *International Journal of Heat and Mass Transfer* 40, no. 5 (1997): 1017-1033.
- Bodell, Bruce R. Distillation of saline water using silicone rubber membrane. US Patent 3361645 A. 1968.
- Bounaceur, Roda, Christophe Castel, Sabine Rode, Denis G. Roizard, and Éric Favre. "Membrane contactors for intensified post combustion carbon dioxide capture by gas-liquid absorption in MEA: A parametric study." *Chemical Engineering Research and Design* 90, no. 12 (2012): 2325-2337.
- Boyd, Claude E. *Water quality management for pond fish culture*. Elsevier Scientific Pub. Co., 1982.

- Coats, A. W., and John P. Redfern. "Thermogravimetric analysis. A review." *The Analyst* 88, no. 1053 (1963): 906-924.
- Courel, Mathilde, Emmanuel Tronel-Peyroz, Gilbert Marcel Rios, Manuel Dornier, and Max Reynes. "The problem of membrane characterization for the process of osmotic distillation." *Desalination* 140, no. 1 (2001): 15-25.
- Dafinov, Antón, Ricard García-Valls, and Josep Font. "Modification of ceramic membranes by alcohol adsorption." *Journal of Membrane Science* 196, no. 1 (2002): 69-77.
- DeMontigny, David D, Paitoon Tontiwachwuthikul, and Amit A. Chakma. "Using polypropylene and polytetrafluoroethylene membranes in a membrane contactor for CO₂ absorption." *Journal of Membrane Science* 277, no. 1-2 (2006): 99-107.
- Drelich, Jaroslaw W, Jan D. Miller, and Robert J Good. "The effect of drop (bubble) size on advancing and receding contact angles for heterogeneous and rough solid surfaces as observed with sessile-drop and captive-bubble techniques." *Journal of Colloid and Interface Science* 179, no. 1 (1996): 37-50.
- Drelich, Jaroslaw W., and Jan D. Miller. "The effect of surface heterogeneity on pseudo-line tension and the flotation limit of fine particles." *Colloids and Surfaces* 69, no. 1 (1992): 35-43.
- Drelich, Jaroslaw, and Jan D Miller. "Effect of solid surface heterogeneity and roughness on the contact angle/drop (bubble) size relationship." *Journal of Colloid and Interface Science* 164, no. 1 (1994): 252-259.
- Drioli, Enrico, Aamer Ali, and Francesca Macedonio. "Membrane distillation: Recent developments and perspectives." *Desalination* 356 (2015): 56-84.
- E. Drioli, A. Criscuoli and E. Curcio. *MEMBRANE CONTACTORS: FUNDAMENTALS, APPLICATIONS AND POTENTIALITIES*. Amsterdam: ELSEVIER, 2006.
- ECOSOC. "United Nations Economic Commission for Europe." http://www.unece.org/fileadmin/DAM/env/documents/2012/EB/ECE_EBAIR_120_EN_G.pdf. February 7, 2014. (accessed January 23, 2016).
- . "United Nations Economic Commission for Europe." http://www.unece.org/fileadmin/DAM/env/documents/2013/air/eb/ECE_EBAIR_119_ENG.pdf. June 17, 2013. (accessed January 23, 2016).
- Fang, Hong, Jianfeng Gao, Huanting Wang, and Chusheng Chen. "Hydrophobic porous alumina hollow fiber for water desalination via membrane distillation process." *Journal of Membrane Science* 403-404 (2012): 41-46.

- Favre, Éric, and Hallvard Fjøsne Svendsen. "Membrane contactors for intensified post-combustion carbon dioxide capture by gas-liquid absorption processes." *Journal of Membrane Science* 407-408 (2012): 1-7.
- Fraken, A., J. Nolten, M. Mulder, D. Bargeman, and C. Smolders. "Wetting criteria for the applicability of membrane distillation." *Journal of Membrane Science* 33 (1987): 315 - 328.
- García-Payo, Carmen C., C. A. Rivier, Ian William Marison, and Urs Von Stockar. "Separation of binary mixtures by thermostatic sweeping gas membrane distillation: II. Experimental results with aqueous formic acid solutions." *Journal of Membrane Science* 198, no. 2 (2002): 197-210.
- García-Payo, M. C., Amparo M. Izquierdo-Gil, and Cristóbal Fernández-Pineda. "Wetting study of hydrophobic membranes via liquid entry pressure measurements with aqueous alcohol solutions." *Journal of Colloid and Interface Science* 230, no. 2 (2000): 420-431.
- Gaydos, J. A., and August Wilhelm Neumann. "The dependence of contact angles on drop size and line tension." *Journal of Colloid And Interface Science*, 1987: 76-86.
- Gazagnes, Laetitia, Sophie A. Cerneaux, Michel I. Peršin, Éric Prouzet, and André L. Larbot. "Desalination of sodium chloride solutions and seawater with hydrophobic ceramic membranes." *Desalination* 217, no. 1-3 (2007): 260-266.
- Ghadiri, Mehdi, Azam Marjani, and Saeed Shirazian. "Mathematical modeling and simulation of CO₂ stripping from monoethanolamine solution using nano porous membrane contactors." *International Journal of Greenhouse Gas Control* 13 (2013): 1-8.
- Good, Robert J., and M. N. Koo. "The effect of drop size on contact angle." *Journal of Colloid And Interface Science* 71, no. 2 (1979): 283-292.
- Gostoli, Carlo. "Thermal effects in osmotic distillation." *Journal of Membrane Science* 163 (1999): 75-91.
- Guillen-Burrieza, Elena, Amelia Servi, Boor Lalia, and Hassan A. Arafat. "Membrane structure and surface morphology impact on the wetting of MD membranes." *Journal of Membrane Science* 483 (2015): 94 - 103.
- Hayashi, Tsukasa, Tatsuya Hazuku, Tomoji Takamasa, and Kenrou Takamori. "Contact angle of water droplets in a high-temperature, high-pressure environment." *Proceedings of the International Conference on Nuclear Engineering (ICONE12)* 1 (2004): 797-800.
- Hendren, Z.D., J. Brant, and M.R. Wiesner. "Surface modification of nanostructured ceramic membranes for direct contact membrane distillation." *Journal of Membrane Science* 331, no. 1-2 (2009): 1-10.

- Jones, Jamie Bryan, and Arthur W. Adamson. "Temperature dependence of contact angle and of interfacial free energies in the naphthalene-water-air system." *Journal of Physical Chemistry* 72, no. 2 (1968): 646-650.
- Khaisri, Sakarin, David deMontigny, Paitoon Tontiwachwuthikul, and Ratana Jiratananon. "CO₂ stripping from monoethanolamine using a membrane contactor." *Journal of Membrane Science* 376, no. 1-2 (2011): 110-118.
- Khayet, M. "Membranes and theoretical modeling of membrane distillation: A review." *Adv. Colloid Interface Science* 164 (2011): 56-88.
- Khayet, Mohamed, Armando Velázquez, and Juan I. Mengual. "Modelling mass transport through a porous partition: Effect of pore size distribution." *Journal of Non-Equilibrium Thermodynamics* 29, no. 3 (2004): 279-299.
- Khayet, Mohamed, M. Paz Godino, and Juan I. Mengual. "Theory and experiments on sweeping gas membrane distillation." *Journal of Membrane Science* 165, no. 2 (2000): 261-272.
- Koonaphapdeelert, Sirichai, and K. Li. "Preparation and characterization of hydrophobic ceramic hollow fibre membrane." *Journal of Membrane Science* 291 (2007): 70-76.
- Koonaphapdeelert, Sirichai, Zhentao Wu, and Kang Li. "Carbon dioxide stripping in ceramic hollow fibre membrane contactors." *Chemical Engineering Science* 64, no. 1 (2009): 1-8.
- Koonaphapdeelert, Sirichai, Zhentao Wu, and Kang Li. "Carbon dioxide stripping in ceramic hollow fibre membrane contactors." *Chemical Engineering Science* 64, no. 1 (2009): 1-8.
- Krajewski, Sebastian R., Wojciech Kujawski, Frédéric Dijoux, Céline Picard, and André Larbot. "Grafting of ZrO₂ powder and ZrO₂ membrane by fluoroalkylsilanes." *Colloids and Surfaces A: Physicochemical and Engineering Aspects* 243, no. 1-3 (2004): 43-47.
- Krajewski, Sebastian R., Wojciech M. Kujawski, Malgorzata Bukowska, Céline Picard, and André L. Larbot. "Application of fluoroalkylsilanes (FAS) grafted ceramic membranes in membrane distillation process of NaCl solutions." *Journal of Membrane Science* 281, no. 1-2 (2006): 253-259.
- Kujawa, Joanna, et al. "Membrane distillation properties of TiO₂ ceramic membranes modified by perfluoroalkylsilanes." *Desalination and Water Treatment* 51, no. 7-9 (2013): 1352-1361.
- Kwok, D.Y., and A.W. Neumann. "Contact angle measurement and contact angle interpretation." *Advances in Colloid and Interface Science* 81, no. 3 (1999): 167-249.

- Larbot, André, Laetitia Gazagnes, Sebastian Krajewski, Malgorzata Bukowska, and Wojciech Kujawski. "Water desalination using ceramic membrane distillation." *Desalination* 168 (2004): 367-372.
- Lawson, Kevin W., and Douglas R. Lloyd. "Membrane distillation." *Journal of Membrane Science* 124 (1997): 1-25.
- Lee, Chul Haeng, and Won Hi Hong. "Effect of operating variables on the flux and selectivity in sweep gas membrane distillation for dilute aqueous isopropanol." *Journal of Membrane Science* 188, no. 1 (2001): 79-86.
- Lee, M., Z. Wu, and K. Li. *Advances in Membrane Technologies for Water Treatment: Materials, Processes and Applications*. Edited by Angelo Basile, Alfredo Cassano and Navin K. Rastogi. Cambridge: Woodhead Publishing, 2015.
- Leger, Christian, Helio De L. Lira, and Russell Pateroso. "Preparation and properties of surface modified ceramic membranes. Part II 1. Gas and liquid permeabilities of 5 nm alumina membranes modified by a monolayer of bound polydimethylsiloxane (PDMS) silicone oil." *Journal of Membrane Science* 120 (1996): 135 - 146.
- Li, Kang, M. S L Tai, and Wah Koon Teo. "Design of a CO2 scrubber for self-contained breathing systems using a microporous membrane." *Journal of Membrane Science* 86, no. 1-2 (1994): 119-125.
- Lü, Jiangang, Youfei Zheng, and Min Dong Cheng. "Wetting mechanism in mass transfer process of hydrophobic membrane gas absorption." *Journal of Membrane Science* 308, no. 1-2 (2008): 180-190.
- Lü, Jian-Gang, You-Fei Zheng, and Min-Dong Cheng. "Wetting mechanism in mass transfer process of hydrophobic membrane gas absorption." *Journal of Membrane Science* 308, no. 1-2 (2008): 180-190.
- Lu, Jun, Yun Yu, Jianer Zhou, Lixin Song, Xingfang Hu, and Andre Larbot. "FAS grafted superhydrophobic ceramic membrane." *Applied Surface Science* 255 (2009): 9092-9099.
- Lv, Yue-Xia, Xin-Hai Yu, Jingjing Jia, Shan-Tung Tu, Jin-Yue Yan, and Erik Dahlquist. "Fabrication and characterization of superhydrophobic polypropylene hollow fiber membranes for carbon dioxide absorption." *Applied Energy* 90, no. 1 (2012): 167-174.
- Lyklema, J. "The surface tension of pure liquids: Thermodynamic components and corresponding states." *Colloids and Surfaces A: Physicochemical and Engineering Aspects* 153, no. 1-3 (1999): 413-421.

- Mack, G. L. "The determination of contact angles from measurements of the dimensions of small bubbles and drops. I: The spheroidal segment method for acute angles." *The Journal of Physical Chemistry* 40 (1936): 159-167.
- Mansourizadeh, Amir, and Abdol Rasoul Pouranfard. "Microporous polyvinylidene fluoride hollow fiber membrane contactors for CO₂ stripping: Effect of PEG-400 in spinning dope." *Chemical Engineering Research and Design* 92, no. 1 (2014): 181-190.
- Mansourizadeh, Amir, and Ahmad Fauzi Auzi Ismail. "CO₂ stripping from water through porous PVDF hollow fiber membrane contactor." *Desalination* 273, no. 2-3 (2011): 386-390.
- Mazzoni, Carolina, Fiorenzo Orlandini, and Serena Bandini. "Role of electrolyte type on TiO₂-ZrO₂ nanofiltration membranes performances." *Desalination* 240, no. 1-3 (2009): 227-235.
- McGuire, Kenneth S, Kevin W Lawson, and Douglas R Lloyd. "Pore size distribution determination from liquid permeation through microporous membranes." *Journal of Membrane science* 99 (1995): 127-137.
- Mengual, J.I., M. Khayet, and M.P. Godino. "Heat and mass transfer in vacuum membrane." *Int. J. Heat Mass Transf* 47 (2004): 865-875.
- Naim, Rosma, Ahmad Fauzi Auzi Ismail, and Amir Mansourizadeh. "Preparation of microporous PVDF hollow fiber membrane contactors for CO₂ stripping from diethanolamine solution." *Journal of Membrane Science* 392-393 (2012): 29-37.
- Newmann, A. W., and D Li. "Equation of State for Interfacial Tension of Solid-Liquid Systems." *Adv. Colloid Interf. Sci* 39 (1992): 299-345.
- Peng, Zanguo, Swin H. Lee, Tong Zhou, Jyhjeng Shieh, and Tai Shung Neal Chung. "A study on pilot-scale degassing by polypropylene (PP) hollow fiber membrane contactors." *Desalination* 234, no. 1-3 (2008): 316-322.
- Petke, F. David, and B. Roger Ray. "Erratum to temperature dependence of contact angles of liquid on polymeric solids." *Journal of Colloid And Interface Science*, 1970: 195.
- Petke, F. David, and B. Roger Ray. "Temperature dependence of contact angles of liquids on polymeric solids." *Source of the Document Journal of Colloid And Interface Science* 31, no. 2 (1969): 216-227.
- Picard, C., A. Larbot, E. Tronel-Peyroz, and R. Berjoan. "Characterisation of hydrophilic ceramic membranes modified by fluoroalkylsilanes into hydrophobic membranes." *Solid State Sciences* 6, no. 6 (2004): 605-612.

- Picard, Céline, André L Larbot, Francine Guida-Pietrasanta, Bernard Boutevin, and Amédée Ratsimihety. "Grafting of ceramic membranes by flourinated silanes: Hydrophobic features." *Separation and Purification Technology* 25, no. 1-3 (2001): 65-69.
- Porcheron, Fabien, and Sophie Drozd. "Hollow fiber membrane contactor transient experiments for the characterization of gas/liquid thermodynamics and mass transfer properties." *Chemical Engineering Science* 64, no. 2 (2009): 265-275.
- Rahbari-Sisakht, Masoud, Dipak Rana, Takeshi Matsuura, Daryoush Emadzadeh, Mahesh Padaki, and Ahmad Fauzi Auzi Ismail. "Study on CO₂ stripping from water through novel surface modified PVDF hollow fiber membrane contactor." *Chemical Engineering Journal* 246 (2014): 306-310.
- Rangwala, Huseni A. "Absorption of carbon dioxide into aqueous solutions using hollow fiber membrane contactors." *Journal of Membrane Science* 112, no. 2 (1996): 229-240.
- Rode, Sabine, Phuc Tien H Nguyen, Denis G. Roizard, Roda Bounaceur, Christophe Castel, and Éric Favre. "Evaluating the intensification potential of membrane contactors for gas absorption in a chemical solvent: A generic one-dimensional methodology and its application to CO₂ absorption in monoethanolamine." *Journal of Membrane Science* 389 (2012): 1-16.
- Saffarini, Rasha B, Bilal Mansoor, Rinku Thomas, and Hassan A Arafat. "Effect of temperature-dependent microstructure evolution on pore wetting in PTFE membranes under membrane distillation conditions." *Journal of Membrane Science* 429 (2013): 282-294.
- Sah, Ashima, Hessel L. Castricum, A. Blik, Dave H. A. Blank, and Johan E. Ten Elshof. "Hydrophobic modification of γ -alumina membranes with organochlorosilanes." *Journal of Membrane Science* 243, no. 1-2 (2004): 125-132.
- Sarti, Giulio Cesare, Carlo Gostoli, and Serena Bandini. "Extraction of organic components from aqueous streams by vacuum membrane distillation." *Journal of Membrane Science* 80 (1993): 21-33.
- Sengupta, Amitava, Patricia A. Peterson, B. D. Miller, Jürgen K. Schneider, and C. W. Fulk. "Large-scale application of membrane contactors for gas transfer from or to ultrapure water." *Separation and Purification Technology* 14, no. 1-3 (1998): 189-200.
- Simioni, Michael A., Sandra E. Kentish, and Geoffrey Wayne Stevens. "Membrane stripping: Desorption of carbon dioxide from alkali solvents." *Journal of Membrane Science* 378, no. 1-2 (2011): 18-27.
- Sun, Xiuyu, Faqiang Xu, Zongmu Li, and Wenhua Zhang. "Photoluminescence properties of anodic alumina membranes with ordered nanopore arrays." *Journal of Luminescence* 121, no. 2 (2006): 588-594.

- Tadmor, Rafael, and Preeti Yadav. "As-placed contact angle for sessile drops." *Journal of Colloids and Interface Science* 317 (2008): 241-246.
- Tai, M. S L, Ivy Chua, Kang Li, Wunjern Ng, and Wah Koon Teo. "Removal of dissolved oxygen in ultrapure water production using microporous membrane modules." *Journal of Membrane Science* 87, no. 1-2 (1994): 99-105.
- Tröger, Jens, Klaus Lunkwitz, and Wolfgang Bürger. "Determination of the Surface Tension of Microporous Membranes Using Contact Angle Measurements." *Journal of Colloid and Interface Science* 194, no. 2 (1997): 281-286.
- UNECE. "United Nations Economic Commission for Europe." <http://www.unece.org/fileadmin/DAM/env/lrtap/full%20text/1999%20Multi.E.Amend.ed.2005.pdf>. November 30, 1999. (accessed January 23, 2016).
- Weber, Christian, and Helge Stanjek. "Energetic and entropic contributions to the work of adhesion in two-component, three-phase solid-liquid-vapour systems." *Colloids and Surfaces A: Physicochemical and Engineering Aspects* 441 (2014): 331-339.
- Wei, Chiao Chien, and K. Li. "Preparation and Characterization of a Robust and Hydrophobic Ceramic Membrane via an Improved Surface Grafting Technique." *nd. Eng. Chem. Res.* 48, no. 7 (2009): 3446-3452.
- Xie, Z., T. Duong, M. Hoang, C. Nguyen, and Bolto. "Ammonia Removal by Sweeping Gas Membrane Distillation." *Water Research* 43 (2009).
- Yang, Mingchien, Ming-Chien, and Edward L. Cussler. "DESIGNING HOLLOW-FIBER CONTACTORS." *AIChE Journal* 32, no. 11 (1986): 1910-1916.
- Yeon, Soon H., Kisub Lee, YuIn Park, Kewho Lee, and Bongkuk Sea. "Application of pilot-scale membrane contactor hybrid system for removal of carbon dioxide from flue gas." *Journal of Membrane Science* 257, no. 1-2 (2005): 156-160.
- Zha, Fu Fang, Anthony Gordon Fane, Christopher Joseph D Fell, and R. W. Schofield. "Critical displacement pressure of a supported liquid membrane." *Journal of Membrane Science* 75, no. 1-2 (1992): 69-80.
- Zhongwei, Ding, Liu Liying, and Ma Runyu. "Study on the effect of flow maldistribution on the performance of the hollow fiber modules used in membrane distillation." *Journal of Membrane Science* 23, no. 1-2 (2003): 11-23.

Membrane characterization.

Summary

1	Introduction	40
2	Membrane Characterization Methods	42
2.1	Thermogravimetric analysis (TGA)	42
2.1.1	Characterization of ceramic membranes by TGA	42
2.1.2	Measuring methods.....	44
2.2	Scanning Electron Microscopy (SEM).....	45
2.3	Gas permeability through macro porous membranes.....	48
2.3.1	Flow regime.....	48
2.3.1.1	Viscous Flow	49
2.3.1.2	Free Molecular Streaming Flow – Knudsen Flow.....	49
2.3.1.3	Transitory Regimes.....	50
2.4	Contact angle	51
2.4.1	Changes with drop size	54
2.4.2	Contact angle in porous materials.....	55
2.4.3	Hysteresis.....	56
2.4.4	Contact angle Temperature dependence.....	57
2.4.4.1	Super-heated water	58
2.4.4.2	Contact angle Temperature dependence – Models	60
2.4.5	Measuring methods.....	63
2.4.5.1	The static sessile drop method	63
2.4.5.2	The dynamic sessile drop method.....	64

2.4.5.3	The capillary rise at a vertical plate.....	64
2.4.5.4	Wilhelmy method.....	64
2.4.5.5	High temperature contact angle measurements	64
2.5	The liquid breakthrough pressure (liquid entry pressure).....	67
2.5.1	Dependence with Temperature.....	70
2.5.2	Measuring methods.....	70
2.5.2.1	Franken Method.....	70
2.5.2.2	Liquid Permeation Technique	71
3	Experimental characterization of MC for high temperature applications	76
3.1	Materials and methods	76
3.1.1	Membranes.....	77
3.1.1.1	Polymeric membranes.....	77
3.1.1.2	Ceramic membranes.....	78
3.1.2	Contact angle measurement	79
3.1.3	Water breakthrough measurements through modified Franken method and flooding curve measurements.....	80
3.1.3.1	Apparatus.....	80
3.1.3.2	Procedure.....	81
3.1.3.3	Data reduction	84
3.1.3.4	Liquid Entry Pressure Definition.....	89
3.1.3.5	Fitting curve modification and pore size distribution.....	90
3.2	Results.....	92
3.2.1	Polymeric membranes.....	92
3.2.1.1	Contact angle	92
3.2.1.2	Water breakthrough.....	93
3.2.2	Ceramic membrane.....	98

3.2.2.1	Contact Angle	98
3.2.2.2	Water breakthrough.....	100
3.3	Analysis and discussion.....	109
4	Conclusions.....	114
5	List of Symbols.....	118
6	Bibliography.....	121

1 **Introduction.**

The key parameter of the membrane contactors (MC) processes is the membrane itself, since it defines the range of the operative conditions and in many cases, it is the most important element to consider for the mass transport operation. Thus it is fundamental to know the characteristics of the membrane, in order to have a safe operation with the maximum potentialities of the membranes and the process.

The characteristics of the membrane can be divided in: morphological characteristics and physical-chemical characteristics. Regarding the morphological characteristics there can be listed properties like pore size (including mean pore size, maximum pore size, and pore size distribution), porosity (active and total), thickness and tortuosity among others. The physical-chemical characteristics are determined mostly by the membrane material and its interaction with solutes and solvents. Examples of these are, the thermal conductivity, thermal stability (phase transition, decomposition, redox...), chemical stability, hydrophobic character (related to interfacial surface tension), mechanical properties, adsorption, desorption and many more.

From the whole set of properties is possible to evaluate phenomena related to the operation like the mass transport coefficient, the pressure of breakthrough or the operative conditions (the phases temperatures and pressures). All this information might be very important to decide which membrane is more suitable to be used on certain MC process (considering the phases and purposes of the process), making possible to predict and to optimize the membrane performance for a given application.

In the introductory chapter there are explained the main conditions for a membrane to be used on a MC process. The membrane must act as a barrier to one or both phases in contact and in order to have a performant operation, the permeability for the diffusive transport should be the highest possible. The optimum equilibrium should be found between the membrane characteristics: E.g., the membrane thickness should be small to promote the mass transport, but (on membrane distillation) if it is too small the heat losses increase. The pore size must be small to contain the phases so to make the pressure of breakthrough the highest, and big enough to have a satisfactory mass transport across the pores.

Different techniques exist to evaluate particular properties, each one suitable or not for a specific membrane. In this chapter there are described the main methods used in the academy and industry to characterize the membranes for MC, with a specific focus on how to identify the hydrophobic character of the membrane and how it might change with the temperature.

The hydrophobic membrane character of the membranes is a critical argument for the MC process and it is one of the main drawback for the massive application of this technology (Drioli, Ali and Macedonio 2015). Many studies aimed to evaluate the hydrophobic character have been performed and continue to be a trend topic on the MC scenario. However, few studies have been performed to evaluate the variation of the hydrophobicity with the temperature and none of them have considered the effect of temperature above the normal water boiling point.

At the end of this section a completely new method will be proposed to estimate the hydrophobic character and secondly a variation of the method currently in use. Both have the aim of evaluating the membrane hydrophobic character at temperatures never explored before.

Moreover, a model based on specific data treatment will be suggested to predict the hydrophobic character and the wettability of the membranes in function of the temperature.

2 *Membrane Characterization Methods*

2.1 *Thermogravimetric analysis (TGA)*

Thermogravimetric analysis is a method of thermal analysis in which changes in mass (loss or gain) are related to changes in physical and chemical properties of materials. Changes in mass are measured as a function of increasing temperature (with constant heating rate), or as a function of time (with constant temperature and/or constant mass loss). Results of **TGA** are typically presented in the diagram known as thermogravimetric curve that relates mass versus temperature (or time) or rate of mass loss (gain) versus temperature curve, known as the differential thermogravimetric curve. (Coats and Redfern 1963).

TGA can provide information about physical phenomena, such as second-order phase transitions, including vaporization, sublimation, absorption, adsorption, and desorption. Also, TGA can provide information about chemical phenomena including chemisorption, desolvation (especially dehydration), decomposition, and solid-gas reactions (e.g., oxidation or reduction).

TGA is a technic used widely for different applications, including analysis of ceramics and thermally stable polymers. Ceramics usually melt before they decompose as they are thermally stable over a large temperature range, thus TGA is mainly used to investigate the thermal stability of polymers.

In membrane science TGA is one of the principal techniques used to characterize the materials. A high number of examples can be found on literature about characterization of membranes with TGA (Jiansheng, et al. 2005); (Sun, Xu, et al. 2006); (Monash and Pugazhenthhi 2011): this is mainly used to verify the thermal stability of the membrane to temperatures going from room temperature to 800 °C – 1000 °C.

An example of TGA analysis for alumina is reported on Figure 2.1. On the Thermogram, three main sections can be identified: 1) From room temperature to 400 °C is observed a low decreases on the mass sample, this is due to the evaporation of the surface humidity and the water present on the pores (Sun, Xu, et al. 2006). 2) From 400 °C to 800 °C, could be an important weight decrease, owing to loss of solvent used in the membrane preparation (Jiansheng, et al. 2005) and to the decomposition and subsequent desorption of synthesis elements (Monash and Pugazhenthhi 2011). 3). Losses between 800 °C to 900 °C, are imputable to the glass transition. Over 900 °C there are no meaningful weight losses.

2.1.1 *Characterization of ceramic membranes by TGA*

The great thermal and chemical stability of ceramic membranes has made of them preferred than polymeric membranes which have a lower range of applicability in terms of pH, and temperature. However the ceramic membranes, produced mainly from metal oxides, are hydrophilic, due to the presence of hydroxyl groups on the surface and the possibility of those to develop Hydrogen Bond.

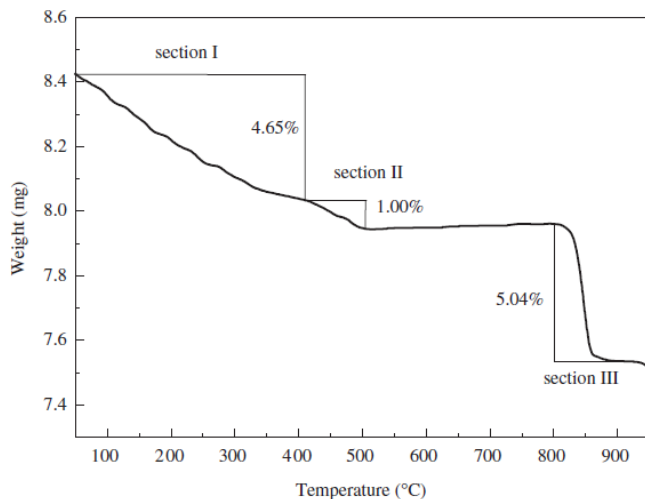


Figure 2.1 TGA characterization of alumina membrane. Three main sections can be identify: I) water desorption; II) decomposition and desorption of synthesis elements; III) glass transition to γ - Al_2O_3 (Sun, Xu, et al. 2006)

With the aim to have hydrophobic membranes able to work at hard temperature and pH conditions, an important research field has been developed: the looking for technics to functionalize the hydrophilic support with polymeric matrices that could turn the ceramic membranes into hydrophobic. This highlighted the possibility of silanize the surface through self-assembling with organofunctional alkoxy silane molecules. Thereby is created a strong bond with the surface and the alkoxy group which generates the desired stern hydrophobicity.

Alami-Younssi et al. (1998) were one of the first to propose the TGA as a technic to characterize alumina functionalized with short chain silanes (metilsilanes). They observed not only the decrease on weight due to the desorption of humidity and synthesis elements, but also between 500 °C and 550 °C a important loss owed to the calcination of the organic groups.

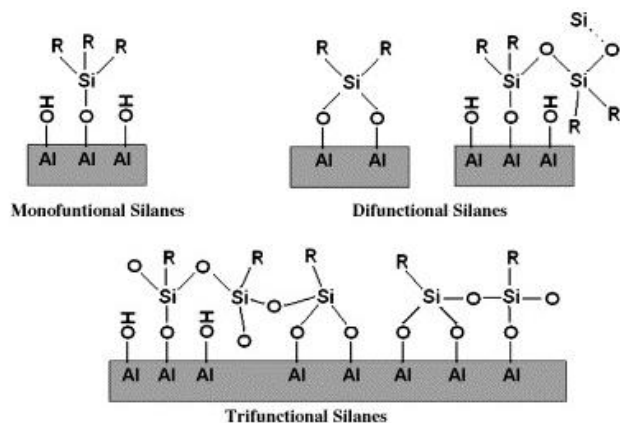


Figure 2.2 Silanization of alkoxy silane on ceramic membranes surface (Koonaphapdeelert and Li 2007)

Alumina hollow fibers were functionalized with fluoroalkylsilane (FAS) and their hydrophobicity as a function of the organic chain length was characterized with different techniques (Koonaphapdeelert and Li 2007). The TGA proved the polymer thermal stability till 250 °C.

Picard et al. (2004) functionalized FAS on zirconia (ZrO₂) membranes. The TGA test, on figure X, show weight loss between 200 °C and 500 °C. The losses are related with the decomposition of the polymer as these grows when the amount of polymer in the membrane surface is higher.

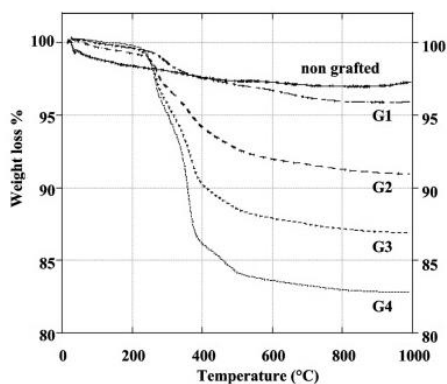


Figure 2.3 Thermogravimetric curve of Zirconia membranes for samples with progressive amounts of polymer on the surface from G1 to G4 (Picard, et al. 2004)

As the in previous case of functionalization, Krajewski et al. (2004) immobilized FAS over Zirconia powders and membranes. They used TGA to optimize the grafting parameters (reagent quantities, contact time, temperature of reaction) of the polymer surface. As for the releasing of fluorocarbons, it starts at 230 °C and terminates at 800 °C: they correlated the loss in this range of temperature to the amount of FAS grafted. Lu et al. (2007) used TGA to investigate the weight loss process (25–800 °C) of the fluoroalkylsilane grafted on Al₂O₃ powders under different grafting conditions to produce “superhydrophobic” membranes, obtaining the same results for polymer decomposition between 230–800 °C

Thermogravimetric analysis is an important technique in the field of membrane characterization. In particular for the characterization of ceramic membranes functionalized with polymers, it is useful to evaluate the temperature of decomposition of the polymer with the loss of the hydrophobic character given by it. If compared with the non grafted membrane the TGA could give important information, like the operational Temperature range and the optimization of the grafting conditions.

2.1.2 Measuring methods.

The measure technique is performed on a thermogravimetric analyzer TGA Q500 (TA Instruments) Auto sampled shown in Figure 2.4



Figure 2.4 TGA Q500 Thermogravimetric Analyzer; Detail of Furnace, Balance and Auto Sampler; Gas flow in the Furnace

This specific instrument allow the measure of mass loss in function of the increasing temperature and of time for a constant temperature. The reaction atmosphere can be controlled with a constant gas flow to create inert or oxidizing atmosphere. The balance prove can be loaded with a minimum weight of 1 mg to a maximum of 1 g. The furnace can set temperatures from room temperature to 1000 °C at a constant heating rate, controlled by a thermocouple set over the sample. A second control thermocouple is set higher than the first one. The sample is loaded by the operator on a sample tray outside the furnace while the balance is loaded by the auto sampler to the furnace. The atmosphere on the furnace is controlled by the horizontal flow of inert gas (N₂ or dehumidify Air) across the sample, the purge of the inert gas allows to have stable atmospheric conditions for the sample.

The data acquisition is controlled by software, as the control of each test. The test procedure is as follow:

- *Selection a tare of the sample holder.*
- *Sample loading*
- *Set the test parameters on the software*
- *Start of the test with the gas flow.*

2.2 Scanning Electron Microscopy (SEM)

The scanning electron microscopy (SEM) is a microscopy technic where the images are the product of the scanning of the sample by a narrow bean of electrons. The narrow beam of electrons hits the atoms on the sample surface, exiting them. Consequently, low energy electrons are emitted by the sample. The signal produced, collected by a special detector contain information about the sample's surface topography and composition. SEM images resolution is in the order of 1 nanometer. The surface must be conductive so frequently the surface is coated with metals like gold.

Generally most SEMs are equipped with the secondary electron detector, yet other kind of signals can be collected by other detectors not always present in every instrument. E.g., back-scattered electrons, characteristic X-rays (to perform spectrographic analysis - composition), specimen current and transmitted electrons.

The results of the interaction between the electrons and the surface atoms of the samples are collected by the detectors. The signal represents an image of the surface of very high resolution, yielding a three-dimensional appearance thanks to the large depth of field produced by the thin electron beam. On Figure 2.5 can be observed an alumina hollow fiber membrane, coated with Fluoroalkyl Silanes (FAS). It can be seen the two different structures along the membrane thickness.

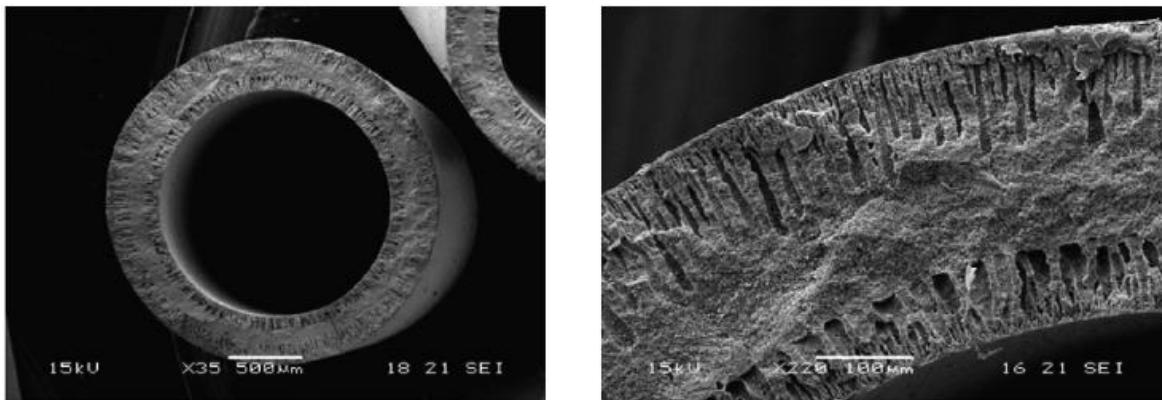


Figure 2.5 Sintered alumina membranes through the phase inversion method (Koonaphapdeelert and Li 2007)

Throughout SEM images is possible to estimate the pore size and pore size distribution, the porosity of the membrane, the thickness of the top layer on a composite membrane and even the surface morphology (Roughness). Numerous authors have used the SEM images to analyze the membrane properties like Calvo et al (2008), they obtain images of the cross section of titania membrane (Figure 2.6) to analyze the top layer thickness and the grain structure of the membrane observing the actual membrane porosity. Through the surface images analysis and its relation with other properties e.g. Lu et al (2009) evaluate the roughness of ceramic samples coated with fluoropolymers to evaluate the relation between the surface roughness with the hydrophobicity across the contact angle (Figure 2.7) after alumina membranes has been coated with Fluoroalkyl Silanes of different concentrations.

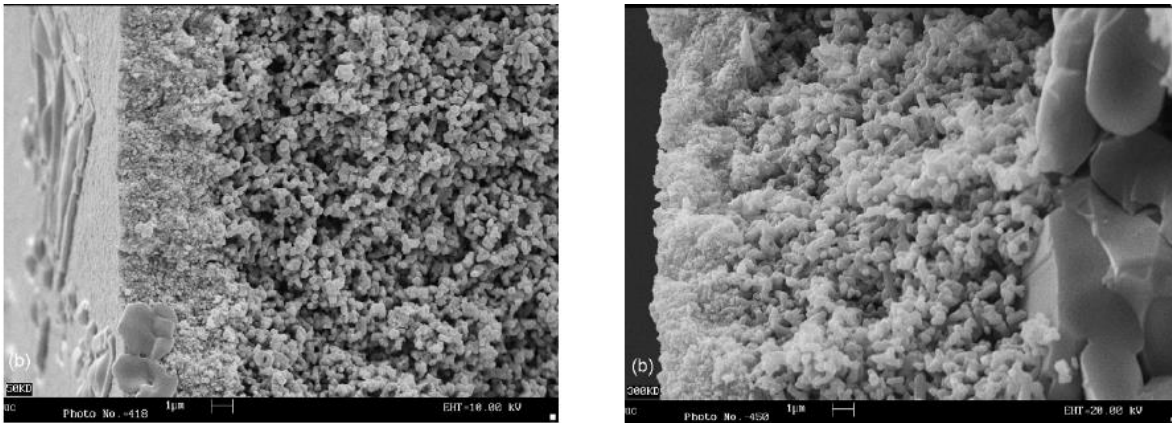


Figure 2.6 Cross section of a titania membrane: top layer and grains diameters (Calvo, et al. 2008)

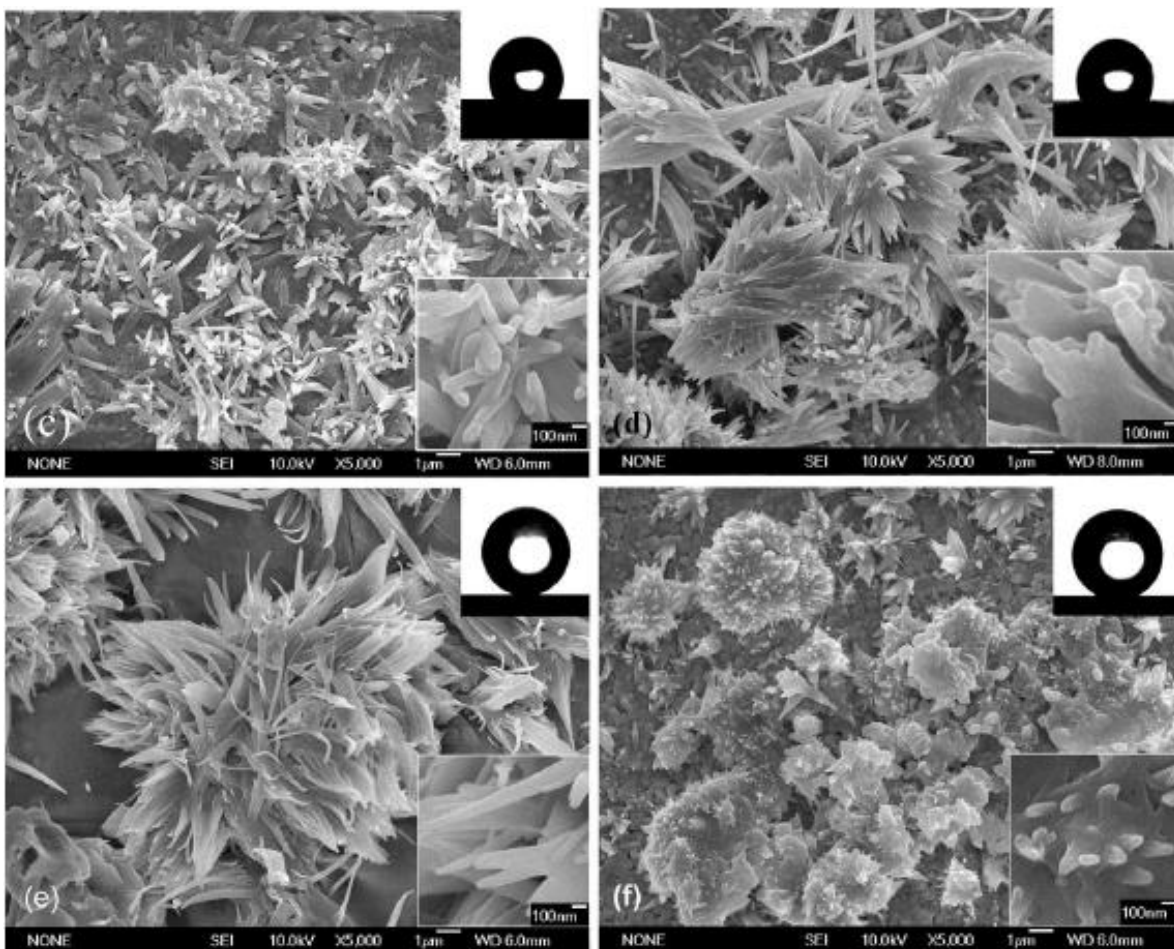


Figure 2.7 Contact angle images along with surface SEM images of Titania membranes coated with FAS (Lu, et al. 2009)

2.3 Gas permeability through macro porous membranes.

2.3.1 Flow regime

The mechanism that rules the gas flux, of one component, through a capillary is related with the ratio of collisions of the molecule with the capillary wall or with other molecules

This ratio is represented by the Knudsen number (Kn), this is an dimensionless number that represent which phenomena is dominant for a given gas component – capillary diameter. Generally Kn represents the ratio between the Mean Free Path (λ) and the physical length scale (L_0) (Present 1958).

$$Kn = \frac{\lambda}{L_0} = \frac{\lambda}{d_p} \quad (2.1)$$

The mean free path represents the distance covered by a single moving particle between collisions with other moving particles, which modify its direction or energy or other particle properties. In kinetic theory the mean free path of a particle is function of the gas viscosity (η), pressure (P), temperature (T), molar mass (MW), related with the ideal gas constant (R).

$$\lambda = \frac{\eta}{P} \sqrt{\frac{\pi RT}{2MW}} \quad (2.2)$$

As said before the calculation of Knudsen number is an indication of the ruling transport mechanism. A Knudsen number below 0.01 ($Kn < 0.01$) indicates a low number of collisions between the particle and the wall (can be neglected) regarding the collisions between particles. This transport mechanism is known as viscous flow.

The opposite case is if Knudsen is grater that 10 ($Kn > 10$), if so, it means that the collisions between the particles and the wall are dominant. This transport mechanism is known as free molecular streaming or Knudsen Flow. If the Knudsen number is between the previously specify ($0.01 < Kn < 10$), we should talk about a transition flow mechanism or slip flow mechanism, depending on the Knudsen number.

Table 2.1 Gas flow regime accordingly with the Knudsen number.

Knudsen Number	Flow regime
$Kn < 0.01$	<i>viscous flow</i>
$0.01 < Kn < 0.1$	<i>slip flow</i>
$0.1 < Kn < 10$	<i>transition flow</i>
$Kn > 10$	<i>Knudsen flow</i>

2.3.1.1 Viscous Flow

The gas flow in the Viscous Flow regime can be described by the Hagen-Poiseuille equation, derived from the Navier–Stokes equations for laminar flow through a pipe of uniform (circular) cross-section. The Hagen–Poiseuille equation relates the pressure drop ΔP across a circular pipe of length (δ_{eff}), to the average flow velocity across a circular section of diameter (d_p).

$$\dot{V} = \frac{\pi \Delta P d_p^4}{124 \eta \delta_{eff}} \quad (2.3)$$

In our particular case a gas has to be considered and so the ideal gas relation could be used. In order to obtain the Hagen-Poiseuille equation for molar flow.

$$\dot{n} = \frac{\dot{V} P}{RT} \quad (2.4)$$

$$\dot{n} = \frac{\pi d_p^4 P}{124 \eta \delta_{eff} RT} \Delta P \quad (2.5)$$

In the case of a porous material (membrane) the equation (2.5) should take into account the number of pores (N_p), where the flux take place, and that the de pores are not all of the same dimensions. So average values should be consider (\bar{d}_p, P_m, T_m) and the channel length δ_{eff} is the channel length (δ) times a tortuosity term (χ)

$$\dot{n} = N_p \frac{\pi \bar{d}_p^4 P_m}{124 \eta \delta \chi RT_m} \Delta P \quad (2.6)$$

Expressing the number of pores of the membrane (N_p) in terms of the porosity (ϵ) and the surface (S_i) the expression above changes as follow.

$$\frac{\dot{n}}{S_i} = \dot{n}'' = \frac{\epsilon P_m \bar{d}_p^2}{\delta \chi 32 \eta RT_m} \Delta P \quad (2.7)$$

2.3.1.2 Free Molecular Streaming Flow – Knudsen Flow

For the Knudsen Flow the expression that defines the molar flux is the following, taking the same considerations of the viscous flow case (Ideal Gas, average conditions, cylindrical channels...).

$$\dot{n}'' = \frac{\epsilon}{\delta \chi} \frac{4}{3} \frac{\bar{d}_p}{\sqrt{2 \pi M W R T_m}} \Delta P \quad (2.8)$$

For Knudsen Flow the Molar Flux will be independent of average Pressure but is dependent from the molecular weight (MW) which can be advantageous in gas separation.

2.3.1.3 *Transitory Regimes*

When Transitory Regimes are consider, Slip Flow or Transition Flow, the collisions between the particles and the channel walls are in the same order of the collision between particles. As both phenomena take place at the same time, the models to describe the flow are of higher complexity.

Among the different models proposed, the most simple will be considered, as many uncertainties has been already introduced and the model will be used only to compare the experimental results. The models with adjustable parameters were excluded, only the ones resulted from the kinetic theory of gases were considered.

The first model propose a correction of the Hagen-Poiseuille equation, since at higher Knudsen numbers the velocity at the wall can't be considered any more to be zero. The slip correction term is:

$$\dot{n}''_{slip} = \frac{\varepsilon \pi}{\delta\chi} \frac{\pi}{4} \frac{\bar{d}_p}{\sqrt{2\pi MWRT_m}} \Delta P \quad (2.9)$$

That added to the Hagen-Poiseuille equation results on:

$$\dot{n}'' = \left(\frac{\varepsilon P_m \bar{d}_p^2}{\delta\chi 32\eta RT_m} + \frac{\varepsilon \pi}{\delta\chi} \frac{\pi}{4} \frac{\bar{d}_p}{\sqrt{2\pi MWRT_m}} \right) \Delta P \quad (2.10)$$

And the permeance is

$$\frac{\dot{n}''}{\Delta P} = \frac{\varepsilon P_m \bar{d}_p^2}{\delta\chi 32\eta RT_m} + \frac{\varepsilon \pi}{\delta\chi} \frac{\pi}{4} \frac{\bar{d}_p}{\sqrt{2\pi MWRT_m}} \quad (2.11)$$

As it can be see the slip flow term is not the same of the Knudsen Flow, as it could be expected to have a continuity with the free molecular streaming when the mean pressure is close to zero. In fact the smaller term of the slip correction, has been confirmed experimentally. The experimental data of permeance vs. mean pressure present a minimum at small values of mean pressure for cylindrical capillary

For a membrane where the pore diameter is not uniformed, so as the effective length, the assumption that, in transitory regime, the permeance can be accounted by the addition of the Viscous Flow term plus the Knudsen flow term, is adequate.

$$\frac{\dot{n}''}{\Delta P} = \frac{\varepsilon P_m \bar{d}_p^2}{\delta\chi 32\eta RT_m} + \frac{\varepsilon 4}{\delta\chi 3} \frac{\bar{d}_p}{\sqrt{2\pi MWRT_m}} \quad (2.12)$$

In any case, if the membrane characteristics are known as well as the fluid properties (viscosity). Both the equations (2.11) and (2.12) can be represented as a linear function where permeance is only function of the mean pressure.

$$\frac{\dot{n}''}{\Delta P} = AP_m + B \quad (2.13)$$

Scott and Dullien (1962) proposed an expression more accurate and more complex. They divided the molecules in two different groups. The molecules that have a high number of collisions with other molecules between two consecutive collision with the wall and the opposite case where the number of collision is low. The fraction of this two groups was quantified by probabilistic considerations.

The total flux is describe by the addition of this two components the first group is describe by the Poiseuille flux modified with the slip and the second group with the Knudsen flow. In the case $Kn \rightarrow 0$ the expression will take Poiseuille form and if $Kn \rightarrow \infty$ will take Knudsen form.

$$\begin{aligned} \frac{\dot{n}''}{\Delta P} = & \left[1 - e^{-\sinh^{-1}(1/Kn)} \right] \left(\frac{\varepsilon}{\delta\chi} \frac{\bar{d}_p^{-2}}{32\eta RT_m} + \frac{\varepsilon \pi}{\delta\chi} \frac{\bar{d}_p}{4\sqrt{2\pi MWRT_m}} \right) \\ & + e^{-\sinh^{-1}(1/Kn)} \frac{\varepsilon}{\delta\chi} \frac{4}{3} \frac{\bar{d}_p}{\sqrt{2\pi MWRT_m}} \end{aligned} \quad (2.14)$$

2.4 Contact angle.

The contact angle is the most diffuse and simplest method to describe the hydrophobic or hydrophilic behavior (wettability) of a material related with a specific liquid.

The contact angle is defined for an ideal surface (not perturbed by porosity, roughness, heterogeneity, etc.) as the angle formed by a liquid droplet on a smooth surface. The angle formed is greater than 90° if the affinity between the liquid and the solid is low, and is lower than 90° if the affinity is high. If the liquid in contact is water, we talk of hydrophobicity or hydrophilicity. (Drioli, Criscuoli and Curcio 2006)

The Young's equation expresses the thermodynamic equilibrium at the point C, where the three phases are in contact (liquid, solid and vapor).

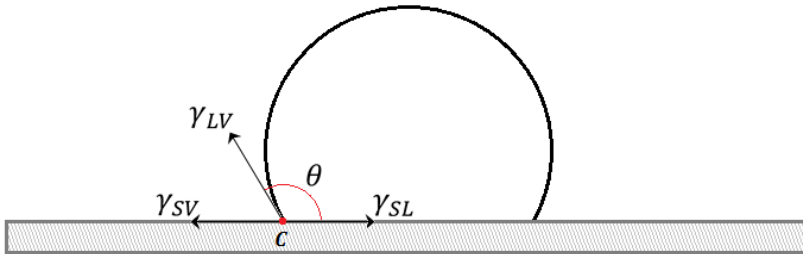


Figure 2.8 Thermodynamic equilibrium at the triple point for a system Vapor-Liquid-Solid

$$\gamma_{LV} \cos \theta = \gamma_{SV} - \gamma_{SL} \quad (2.15)$$

The expression above represents the equilibrium at point C, on it, γ_{LV} , γ_{SV} and γ_{SL} are the interfacial tensions for Liquid-Vapor, Vapor-Solid and the Solid-Liquid interfacial, respectively.

In Young's equation only two direct measurable quantities can be identify, the contact angle θ and the liquid-vapor surface tension γ_{LV} . The lack of mobility, made the solid interface very different from the liquid-fluid interface, and hence the interfacial tension involving a solid cannot be measured directly. To calculate the values of solid-vapor surface tension γ_{SV} and solid-liquid interfacial tension γ_{SL} , a second independent relation of these quantities should be found. From the previous statement it could be inferred that, whit the measurements of the contact angle on solid and γ_{LV} is not possible to calculate the solid surface tension γ_{SV} and the solid-liquid interfacial tension γ_{SL} .

To overcome the difficulties in the calculation of the solid surface tension γ_{SV} and the solid-liquid interfacial tension γ_{SL} many authors have proposed different methods in order to eliminate one of the unknown quantities.

One of the first approximations made uses of the concepts of work of adhesion and the combining rules. The work of adhesion is defined as the work required to cleave a bulk sample, creating two surfaces, isothermally and reversibly. In similar fashion, the cleaving of the interfacial contact between species 1 and 2 in a medium of species 3, requires energy to build a unit area of surface between species 1 and 3 as well as between species 2 and 3.

The mathematical formulation of the work of adhesion is due to (Dupré 1869). In the equation proposed, the work of adhesion is represented, by the surface tension of the two new surfaces ($\gamma_\alpha, \gamma_\beta$) minus the interfacial tension of the contact between α and β .

$$W_{adh} = \gamma_\alpha + \gamma_\beta - \gamma_{\alpha\beta} \quad (2.16)$$

The combining rules according with (Weber and Stanjek 2014), proposed by Rayleigh, are empirical relations used to relate Van der Waals interaction energies.

$$\sqrt{\gamma_{\alpha\beta}} \approx \sqrt{\gamma_\alpha} - \sqrt{\gamma_\beta} \quad (2.17)$$

Considering the work of adhesion (2.16) and the combining rules (2.17), Young's equation can be rewritten like follows.

$$\cos \theta \approx 2 \sqrt{\frac{\gamma_{SV}}{\gamma_{LV}}} - 1 \quad (2.18)$$

This first aproximation, using combining rules, didn't work properly with many systems. The combining rules overestimate the surface tensions as they can be applied to thermodynamic properties. Taking account of this fact (Girifalco and Good 1957) proposed a corrective factor Φ .

$$\Phi = \frac{W_{adh}}{\sqrt{W_{coh,\alpha}W_{coh,\beta}}} \quad (2.19)$$

In equation (2.19) $w_{coh,\alpha}$ is the work of cohesion $w_{coh,\alpha}=2\gamma_\alpha$ the equation (2.18) becomes as below and can be directly resolve as Φ is known.

$$\cos \theta = 2\Phi \sqrt{\frac{\gamma_{SV}}{\gamma_{LV}}} - 1 \quad (2.20)$$

Fowkes, (1964) approach to the problem involved two assumptions. The surface tension is the sum of the contributions of the dispersion forces γ^d (London-van der Waals) and the contributions of specific interactions (such as hydrogen bonds, γ^h) being γ^d prevalent in many systems, being the only one having sufficiently long range. The second assumption was that the dispersion force attraction between immiscible phases (α and β) could be predicted by $2(\gamma_1^d\gamma_2^d)^{1/2}$, the geometric mean base on Berthelo's principle, arriving to the conclusion.

$$\cos \theta = \frac{2}{\gamma_{LV}} \sqrt{\gamma_{SV}^d \gamma_{LV}^d} - 1 \quad (2.21)$$

Again fowkes assumes the treating of surface tension a mechanical quantity and not a thermodynamic one, independent of Temperature. Fowkes approach fail describing many systems indicating that non only dispersive forces should be counted.

Newmann et al. 1974, proposed an equation of state that could relate $\gamma_{SL}=f(\gamma_{SV}, \gamma_{LV})$. The main hypothesis was that a liquid will wet a solid (the contact angle is zero) when the interfacial tension between both is equal to zero ($\gamma_{SL}=0$), and so, the liquid surface tension is equal to solid surface tension ($\gamma_{SV}=\gamma_{LV}$). By the observation that contact angle of many liquid decrease as the liquid surface tension decrease they calculate the solid surface tension and formulate the next equation.

$$\gamma_{SL} = \frac{\gamma_{SV} + \gamma_{LV} - 2\sqrt{\gamma_{LV}\gamma_{SV}}}{1 - 0.015\sqrt{\gamma_{LV}\gamma_{SV}}} \quad (2.22)$$

That combined with Young's equation could calculate the Solid surface tension from liquid surface tension and contact angle.

$$\cos \theta = \frac{(0.015\gamma_{SV} - 2)\sqrt{\gamma_{LV}\gamma_{SV}} + \gamma_{LV}}{\gamma_{LV}(0.015\sqrt{\gamma_{LV}\gamma_{SV}} - 1)} \quad (2.23)$$

Subsequently they Li and Neumann (1990) proposed a reformulation of the equation of state realizing to the possibility of numerator, on previous EOS, to become zero for large values of the product $\gamma_{LV} \gamma_{SV}$

$$\cos \theta = -1 + 2 \sqrt{\frac{\gamma_{SV}}{\gamma_{LV}}} e^{-\beta(\gamma_{SV} - \gamma_{LV})^2} \quad (2.24)$$

Where β is a constant fit parameter independent of the solid and the liquid. By the fit of many different systems Kwok and Neumann (1999) deduce β to be equal to 0.0001247 (din/cm²).

Though the contact angle and the γ_{LV} are easily measurable, and has been proposed a valid equation of state where $\gamma_{SV}=f(\theta, \gamma_{LV})$. This equation is applicable only for surface, solid, smooth, homogeneous, rigid, chemically inert and insoluble to the liquid. The contact angle measurement at the previous conditions should give us the Young's contact angle (θ_Y), the ideal contact angle to be use in Li-Neumann's equation, as derived from Young's one.

2.4.1 Changes with drop size

After observed changes (55%) in contact angle when the drop volume was changed from 3.65 to 0.4 μ l. Mack. (1936) proposed that the contact angle is a function of the radius and volume of liquid drop. He developed an equation for evaluating the effect of gravitational force upon the form of the drop. Later on several authors will reject the hypothesis of the effect of gravity. (Vesselovsky and Pertzov 1936), proposed the line tension modification of Young's equation, to take account of the line tension: the excess free energy in the region of the triple interface.

$$\gamma_{LV} \cos \theta + \frac{\gamma_{SLV}}{r} = \gamma_{SV} - \gamma_{SL} \quad (2.25)$$

r is the drop radius and γ_{SLV} is the line tension. This equation is applicable for homogenous, rigid, flat, horizontal, and smooth solid surface, though the line tension values proposed to correct the Young equation were much larger than those that would be expected from intermolecular interactions.

Numerous authors ((Gaydos and Neumann 1987), (Jańczuk and Białopiotrowicz 1991), (Drelich and Miller 1992) (Drelich and Miller 1994)) used the line tension modification of Young's equation, for the interpretation of contact angles and its relation with the drop size; but it worked only for ideal three face systems with pure liquids and solid surfaces cleaned and prepared (For all the other systems it was rejected). On further experiments, however, the calculation of the line tension, calculated from experimental results, were closer to those predicted theoretically

Good and Koo. (1979), proposed that the surface heterogeneity could be the reason for the contact angle/drop size relation-ship observed, they suggest that the term γ_{SLV} in the expression should be consider as a pseudo-line tension for non-ideal systems and that it doesn't describe the excess free energy. The hypothesis was supported experimentally by Drelich & Miller (1994), confirming not only the Good and Koo hypothesis but also adding and evaluating the effect of the roughness on the contact angle/drop size relationship. Despite this confirmation they also observe that for the advancing and receding contact angle the effect are

neglected, confirmed experimental for advancing contact angle from 1mm to 7 mm. Drelich, (Drelich, Miller and Good 1996)

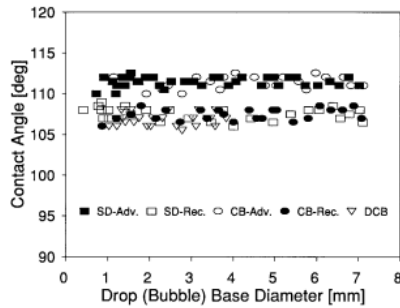


FIG. 2. The effect of drop (bubble) size on advancing (Adv.) and receding (Rec.) contact angles for the air/water/(dodecanethiol on gold) system as obtained with the static sessile-drop (SD), static captive-bubble (CB), and dynamic captive-bubble (DCB) techniques.

Figure 2.9 Effect of drop (bubble) size on advancing and receding contact angle for the air, water, Dodecanethiol on gold (Drelich, Miller and Good 1996)

2.4.2 Contact angle in porous materials

(Courel, et al. 2001), proposes an equation that corrects the effect of surface heterogeneity on contact. The equation relates the fractions of liquid-solid and liquid-air surface with the theoretical contact angle.

$$\cos \theta' = y \cos \theta - (1 - y) \quad (2.26)$$

Being y the fraction of membrane surface made of solid material. It's been proved by (Fraken, et al. 1987), that for polymers with surface porosity lower than 0.5. The surface porosity of the polymer that it's consider to be a relation of the porosity ε and the tortuosity τ being $y = \varepsilon/\tau$.

Also for porous materials Tröger et al, 1997, proposed a derived relation for the three-phase equilibrium minimum energy. Relation derived under the assumption that the angle formed by the drop on the surface is equal to the angle formed on each pore. The relation between the ideal angle and the observable angle is presented below.

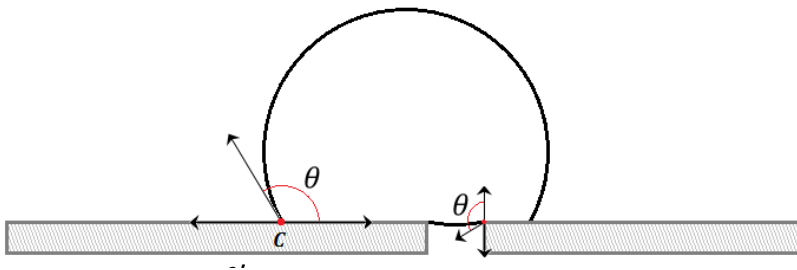


Figure 2.10 Hypothesis by Tröger et al, 1997. The contact angle formed by the drop on the surface is equal to the angle formed on each pore.

$$\gamma_{LV} \left(\cos \theta' - \frac{4\varepsilon \cos \theta' + 1}{1 - \varepsilon \cos \theta' - 1} \right) = \gamma_{SV} - \gamma_{SL} \quad (2.27)$$

$$\cos \theta' - \frac{4\varepsilon \cos \theta' + 1}{1 - \varepsilon \cos \theta' - 1} = \cos \theta \quad (2.28)$$

θ' stands for the angle observed on the porous surface rather than on an ideal one.

2.4.3 Hysteresis

If the interfacial tensions γ_{LV} , γ_{SV} and γ_{LS} are thermodynamics properties, it should be a single value of contact angle (the Young's one), however experimentally the equilibrium contact angle changes with many parameters (as seen before). Changes in the roughness, the drop size, the porosity or the tilt of the surface can change the absolute value of the equilibrium contact angle. The contact angle possesses a spectrum among two limits, the advancing contact angle (θ_a) and the receding contact angle (θ_r). The hysteresis (H) in the contact angle can be easily evidenced; if a small amount of liquid is added to a drop, an increase in the contact angle will be seen; similarly, when a small amount of liquid is removed from a drop, the contact angle will decrease. A drop placed on a surface has an equilibrium contact angle (θ) somewhere between θ_a and θ_r . The contact angle hysteresis is defined as $\theta_a - \theta_r = H$ and nearly all solid surfaces exhibit this (Tadmor 2004).

Apart from the surface tensions, also the three-phase contact line contributes to the total energy of the system. This is the reason for the existence of the hysteresis spectrum of contact angles. The energy line is the result of defects in the smoothness (either chemical or structural) of the solid surface. The value of the energy line has a local character being related with the local type and concentration of those imperfections, and so, having different values for the energy line at different regions of the line it is common if the concentration or type of imperfection is different in those regions.

The imperfections in the surface "fix" the contact line, this fixing effect is what develop the angle hysteresis. However, the same imperfection, might fix the line on a different way for the advancing direction or the receding one. For example on the way the surface supporting the drop is tilted, but not only. The deviation of the maximal advancing (θ_a) and minimal receding (θ_r) from the equilibrium Young angle might be different one to other. Nevertheless the interaction associated with the maximal advancing angle should equal the negative of the interaction associated with a minimal receding angle.

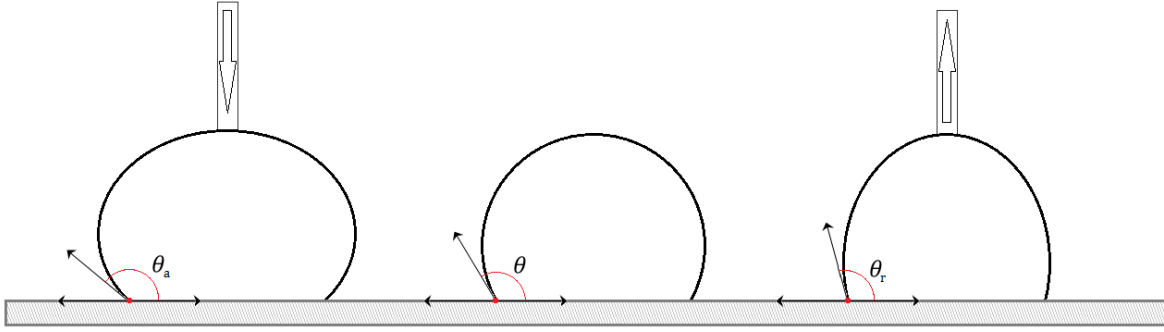


Figure 2.11 Representation of Advancing (liquid is added to the drop), equilibrium and Receding (liquid is removed from the drop)

Elimination or minimization of the H, should be required for accurate and reproducible wetting characterization of solid surface, this is usually accomplished by solid surface preparation (polishing and cleaning), handling and preserving. Even after the surface preparation, however, there will be hysteresis though is of a few degrees. The equilibrium contact angle θ can be calculated from θ_a and θ_r as was shown theoretically and verified with experimental data by Tadmor.

$$\theta = \cos^{-1} \left(\frac{r_A \cos \theta_A + r_R \cos \theta_R}{r_A r_R} \right) \quad (2.29)$$

$$r_A = \left(\frac{\sin^3 \theta_A}{2 - 3 \cos \theta_A + \cos^3 \theta_A} \right)^{1/3} \quad (2.30)$$

$$r_R = \left(\frac{\sin^3 \theta_R}{2 - 3 \cos \theta_R + \cos^3 \theta_R} \right)^{1/3} \quad (2.31)$$

On a surface that is rough or contaminated, there will also be contact angle hysteresis, but now the local equilibrium contact angle (the Young's equation is now only locally valid) may vary from place to place on the surface. The same expressions are valid in these cases.

2.4.4 Contact angle Temperature dependence

The effect on contact angle with temperature is not well understood and hasn't been studied deeply enough. It is reported to increase, decrease and remain constant with increasing temperature. Most part of publications have reported the contact angle to decrease linearly when temperature increases.

Table 2.2 Temperature dependence of contact angle reported on literature

<i>Solid surface</i>	<i>Liquid drop</i>	<i>Temperature range</i>	<i>Observation</i>	<i>Authors</i>
<i>fluoropolymer</i>	<i>hexadecane</i>	22 - 150	$\theta_A = cst$ $\theta_R = low\ decr$	(Johnson and Dettre 1965)
<i>siliconized glass</i>	<i>water</i>	4 - 75	$\theta_A = line\ decr$ $\theta_R = line\ decr$	(Phillips and Riddiford 1965)
<i>Oxyparaffinic hydrocarbon</i>	<i>water</i>	22 - 75	$\theta_A = line\ decr$ $\theta_R = line\ decr$	
<i>polyethylene</i>	<i>water</i>	0 - 100	<i>constant value</i>	(Schonhorn 1966)
	<i>Glycerol</i>	20 - 90	<i>constant value</i>	
<i>naphthalene</i>	<i>formamide</i>	0 - 75	<i>constant value</i>	(Jones and Adamson 1968)
	<i>water</i>			
<i>PTFE</i>	<i>n-alkanes (C10-C16)</i>	20 - 70	<i>linear decrease</i>	(Neumann, Haage and Renzow 1971)
<i>siliconized glass</i>	<i>alkanes</i>	20 - 70	<i>linear decrease</i>	(Neumann 1974)
	<i>water</i>	20 - 40	<i>linear decrease</i>	
<i>hexatrioctane</i>		20 - 60	<i>linear decrease</i>	
<i>Teflon</i>	<i>water</i>	25 - 100	<i>Decreases 6%</i>	(Yekta-Fard and Ponter 1988)
<i>SS 303</i>				
<i>gold</i>				
<i>copper</i>				
<i>Butyl Rubber and Dow Corning 236</i>	<i>glycerol</i>	23 - 120	$d\theta_A/dT=0.062$	(Budziak, Vargha-Butler and Neeumann 1991)
	<i>Ethylene Glycol</i>		$d\theta_A/dT=0.021$	
	<i>Diethylene Glycol</i>		$d\theta_A/dT=0.022$	

Almost all experimental results, for contact angle (equilibrium, advancing, receding, as-place etcetera) dependence with temperature have shown a temperature derivative of θ close to 0.1 deg K⁻¹ for many liquid-solid couples, in a moderate temperature range. The models proposed to approach the problematic of temperature dependence of contact angle (Li-Neumann's equation), have shown a lack of accuracy by not taking into account the entropic contributions to Surface/interphase tension that can arrive to be 30-50 % of Helmholtz free energy. (Weber and Stanjek 2014).

2.4.4.1 *Super-heated water*

Petke and Ray (1969) test the dependence of contact angles of different liquids with temperature. The contact angle was measured in the temperature range from 5 to 160 °C on the surface of five different polymers (polyethylene, polystyrene, polyacetate, polycarbonate, polyethylene terephthalate and "PTFE" Petke and ray, 1970). Stable advancing and receding

contact angle of water, glycerol, formamide, ethylene glycol, α -bromonaphalene and bromobenzene were measured in function of the temperature on a pressure cell saturate with the contact angle liquid. All the liquid - Solid couples contact angles follow a linear fashion trend in the considered temperature range (same results are observed by Jones & Adamson, 1968), all but water. After 100 - 120 °C the contact angle of water on all six polymers critically decreases. The results were supposed to be related with solubility or swelling of the polymeric matrix and dissolution or decomposition.

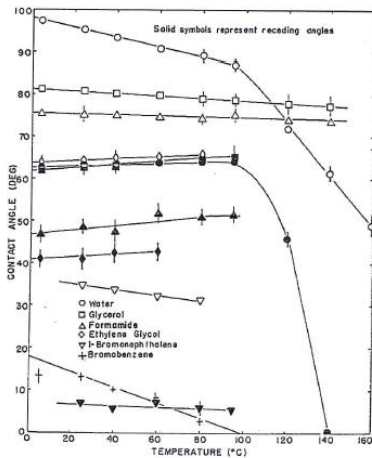


Fig. 2. Temperature dependence of contact angles of liquids on polyethylene.

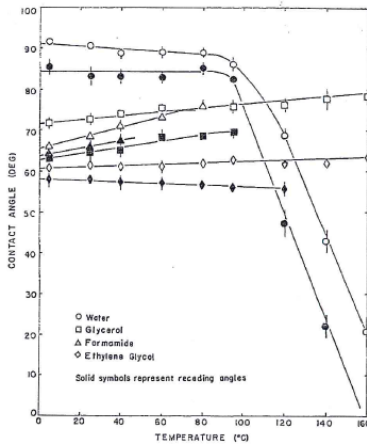


Fig. 3. Temperature dependence of contact angles of liquids on polystyrene.

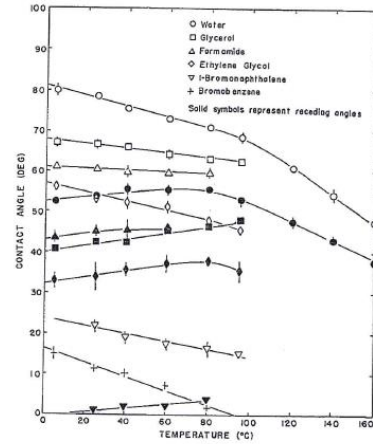


Fig. 4. Temperature dependence of contact angles of liquids on polyacetal.

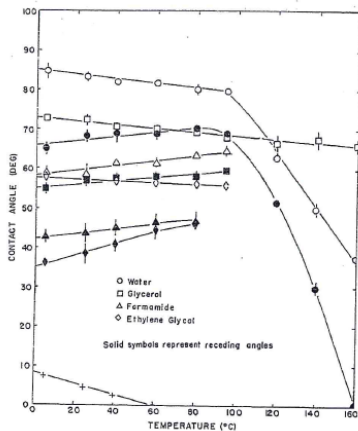


Fig. 5. Temperature dependence of contact angles of liquids on polycarbonate.

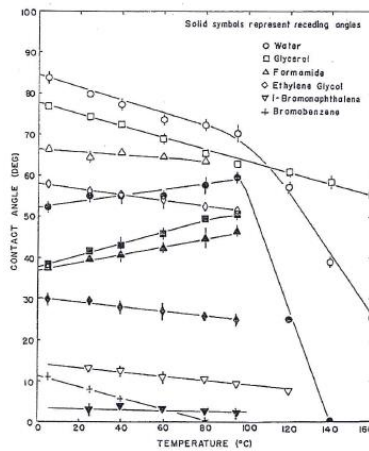


Fig. 6. Temperature dependence of contact angles of liquids on poly(ethylene terephthalate).

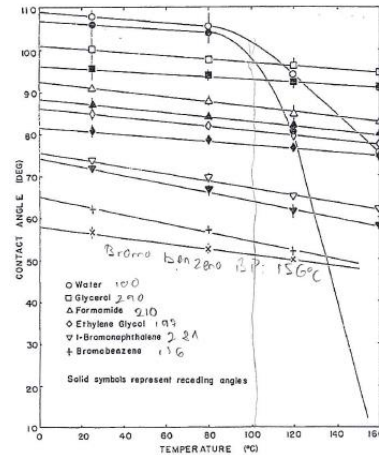


Fig. 7. Temperature dependence of contact angles of liquids on FEP fluoropolymer.

Figure 2.12 Advancing and receding contact angle of water on Polyethilene, Polystyrene, Polyacetal, Polycarbonate, Polyethylene terephthalate and Politetrafluoroetilene (Petke and Ray 1969)

(Bernardin, et al. 1997) performed measurements of contact angle on smooth aluminum surface on the range of temperature from 25 to 170 °C, the measurements were performed again on a pressure chamber at different fixed pressures (101.3 to 827.4 kPa), obtaining the same results observed by Petke et al, that is, Two distinct temperature-dependent regimes. A lower temperature regime bellow 120 °C, were the contact angle remains nearly constant with temperature (around 90 °) and high temperature regime (above 120 °C) where there is a drastic

decrease of the contact angle in a linear manner. At the temperature of 170 °C the contact angle was higher than zero (the pseudo-critical temperature was not reached).

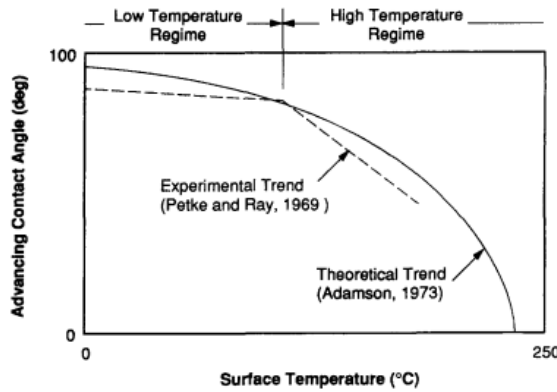


Figure 2.13 J. D. Bernardin, I. Mudawar, C. B. Walsh and E. I. Franses, Contact angle temperature dependence for water droplets on practical aluminum surfaces, *Int. J. Heat Mass Transfer*, 40 (1997), pp. 1017–1033

Later on Hayashi et al (2004) repeated the experiment on smooth stainless steel surface arriving to higher temperatures (300 °C, pressure of 15 MPa), they were looking for the pseudo-critical temperature where the contact angle was zero for the couple water- stainless steel 304. They observed that the contact angle stabilized at a constant value for values of temperature higher than 250 °C.

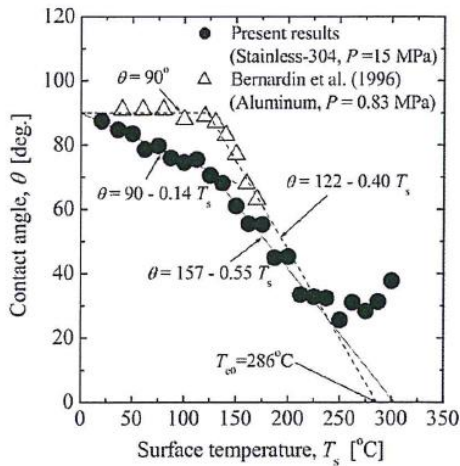


Figure 2.14 Hayashi, T., Hazuku, T., Takamasa, T., & Takamori, K. (2004). Contact angle of water droplets in a high-temperature, high-pressure environment. *Proceedings of the International Conference on Nuclear Engineering (ICONE12)*, 1, 797-800.

Fig. 4 Temperature dependence of the contact angle of water droplets

2.4.4.2 Contact angle Temperature dependence – Models

Adamson, 1973, derived a semi theoretical equation for the effect of temperature on contact angle of a liquid droplet base on molecule absorption theory on a solid surface. He predicted a theoretical trend where the contact angle has a slow decrease on a regime of low temperature and a critical decrease, arriving to zero, on a high temperature regime. To do this he used the Gibbs adsorption isotherm, thermodynamics, and a molecular interaction model to arrive at the following equation:

$$\cos \theta = 1 + C(T_{co} - T)^{a/(b-a)} \quad (2.32)$$

Where T_{co} is the pseudo-critical temperature, temperature where the contact angle goes to zero, C is an integration constant and, a and b are temperature-independent constants from a balance

Weber & Stanjek (2014) proposed an equation with the potentialities to predict the wettability of a system, for which the temperature dependence of contact angle is not known. Following the approach of (Lyklema 1999) to obtained, from the temperature dependency of surface and interfacial tensions, the surface excess energy and entropy per unit area.

From the general definition of surface tension:

$$\gamma = F_a^\sigma - \sum_i \Gamma_i \mu_i \quad (2.33)$$

Where μ_i the chemical potential of component i , Γ_i the surface concentration of component i and F_a^σ the excess Helmholtz free energy taken per unit of interface area. Considering only one component liquid, for which only one surface excess remains, which in the Gibbs convention is set zero ($\Gamma_1 = 0$), the surface tension becomes:

$$\gamma = F_a^\sigma = U_a^\sigma - TS_a^\sigma \quad (2.34)$$

U_a^σ is the excess energy and S_a^σ is the excess entropy. If the surface tension is known as a function of the temperature, the excess energy and the excess entropy can be found by differentiation of the expression above with respect to the Temperature for constant Pressure (the effect of pressure on interface tension with liquid is small) (Lyklema 1999).

$$S_a^\sigma = - \left(\frac{\partial \gamma}{\partial T} \right)_p \quad (2.35)$$

$$U_a^\sigma = \gamma - T \left(\frac{\partial \gamma}{\partial T} \right)_p \quad (2.36)$$

The Gibbs convention implies that F_a^σ , U_a^σ and S_a^σ are referred to the Gibbs dividing plane (GDP) the location of which is defined by setting $\Gamma \equiv 0$. Hence, U_a^σ and S_a^σ are sensitive to this choice. However, as $F_a^\sigma = \gamma$ and the latter is a measurable quantity F_a^σ must be invariant to the choice of the GDP.

As Dupré (1869) formulated, the work of adhesion W_{adh} is the work to be done to tear apart two phases in contact isothermally and reversibly. This is related with the interfacial tension of the contact phases.

$$W_{adh} = \gamma_{LV} + \gamma_{SV} - \gamma_{LS} \quad (2.37)$$

If all the surface tension are linearly dependent whit temperature this would meant that S_a^σ and U_a^σ will be constant and so the Dupré expression can be written in terms of excess energy and entropy.

$$\Delta_{adh}U_a^\sigma = U_{a,LV}^\sigma + U_{a,SV}^\sigma - U_{a,LS}^\sigma \quad (2.38)$$

$$\Delta_{adh}S_a^\sigma = S_{a,LV}^\sigma + S_{a,SV}^\sigma - S_{a,LS}^\sigma \quad (2.39)$$

$$W_{adh} = \gamma_{LV} + \gamma_{SV} - \gamma_{LS} = \Delta_{adh}U_a^\sigma - T\Delta_{adh}S_a^\sigma \quad (2.40)$$

This take us to the equation propose by Weber & Stanjek (2014) who convined Dupre expressions, in terms of Excess energy and Excess Entropy of adhesion, whit Young's equation arrive to the expression that relates the contact angle directly whit Temperature.

$$\cos \theta = -1 + \frac{\Delta_{adh}U_a^\sigma}{\gamma_{LV}} - \frac{T\Delta_{adh}S_a^\sigma}{\gamma_{LV}} \quad (2.41)$$

The equation above has been tested for several systems (Two components three phases) reported in literature. From the data contact angle and liquid surface tension Excess energy and Excess Entropy of adhesion has been caolculated as fallow.

The work of adhesion is calculated directly by the contact angle, surface tension data in function of temperature.

$$W_{adh}(T) = \gamma_{LV}(T) * (1 + \cos \theta(T)) \quad (2.42)$$

The excess entropy and excess energy of adhesion are calculated from the derivative of the work of adhesion with T.

$$\Delta_{adh}S_a^\sigma = -\left(\frac{\partial W_{adh}}{\partial T}\right)_P \quad (2.43)$$

$$\Delta_{adh}U_a^\sigma = W_{adh} - \left(\frac{\partial W_{adh}}{\partial T}\right)_P \quad (2.44)$$

From the different systems studied are of particular interest the three different contact angle studies of N-alkanes over water (Zepierrri et al. (2001); Motomura et al (1983); Haydon (1965)). For all the system studied similar values of Excess entropy of adhesion and Excess energy of water were obtain. Liquid - Solid systems $\theta(T)$ were also studied. The main conclusion is that there is not direct trend for the data of $\Delta_{adh}S_a^\sigma$ vs $\Delta_{adh}U_a^\sigma$ with values for excess entropy of adhesion in the range of 0.03 to 0.2 mJ/m²K and values of excess energy of adhesion between 60 and 160 mJ/m².

To test the ability of the equation to predict wettability (contact angle) of systems in function of Temperature. Due to, the lack of extensive data of contact angles in function of temperature; data of several liquids (different γ_{LV} but similar $\Delta_{adh}S_a^\sigma$ and $\Delta_{adh}U_a^\sigma$) over the same surface FC-7222-coated mica (Kwok and Neumann 1999) were plot and compared with the results of the Weber's equation with the use of average $\Delta_{adh}S_a^\sigma$ and $\Delta_{adh}U_a^\sigma$. The results capture the trend of the data.

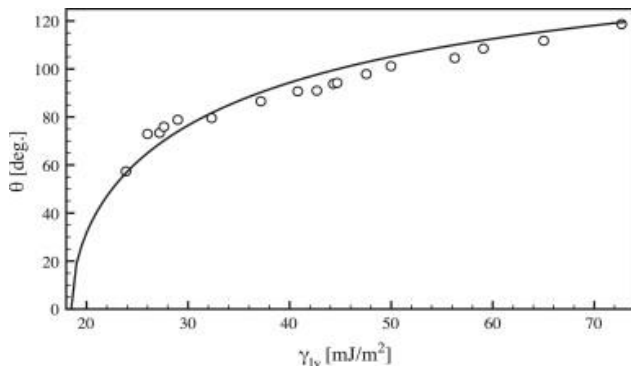


Figure 2.15 Contact angles on FC-722-coated mica at 20 °C reported by Kwok & Neumann, 1999 compared with the equation proposed by Weber and Stanjek (2014)

Berim and Ruckenstein (2011) arrived to a similar conclusion using the Density Functional Theory (DFT). They performed a theoretical study of the liquid nano-drops (extendible to macro-drops) on solid surfaces. The main conclusion was that contact angle is linearly dependent of the fluid solid energy parameter, a measurement of the solid liquid interaction, related with the Lennard-Jones Potentials (if this type of interactions can be assumed).

They proposed an expression that relates the change of contact angle with temperature $\frac{d\theta}{dT}$ only to the energy interaction. This expression made possible that the absolute value of $\frac{d\theta}{dT}$ increases with increasing Temperature or even remains constant.

Nevertheless the analysis performed had a great number of assumptions behind and is difficult to extrapolate the results to a macro level, and higher temperature conditions.

2.4.5 *Measuring methods.*

The most common way of measuring the contact angle is with a goniometer, which makes a visual measure of the contact angle. With a syringe pointed vertically a droplet is deposited on the sample surface, and a high resolution camera captures the image. Then the image is analyzed either by eye (with a protractor) or using image analysis software.

2.4.5.1 *The static sessile drop method*

In the static sessile drop method described by (Neumann and Good 1979) the contact angle is measured in its static form. Once the droplet is deposited gently on the sample the image is analyzed after the equilibrium has been reached. Older systems used a microscope optical

system with a back light. Current-generation systems employ high resolution cameras and software to capture and analyze the contact angle.

2.4.5.2 *The dynamic sessile drop method*

In the dynamic sessile drop method requires the drop to be modified. A common type of dynamic sessile drop study determines the largest contact angle possible without increasing its solid/liquid interfacial area by adding volume dynamically. This maximum angle is the advancing angle. Volume is removed to produce the smallest possible angle, the receding angle. The difference between the advancing and receding angle is the contact angle hysteresis.

2.4.5.3 *The capillary rise at a vertical plate.*

This method proposed by Neumann (1974) measured the contact angle indirectly. A plate is partially submerged on the testing liquid and is measured the capillary rise or depression of the liquid and the plate. The contact angle is calculated by the level (h) of the liquid level and the capillary wetting of the solid. If the density difference between liquid and gas is known as the gravitational force and the surface tension.

$$\sin \theta = 1 - \frac{\Delta \rho g h^2}{2 \gamma_{LV}} \quad (2.45)$$

2.4.5.4 *Wilhelmy method*

The Wilhelmy method is a dynamic measure of the contact angle (Koonaphapdeelert and Li 2007). For this method, a flat solid plate is submerged, dynamically, on the liquid of interest, which applies a buoyancy force and the force due to the surface tension. Instruments connect to the solid measure the total force applied to submerge a certain length of the solid into the liquid. Advancing and receding contact angle can be measure immersing or emerging the plate through the equation bellow.

$$\cos \theta = \frac{F - B}{L \gamma_{LV}} \quad (2.46)$$

F is the measured total force, B is the buoyancy force, L is the length of the submerged plate and liquid surface tension is calculated. This method is widely used to test the dynamic contact angles of samples in different shapes other than flat sheet with greater accuracy of the measurement. However, it requires a sophisticate apparatus and samples with homogenous surface.

2.4.5.5 *High temperature contact angle measurements*

Petke and Ray (1969) performed contact angle measurements at high temperature by the *dynamic sessile drop method*. A pressure cell (Figure 2.16), pressure range from void to 25 atm,

is filled with the contact angle liquid, allowing saturation of air. The cell is heated externally with resistance wire and is insulated. Drops of 2 – 3 mm diameter are formed withdrawing the liquid with a syringe driven by a screw and advancing contact angles were accomplished lowering the capillary tip to the polymer. Separate drops (5 to 10) readings were taken after 5 min allowing stable angles and average and standard deviation were calculated. Receding contact angles were measured after the advancing ones, removing some of the liquid until the drop periphery receded back across the surface.

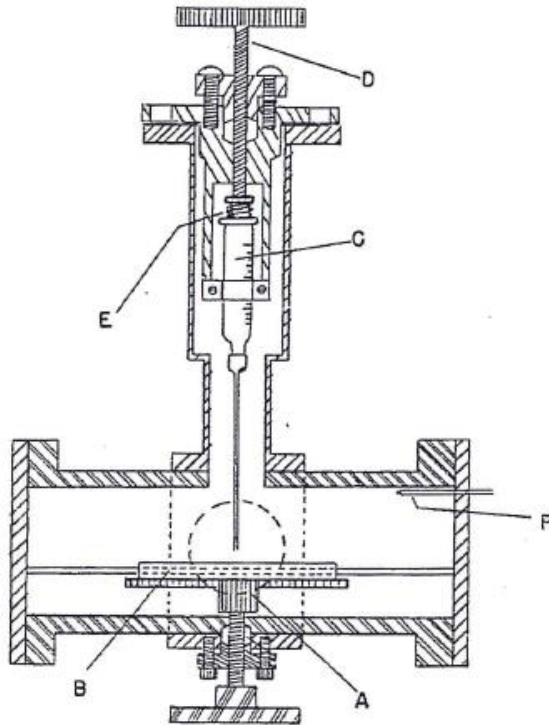


Figure 2.16 Experimental Pressure Cell for contact angle measurements at high temperature. (Petke and Ray 1969)

Bernardin (1996) use the above apparatus to perform measurements of dynamic advancing, quasi static and dynamic receding contact angle of water drops on Smooth aluminum surface.

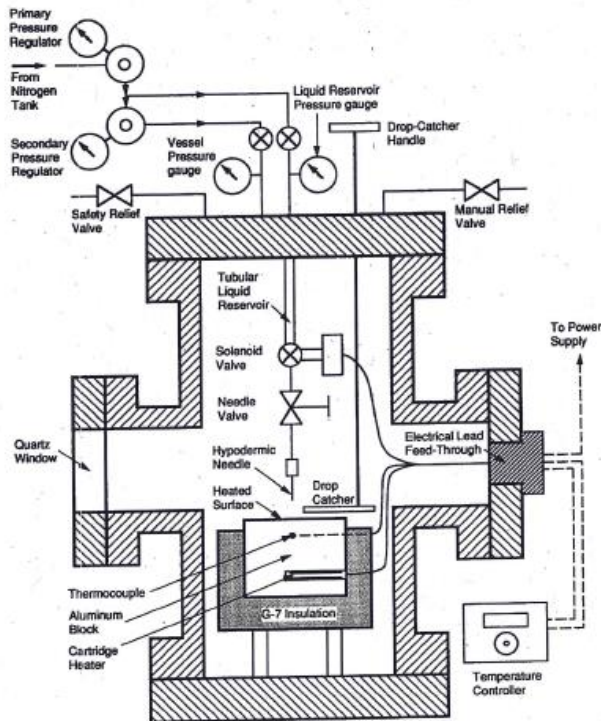


Figure 2.17 Pressure Cell use to performed measurements of dynamic advancing, quasi static and dynamic receding contact angle at high temperature. (Bernardin, et al. 1997)

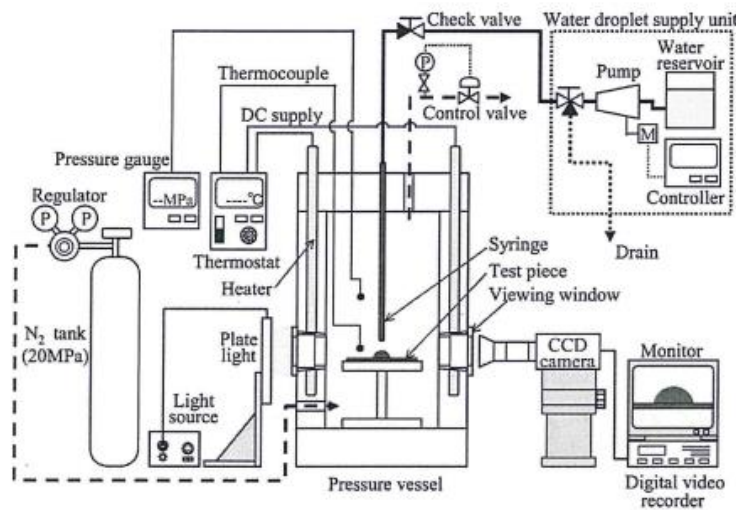


Figure 2.18 High Temperature High Pressure apparatus (Hayashi, et al. 2004)

Hayashi et al, 2004, performed a similar experiment at high temperature an pressure, with the aparattus show in Figure 2.18. *The static sessile drop method* over SS 304 was recorded. The withdrwal method was changed and a controled pump with check valve was used to provide the drop 5 mm avobe the plate.

2.5 The liquid breakthrough pressure (liquid entry pressure)

In membrane contactors process, the non-wettability condition should always be constant, in order to have the phases separated by the membrane, and have an efficient operation. The non-wetting fluid should not pass through the pores, partially or completely, to avoid bubbling, flooding, fouling and its consequences, phase mixing, reduction of mass transport, heat losses, etc. Membranes with low affinity to the feed fluid and differences in pressure between the two phases are used to keep the non-wettability condition.

In the case of water, the use of hydrophobic membranes should avoid water to penetrate through the pores of the membranes, if pressure is kept below a critical pressure value. This value of pressure is known as breakthrough pressure or liquid entry pressure (LEP).

The LEP is defined as the limit pressure, or difference in pressure between the two phases in contact, before the membrane starts getting wet. Traditionally has been described by the Laplace-Young equation, derived from the capillary model. The equation relates the pore size and the three-phase equilibrium (the affinity of the membrane to phases in contact). This simple equation, tries to calculate the value of pressure across the membrane, when the largest of its pores starts to be flooded.

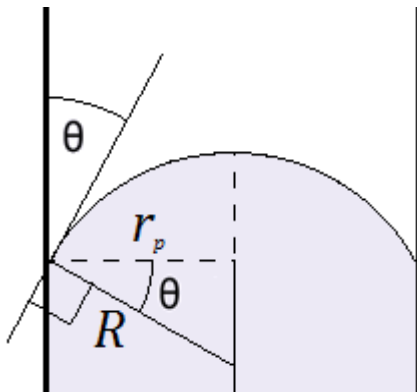


Figure 2.19 Spherical meniscus inside a capillary of radius r_p

$$\Delta P_{min} = \frac{-2\gamma_{LV} \cos \theta}{r_{p,max}} \quad (2.47)$$

Where γ_{LV} is the liquid surface tension, θ is the angle formed between the liquid and the solid membrane and $r_{p,max}$ is the radius of the biggest pore in the membrane. The same expression is equivalent for each pore on the membrane, and correlates the pore radius with the pressure at which it is flooded.

However, the capillarity model, does not take into account deviations from the ideality; this assume the pore to be perfectly cylindrical with smooth pore wall and the contact angle to be a

unique value (exempt from the hysteresis effect), calculated from the equilibrium of the interphase tensions. Franken et al. (1987), introduced a geometry coefficient (B) in order to take into account the irregularities of the pores, as the Laplace-Young equation describe systems with cylindrical pores and small enough that the surface curvature radius can be assumed to be constant. The geometric coefficient B is equal to 1 for cylindrical pores and between 0-1 for non-cylindrical pores. On literature can be found values of B for different type of membranes and stretched membranes (e.g. PTFE): a common value for B is 0.4 – 0.46 (Saffarini 2013). The B value has been calculated from the deviation of the experimental value from Laplace-Young equation.

$$\Delta P_{min} = \frac{2B\gamma_{LV} \cos \theta}{r_{p,max}} \quad (2.48)$$

Using Franken's models the calculated LEP, for membranes without circular pores, will always have a lower LEP than one with the same LEP maximum pore radius but with circular pores.

The model proposed by Franken takes into account only the deviation of pore shape from a circle, and so only the radial deviation from a cylinder and does not consider the tortuosity of most membranes pores in nature like deviations from the axial coordinate. Zha et al. 1992, proposed an expression to take account of non-cylindrical pores on the radial and the axial coordinate.

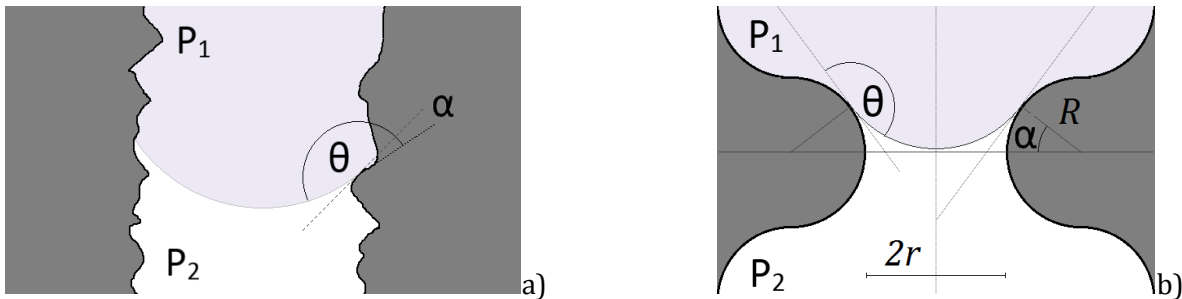


Figure 2.20 a) Irregular pore structure and angle between a pore wall element and the normal to the membrane surface in the axial direction b) Neck structure in a membrane pore. Modified from (Zha, et al. 1992)

On Zha's model the pore is describe by two main parameters: the hydraulic radius ($r_h = 2A / \text{wetted perimeter}$) that describe the deviation from a circle and the "Structure Angle" (α) that is the angle between the pore wall element and the ordinate vertical axis. As α change along the pore, the average value of α was considered for calculations Figure 2.20.

Zha and colleges describe smallest restriction of the pore as a "neck" of radius r and connected by an arc of radius R Figure 2.20 b). Along this restriction the structure angle change from a maximum (α_i) to ($-\alpha_i$). The hydraulic radius can be calculated at any section of the restriction with the expression below.

$$r_h = r + R(1 - \cos \alpha) \quad (2.49)$$

With the expression for the hydraulic radius we can obtain the expression for the calculation of the LEP.

$$\Delta P = -\frac{2\gamma_{LV}}{r} \frac{\cos(\theta - \alpha)}{1 + \frac{R}{r}(1 - \cos \alpha)} = -\frac{2\gamma_{LV}}{r} \cos \theta_{eff} \quad (2.50)$$

R and r are characteristics of a certain type of membrane; their values could be obtained from electron micro graph or by nonlinear regression of the experimental results. (Guillen-Burrieza, et al. 2015) Mathematically the LEP is the maximum value of the expression above. The derivation of the function with respect to α , equated to zero give us the expression to calculate α with the values of R/r (the expression below). The model equation take us to the conclusion that θ_{eff} can't take values below 90° without checking flooding of the membrane. Even though the model allows spontaneous wetting (LEP ≈ 0) when the contact angle θ is below 90° when r/R is very small. Spontaneous wetting can be verified experimentally.

$$\sin(\theta - \alpha) = \frac{\sin \theta}{1+r/R} \quad (2.51)$$

The LEP is a function of the surface tension of the solid-liquid interphase (γ_{SL}) as $\gamma_{LV} \cos \theta = \gamma_{SV} - \gamma_{SL}$. Variations on the composition of the liquid, that can change γ_{SL} , change drastically the LEP. Detergents, surfactants or solvents with the same behavior as alcohols (polar liquids that affect the polarity difference between the liquid and the membrane) are components that can influence the value of γ_{SL} . Garcia-Payo et al. 2000, studied the dependence of LEP to the process parameters: Membrane type, pore size, temperature, alcohol type and concentrations observing a strong dependence for each of the studied parameters. Even though the LEP change differently for each of this parameters, they all converge to a single value of vapor-liquid surface tension γ_{LV} , for a certain membrane, when LEP is equal to zero. The value of surface tension when the membrane spontaneously wets (LEP ≈ 0) was called wetting surface tension γ_{LV}^w and the expression deduced that relates the change in LEP with the surface tension is described below.

$$\Delta P_{min} = \frac{2}{r_{p,max}} (\gamma_{LV} - \gamma_{LV}^w) \quad (2.52)$$

The deduction of this expression assumes the dispersion component of the surface tension to be constant, which is not true for polar liquids, so this expression is valid for certain alcohol concentrations.

2.5.1 *Dependence with Temperature.*

The relation of the breakthrough pressure (and hydrophobicity in general) with the operative temperature hasn't been widely discussed, though these have a close relation. Changes on all the parameters in the three phase equilibrium $\gamma_{LV} \cos \theta = \gamma_{SV} - \gamma_{SL}$ are directly related with changes on the temperature system.

Some studies have evaluate the performance of membrane contactors at elevate Temperature (Singh and Sirkar 2014). However the Liquid Entry Pressure has never been evaluated at the process conditions. Membrane contactors test have been performed at low transmembrane pressures close to zero.

The effect of temperature on pore wetting has been studied for membranes of PTFE (Saffarini et al 2013). Arriving to a temperatures of 70 °C. LEP values changes between 20-30 % for test performed at 25 °C and 70 °C. The same study measure enlargements of 4-8 % in the mean pore size and decreasing of 4 % of the contact angle. In the same range of temperature (25 – 70 °C) the water surface tension decrease a 12%.

2.5.2 *Measuring methods*

2.5.2.1 *Franken Method*

As defined by the Laplace-Young equation, the liquid entry pressure (LEP) value is that when a non-wetting liquid has flooded the biggest of the pores in a porous membrane matrix and so, at the same pressure, flow can be verified across the pore. Experimentally Franken and colleagues (1987) gave the first guidelines to measure the LEP, proposing the LEP value to be the value of pressure when the first liquid drop can be verified in the permeate side of the membrane (Figure 2.21). The same procedure have been reproduced by several authors (Khayet et al, 2002; Garcia-Payo et al, 2010; Saffarini et al, 2014; Hereijgers et al, 2015). For the measurement of LEP, the membrane is carefully installed on a support, allowing the contact with a non-wetting liquid on one side and with a gas (usually air) on the other side. The pressure of the non-wetting liquid is raised gradually and when the first drop passes across the membrane (permeate side), the value of pressure of the feed side is registered as the LEP. The moment when the liquid-drop comes out on the permeate side, is verified by visual inspection, and so, the accuracy of the measurement depends on the operator criteria (as usually is) of what he considers a liquid drop.

This is a simple method to evaluate the capacity of a membrane to hold a pressurized liquid. Its effectiveness is confirmed by several authors and is still used (with minor variations) giving good reproducibility of the data, even by different authors. Some publications, aware that the main limitation of the method is the dependence from the operator criteria, performed repetitions of the same experiment, calculating a dispersion in the results of around 10 % (Saffarini, et al. 2013).

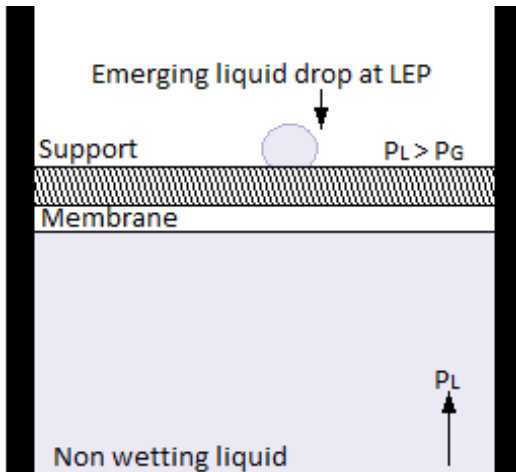


Figure 2.21 Scheme of Liquid Entry Pressure measurements base on the description of Franken's experiments. Modified figure from (Saffarini, et al. 2013)

Another problem of the method previously described is that assumes the membrane pore distribution is very homogeneous. This assumption makes possible that some measurements of LEP involving defects (very low quantity of pores with larger pore size than the standard) get to be representative of the wettability of the membrane material. The main consequence of this is the widening of the experimental distribution of the results and the LEP data.

2.5.2.2 Liquid Permeation Technique

McGuire et al, 1994 developed a procedure to evaluate the pore size distribution of micro-ultrafiltration membranes with a non-wetting liquid. On the liquid permeation technique, the transmembrane flux of a low affinity liquid (usually water, when testing hydrophobic membranes), is measured in function of the applied transmembrane pressure at room temperature (cst). At increasing pressure, smaller pores get flooded, increasing permeability. When all the pores get flooded, the flux becomes proportional to the transmembrane pressure following Darcy's law ($J_v/\Delta P = cst$). Reducing the apply pressure does not restore the hydrophobicity and the flux will continue to be proportional to the transmembrane pressure, as shown in the figure bellow.

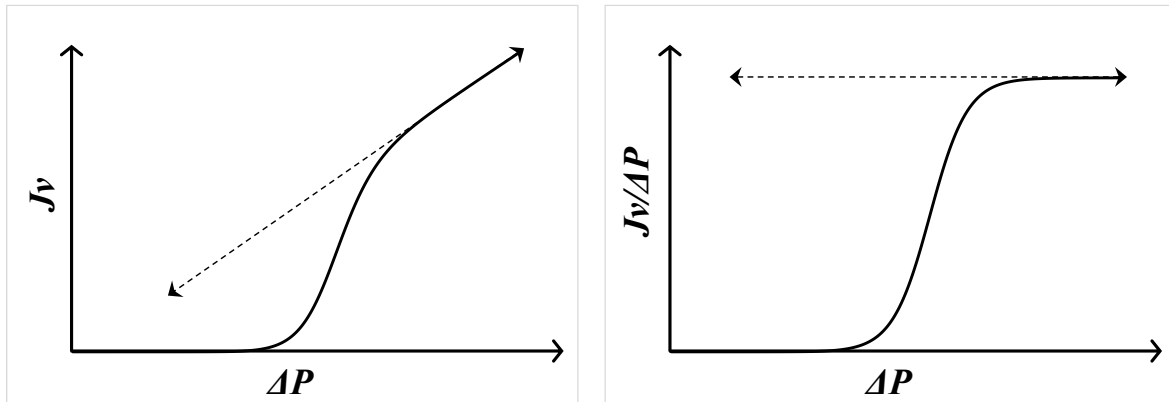


Figure 2.22 Presentation of the flooding curve; where Flux is presented in function of transmembrane Pressure; the dotted line shows flux of a complete flooded membrane following Darcy's Law

The main concept for the measurement, is putting in contact both sides of the membrane with the low affinity liquid (generally water to test the hydrophobicity of the membrane) inside a membrane holder. On the membrane holder a pressure gradient can be created between both sides of the membrane. The pores of the membrane are initially full of gas; at zero differential pressure the liquid doesn't wet the membrane because of the low affinity with it.

Increasing the liquid pressure, on the feed side of the membrane, creates a differential pressure across it. If the pressure is slowly raised up, at some point, the liquid will start flowing across the membrane (considering the force balance on a capillary pore (2.47)). The liquid entry pressure is defined as the pressure when "the biggest" of the pores in the membrane gets flooded. If the transmembrane pressure is held, constant liquid flux can be verified (before the flux should be equal to zero). As the pressure on the feed subsequently increases, smaller pores will be flooded. When all the pores in the membrane are flooded the flux will be proportional to the differential pressure, accordingly with Darcy's law. On Figure 2.22 it can be observed an example of the flux vs. differential pressure: Initial zero flux is measured, after LEP, the flux will follow the pore size distribution increasing while further pores get flooded until the flux follows Darcy's law. From the elaboration of the data is possible to measure not only the liquid entry pressure but, if data is treated is possible to obtain the pore size distribution as proposed by (McGuire, Lawson and Lloyd 1995) and (García-Payo, Izquierdo-Gil and Fernández-Pineda 2000)

2.5.2.2.1 Pore size distribution determination from liquid permeation technique

If the membrane is sufficiently large, the pore size distribution could be considered continuous. If so, it can be represented by a continuous distribution function $f(r)$ (Figure 2.23) and the number of pores between r and $r + dr$ is obtained by integrating the function $f(r)$. If the Laplace-Young equation is elaborated and considered for all the pores of the membrane (2.54) the flooded pore radius will be a function of pressure across the membrane, for a given pore distribution it is possible to evaluate the number of flooded pores at a given pressure.

$$N_{p,tot} \int_{r(\Delta P)}^{r_{max}} f(x) dx = N_p \quad (2.53)$$

N_{tot} is the total number of pores, $r(\Delta P)$ is the smallest flooded pore and r_{max} is the radius of the largest membrane pore.

$$r_p(\Delta P) = \frac{-2\gamma_{LV} \cos \theta}{\Delta P} = \frac{C_1}{\Delta P} \quad (2.54)$$

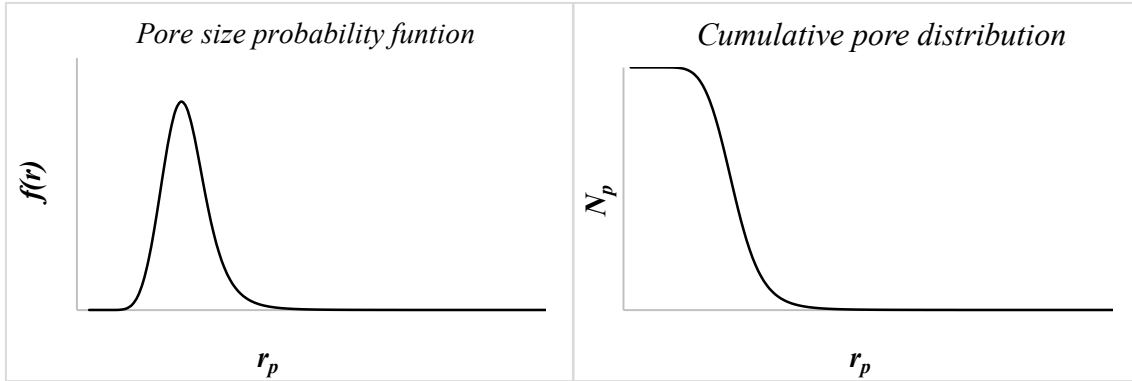


Figure 2.23 Pore size distribution and cumulative pore distribution

In order to obtain the pore size distribution from a flooding curve an assumption has to be made about the geometry of the pores. The pores of the membrane are assumed to be cylindrical with a tortuosity χ . In a cylindrical pore the laminar flow will be given by the Hagen-Poiseuille Equation.

$$Q_p = \frac{\Delta P \pi r_p^4}{8\eta \delta \chi} \quad (2.55)$$

The expression above is the flow on a cylindrical pore in function of the pressure drop, δ is the thickness of the membrane, χ is the tortuosity of the pore, η is the viscosity of the fluid and r_p is the pore diameter.

If we consider a homogenous thickness over the whole membrane and that the flow through each pore is independent from the others. The total flow through the membrane at a given $\Delta P > LEP_{min}$ is given by.

$$Q = \frac{N_{tot} \pi \Delta P}{8\eta \delta \chi} \int_{r(\Delta P)}^{r_{max}} x^4 f(x) dx = C_2 \Delta P \int_{r(\Delta P)}^{r_{max}} x^4 f(x) dx \quad (2.56)$$

Deriving Q in terms of ΔP and with the proper rearrangements and substitutions the pore size distribution could be expressed in terms of Q and ΔP .

$$f(x) = \left(\frac{dQ}{d(\Delta P)} - \frac{Q}{\Delta P} \right) \frac{\Delta P^5}{C_1^5 C_2} \quad (2.57)$$

C_1 and C_2 are constants that take into account information about the structural properties of the membrane, the fluid properties and the fluid - membrane interactions. (McGuire et al, 1995), (Piątkiewicz et al, 1999).

The flooding curve is usually “S shaped”, related to the pore size distribution. For this method McGuire proposed the smoothing spline line the only function for fitting the flow-pressure data to be used on the equation describing the pore size probability function. Though the spline derivate could present discontinuities. Garcia-Payo et al (2000) proposed an empirical equation to fit the data for the curve of flux vs pressure drop. The empirical equation is related with three parameters b , Lp_{max} , and ΔP_0 ; ΔP_0 corresponds to the pressure difference when $\frac{Q}{\Delta P} = \frac{Lp}{2}$, Lp is the liquid permeability when the membrane is completely flooded and b is a fitting parameter related with the dispersion in the pore size distribution.

The fitting function could be evaluated on the expression above obtaining the pore size distribution function.

$$\frac{Q}{\Delta P} = \frac{Lp_{max}}{e^{-b(\Delta P - \Delta P_0)} + 1} \quad (2.58)$$

$$\frac{dQ}{d(\Delta P)} = \frac{Lp_{max}}{e^{-b(\Delta P - \Delta P_0)} + 1} + \frac{Lp_{max} b \Delta P e^{-b(\Delta P - \Delta P_0)}}{e^{-b(\Delta P - \Delta P_0)} + 1} \quad (2.59)$$

The main disadvantage reported for this method is the loss in the resolution of the pore size distribution as the pore sizes decrease to values much below the largest pore size. On equation (2.55) it can be appreciated that flow is proportional to the fourth power of the radius and so at higher pressure values the high flow across the larger pores masks the small flowrate through the newly flooded pores. Nevertheless the method present also advantages respect other methods to measure the pore size distribution, as mercury porosimetry or images analysis of scanning electron microscopy (SEM). The liquid permeation technique measure only the pores that connect both sides of the membrane (pores where the flux can come on) while mercury porosimetry measure the complete porosity of the membrane (even the close pores). (Calvo, et al. 2008)

Regarding the disadvantage reported on the previous paragraph, (Lee, et al. 1997) proposed a modification in the method. They performed, as in the original method, the increase in the feed pressure to flood smaller pores. Then, after each pressure raise the feed pressure was set at a lower value (constant for each point) to perform the flux measurements.

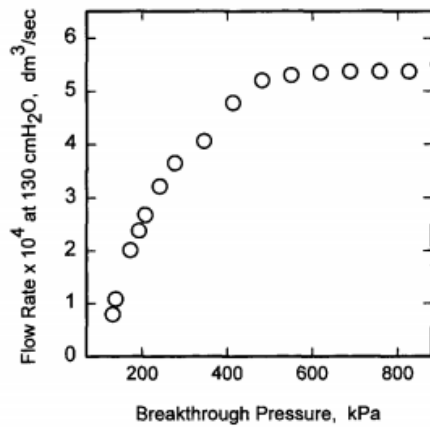


Fig. 3. Typical liquid flow rates measured at standard pressure of 130 mm H₂O through pores penetrated at breakthrough pressure with permeating liquid.

Figure 2.24 Flux vs. Breakthrough Pressure measure at constant transmembrane pressure (Lee, et al. 1997)

3 *Experimental characterization of MC for high temperature applications*

3.1 *Materials and methods*

As seen on the previous section very few authors have been interested in the measurement of the hydrophobic character of membrane contactors at high temperatures, especially at temperatures above the bubble point.

Some measurement of water contact angle over different surfaces, including polymeric and metallic surfaces, have left the doubt, that water contact angle at higher temperatures change the linear trend, many times reported, in function of Temperature. The results of this experiments have shown that a certain value of temperature, water contact angle decrease rapidly, approaching to zero at values of temperature well below the critical temperature.

The measurements of contact angle might be the most representative parameter of the hydrophobic character. However the wide hysteresis phenomena, present in pretty much all samples, the difficulties of measure it on samples of different shapes than flat surfaces and the very sophisticated apparatus to perform measurements at temperature above the boiling point made of the contact angle hard to measure and a parameter with many uncertainties. On the other hand the liquid entry pressure is a parameter that can adequately evaluate the hydrophobic character of a membrane, and even more, is a direct parameter of the membrane contactors operation.

On the study of the state of the art of characterization method for membrane contactors at high temperature, it was evident the lack of a suitable method to evaluate on a simple and economic way the hydrophobic character. Especially there are no reference for the measurement of liquid entry pressure (LEP) at temperatures above 70 °C (Saffarini, et al. 2013). Even more, the method use to perform this measurements is not suitable to be used at higher temperature because evaporation phenomena across the membrane starts to be relevant.

With this aim the liquid permeation technique was modified to perform tests at higher temperatures and, in an innovative way, in function of temperature at constant differential pressure.

Performing the liquid permeation technique with this modifications we were able to obtain for the first time the liquid entry pressure at temperature above the boiling point and a new operative parameter, named, LIQUID ENTRY TEMPERATURE. The arbitrary definition of liquid entry pressure proposed by (García-Payo, Izquierdo-Gil and Fernández-Pineda 2000), as well as the fitting equation, were change. Through this changes, we were able to compare results at different temperatures and obtain a trend of LEP vs Temperature.

3.1.1 Membranes

3.1.1.1 Polymeric membranes

3.1.1.1.1 Flat sheet

Two different commercial polymeric membranes have been characterized. The membranes of hydrophobic nature are presented in the flat sheet form. The main characteristics from obtain from data sheet are reported in Table 3.1. In addition to the data sheet information other characteristic reported in literature are in the same table.

Table 3.1 Polymeric membranes characteristics (¹ Khayet, Velázquez and Mengual 2004)

<i>Properties</i>	<i>MSI TefSep</i>	<i>Pall TF200</i>
<i>Material</i>	<i>PTFE</i>	<i>PTFE</i>
<i>Support</i>	<i>Polypropylene</i>	<i>Polypropylene</i>
<i>Mean pore size</i>	<i>0.22 μm</i>	<i>0.2 μm</i>
<i>Porosity</i>		<i>60 % - 80 %¹</i>
<i>Membrane Thickness δ</i>		<i>60 μm¹</i>
<i>Total Thickness δ</i>	<i>175 μm</i>	<i>135 μm – 165 μm¹</i>
<i>Max Operative T</i>	<i>130 °C</i>	<i>100 °C (water) - 149 °C (air)</i>
<i>Bubble Pressure (IPA)</i>		<i>1.0 bar</i>
<i>Water entry Pressure</i>		<i>2.8 bar</i>

3.1.1.1.2 Hollow fiber module.

The LiquiCel ® 2.5 x 8 EXTRA-FLOW is a commercial polymeric membrane module. The “Extra-Flow” are cross flow modules of great membrane area, due to the number of fibers on the bundle. Has been design for gas transport application, degassing of liquid streams, absorption of gas on liquid streams, particularly tested with CO₂. The polypropylene structure limit the maximum application temperature to 70 °C.

The characteristics of membranes and module are available on the data sheet of the product (3M Company 2016) other part of the characteristics were taken from (Schöner, et al. 1998) and form direct communication of the producer (classified information). The Characteristics are present on Table 3.2.

Table 3.2 LiquiCel ® 2.5 x 8 EXTRA-FLOW: module and membrane technical characteristics.

<i>Module</i>	<i>EXTRAFLOW 2.5 x 8</i>	<i>Membrane</i>	X50
N_t	-	<i>Material</i>	PP
$l^{eff} (cm)$	18	<i>Mean pore size</i>	0.04 μm
$d_s (cm)$	5.5	<i>Porosity</i>	40%
$d_c (cm)$	-	d_o	300 μm
$\varepsilon \%$	60.6%	d_i	220 μm
$V_{lumen} (mL)$	150	<i>Thickness δ</i>	40 μm
$V_{Shell} (mL)$	400	<i>Max Operative T liquid</i>	70 °C
$A_i (cm^2)$	14000	<i>Max Operative T Gas</i>	30 °C
$A_o (m^2)$	19091		
$A_{Av} (m^2)$	16546		

3.1.1.2 Ceramic membranes

The ceramic membranes has been developed in partnership with the Fraunhofer Institute for Ceramic Technologies and Systems. These are titania multi-layer membranes coated on the last layer with polymeric resins to add an hydrophobic character. For the study has been supplied flat disk samples and single channel tubes. The titania base was coated with four different resins and all four has been tested to evaluate the hydrophobic character.

On Table 3.3 are reported the characteristics of the hydrophobic layer, the mean pore size diameter reported by the supplier and the polymer resin coated on the membrane surface.

Table 3.3 Ceramic membranes characteristics

<i>Membrane</i>	<i>P</i>	<i>F</i>	<i>P+F</i>	<i>Silicone</i>
<i>Coating material</i>	polyester resin	FAS	polyester resin + FAS	Silicone
<i>Coating pore size</i>	0.1-0.25 μm	0.1-0.25 μm	0.1-0.25 μm	0.1-0.25 μm
<i>Support</i>			TiO ₂	

Table 3.4 summarized the morphological characteristics of the membrane samples and Table 3.5 report the characteristics of each layer on the titania support. The layer characteristics has been published before by the producers. (Weyd, et al. 2008)

Table 3.4 Ceramic membrane morphological characteristics.

<i>Shape</i>	<i>tubular</i>	<i>Flat disk</i>
<i>Inner Diameter (mm)</i>	7	-
<i>Outer Diameter (mm)</i>	10	-
<i>Total Length (mm)</i>	250	-
<i>Effective Length (mm)</i>	224	-
<i>Diameter (mm)</i>	-	25
<i>Thickness (mm)</i>	-	1
<i>Area (cm²)</i>	49.26	4.90

Table 3.5 Ceramic support membrane characteristics (Weyd, et al. 2008)

<i>Layer</i>	<i>Layer thickness</i>	<i>Pore diameter</i>	<i>Porosity</i>	<i>Tortuosity</i>	ϵ/χ	<i>K</i>	<i>B</i>
<i>[μm]</i>	<i>[μm]</i>	<i>[μm]</i>	<i>[-]</i>	<i>[-]</i>	<i>[-]</i>	<i>[m]</i>	<i>[m²]</i>
<i>support</i>	1500	4.5	0.33	2.92	0.11	$1.27 \cdot 10^{-7}$	$7.14 \cdot 10^{-14}$
<i>1. layer</i>	30	0.8	0.34	1.68	0.20	$4.07 \cdot 10^{-8}$	$4.08 \cdot 10^{-15}$
<i>2. layer</i>	30	0.25	0.39	1.15	0.34	$2.16 \cdot 10^{-8}$	$6.76 \cdot 10^{-16}$
<i>3. layer</i>	10	0.1	0.47	1.91	0.25	$2.09 \cdot 10^{-9}$	$8.89 \cdot 10^{-18}$

K = effective Knudsen coefficient, B = effective permeability constant reported by Weyd, et al

3.1.2 Contact angle measurement.

The measurements of the contact angle are performed by the static sessile drop method taking a photo of a drop over the membrane surface. The photo is taken with a photo camera Canon 350 D – lens Canon macro EF 100 mm 1:2.8. The picture is taken with artificial light, to have pictures equally illuminated. The magnifying lens allows the operator to have a picture with a great quality to perform analysis of the contact angle on the surface.

To have good reproducibility of the test, the drop should be always the same size and the temperature of the surroundings should be known to take it into account. A constant volume drop of 30 μL , is deposited over the surface with a micro syringe of 100 μL and the temperature of the surroundings is controlled with temperature probe PT 100.

The measurements at controlled temperature are performed inside an electric oven Kennex KWS1319J-F3UT, this perform the atmospheric temperature control. In order to avoid the drop evaporation the atmosphere is saturated with the test fluid present inside the oven on a beaker. Otherwise the pictures are performed at atmospheric conditions.

The analyses are performed in the software Geogebra, which measure the angle between two lines. The software operator should perform the selection of the base line and the tangent line to the drop. The measurement influenced by the operator criteria, the measurement should be performed repeatedly in order to obtain a distribution of the measurement.

On each sample a total of five drops are registered separately. Each liquid drop, randomly placed, is photographed three times and from each shoot both visible angles are measured. A total of 30 measurements by sample are performed.

Measurement of the same drop vs time were performed with the same procedure. The drop is randomly placed on the sample surface, three consecutive shoots are performed at each time and from each photography both the visible contact angles are measured.

3.1.3 *Water breakthrough measurements through modified Fraken method and flooding curve measurements.*

3.1.3.1 *Apparatus*

Measurements have been performed by the modified Fraken method and the combined method liquid breakthrough - Flooding curve. The experimental apparatus used to perform the measurements is shown in Figure 3.1.

Two membrane cells were used, shown in Figure 3.2. The first one is a cell for flat sheet membranes, with 10.75 cm² of total membrane area, the second is a vessel for tubular membranes of 10 mm OD and 25 cm total length.

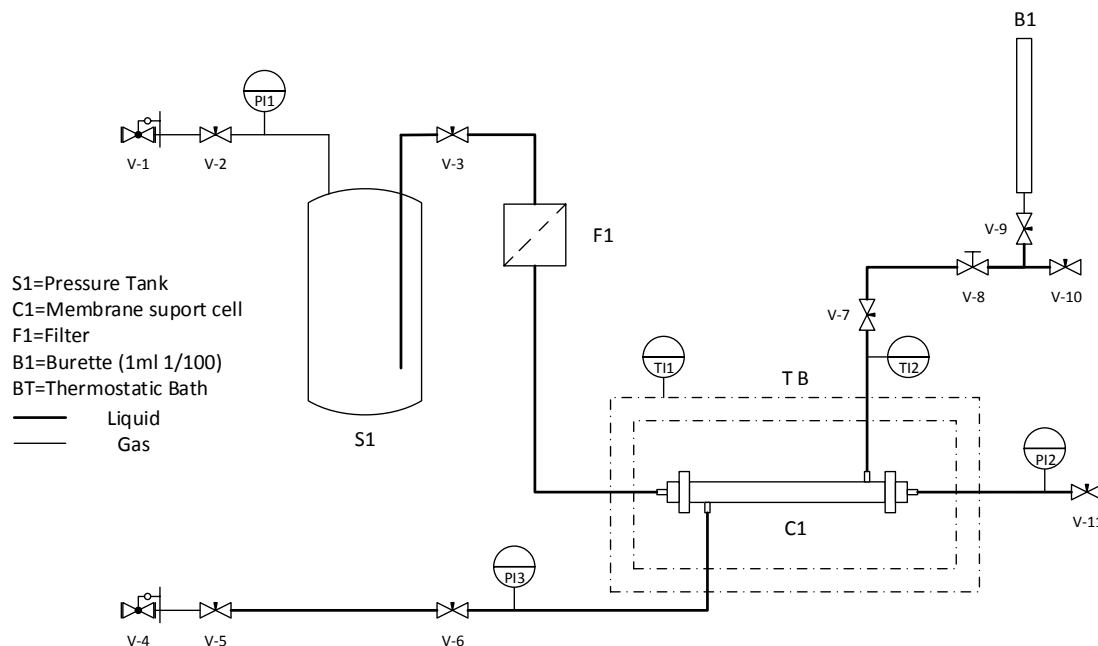


Figure 3.1 Experimental apparatus for liquid entry pressure – flooding curve measurements

The setup of the apparatus as shown in Figure 3.1 consist of: a stainless steel pressure tank (S1), reservoir of the non-wetting liquid pressurized with compressed air. The liquid is filtered with a cellulose filter (F1) of 2.5 μm , nominal size, before is feed to the membrane holder. Two kinds of membrane holder (C1) can be used to support different membranes. A AISI 316 L cell, design to hold flat sheet membranes with 10.75 cm^2 of total membrane area, consisting of a high pressure chamber (feed side) and a low pressure chamber (permeate side). The second housing (AISI 316 H) is made for tubular membranes of 10 mm OD and 25 cm total length, the non-wetting liquid is feed from the lumen side (feed side) and the permeate is collected on the shell side (permeate side).

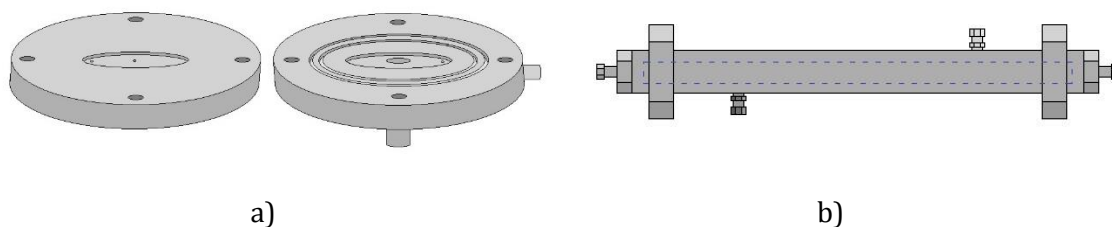


Figure 3.2 Support cell for LEP measurements C1. a) flat sheet membrane b) tubular membrane

The pressure is measured with analogic gauge manometers (0 – 10 bar) on the pressure tank, the high-pressure chamber (feed side) and the low-pressure chamber (permeate side). The pressure on each chamber of the membrane is controlled by the regulation valves of the compressed air line (V-1 and V4 in Figure 3.1) and a back pressure valve (V-8) before the flow measuring system. The housing is immersed on a thermostatic bath (30 – 180 $^{\circ}\text{C}$) Memmert one 7-45 (BT) to keep constant the inlet temperature and the outlet temperature. The temperature is measured in the bath and in the outlet of the housing with a Thermoresistance PT 100 connected with data logger (Delta OHM HD 2127.2). In the outlet of the system, the flow is measured with micropipette (1/100 and 5/100 mL) and a chronometer.

3.1.3.2 Procedure

3.1.3.2.1 Modified Fraken method

For the measurement of LEP, the membrane is carefully installed on a support cell allowing the contact with a non-wetting liquid on both sides of it and the pores remain full of gas (usually air). The pressure of the non-wetting liquid is upraised gradually on the feed side of the support cell. When the first air bubble is verified across the membrane (permeate side), the value of pressure of the feed side is registered as the LEP-A. The air bubbles came from the gas inside the membranes pushed out by the non-wetting liquid during the membrane flooding. The feed side is pressurized furtherly until the liquid flux is evident on the permeate side. This is registered as the LEP-B. The mean value between LEP-A and B is the registered as the water breaking pressure at the operative temperature. As in Fraken method the value of LEP is verified by visual inspection, and so, the accuracy of the measurement depends on the operator criteria

The action of the thermostatic bath allow the control of the test temperature, which can be performed at a constant temperature up to a temperature of 160 °C, depending on the material resistance.

3.1.3.2.2 ***Flooding curve at constant Temperature T_{cst} (Jv vs. ΔP) - Temperature > 80 °C***

The membrane is set on the housing and both chambers of it get filled with the test liquid (between valves 3-6-8 and 11 should be only the testing liquid). With the valve 8 completely closed the pressure on the feed side and on the permeate side is set at the same value avoiding to set a transmembrane differential pressure. The Pressure should be the maximum allowed by the setting on this way the maximum transmembrane pressure will be the starting pressure on the feed side. With gas pressure inlet opened (V-1, V-2) and fixed, the Temperature is raised up at the operative Temperature in order that vapor pressure raising doesn't increase pressure on the system.

When the Temperature of the system is steady, the inlet pressure valve (V-6) of the permeate side is closed and the test may start. To create a transmembrane pressure the back pressure valve (V-8) is slightly open. The opening of this valve decrease the pressure on the permeate side while the pressure on the feed side remains constant. The feed is continuously pressurized by the inlet gas (V-1). The pressure difference between feed and permeate creates a flow across the membrane that stabilizes the pressure on the permeate side. The arrival to steady state is long, usually one hour.

After the system have reached the steady state the pressure on the feed and permeate side are registered and the flux is measured with the most suitable volumetric pipette (B1). At this moment a higher differential pressure can be set on the system. Small steps should be considered, in order to have the higher number of points and perform better analysis. The back pressure valve (V-8) is opened a bit more and the system is again leave for stabilization and flux measurement. After consecutive flux measurements for the increasing differential pressure the test will be over when the maximum differential pressure is reached (the minimum pressure in the permeate side must be in any case higher than the vapor pressure at the operative test Temperature) or if the fluid Temperature in the pipette is close to the standard boiling point and bubbling stars to take place.

3.1.3.2.3 ***Flooding curve at constant Temperature T_{cst} (Jv vs. ΔP) - Temperature < 80 °C***

To perform the flooding curve measurements at temperatures below 80 °C the standard procedure was followed, described by McGuire et al and later on improved by Garcia-Payo et al. On the same way the membrane is set on the housing and the circuit is filled up to avoid the presence of bubbles. In this case, as the evaporative phenomena is lower, the presence of the back pressure valve V-8 is not needed. The outlet pressure from the membrane will be the atmospheric pressure and so the starting pressure on the feed side.

As for the differential pressure, it is only set by the inlet pressure and so by the gas pressure on the reservoir (S1). The control of the operative parameters is much easier (the fact that, at higher temperatures, the differential pressure is set by the pressure drop on the membrane plus the valve V-8 made the previous case difficult to control and the stabilization times longer).

The pressure on the inlet is set opening the valve V-1, in order to perform a wide range of measurements the first pressure set should be the lowest possible. The system should be at steady state to performed flux measurements. An hour has been established as the standard stabilization time. After the stabilization hour the flux is measured at least four times or until the flux measurement is steady. The pressure can be increased to the next value.

Both methods, with and without the back pressure valve, are equivalent. No difference between the results obtained with one method or the other has been appreciated for the same sample.

3.1.3.2.4 ***Flooding curve at constant differential Pressure ΔP_{cst} (J_v vs. T)***

As in the constant Temperature case the membrane is set on the housing, the circuit is completely filled with the test liquid, it should be avoid the presences of any gas bubble. Then the circuit can be submerge on the thermal bath.

The operative transmembrane pressure is set taking into account that the absolute pressure on the feed side and the permeate side should be always higher than the vapor pressure of the liquid at T . Having done this, we can be sure there is only liquid flux across the membrane, regardless the temperature reached on the test. Again, as for constant temperature, is advisable to set the highest pressure possible on the feed side. Yet, the startup of the pressure setting should be carefully performed. The differential pressure must never go over the nominal for the test. So the pressure will be raised up one step at the time, increasing simultaneously the feed side and the permeate side (with the reduction valves V-1 and V-4, Figure 3.1) until the pressure is the maximum and equal on both sides.

When the Temperature of the system have reached a steady state, the back pressure valve V-8 is slightly opened in order to stablish the differential pressure decreasing the pressure on the permeate side. When the system has reached the steady state, temperature, transmembrane pressure, and flux are constant, the flux measurement can be performed and the temperature can be furtherly raised up.

For increasing Temperature the pressure on the permeate side increase as well due to the vapor pressure, the differential pressure trend to arrive to zero. To reestablish the differential pressure, the back pressure valve should be furthermore open and so the flux increase.

3.1.3.3 Data reduction

On Figure 3.3 is represented the curve resulting from the procedures describe above. The continuous curve of flux vs. Transmembrane Pressure (T_{cst}) or vs. Temperature (ΔP_{cst}), is obtained for an infinite number of experimental points and considering the range of ΔP s or T s where none of the pores has been flooded to the condition when all of them are flooded and the flux follows Poiseuille law.

In order to simplify, only the test of flux measurements for increasing transmembrane pressure (at constant Temperature) will be considered to explain the data reduction. Nevertheless the conclusions are the same for the case of increasing Temperature (at constant transmembrane pressure).

Two curves can be observed. The dotted line represents the ideal membrane, with none pore size. In this case the flux will be zero until certain combination of the array transmembrane pressure-temperature values, the LEP. At this point all the pores in the membrane get flooded, increasing furtherly the transmembrane pressure, the flux will follows the poiseuille's. The red line represents a standard membrane with a pore size distribution.

Can be appreciate that the red line, relative to the flooding of a hydrophobic membrane in function of the operative parameters, follows a pore size distribution with a well-defined maximum and minimum pore size. As the flows is zero until LEP (or LET), when the flow starts growing accordingly with the number of pores flooded at the operative conditions.

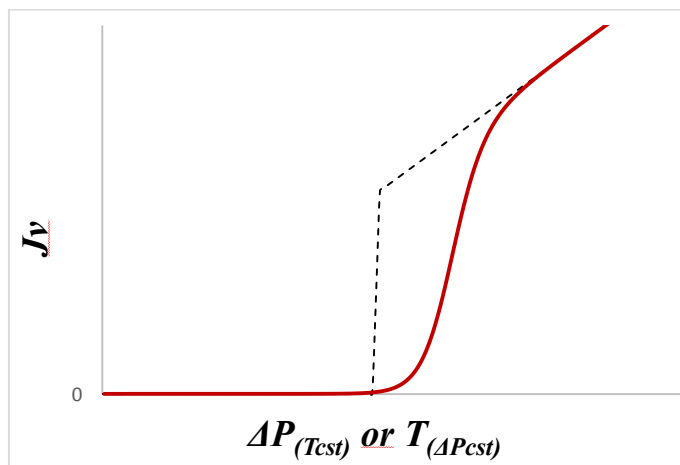


Figure 3.3 Flooding curve of hydrophobic membrane: flux vs. Transmembrane Pressure ($\Delta P_{(T_{cst})}$) at constant Temperature or Temperature ($T_{(\Delta P_{cst})}$) at Constant Pressure.

However as the pores size in a membrane are usually distributed in a normal fashion, it is possible that at atmospheric conditions the biggest (even the biggest part of the distribution) of the pores has been already flooded (at a very low pressure), let's call this pores "defects". If we consider that the distribution, generally, are not perfectly continuous. For a certain range of pressure no more pores will be subsequently flooded, after defects has been flooded. For this

reason, on the initial part of the flooding curve, the flow across the membrane could follow a linear trend in function of increasing pressure instead of being zero.

Even at low values of transmembrane pressure, low flux can be measured across a hydrophobic membrane. The definition of LEP, as state by previous authors, is not valid. Experimentally LEP has been defined with an arbitrary concept, Garcia-Payo et al defined the LEP as the pressure when the flux reached a certain defined value.

In Figure 3.4 is shown the again the difference between an ideal membrane (no pore size distribution) the membrane with no defects and the so called standard membrane. The value of LEP is well defined for the first two cases, being clear that, when the flux is different from zero the membrane has starts to flood. The real membranes are long away from being ideal's and is also difficult to found a membrane with any "defect" or pores creating discontinuities, especially on the extremes of the distribution. This defects create the phenomena observed on Figure 3.4 where the red line starts growing from the beginning and for a certain range of increasing transmembrane pressure follows the Poiseuille Flow.

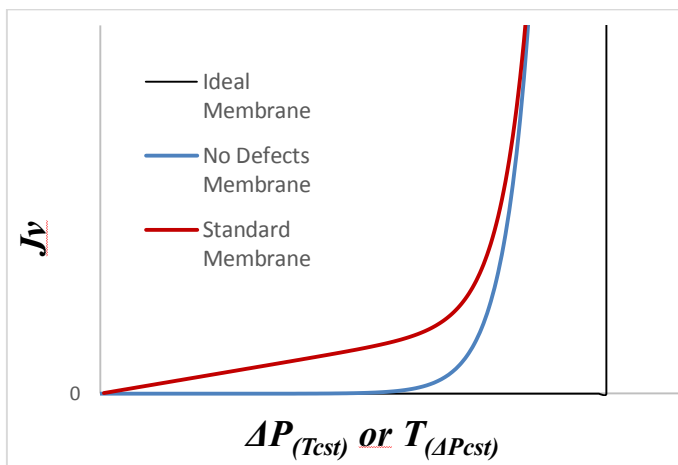


Figure 3.4 Flooding curve for increasing Transmembrane Pressure – Temperature: Low Pressure Range.

One example of the previously stated is represent by the experimental results of Figure 3.5 and Figure 3.6. The polymeric membrane Pall TF200 was used for the development of the method and from the analysis of the results was elaborated for the data reduction.

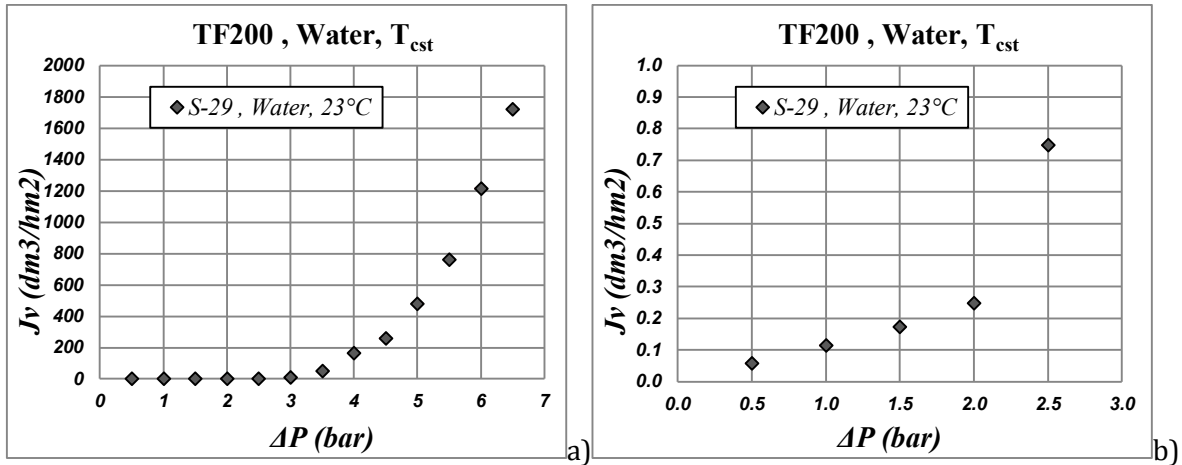


Figure 3.5 TF200 flooding curve vs. Transmembrane Pressure at 23 °C: a) whole pressure range b) detail for low flux

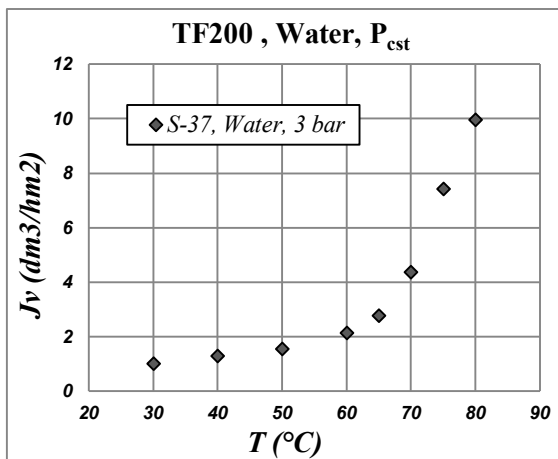


Figure 3.6 TF200 flooding curve vs. Temperature at 3 bar

On the figures above it can be seen that for both cases (J_v vs. ΔP (T_{cst}), J_v vs. T (ΔP_{cst})), on the initial part of the flooding curve, there is the linear trend, evidence of Poiseuille flow across a constant number of pores.

García-Payo et al. 2000 suggest the calculation of the permeability in order to fit the experimental results to the equation (2.48). The permeability of a porous membrane is generally defined in terms of the flux over the driving force, on this case the transmembrane pressure, resulting in the expression below, where ε refers to the porosity of the membrane and r is the mean pore radius.

$$L_p = \frac{J_v}{\Delta P} = \frac{\varepsilon \bar{r}_p^2}{8\eta\delta\chi} \quad (3.1)$$

However the permeability defined on that way, made reference to a membrane where flux came across all the pores in the membrane. The porosity term accounts the number of pores and the total surface of the membrane as follows:

$$\varepsilon = \frac{N_p \pi \bar{r}_p^2}{S_l} \quad (3.2)$$

In the case of the flooding curve the measured flow doesn't come across all the pores in the membrane. As the membrane material has low affinity with water, at the beginning of the test flow came across a low number of pores. Further pores get flooded as the transmembrane pressure increases.

$$\frac{Jv}{\Delta P} = \frac{(N_p \pi \bar{r}_p^2) \bar{r}_p^2}{8\eta \delta \chi S_l} = \frac{Q_p N_p}{\Delta P S_l} \quad (3.3)$$

The flux can be express as the flow on a single pore times the number of pores of the membrane over the membrane surface and so the flow of a single pore is function of the geometrical parameters, the fluid properties and the driving force.

$$Q_p = \frac{\Delta P \pi r_p^4}{8\eta \delta \chi} \quad (3.4)$$

Even if the flux over differential pressure is usually related with the concept of permeability, the calculation of this made account of the transmembrane pressure, not as a driving force, but as a way of breaking through the hydrophobic pores.

On Figure 3.7 we can see the plot of the flux over differential pressure for the flooding curve at increasing $\Delta P_{(T_{cst})}$ and $T_{(\Delta P_{cst})}$. The plot for increasing $\Delta P_{(T_{cst})}$ shows initially a constant value of permeability indicating that the number of flooded pores remains constant, which is the same trend observed when the membrane is completely flooded. The flooding curve for increasing $T_{(\Delta P_{cst})}$ keeps the same shape, as the test is performed at constant transmembrane pressure. Here the pressure acts only as a driving force, the breaking through effect is performed by the increasing Temperature, changing the Interfacial Surfaces and so the contact angle. The equation (2.54) can be reordered in order to observe this effect.

$$r_p(T) = \frac{-2\gamma_{LV} \cos \theta}{\Delta P} = \frac{-2[\gamma_{LV}(T)] \cos[\theta(T)]}{\Delta P} \quad (3.5)$$

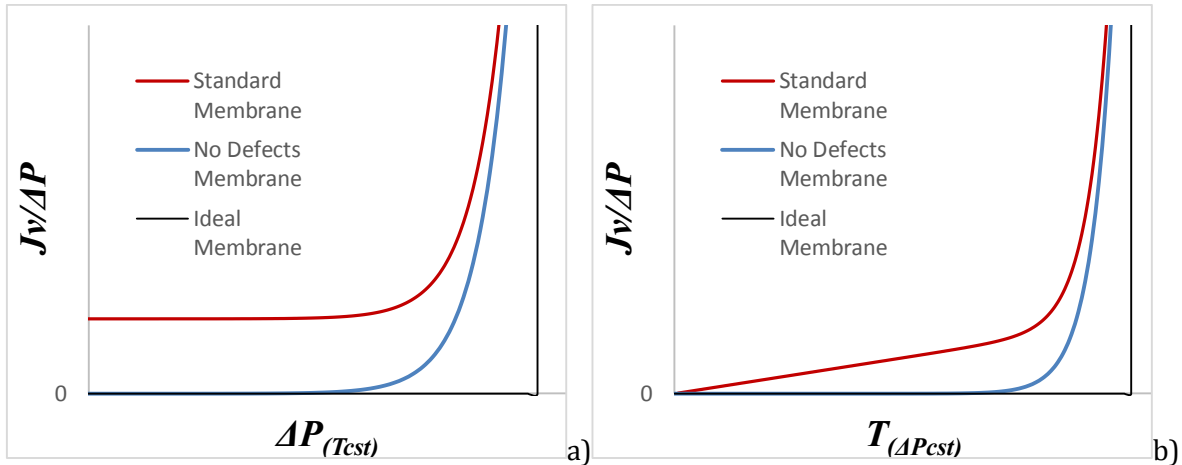


Figure 3.7 flooding curve Permeability for increasing a) Transmembrane Pressure b) Temperature

The same initial linear trend is observed for $J_v/\Delta P$ vs. $T_{(\Delta P_{cst})}$ implying again constant permeability. Assuming that geometric parameters doesn't change with Temperature, only the fluid properties can be responsible of the increasing in the flux. An extra normalization should be performed in terms of the viscosity at T. Normalizing the flux with transmembrane pressure and viscosity, the effect of ΔP and T on the flooding curve accounts only the pores flooded.

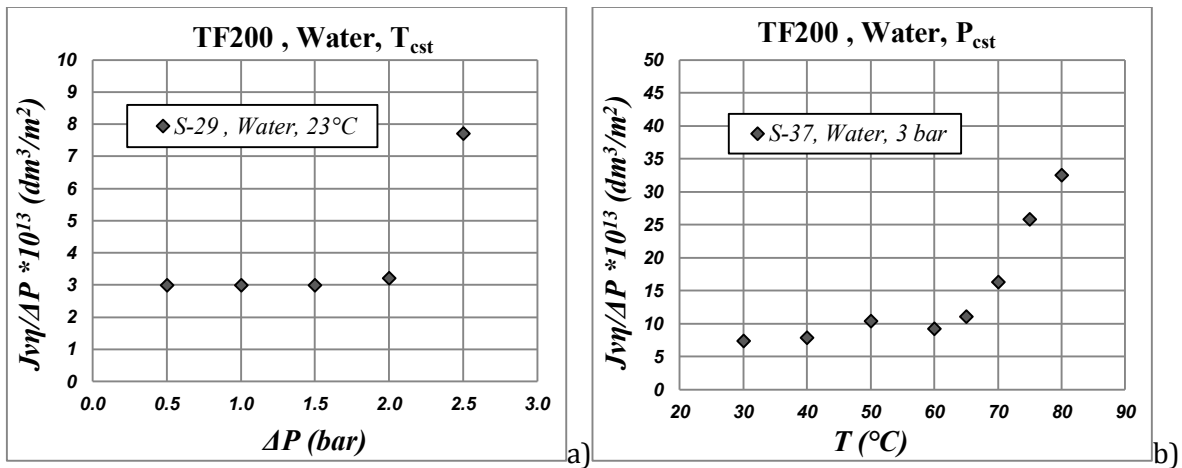


Figure 3.8 TF200 flooding curve: viscosity normalized permeability. a) increasing $\Delta P_{(T_{cst})}$ b) increasing $T_{(\Delta P_{cst})}$.

On Figure 3.8 it can be seen the effect of the process of normalization with transmembrane pressure and the temperature across the viscosity. On both cases the permeability present a constant value on the initial part of the test regardless the magnitude of it. The constant permeability value is a clear evidence that the number of pores where the flow is coming through is constant.

3.1.3.4 Liquid Entry Pressure Definition

The definition of Liquid entry Pressure came through the analysis of the Laplace-Young equation. This is the differential pressure where the biggest of the pores in a porous membrane get flooded. As we have seen during this discussion, since a differential pressure across the membrane exists there is the possibility of flow across the so called defects. The defects are larger pores creating discontinuities along the pore size distribution or pores where the hydrophobic character hasn't been well established (in the case of coating).

Previous authors observe the same behavior and defined the LEP to be the value of differential pressure when the flux reach certain arbitrary value (1 mm³/s in the case of Garcia-Payo et al 2000). As this definition is support on an arbitrary value, changes on the conditions considered for the selection of the flux could not be not valid for the value selected. This is the case of test at different Temperatures where the changes of viscosity increase the flux for increasing Temperature.

On

Figure 3.9 it can be seen the hypothetical case where the same membrane is flooded at different temperatures. Is evident that flooding curves at different temperatures could intercept the arbitrary line of the LEP_{min} Flux (red line) only for a matter of change of viscosity or even intercepted when the initial linear trend is still constant.

Calculating the permeability by the normalization of flux with transmembrane pressure and the viscosity, for the same membrane the initial permeability is a constant value regardless the working temperature or the differential pressure until further pores start to get flooded.

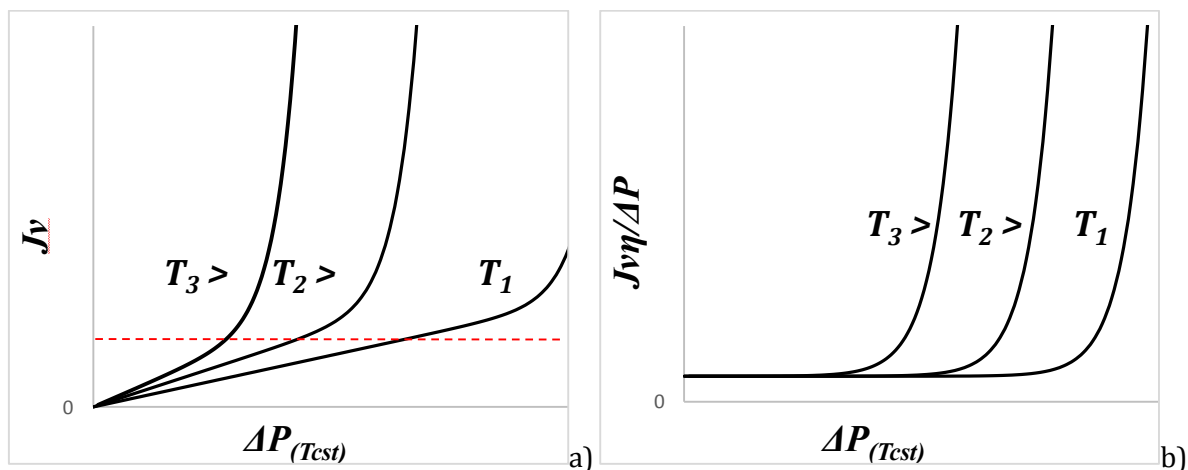


Figure 3.9 flooding curve for increasing transmembrane Pressure: a) Jv vs. $\Delta P_{(Tcst)}$ Test at different temperatures b) $Jv\eta/\Delta P$ vs. $\Delta P_{(Tcst)}$ Test at different temperatures

Through this analysis the concept of **Liquid Entry Pressure (LEP)** is now an absolute definition and not relative to the operative conditions not either the operator criteria. The LEP is the value

of transmembrane pressure (ΔP), for a given value of temperature (T_{cst}), when further pores (extra to the so called defects) start to get flooded. This value of pressure can be recognized, through the liquid permeation technique for increasing transmembrane pressure, when the initial constant permeability changes its absolute value and starts to grow.

Likewise the concept of **Liquid Entry Temperature (LET)** is the value of temperature, for a given value of transmembrane pressure (ΔP_{cst}), when further pores start to get flooded. Through the same data reduction method, like the case of increasing pressure, is easily recognizable the moment when the permeability is not anymore constant.

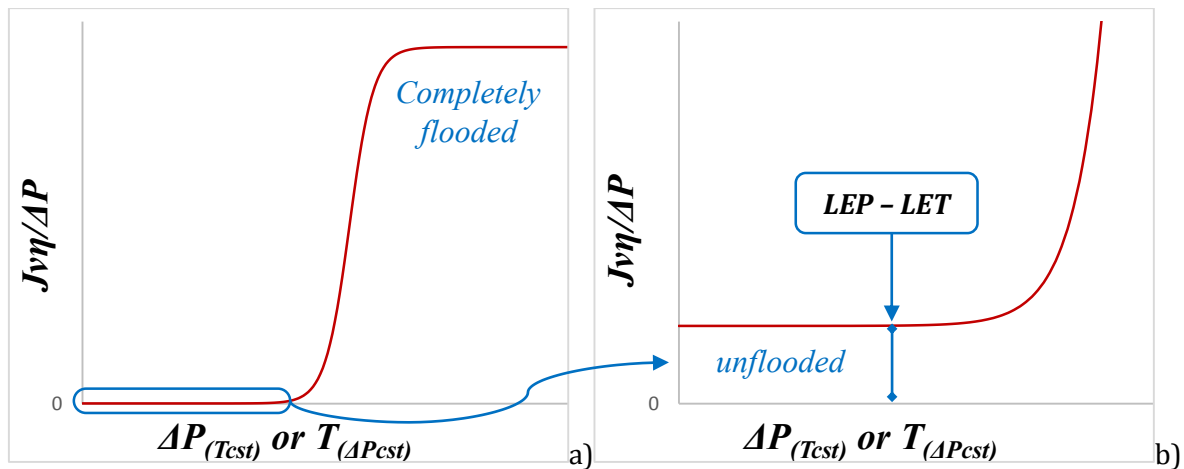


Figure 3.10 LET and LEP from normalized flooding curve.

3.1.3.5 Fitting curve modification and pore size distribution.

From the analysis performed before is evident that the fitting curve propose by García-Payo et al (section 2.5.2.2.1) is no longer valid and there is a missing parameter to complete it. The value of the minimum permeability will goes to fit the curve section where the number of pores flooded is constant and minimum.

$$\frac{Q}{\Delta P} = \frac{Lp_{max}}{e^{-b(\Delta P - \Delta P_0)} + 1} + Lp_{min} \quad (3.6)$$

Nevertheless the equation proposed doesn't change the procedure to perform the pore size distribution analysis and might be used for the same purposes.

It should be also possible to perform the same pore size distribution analysis throughout the test at constant transmembrane pressure, on this case the variable will be the temperature that will go to change directly the fluid viscosity, the liquid-vapor surface tension and the solid-liquid contact angel. On this way equation (2.55) will be explicit in terms of temperature, assuming that viscosity follows Arrhenius law:

$$Q_p = \frac{\Delta P \pi r_p^4}{8 \left(\eta_0 \exp \left(\frac{E}{RT} \right) \right) \delta \chi} \quad (3.7)$$

The flooded pore radius at the temperature T is defined by the change of surface tension and contact angle.

$$r_p(T) = \frac{-2\gamma_{LV} \cos \theta}{\Delta P} = \frac{-2[\gamma_{LV}(T)] \cos[\theta(T)]}{\Delta P} \quad (3.8)$$

$$Q = \frac{N_{tot} \pi \Delta P}{8\eta(T) \delta \chi} \int_{r_p(T)}^{r_{max}} x^4 f(x) dx = C_2 \Delta P \int_{r(\Delta P)}^{r_{max}} x^4 f(x) dx \quad (3.9)$$

In order to complete the analysis and obtain the theoretical expression for the pore size distribution its necessary an explicit relation between the material contact angle with the temperature, which is the part of the objectives on this study.

3.2 Results

3.2.1 Polymeric membranes

Flat sheets polymeric membranes were used to tune the experimental procedures and to evaluate the hydrophobic character at moderate temperatures. The membranes selected to performed the measurements were commercial membranes of PTFE, among which the TF200. The TF200 is a widely used membrane, used to perform studies of hydrophobicity throughout contact angle experiments and liquid entry pressure and so the results obtain for this membranes are easily comparable making possible the development of our own measurement procedure.

The TF200 was used to perform test of contact angle in function of the temperature and water breakthrough test at constant temperature and constant transmembrane pressure.

3.2.1.1 Contact angle

The membrane TF200 was used to perfume contact angle test vs. Temperature with two different fluids. Was measured the water contact angle of water up to a temperature of 65 °C and the glycerol contact angle up to a temperature of 120 °C.

As the measurement system was open, even if the surroundings were saturated with vapor, the evaporation of water was evident after 60 °C. Among other fluids the glycerol was selected to compare its behavior with water because it similar vapor-liquid surface tension and the higher boiling point compare with the water. The test were performed with a glycerol-water solution of 66 %, from now glycerol will be intended as the solution.

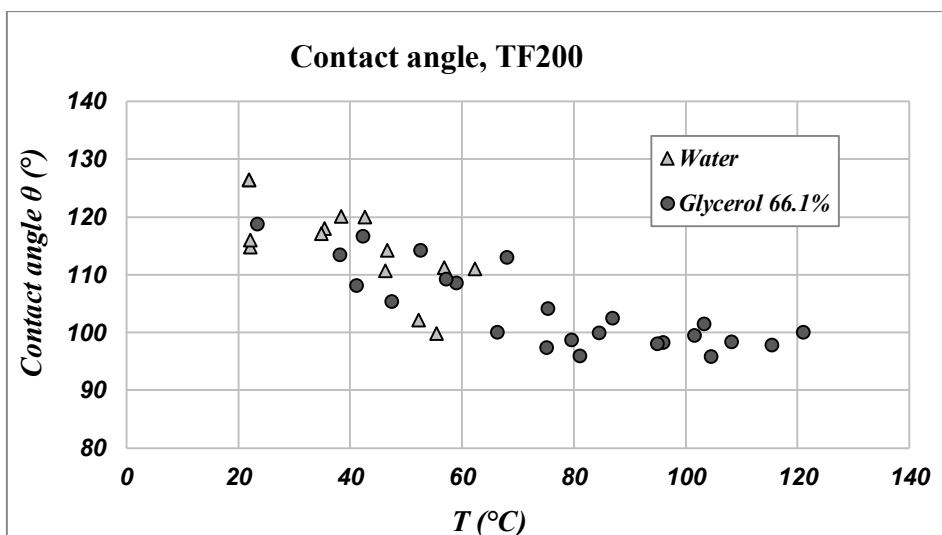


Figure 3.11 Water and Glycerol contact angle vs. Temperature.

The Figure 3.11 presents the summary of the contact angle measurements performed on different samples of flat sheet membrane. Apparently the water and glycerol contact angle present similar contact angle values and trends vs. Temperature, at least on the considered temperature range ($< 60\text{ }^{\circ}\text{C}$). The glycerol drops are stable at higher temperatures and the contact angle test proceed up to temperatures close to $120\text{ }^{\circ}\text{C}$. The overall contact angle vs. temperature trend can be linear like, the same results has been observed elsewhere (Petke and Ray 1969).

Never the less even if the contact angle result are similar at temperatures below $60\text{ }^{\circ}\text{C}$ it cannot be assumed that the water will keep it's linear trend and follow the glycerol's trend.

3.2.1.2 *Water breakthrough.*

3.2.1.2.1 *Modified Fraken method*

Through the modified Fraken method (described on section 3.1.3.2.1) was initially evaluated the LEP of the polymeric membranes TF200 and MSI, both PTFE membranes of 200 nm (mean pore size).

The test were performed to evaluate the effect of thee temperature on the liquid entry pressure. For this the same membrane was tested at different temperatures. On Figure 3.12 are reported the results for 4 membrane samples, each point is the result of one single test. The test were performed at constant temperature, after each test the membrane was dried inside the membrane holder (to avoid the membrane damage) with air flow through each side of the membrane holder and throughout the membranes for 60 minutes (each).

The tests series for each membrane were performed at increasing test temperature starting from the test at room temperature (asterisk). The sequence of the tests performed on sample 7 (Figure 3.12-a) are performed as indicated by the arrows, starting at room temperatures subsequence test were performed at higher temperatures. Finally the test was performed at again at room temperature. The tests show clearly that LEP decreases for increasing temperature and that after the test at higher temperatures there is a permanent modification effect on the membrane.

The test with further membranes (samples 9 – 12 – 16 on Figure 3.12-b, c and d respectively) follow the next sequences: after each test at higher temperature a test at room temperature was performed. The subsequent room T trial after the trial at higher temperature is reported in the figure with the same symbol with light grey, as clearly indicated by the arrows on figure b.

The figures illustrates how the membranes modification is irreversible after trials at temperatures higher than $50\text{ }^{\circ}\text{C}$.

The modification on the membrane, provably a dilatation of the pores, made the effect of the temperatures on the LEP to be triple, the surface tension, the contact angle and the pores size.

Only the surface tension can be predicted, so is not possible arrive to conclusions of the effect of the temperature on the hydrophobicity.

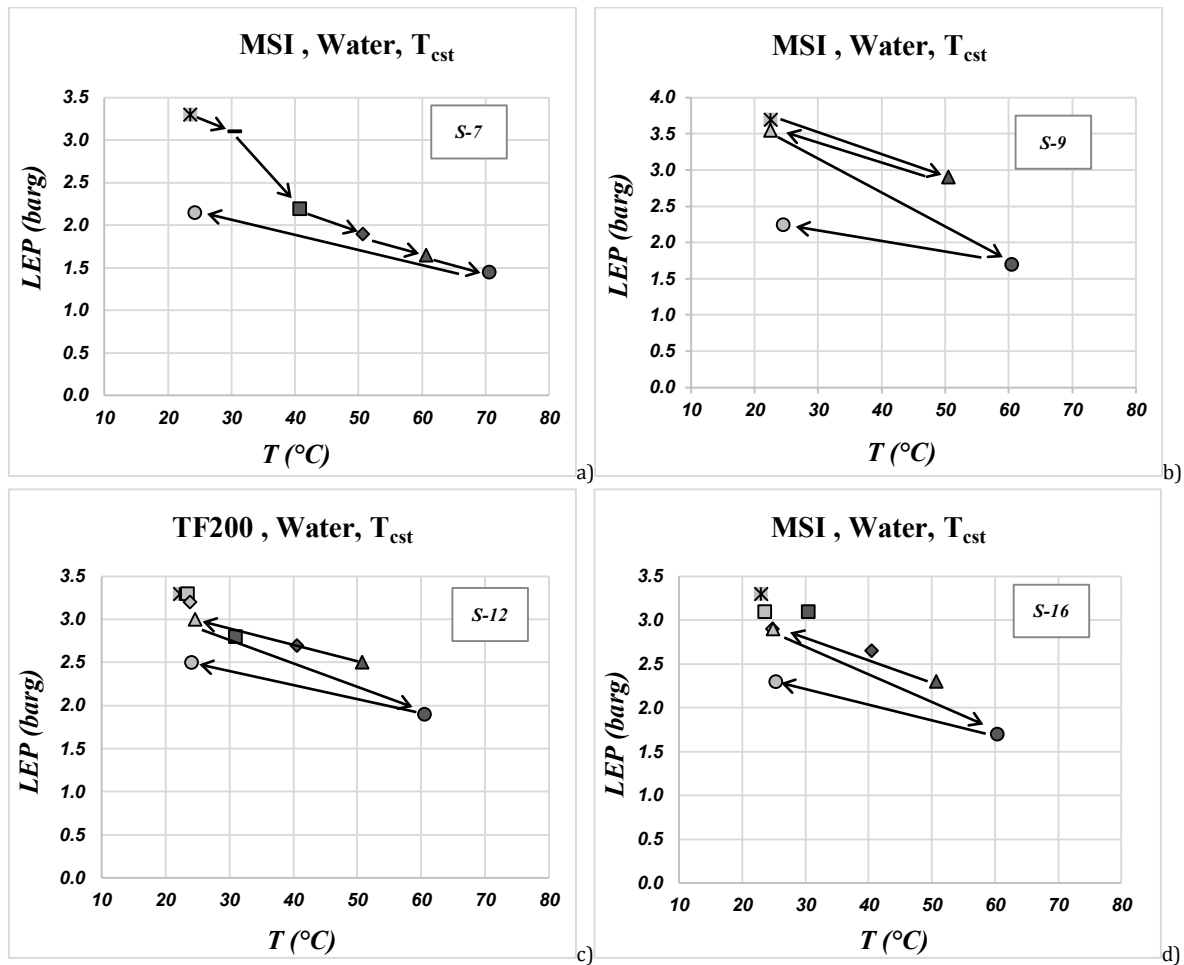


Figure 3.12 Test of LEP on four samples of PTFE, test performed at increasing test temperature.

3.2.1.2.2 Flooding curves

Flat sheet membranes

The water breakthrough measurements were performed through the flooding curve test described on section 3.1.3 with the polymeric membranes TF200 (section 3.1.1.1). test were performed at constant temperatures, for increasing transmembrane pressure and at constant transmembrane pressure for increasing temperature.

The flooding curves obtain from the test are reported on Figure 3.13 to Figure 3.15. Were performed tests, exclusively with new membranes, at different constant temperatures between room temperature and 60 °C. Furtherly were performed test at constant differential pressure, increasing temperature, up to a temperature of 80 °C.

On Table 3.6 is reported the summary of the test performed on TF200 membranes. On the table can be found the test configuration and the value of breakthrough, liquid entry pressure (LEP) if T_{cst} or liquid entry temperature (LET) if ΔP_{cst} .

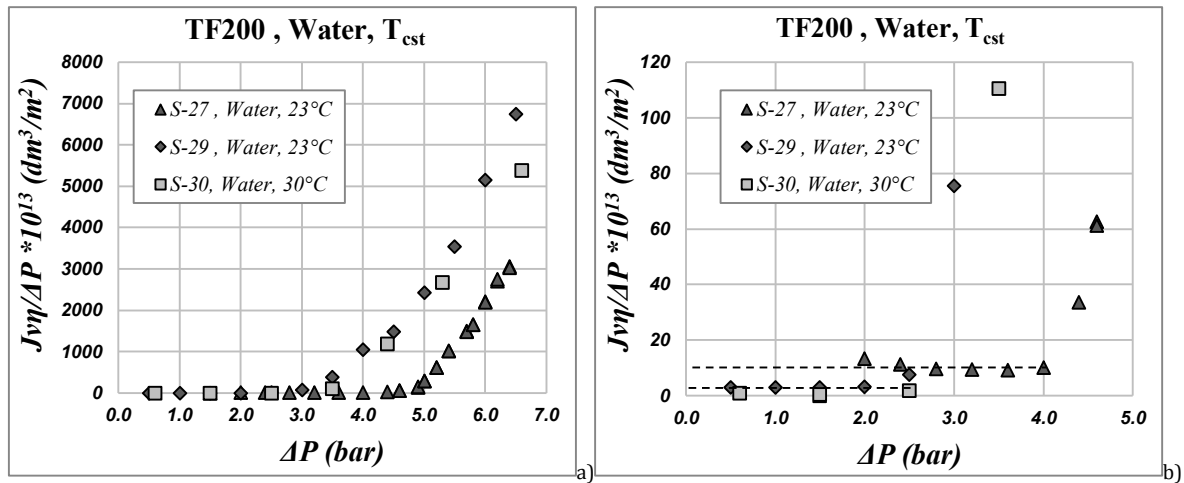


Figure 3.13 Different Samples TF200 flooding curve at room Temperature

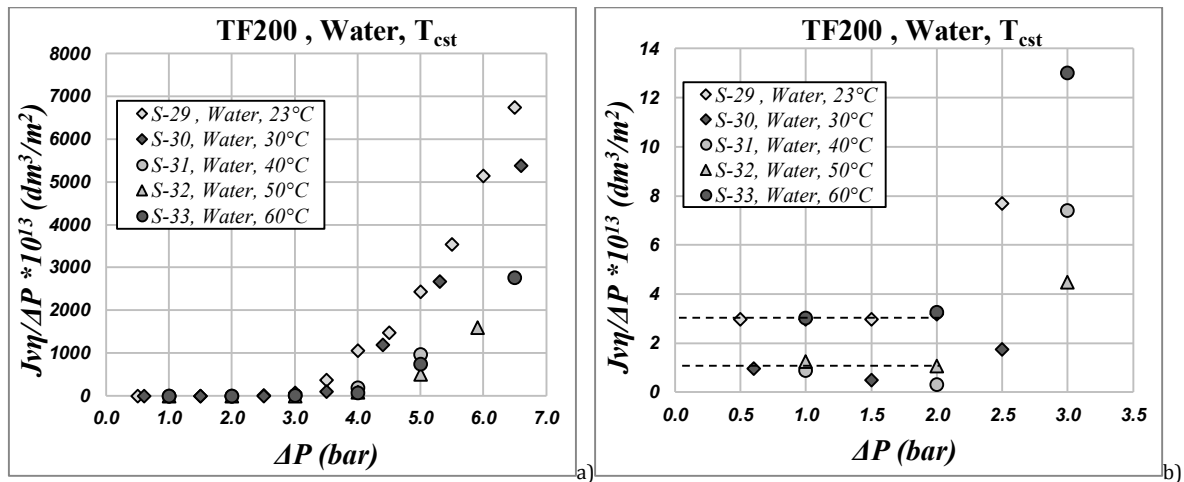


Figure 3.14 Different Samples TF200 flooding curve at different constant Temperature.

On the table below are reported the values of LEP if the test was performed at T_{cst} and LET if ΔP_{cst} . If the operative variable is the differential pressure, the operative constant temperature is reported on the column LET-T, otherwise the constant pressure is reported on LEP- ΔP column.

As it is virtually impossible to obtain a continuative flooding curve, the value of LEP-LET reported is the value of the previous condition, before the flooding start to take place (as described on section 3.1.3.4). The exact condition when the membrane begins to flood, when the permeability is no longer constant, could be not registered among the experimental values

and so the error in the measurement ($\sigma_a+0.1$) is proportional to the experimental step took during the experimental procedure.

Last but not least is reported the corresponding flux to the breaking through condition. The higher this value is, the defects on the membrane are bigger. Meaning the membrane is not yet flooded but doesn't act as a proper barrier.

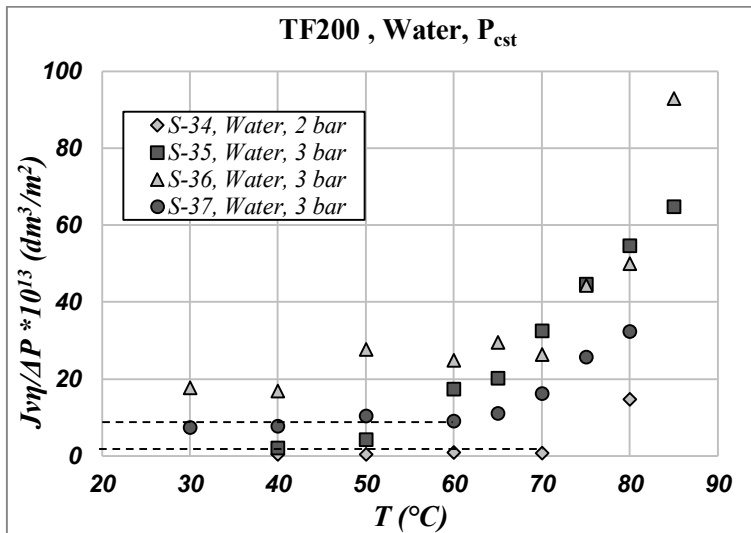


Figure 3.15 Different Samples TF200 flooding curve at different constant Transmembrane Pressure

Table 3.6 Water breakthrough $\Delta P - T$ and correspondent flux at breakthrough: TF200 membranes.

Test	pore size (nm)	Sample	LEP- ΔP (bar)	$\sigma_a+0.1$ (bar)	LET-T (°C)	J_v at LEP ($dm^3 h^{-1} m^{-2}$)
<i>T cst</i>	200	26	3.2	0.2	22.6	0.18
<i>T cst</i>	200	27	4	0.2	23.1	1.60
<i>T cst</i>	200	28	2.4	0.2	59.2	0.03
<i>T cst</i>	200	29	2.0	0.5	22.5	0.25
<i>T cst</i>	200	30	2.5	0.8	30.0	0.20
<i>T cst</i>	200	31	2.0	0.9	40.0	0.04
<i>T cst</i>	200	32	2.0	0.8	50.0	0.14
<i>T cst</i>	200	33	2.0	0.9	60.0	0.50
<i>$\Delta P cst$</i>	200	34	2.0	1.0 (°C)	80.0	0.15
<i>$\Delta P cst$</i>	200	35	3.0	1.0 (°C)	65.0	0.84
<i>$\Delta P cst$</i>	200	36	3.0	1.0 (°C)	70.0	5.80
<i>$\Delta P cst$</i>	200	37	3.0	5.0 (°C)	65.0	2.13

The experimental results show a big variability of the membranes. Besides the variability of the single value of LEP for test at similar conditions, the flooding curves show different behaviors.

The Figure 3.13 summaries some test performed at room temperature, the flooding curves, in some cases, are completely different one to the other. The initial constant permeability presents different values and the value of breaking through differential pressure are on a wide range of values (between 2 and 4 bar).

On Figure 3.14 are present a sequence of test performed with new membranes at different temperatures. Again, the inconsistency of the results is quite appreciable. Can be appreciated (particularly on figure b) two groups of membranes where the permeability ($Jv\eta/\Delta P$) is the same. One group are the test at 23 and 60 °C ($Jv\eta/\Delta P \approx 3 \text{ E-13 dm}^3/\text{m}^2$), and the group of test at 30, 40 and 50 °C ($Jv\eta/\Delta P \approx 1 \text{ E-13 dm}^3/\text{m}^2$). However the value of breakthrough is very similar (around 2 bar).

The test at constant pressure are a little more regular, even if the permeability change on a wide range, the value of breaking through e quite the same.

The polymeric membranes TF200 present a small area and the defects on them are rather variable. Even more the temperature could expand the polymer and the pores in the membrane, which made untrustworthy the test at different temperatures with different membranes.

A proper study, to evaluate the effect of temperature on the breaking through condition and so on the hydrophobicity, should be performed with the same membrane sample and with membranes that does not changed its morphology with temperature.

Hollow fiber module

On the hollow fiber was performed only on test of flooding curve at room temperature. This modules should be used on SGMD test and so is preferable avoid flooding the membrane and probably reduce its performance on the process.

The flooding curve show the typical initial constant linear trend, which indicated the membrane hasn't been flood. The flux come across only few pores. The magnitude of the normalized flux make think the defects on this membrane are insignificant, which can be expected if the mean pore size is consider (40 nm).

The magnitude of the normalized flux should be considered the objective of a non-flood membrane.

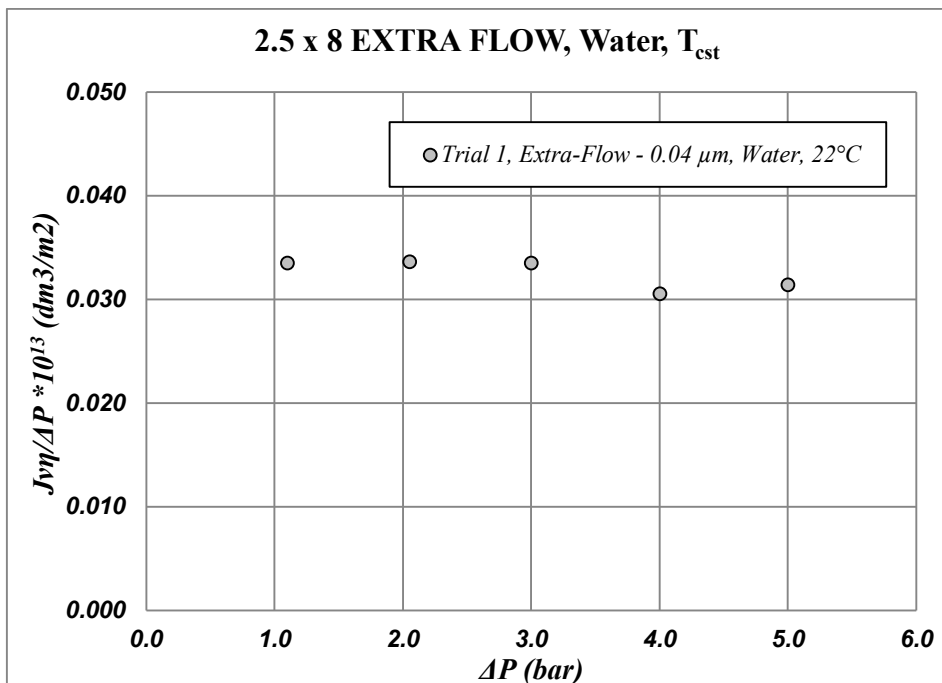


Figure 3.16 Extra-Flow 2.5x8 flooding curve at constant temperature.

3.2.2 Ceramic membrane

Titania (TiO₂) membranes (described on section 3.1.1.2) coated with four different polymers were tested in order to characterize its hydrophobicity. Test of contact angle and water breakthrough were performed to evaluate its hydrophobic performance. Contact angle test are focused on the *membrane* surface hydrophobic character and breakthrough test to allow to identify the inner hydrophobic character. The breakthrough test allow to evaluate on its complex the *material* contact angle, and the barrier effect of the membrane to some fluid and its dependence with the transmembrane pressure (ΔP) and Temperature (T).

3.2.2.1 Contact Angle

The water contact angle reported on the Figure 3.17 are the results of the mean value of 5 different water drops randomly place over the membrane surface. For each drop, three photoshoot were performed, and both of the contact angles visible on each photo (left and right) were measured. The error bar is representative of the standard deviation of the thirty contact angles measured on each sample.

Test were performed with flat disk of ceramic membranes coated with two different polymers, the first one, coded as P+F, is a mix of polyester resin + FAS the second one is a silicone resin. Both are coated on one surface of the disk, on which the test were performed.

The contact angle measurements are described on section 3.1.2. The as placed contact angle was measured through photographic register of the different drops over the same surface and

for the same drop in function of time. The results for the membranes new are summarized on Figures Figure 3.17 and Figure 3.18.

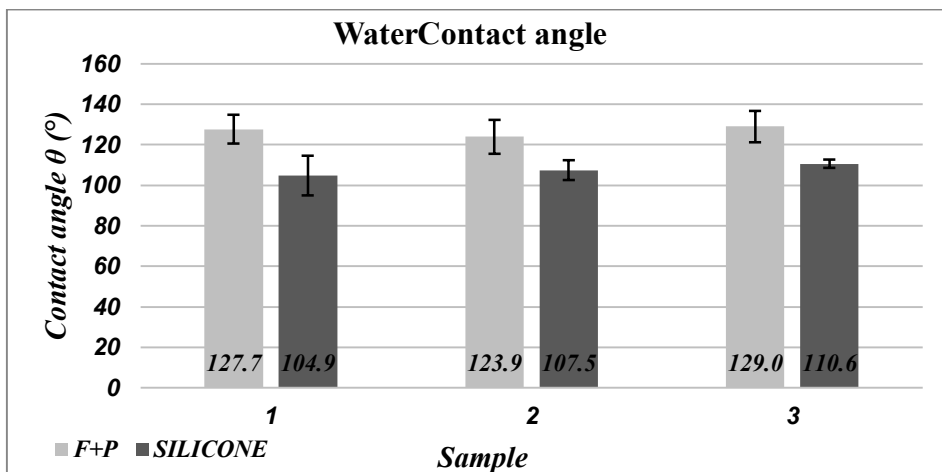


Figure 3.17 Water Contact angle: TiO_2 P+F and Silicone coated membrane

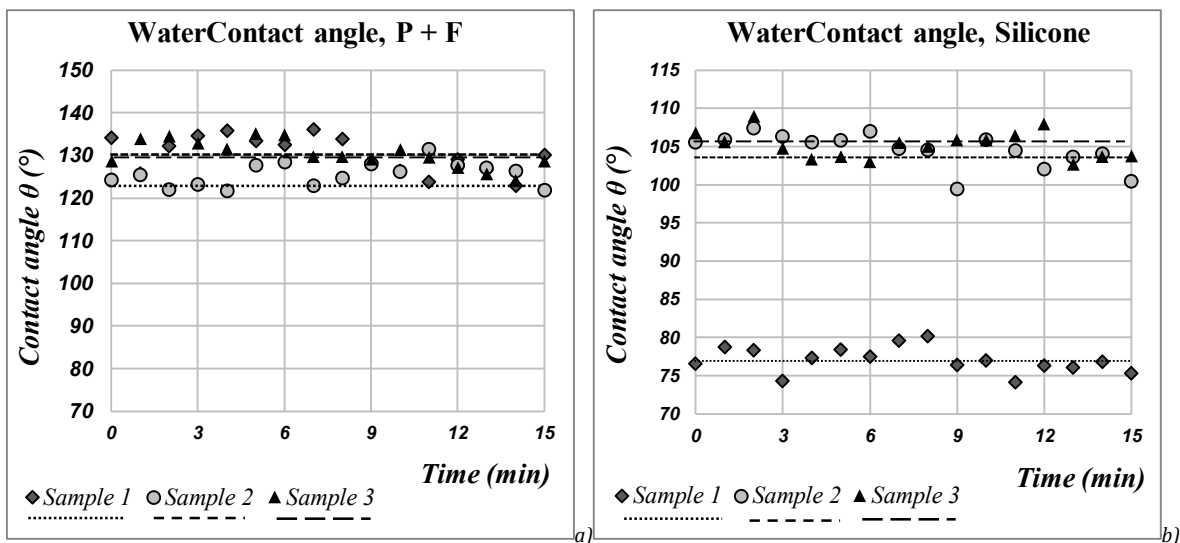


Figure 3.18 Water Contact angle vs. Time: TiO_2 P+F (a) and Silicone (b) coated membrane

The contact angles registered on the new membranes present a value around 126.9° with a standard deviation of 7.7° for the P+F samples and $107.7^\circ - 5.5^\circ$ for the silicone samples. Both membranes presents a clear hydrophobic character, being P + F exceptionally high.

The membranes present a constant value of contact angle during the first 15 minutes, going further in time could not be trustworthy due to evaporation phenomena.

3.2.2.2 *Water breakthrough.*

3.2.2.2.1 *Water flooding curves*

The test of water breakthrough were performed on all the four categories of coating described on the materials and methods section. Throughout the flooding curve, was evaluated the breakthrough conditions. Two pores sizes membranes, of all the coating material were tested at constant room temperature.

A particular coating material presents outstanding values of LEP. The membranes of this category were furtherly tested at higher temperatures. A complete study of the breaking through conditions, dependence with temperature, was performed.

On the tables below are reported the values of LEP if the test was performed at T_{cst} and LET if ΔP_{cst} . If the operative variable is the differential pressure, the operative constant temperature is reported on the column LET-T, otherwise the constant pressure is reported on LEP- ΔP column.

The experimental impossibility to obtain a continues flooding curve, made necessary a convention for the value of LEP-LET reported. This is the value of the previous condition, before the flooding start to take place (as described on section 3.1.3.4). The exact condition when the membrane begins to flood, when the permeability is no longer constant, could be not registered among the experimental values and so the error in the measurement ($\sigma_a+0.1$) is proportional to the experimental step took during the experimental procedure.

Last but not least is reported the corresponding flux to the breaking through condition. The higher this value is, the defects on the membrane are bigger. Meaning the membrane is not yet flooded but doesn't act as a proper barrier.

P coated membranes.

Table 3.7 Water breakthrough $\Delta P - T$ and correspondent flux at breakthrough: $TiO_2 - P$ coated membranes.

<i>Test</i>	<i>pore size (nm)</i>	<i>Sample</i>	<i>LEP-ΔP (bar)</i>	<i>$\sigma_a+0.1$ (bar)</i>	<i>LET-T (°C)</i>	<i>Jv at LEP ($dm^3h^{-1}m^{-2}$)</i>
<i>T cst</i>		<i>C1765</i>	<i><0.3</i>	<i>-</i>	<i>22.3</i>	<i>43.22</i>
<i>T cst</i>	<i>100</i>	<i>C1782</i>	<i><0.3</i>	<i>-</i>	<i>21.8</i>	<i>21.38</i>
<i>T cst</i>		<i>C1783</i>	<i><0.3</i>	<i>-</i>	<i>23.8</i>	<i>3.48</i>

F coated membranes.Table 3.8 Water breakthrough $\Delta P - T$ and correspondent flux at breakthrough: TiO₂ – F coated membranes.

<i>Test</i>	<i>pore size (nm)</i>	<i>Sample</i>	<i>LEP-ΔP (bar)</i>	<i>$\sigma_a+0.1$ (bar)</i>	<i>LET-T (°C)</i>	<i>Jv at LEP (dm³h⁻¹m⁻²)</i>
<i>T cst</i>		<i>C1899</i>	<i>n.p.</i>	-	-	-
<i>T cst</i>	<i>100</i>	<i>C1900</i>	<i>3.1</i>	<i>0.3</i>	<i>21.5</i>	<i>61.85</i>
<i>T cst</i>		<i>C1901</i>	<i>2.0</i>	<i>0.6</i>	<i>22.3</i>	<i>1.53</i>
<i>T cst</i>		<i>C1904</i>	<i>2.6</i>	<i>0.6</i>	<i>22.1</i>	<i>1.50</i>
<i>T cst</i>	<i>250</i>	<i>C1905</i>	<i>3.6</i>	<i>0.4</i>	<i>23.9</i>	<i>3.78</i>
<i>T cst</i>		<i>C1906</i>	<i>3.1</i>	<i>0.2</i>	<i>23.0</i>	<i>2.62</i>

F modified coated membranes.Table 3.9 Water breakthrough $\Delta P - T$ and correspondent flux at breakthrough: TiO₂ – F (modified) coated membranes.

<i>Test</i>	<i>pore size (nm)</i>	<i>Sample</i>	<i>LEP-ΔP (bar)</i>	<i>$\sigma_a+0.1$ (bar)</i>	<i>LET-T (°C)</i>	<i>Jv at LEP (dm³h⁻¹m⁻²)</i>
<i>T cst</i>		<i>C1989</i>	<i>1.6</i>	<i>0.2</i>	<i>23.9</i>	<i>0.14</i>
<i>T cst</i>	<i>100</i>	<i>C1990</i>	<i>1.8</i>	<i>0.1</i>	<i>24.5</i>	<i>3.46</i>
<i>T cst</i>		<i>C1991</i>	<i>3.35</i>	<i>0.1</i>	<i>25.0</i>	<i>0.04</i>
<i>T cst</i>		<i>C1994</i>	<i>n.p.</i>	-	-	-
<i>T cst</i>	<i>250</i>	<i>C1995</i>	<i>2.1</i>	<i>0.6</i>	<i>22.8</i>	<i>0.12</i>
<i>T cst</i>		<i>C1996</i>	<i>n.p.</i>	-	-	-

Silicone-coated membranesTable 3.10 Water breakthrough $\Delta P - T$ and correspondent flux at breakthrough: TiO₂ – Silicone coated membranes.

<i>Test</i>	<i>pore size (nm)</i>	<i>Sample</i>	<i>LEP-ΔP (bar)</i>	<i>$\sigma_a+0.1$ (bar)</i>	<i>LET-T (°C)</i>	<i>Jv at LEP (dm³h⁻¹m⁻²)</i>
<i>T cst</i>		<i>C2019</i>	<i>3.6</i>	<i>0.3</i>	<i>23.0</i>	<i>0.13</i>
<i>T cst</i>		<i>C2020</i>	<i><0.4</i>	-	<i>25.5</i>	<i>2.08</i>
<i>T cst</i>	<i>100</i>	<i>C2021</i>	<i><0.5</i>	-	<i>24.8</i>	<i>0.07</i>
<i>T cst</i>		<i>C2037</i>	<i><0.6</i>	-	<i>22.5</i>	<i>7.31</i>
<i>T cst</i>		<i>C2038</i>	<i>n.p.</i>	-	-	-
<i>T cst</i>		<i>C2024</i>	<i>3.5</i>	<i>0.5</i>	<i>23.0</i>	<i>0.71</i>
<i>T cst</i>		<i>C2025</i>	<i>3.5</i>	<i>0.5</i>	<i>24.7</i>	<i>1.41</i>
<i>T cst</i>	<i>250</i>	<i>C2026</i>	<i>3.2</i>	<i>0.9</i>	<i>22.8</i>	<i>1.63</i>
<i>T cst</i>		<i>C2040</i>	<i>3.1</i>	<i>0.3</i>	<i>23.8</i>	<i>1.31</i>
<i>T cst</i>		<i>C2041</i>	<i>2.3</i>	<i>0.7</i>	<i>23.6</i>	<i>0.08</i>

P+F coated membranesTable 3.11 Water breakthrough $\Delta P - T$ and correspondent flux at breakthrough: $TiO_2 - P+F$ coated membranes. Pore size 100 b1 and b2 corresponds to 2 different batches.

<i>Test</i>	<i>pore size (nm)</i>	<i>Sample</i>	<i>LEP-ΔP (bar)</i>	<i>$\sigma_a+0.1$ (bar)</i>	<i>LET-T (°C)</i>	<i>Jv at LEP (dm³h⁻¹m⁻²)</i>
<i>T cst</i>		<i>C1919</i>	<i>>6.5</i>	<i>-</i>	<i>23.4</i>	<i>-</i>
<i>T cst</i>		<i>C1920</i>	<i>>6.0</i>	<i>-</i>	<i>22.6</i>	<i>-</i>
<i>T cst</i>	<i>100 (b1)</i>	<i>C1921</i>	<i>>5.2</i>	<i>-</i>	<i>60.0</i>	<i>-</i>
<i>T cst</i>		<i>C2043</i>	<i>5.1</i>	<i>0.1</i>	<i>60.0</i>	<i>0.32</i>
<i>T cst</i>		<i>C2044</i>	<i>>5.7</i>	<i>-</i>	<i>60.0</i>	<i>-</i>
<i>T cst</i>		<i>C2515</i>	<i>3.9</i>	<i>0.5</i>	<i>60.0</i>	<i>0.11</i>
<i>T cst</i>		<i>C2516</i>	<i>3.3</i>	<i>0.1</i>	<i>60.0</i>	<i>0.35</i>
<i>T cst</i>	<i>100(b2)</i>	<i>C2518</i>	<i>2.6</i>	<i>0.3</i>	<i>60.0</i>	<i>0.18</i>
<i>T cst</i>		<i>C2519</i>	<i>2.7</i>	<i>0.3</i>	<i>60.0</i>	<i>0.16</i>
<i>T cst</i>		<i>C2521</i>	<i>2.7</i>	<i>0.3</i>	<i>60.0</i>	<i>0.37</i>
<i>T cst</i>		<i>C2522</i>	<i>2.5</i>	<i>0.3</i>	<i>60.0</i>	<i>1.73</i>
<i>T cst</i>		<i>C1924</i>	<i>4.4</i>	<i>0.6</i>	<i>23.8</i>	<i>0.22</i>
<i>T cst</i>		<i>C1925</i>	<i>4.5</i>	<i>0.8</i>	<i>23.3</i>	<i>8.15</i>
<i>T cst</i>	<i>250</i>	<i>C1926</i>	<i>3.5</i>	<i>0.8</i>	<i>23.0</i>	<i>0.17</i>
<i>T cst</i>		<i>C2046</i>	<i>3.7</i>	<i>0.6</i>	<i>22.0</i>	<i>0.65</i>
<i>T cst</i>		<i>C2047</i>	<i>1.8</i>	<i>0.5</i>	<i>22.5</i>	<i>0.34</i>

The breakthrough results for some of the categories are quite poor, like the P coated membranes, was not possible to measure the LEP. The membranes were already flooded at low values of differential pressure. Even more, from the beginning of the test, the flux were remarkably high.

The case of the F and F modified coated membranes is very interesting. In both cases the membranes presented medium-high values of LEP.

The LEP values for the silicon coated membranes were interesting (moderate LEP values and high reproducibility of the results) for the 250nm pore size membranes while the 100 nm flooded at very low transmembrane pressure values.

Finally the P+F coated membranes presented at room temperature, indeed in some cases (100 nm membranes) it was not possible to achieved the flooding at the maximum operation conditions of the system (at room temperature). It was decided to perform the test at a higher temperature (60 °C), and even at this temperature the results were satisfactory.

The P+F coating was interesting to be tested at higher temperatures, even temperatures over the fluid boiling point. Particularly the 100 nm membranes.

For different reasons, some inherent to the project, of the eleven membranes samples only four were available to be tested at higher temperatures.

Two membranes were from the bath “b1” the others are from the batch “b2”.

The results of the flooding curves at different temperatures and at constant differential pressure are presented on the figures bellow. Each figure presents the results of the test performed on the single membrane and the table next to the figures summarized the conditions of Temperature and differential pressure when the water breaks through.

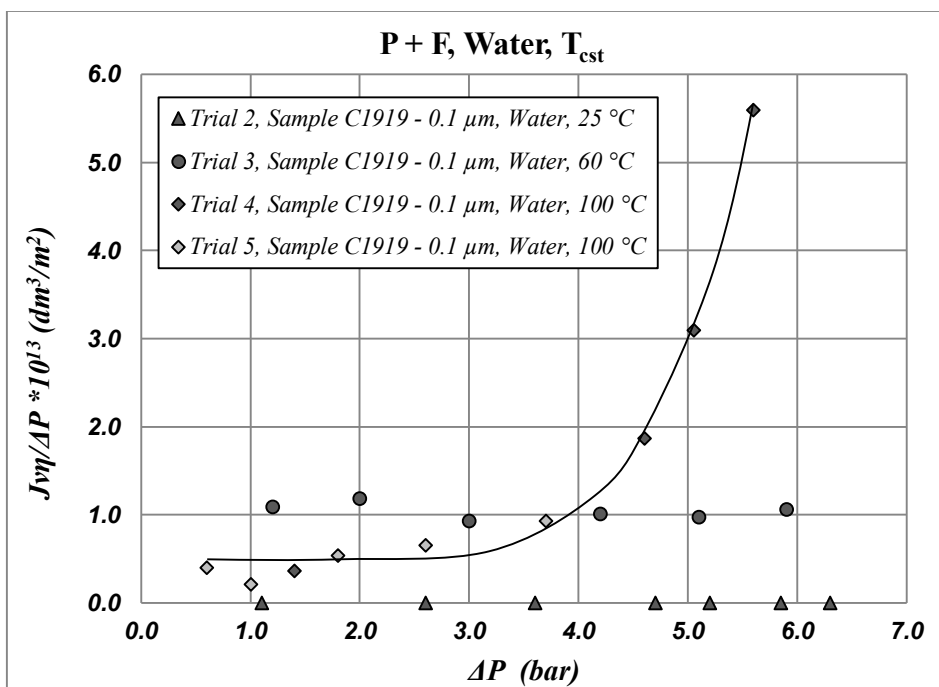


Figure 3.19 P+F coated sample C1919: flooding curve at various constant Temperature.

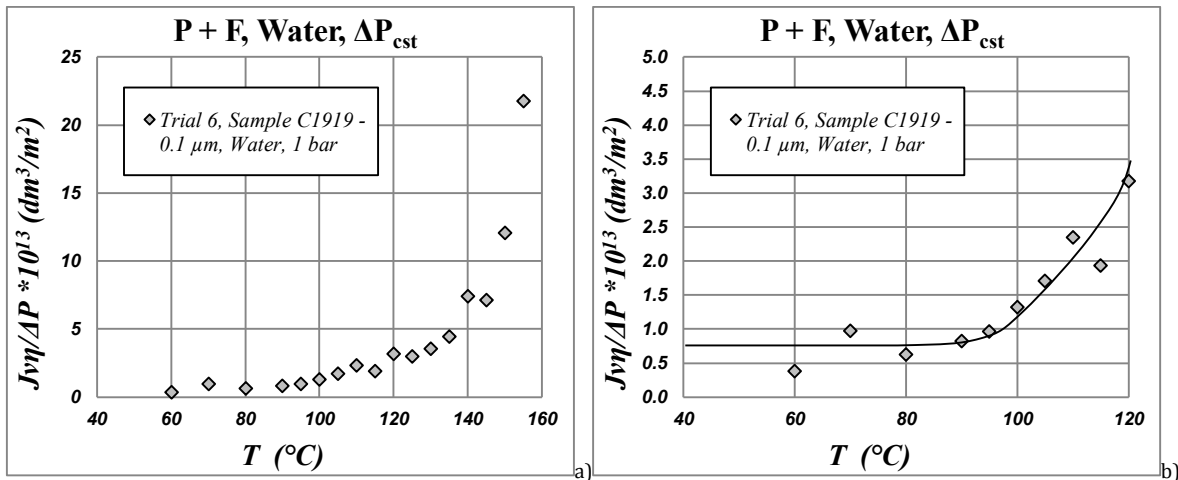


Figure 3.20 P+F coated sample C1919: flooding curve at constant transmembrane pressure equal to 1 bar

Table 3.12 Water breakthrough $\Delta P - T$ and correspondent flux at breakthrough: $\text{TiO}_2 - \text{P+F}$ coated membranes. Sample C1919.

Test	pore size (nm)	Sample	LEP- ΔP (bar)	$\sigma_a+0.1$ (bar)	LET-T ($^\circ\text{C}$)	Jv at LEP ($\text{dm}^3\text{h}^{-1}\text{m}^{-2}$)
T cst			>6.5	-	23.4	-
T cst			>6.3	-	25.0	-
T cst	100	C1919	>5.9	-	59.9	-
T cst			1.4	2.7	100	0.05
T cst			2.6	0.1	100	0.08
ΔP cst			1.0	1.0 ($^\circ\text{C}$)	95	0.09

On figures Figure 3.19 and Figure 3.20 are presented the flooding curves at the constant temperatures of 25, 60, and 100 °C and the flooding curve at differential pressure of 1 bar. At the moment, when the test on the sample C1919 were performed, the maximum differential pressure of the system was 6-7 bar. At the maximum differential pressure at room temperature and 60 °C the membranes were not flooded. Only at 100 °C was possible to flood the membrane.

For the five tests performed on the membrane C1919 the value of permeability ($Jv\eta/\Delta P$) are very similar one to the other (including the test vs. temperature) around $0.7 \text{ E-13 dm}^3/\text{m}^2$. This result confirmed the hypothesis made during the development of the Data reduction (section 3.1.3.3) process.

The test in function of temperature are very interesting, even if the experimental procedure is much more difficult and the stabilization times are longer it is clear that the permeability keeps constant in the low temperature range, the membrane starts flooding around 95 °C.

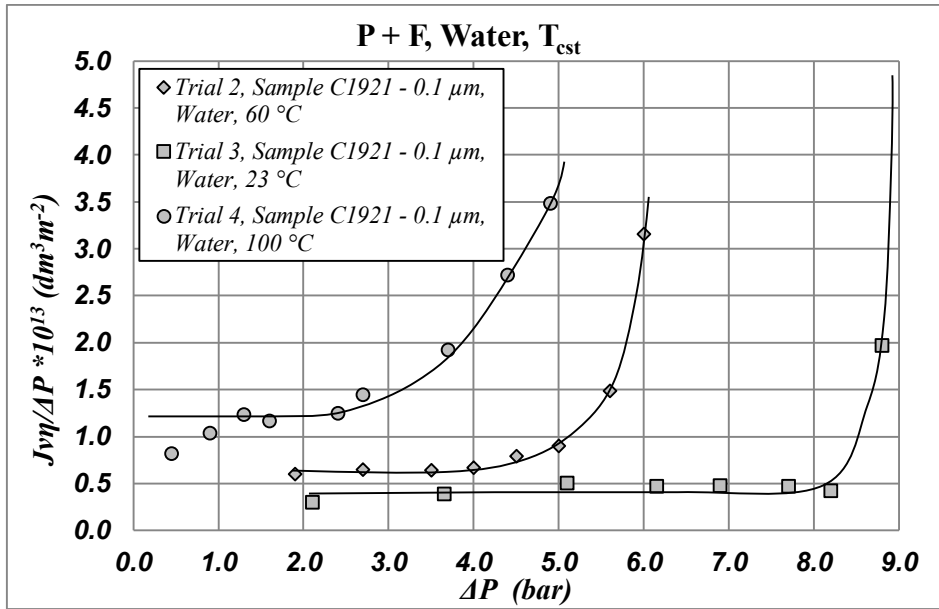


Figure 3.21 P+F coated sample C1921: flooding curve at various constant Temperature

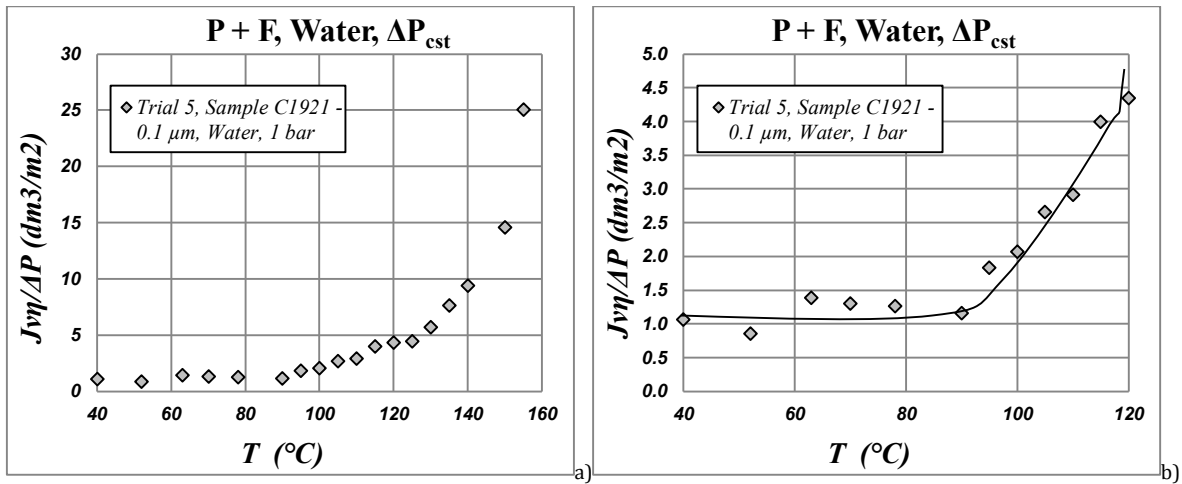


Figure 3.22 P+F coated sample C1921: flooding curve at constant transmembrane pressure equal to 1 bar

Table 3.13 Water breakthrough $\Delta P - T$ and correspondent flux at breakthrough: $TiO_2 - P+F$ coated membranes. Sample C1921.

Test	pore size (nm)	Sample	LEP- ΔP (bar)	$\sigma_a+0.1$ (bar)	LET-T (°C)	J_v at LEP ($dm^3 h^{-1} m^{-2}$)
T_{cst}			>5.2	-	60.0	C1921
T_{cst}			4.5	0.5	60.0	0.27
T_{cst}	100	C1921	8.2	0.6	21.8	0.02
T_{cst}			2.4	0.3	100.0	0.19
ΔP_{cst}			1.0	1.0 (°C)	90.0	0.13

The sample C1921 and C2515 gather the most comprehensive results. It should be remember that this membranes belongs to different batches (the producer reports minor changes on the coating process).

In both cases was possible to perform a complete set of test at different temperatures. The membrane was flooded each time, obtaining the value of differential pressure when the water breaks through. A total of three point, for the sample C1921 and five point for the sample C2515 were achieved. Is remarkable how the flooding curve shift to lower values of pressure keeping the same shape as predicted on the data reduction section (

Figure 3.9). Also for this membranes can be appreciated that the initial constant permeability value ($Jv\eta/\Delta P$) is similar on both membranes along the test performed.

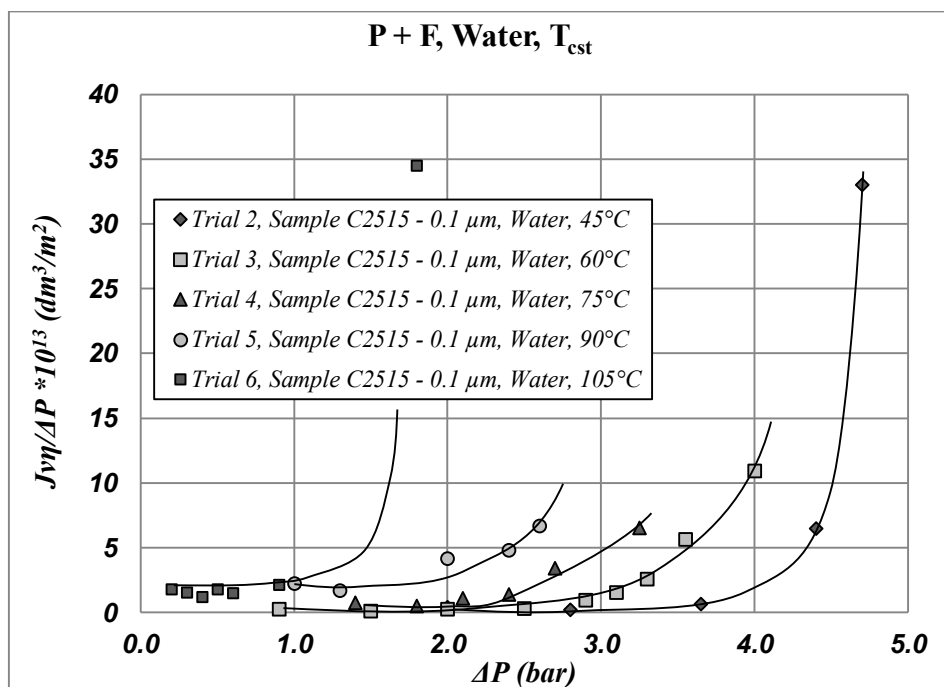


Figure 3.23 P+F coated sample C2515: flooding curve at various constant Temperature

Table 3.14 Water breakthrough $\Delta P - T$ and correspondent flux at breakthrough: $TiO_2 - P+F$ coated membranes. Sample C2515

Test	pore size (nm)	Sample	LEP- ΔP (bar)	$\sigma_a+0.1$ (bar)	LET-T (°C)	Jv at LEP ($dm^3 h^{-1} m^{-2}$)
T cst			3.9	0.5	60.0	0.11
T cst			3.7	0.5	45	0.15
T cst	100	C2515	2.5	0.3	60	0.06
T cst			2.1	0.3	75	0.22
T cst			1.3	0.7	90	0.25
T cst			0.6	0.3	105	0.12

The tests with samples C2515 and C2516 put in evidence a phenomena not seen before, due to the defined procedure.

It is evident on figures Figure 3.23 and Figure 3.24 that after the first trial some changes came on the coating material. The second trial at the same temperature showed a reduction in the hydrophobicity.

The results of sample C2516 are very close to the ones of sample C2515. However the few number of trials don't allow to arrive to further conclusions.

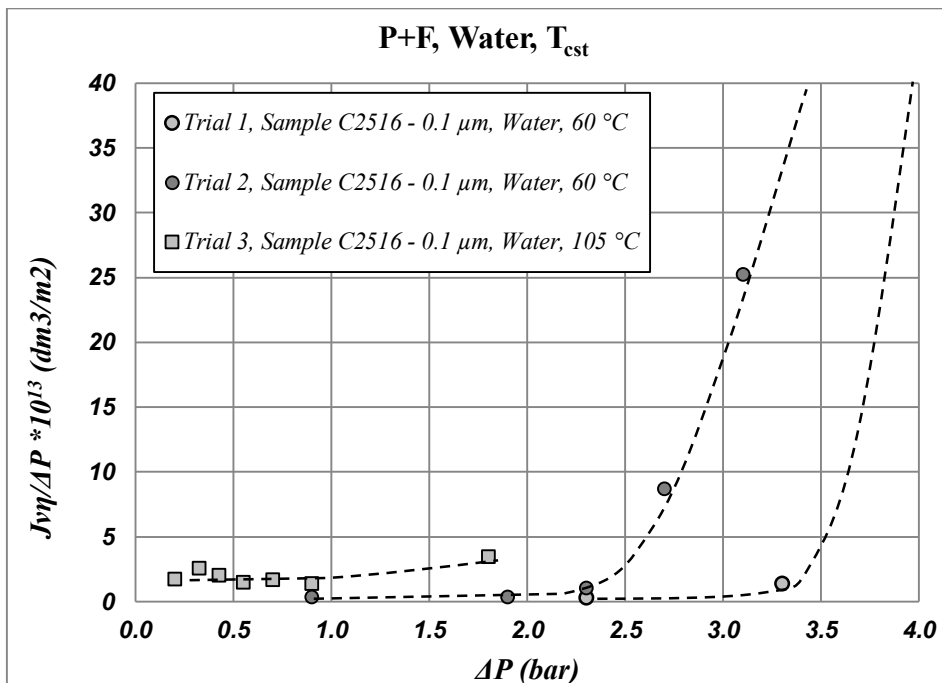


Figure 3.24 P+F coated sample C2516: flooding curve at various constant Temperature

Table 3.15 Water breakthrough $\Delta P - T$ and correspondent flux at breakthrough: $\text{TiO}_2 - \text{P+F}$ coated membranes. Sample C2516.

Test	pore size (nm)	Sample	LEP- ΔP (bar)	$\sigma_a+0.1$ (bar)	LET-T (°C)	Jv at LEP ($\text{dm}^3\text{h}^{-1}\text{m}^{-2}$)
T cst			3.3	0.1	60	0.35
T cst	100	C2516	2.3	0.3	60	0.05
T cst			0.9	0.1	105	0.17

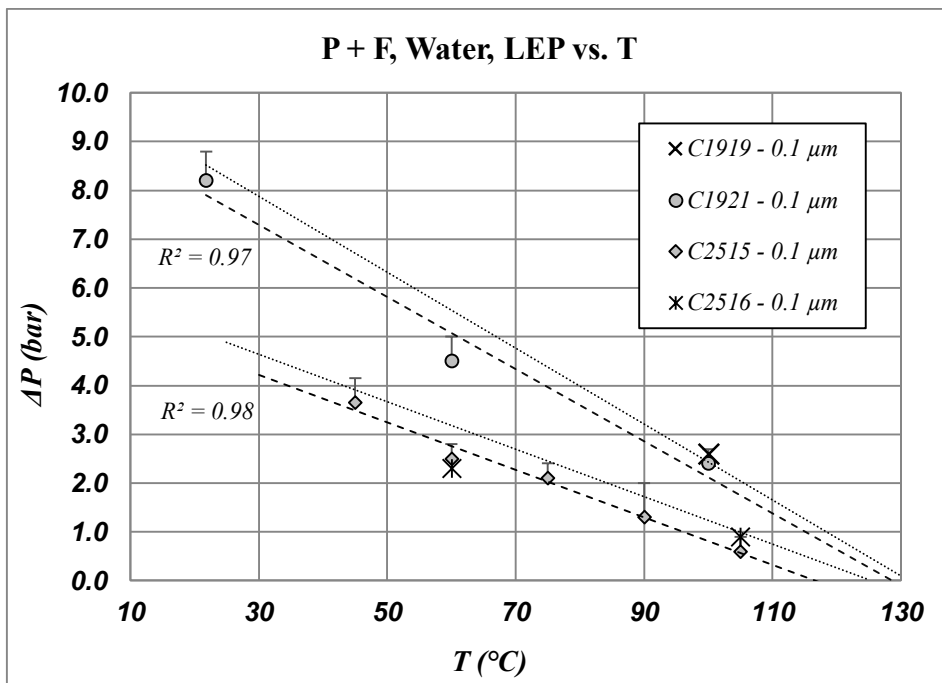


Figure 3.25 P+F coated values of LEP vs. operative Temperature: Samples C1921 and C2515

The Figure 3.25 summarized the results of the set of test performed for the study of the hydrophobic character. The test evaluate the change in the hydrophobic character with Temperature, through the flooding curve test and the value of breakthrough.

For two membranes was possible to obtain a set of data of transmembrane pressure of breakthrough (LEP) vs. the operative temperature. The second couple of membranes give few data that can be plotted alongside the membrane of the same category (batch). The experimental data and the fitting lines are reported on the figure above.

The experimental data of each sample can be clearly fitted with a linear regression line with a good coefficient of determination (R^2). Particularly the sample with the biggest set of data. Both the fitting lines seem to go towards a common point, between 120 and 130 °C.

3.3 Analysis and discussion.

Through the availability study for the proper membranes to be used on a particular Sweeping Gas Membrane Distillation (SGMD) process. Was studied the effect of temperature on the water wettability of hydrophobic macroporous membranes. The process requires the membranes to withstand elevated temperatures (between 100 and 130 °C) and highly concentrated salt solutions, maintaining the hydrophobic character.

During this study were evaluated different membranes, among them, polymeric commercial membranes (PTFE) and tailored ceramic membranes (TiO₂), produced for the project and coated with hydrophobic polymers, to give a hydrophobic character to the ceramic matrix.

The hydrophobic character and the wettability of materials and particularly membrane material, has been evaluated across two simple methods widely used and studied. The surface contact angle and the breakthrough pressure. Nevertheless the Temperature effect on the hydrophobic character hasn't been properly studied and is not well understood.

Both techniques are deeply related, in both, the equilibrium of interfacial forces rules the affinity of the solid and the liquid (in our case of interest, water) and so the wettability. But, the contact angle is a measure of the material surface affinity, which takes into account the material roughness, porosity and the contact area between the solid and the liquid. On the other hand the breakthrough pressure is a process parameter, which fix the maximum transmembrane pressure before the membrane pores start flooding. Usually represented as the force equilibrium on a capillary pore, the breakthrough pressure relates the diameter of the capillary, the interface equilibrium forces and macroscopic forces like transmembrane pressure difference, embodied on the Laplace-Young equation.

$$\Delta P = \frac{2\gamma_{lv} \cos \theta}{r_p} \quad (3.10)$$

The Laplace Young equation relates geometrical (r_p), physical (materials thermodynamic properties) and operative parameters. All of them can be modified by the effect of temperature. To understand the whole, each one should be studied separately.

$$\gamma_{lv} \cos \theta = \gamma_{sv} - \gamma_{sl} \quad (3.11)$$

The contact angle is a macroscopic measurement, representing an interfacial molecular equilibrium. The experimental angle measured is not truly the result of the interfacial forces, as many parameters are involved in the measurement and are not accounted on the Young's expression (3.11), especially if the surface is porous, like a membrane. Change in the surface like, roughness, porosities or materials matrix can change the contact angle diverting the experimental value from the theoretical. The contact angle measurements should be considered as a macroscopic indication of the hydrophobic character. Though the experimental values are

not always trustworthy to perform predictions at microscopic level, as for example on the Laplace young equation. Often the surface contact angle has divert from the contact angle calculated from the breakthrough pressure.

Experimentally, the effect of temperature on contact angle has been difficult to correlate, particularly with water which proximity to boiling point made the measurement technically demanding (see section 2.4.5.5). Furthermore, the results have not been compared with models confirming the experimental observations.

During this study were performed contact angle measurements on polymeric membrane (3.2.1.1) and on coated ceramic membranes 3.2.2.1. On both is confirmed a well-defined hydrophobic character. But, even if, on the polymeric membranes were performed test vs. temperature the results are going to be considered only as the confirmation of the macroscopic hydrophobic character and on the ceramic membranes as an initial selection technique for the membranes of the process of interest.

The results of contact angle vs. temperature, obtained for water and glycerol on PTFE membranes suggest that these changed on a linear fashion way and that water and glycerol behave similarly. However the reasons exposed previously and the fact that membranes morphology changes with temperature made the results untrustworthy.

The contact angle measurements suggest that, the ceramic membranes with the surface coating P+F are the most interesting. The mean contact angle, at room temperature is close to 130 °C. This is an outstanding value, suggesting the possibility of further and deeper studies.

How do the breakthrough pressure change with Temperature?

Even if the contact angle experimental measurements are untrustworthy for predicting the wettability change with temperature. This doesn't mean that shouldn't be taken a theoretical approach. The contact angle, as the interfacial forces equilibrium, will depend only on how change this interfacial forces.

The approach taken by Lyklema (1999) (explained on section 2.4.4.2) entail that all the interfacial surface tensions (Liquid-Vapor, Liquid-Liquid, Liquid-Solid and Solid-Vapor) changes with temperature are nearly constant. This is true if the excess entropy of the system remains constant, consideration confirmed by Weber & Stanjek (2014).

$$\left| \frac{\partial \gamma_{\alpha\beta}}{\partial T} \right|_p \approx cst \quad (3.12)$$

The fact that all interfacial tensions can be assumed approximately linearly dependent of the temperature (this assumption can be confirmed at least for liquids), made the breakthrough predictions simpler.

Though, the magnitude of the interfacial tension changes is unknown, for solid-liquid and solid-vapor, is known the fact that the addition of the changes will be a constant magnitude and so the product of the surface tension and the contact angle cosine.

$$\gamma_{lv} \cos \theta = \gamma_{sv} - \gamma_{sl} \approx mT + b \quad (3.13)$$

The expression above can be directly replaced on the Laplace-Young equation. Taking us to the conclusion that the minimum breakthrough pressure is linearly dependent of the temperature, only if the maximum pore radius of the membrane is constant.

$$\Delta P_{min} = \frac{2\gamma_{lv} \cos \theta}{r_{p,max}} \approx \frac{(mT + b)}{r_{p,max}} \quad (3.14)$$

This can be the case of ceramic membranes, contrary to polymeric membranes, the pore size distribution does not have critical changes when the temperature is increased. Complementary to the mechanical membrane properties, the data reduction proposed on section 3.1.3.3 made the analysis of the flooding curves independent of the process conditions and so the determination of the breakthrough conditions.

This is the case of the results obtained for the P+F coated Titania membranes. On Figure 3.25 is evident the linear dependence of breakthrough pressure with the test temperature. The results were confirmed on the samples where this analysis was performed.

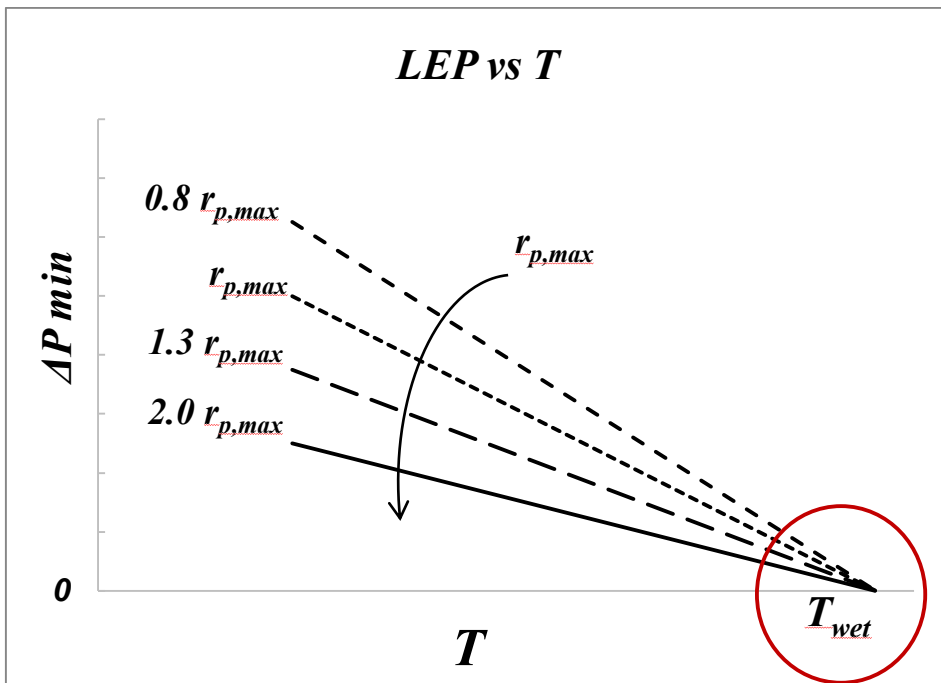


Figure 3.26 Wetting temperature indication.

However there are some differences between the results of two groups of membranes, even if the nominal pore size and coating are the same. This is indicative of difference on the maximum pore size and not of changes on the hydrophobic character of the membrane.

The expression on equation (3.14) indicates that the function will arrive to zero at a value of temperature independently of the pore radius. Different membranes with same hydrophobic character but different maximum pore radius will go towards, zero breakthrough pressure at the same value of temperature indicating a spontaneous membrane wetting. We have defined this value the **wetting temperature**, a unique value for the couple liquid – solid material. The wetting temperature indicates an operative limit for the process with this membranes independently of the pore size. This effect has been illustrated theoretically on Figure 3.26 and is the same result observed on the experimental results of Figure 3.25.

The same results were observed on the polymeric membranes. The results of section 3.2.1.2.1 show a decrease on the breakthrough pressure and the irreversible modification of the membrane pore size distribution after the LEP was measured at temperatures above 50 °C. Pore size distribution modification after an annealing process was registered previously by Saffaini et al (2013). It was observed a permanent modification of the polymeric matrix structure and that mean pore size increases for higher annealing temperature.

The test where breakthrough pressure was measured at room temperature after a previous test at higher temperature, especially above 50 °C, showed a reduction on the breakthrough pressure. The higher was the reduction when the temperature of the previous test was higher.

If the pore dilatation during tests at temperatures above 50 °C is considered completely irreversible. The line that fits the room temperature value of LEP with the previous results at high T (Above 50°C) were extrapolated in order to find the wetting temperature.

The lines were fit for the test at temperature higher than 50 °C (50, 60 and 70 °C). On all cases the extrapolation of the fitted lines goes towards the same value. For the same membrane the lines met at the same wetting temperature and further more for three different membranes this temperature was very close to 170 °C and only one sample the lines met at a temperature close to 160 °C.

The trend of the LEP vs. T for the PTFE membranes indicates the LEP might reach the value of zero at a temperature well below the 160 – 170 °C indicated previously. Nevertheless PTFE membranes, with similar pore size, has been used at temperature close to 120 °C (Singh and Sirkar 2014) without suffering wetting or leakages. It should be lay down that during the process the absolute transmembrane pressure was always close to zero.

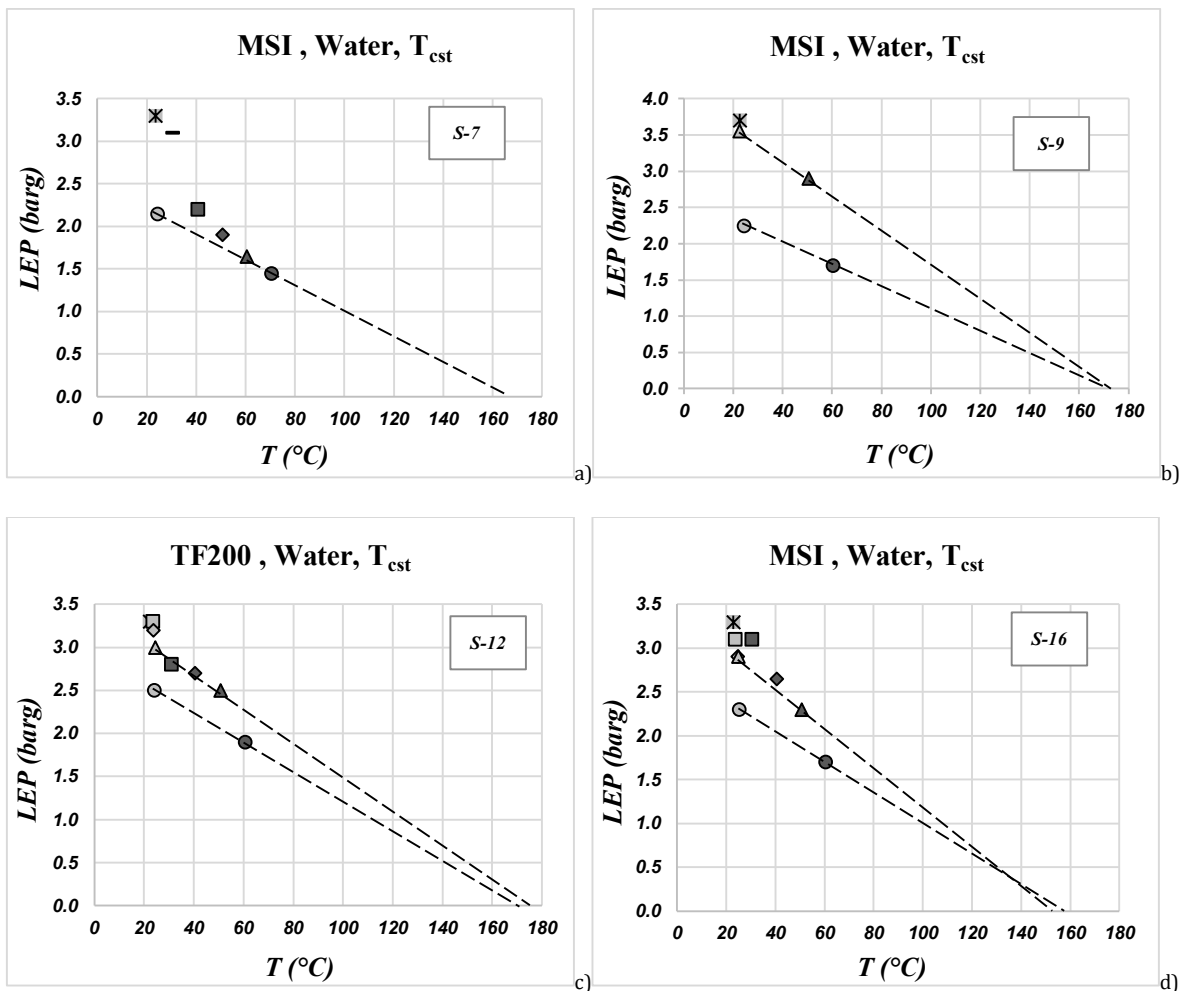


Figure 3.27 Test of LEP on four samples of PTFE, test performed at increasing test temperature. Extrapolation to wetting Temperature.

The results obtain from the tests at constant differential pressure show that, after the theoretical wetting temperature the permeability is not constant as should be if all the membrane pores are completely flooded. However should be remember that the analysis was performed assuming the pores cylindrical (smooth), a single contact angle value and a uniform porous matrix (same material). This is not the case of the ceramic coated membrane, where the coating deposition is not uniform along the membrane and the pores are not cylindrical. Never the less is evident that between 120 and 130 °C the permeability increase at a rate much higher than after the LET.

4 *Conclusions*

The main objective of this PhD work is to evaluate the general availability for the implementation of the membrane contactors (MC) technology, to the stripping of the reaction product of an endothermic equilibrium reaction. The key parameter for the implementation of the MC technology to this process is the existence of membranes and membrane modules able to work at the process conditions for the development of the chemical reaction, particularly the high temperature when the reaction products start to be available for an effective stripping process.

The membrane defines the barrier between the two phases in contact and avoids the phase mixing or dispersion. The barrier effect is generally performed by the low affinity of the membrane to one or both of the phases in contact, hydrophobic membranes are used to hold aqueous phases and hydrophilic membranes are used to hold organic phases. The barrier effect must be permanent in order to have a successful operation.

The studied application involves the mass exchange operation between a liquid phase and a gas. It was selected to work with hydrophobic membranes and higher pressure on the aqueous phase in order to keep the phases separated. The hydrophobic membranes are preferable as the diffusive mass transport through a gas (phase inside the membrane pores) is much more effective than through a liquid matrix, furthermore, phenomena like fouling by crystallization of the salt solution is avoid inside the pores.

The membrane hydrophobic character is a matter of great importance for the process reliability. If liquid phase floods the membrane, partially or completely, the complete operation might be compromised. After the flooding we can verify the transport of non-volatile components, phases mixing, the membrane fouling and the decrease of mass transport.

Identify the main characteristics that made the membrane suitable to be used on a particular application was the central objective of the first part of this thesis, particularly the hydrophobic character of the macroporous membranes and its dependency with the temperature. A deep study of the hydrophobic character was performed, the theoretical bases, the key parameters that modifies the hydrophobic behavior and the experimental methods to evaluate it, were the focus of the state of the art study.

The study of the state of the art allows to identify the necessity of deeper studies on the matter of hydrophobic character dependence with temperature, especially with water at temperatures above the bubble point.

The most diffused methodologies for the measurement of the hydrophobic character are the liquid contact angle over flat surfaces and the break through pressure of a non-wetting phase. Both methodologies provide information about the affinity of the membrane with a liquid and allow to obtain practical information for the selection of a membrane and the operative limits during the MC operation. Both methodologies have their pros and cons, but there is an evident

lack on both procedures, to measure the hydrophobic character at higher temperatures. This have shown some contradictory results on the study of the hydrophobic character vs temperature.

Some measurement of water contact angle over different surfaces, including polymeric an metallic surfaces, have leave the doubt, that water contact angle at higher temperatures change the linear trend, many times reported, in function of Temperature. The results of this experiments have shown that a certain value of temperature, water contact angle decrease rapidly, approaching to zero at values of temperature well below the critical temperature.

The measurements of contact angle might be the most representative parameter of the hydrophobic character. However the wide hysteresis phenomena, present in pretty much all samples, the difficulties of measure it on samples of different shapes than flat surfaces and the very sophisticate apparatus to perform measurements at temperature above the boiling point made of the contact angle hard to measure and a parameter with many uncertainties. On the other hand the liquid entry pressure is a parameter that can adequately evaluate the hydrophobic character of a membrane, and even more, is a direct parameter of the membrane contactors operation.

On the study of the state of the art of characterization method for membrane contactors at high temperature, it was evident the lack of a suitable method to evaluate on a simple and economic way the hydrophobic character. Especially there are no reference for the measurement of the break through pressure or liquid entry pressure (LEP) at temperatures above 70 °C (Saffarini, et al. 2013). Even more, the method use to perform this measurements is not suitable to be used at higher temperature because evaporation phenomena across the membrane stars to be relevant.

With this aim the liquid permeation technique was modified to perform tests at higher temperatures and, in an innovative way, in function of temperature at constant differential pressure.

In order to perform this tests, the regular equipment used to perform the flooding curves was modify and the complete procedure was redefined. With this configuration and procedure we were able to perform for the first time ever the flooding curve at temperatures above the fluid normal bubble point and obtain the value of the break through pressure-Liquid entry pressure. With the same equipment configuration and changing the procedure, was proposed to perform the flooding curve in function of the temperature, at constant transmembrane pressure and was defined a new operative parameter of breakthrough, the LIQUID ENTRY TEMPERATURE (LET).

With the aim of comparing the results at different temperatures and obtain correlations of LEP vs T was defined a successful new way to elaborate the flooding curve data, and the concept itself of breakthrough was redefined, taking into account the experimental results and avoiding and arbitrary definition like the one propose by Garcia-Payo and colleagues.

The hydrophobic character was studied on commercial polymeric membrane and on prototype ceramic membranes, throughout the contact angle measurement and the flooding curve for the determination of LEP and LET.

The LEP and LET results with polymeric membranes were less trustworthy. The small membrane area generates a great dispersion in the experimental results and the temperature modifies the polymeric matrix (on a unique way for each membrane) and the pores morphological configuration. This last parameter was not considered on the data elaboration, focusing only on the hydrophobic character of the membranes. Never the less the test were useful to set up the experimental procedure comparing the results with the ones reported on literature.

Titania membranes coated with four different polymers were tested in order to characterize its hydrophobicity. Throughout the flooding curve, was evaluated the breakthrough conditions of all the coating material for two membrane pores sizes. The tests were performed at constant room temperature.

The membranes with coating material P+F presented remarkably high values of LEP. The membranes of this category were furtherly tested at higher temperatures. A complete study of the breaking through conditions, dependence with temperature, was performed.

For two membranes was possible to obtain a set of data of transmembrane pressure of breakthrough (LEP) vs. the operative temperature. A second couple of membranes give few data that can be plotted alongside the membrane of the same category (batch). The experimental data and the fitting lines are reported on the figure below.

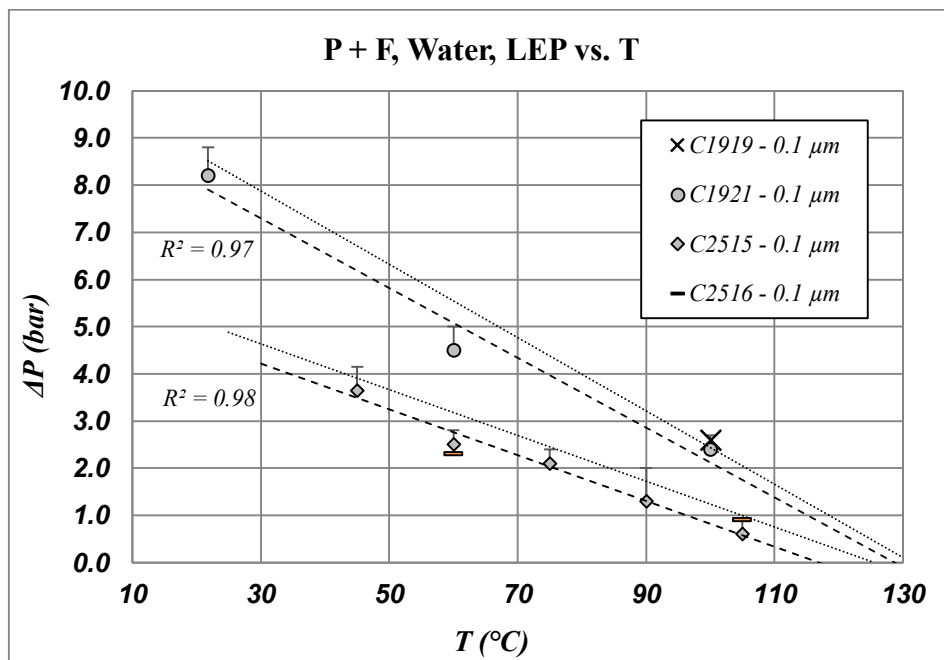


Figure 4.1 P+F coated values of LEP vs. operative Temperature: Samples C1921 and C2515

The experimental data of each sample was fitted with a linear regression line with a good coefficient of determination (R^2). Particularly the sample with the biggest set of data. Both the fitting lines seem to go towards a common point, between 120 and 130 °C.

The experimental results were analyzed through the theoretical background, defining a linear dependence of the pressure of breakthrough (LEP) with the operative temperature when the maximum pore radius of the membrane is constant (ceramic membranes).

Was defined a new operative parameter, the **wetting temperature**, a unique value for the couple liquid – solid material. The wetting temperature indicates the value of temperature when all the membrane pores get flooded, regardless the pore size. This is a clear operative limit for the membrane material independently of the pore size.

After the ceramic membranes results analysis, the results with polymeric membranes were reevaluated. These revalidate the observation of the wetting temperature when a permanent temperature deformation was assumed.

The search for a suitable membrane, to be used on the stripping of the reaction product of an endothermic equilibrium reaction, give as a result that: titania membranes coated with a particular hydrophobic layer, are the most performant membranes to work at high temperatures keeping its hydrophobicity even at temperatures above normal boiling point. Furthermore the search reveal a general trends of the hydrophobic character behavior in function of the temperature and identify a temperature limitation for each couple of membrane material and liquid.

5 List of Symbols

Symbol	Meaning
Kn	<i>Knudsen number</i>
λ	<i>Mean free path</i>
L_0	<i>Physical length scale</i>
d_p	<i>Pore diameter</i>
η	<i>Viscosity</i>
P	<i>Pressure</i>
ΔP	<i>Transmembrane pressure</i>
π	<i>Pi number</i>
R	<i>Universal gas constant</i>
T	<i>Temperature</i>
MW	<i>Molecular weight</i>
δ_{eff}	<i>Effective pore length</i>
$\dot{V} = Q$	<i>Volumetric flow rate</i>
\dot{n}	<i>Molar flow rate</i>
N_{tot}	<i>Number of pores in the membrane</i>
$\overline{d_p}$	<i>Mean pore diameter</i>
ε	<i>Membrane porosity</i>
δ	<i>Pore length</i>
χ	<i>Pore tortuosity</i>
P_m	<i>Average Pressure</i>
T_m	<i>Average Temperature</i>
S_l	<i>Membrane surface</i>
\dot{n}''	<i>Molar Flux</i>
K	<i>Overall membrane transport coefficient</i>
γ	<i>Interfacial tension</i>
θ	<i>Contact angle</i>
w_{adh}	<i>Work of adhesion</i>
w_{coh}	<i>Work of cohesion</i>

Φ	<i>Girafalco corrective factor</i>
γ^d	<i>Dispersion force</i>
β	<i>Li and Neumann fitting parameter</i>
γ_{SLV}	<i>Line tension</i>
r	<i>Drop radius</i>
θ'	<i>Apparent contact angle</i>
H	<i>Contact angle hysteresis</i>
θ_A	<i>Advancing contact angle</i>
θ_R	<i>Receding contact angle</i>
r_A	<i>Defined by equation (2.30)</i>
r_R	<i>Defined by equation (2.31)</i>
T_{co}	<i>Pseudo-critical temperature</i>
F_a^σ	<i>Excess Helmholtz free energy</i>
Γ_i	<i>Surface concentration of component i</i>
μ_i	<i>chemical potential of component i</i>
U_a^σ	<i>excess energy</i>
S_a^σ	<i>excess entropy</i>
ρ	<i>Density</i>
g	<i>Gravitational force</i>
h	<i>Liquid level</i>
F	<i>Force</i>
B	<i>Flotation force</i>
r_p	<i>Pore radius</i>
r_h	<i>Hydraulic radius</i>
R	<i>Radius of pore arc</i>
α	<i>Structure angle</i>
γ_{LV}^w	<i>Wetting surface tension</i>
Q_p	<i>Single pore volumetric flow rate</i>
L_p	<i>Liquid permeability</i>
$f(r)$	<i>Probability pore size funtion</i>
r_{max}	<i>Radius of the biggest membrane pore</i>

C_1	<i>Hydrophobic parameters constant equation (2.54)</i>
C_2	<i>Geometric parameters constant equation (2.56)</i>
Lp_{max}	<i>Permeability of the complete flooded membrane</i>
ΔP_0	<i>Transmembrane pressure to flood the half of the pore distribution</i>
ΔP_{cst}	<i>Transmembrane constant pressure</i>
T_{cst}	<i>Constant temperature</i>
Jv	<i>Volumetric flux</i>
N_p	<i>Number of flooded pores</i>
Lp_{min}	<i>Minimum membrane permeability</i>
t	<i>Time</i>
T_{wet}	<i>Wetting temperature</i>

6 Bibliography

- 3M Company. «Liqui-Cel.» www.liquicel.com/. January 2016. <http://www.liquicel.com/uploads/documents/2%205x8ExtraFlow-D59Rev16%204-15.pdf>.
- Adamson, Arthur W. «Potential distortion model for contact angle and spreading. II. Temperature dependent effects.» *Journal of Colloid And Interface Science* 44, n. 2 (1973): 273-281.
- Alami-Younssi, Saad, Carolin Kiefer, Andre Larbot, Michel Persin, e Jean Sarrazin. «Grafting γ alumina microporous membranes by organosilanes:: Characterisation by pervaporation.» *Journal of Membrane Science* 143, n. 1-2 (1998): 27–36.
- Berim, G. O., and E. Ruckenstein. "Universality in the dependence of the drop contact angle on liquid-solid interactions and temperature obtain by the density funtional theory." *The European Physical Journal Special Topics* 197 (2011): 163-178.
- Bernardin, John D, Issam A Mudawar, Christopher B Walsh, and Elias I Franses. "Contact angle temperature dependence for water droplets on practical aluminum surfaces." *International Journal of Heat and Mass Transfer* 40, no. 5 (1997): 1017-1033.
- Budziak, C J, E I Vargha-Butler, and A W Neeumann. "Temperature dependence of contact angles on elastomers." *Journal of applied polymers science* 42 (1991): 1959-1964.
- Calvo, José Ignacio, Aldo Bottino, Gustavo Capannelli, e Antonio Hernández. «Pore size distribution of ceramic UF membranes by liquid-liquid displacement porosimetry.» *Journal of membrane science* 310 (2008): 531-538.
- Coats, A. W., and John P. Redfern. "Thermogravimetric analysis. A review." *The Analyst* 88, no. 1053 (1963): 906-924.
- Courel, Mathilde, Emmanuel Tronel-Peyroz, Gilbert Marcel Rios, Manuel Dornier, e Max Reynes. «The problem of membrane characterization for the process of osmotic distillation.» *Desalination* 140, n. 1 (2001): 15-25.
- Drelich, Jaroslaw W, Jan D Miller, and Robert J Good. "The effect of drop (bubble) size on advancing and receding contact angles for heterogeneous and rough solid surfaces as observed with sessile-drop and captive-bubble techniques." *Journal of Colloid and Interface Science* 179, no. 1 (1996): 37-50.
- Drelich, Jaroslaw W., e Jan D. Miller. «The effect of surface heterogeneity on pseudo-line tension and the flotation limit of fine particles.» *Colloids and Surfaces* 69, n. 1 (1992): 35-43.

- Drelich, Jaroslaw, e Jan D Miller. «Effect of solid surface heterogeneity and roughness on the contact angle/drop (bubble) size relationship.» *Journal of Colloid and Interface Science* 164, n. 1 (1994): 252-259.
- Drioli, E., A. Criscuoli, and E. Curcio. *MEMBRANE CONTACTORS: FUNDAMENTALS, APPLICATIONS AND POTENTIALITIES*. Amsterdam: ELSEVIER, 2006.
- Drioli, Enrico, Aamer Ali, e Francesca Macedonio. «Membrane distillation: Recent developments and perspectives.» *Desalination* 356 (2015): 56-84.
- Dupré, A M. *Théorie mécanique de la chaleur*. Paris: Gauthier-Villars, 1869.
- Fowkes, Frederick M. «Attractive forces at interfaces.» *Ind. Eng. Chem* 56, n. 12 (1964): 40-52.
- Fraken, A., J. Nolten, M. Mulder, D. Bargeman, e C. Smolders. «Wetting criteria for the applicability of membrane destillation.» *Journal of Membrane Science* 33 (1987): 315 - 328.
- García-Payo, M. C., Amparo M. Izquierdo-Gil, e Cristóbal Fernández-Pineda. «Wetting study of hydrophobic membranes via liquid entry pressure measurements with aqueous alcohol solutions.» *Journal of Colloid and Interface Science* 230, n. 2 (2000): 420-431.
- Gaydos, J. A., e August Wilhelm Neumann. «The dependence of contact angles on drop size and line tension.» *Journal of Colloid And Interface Science*, 1987: 76-86.
- Girifalco, Louis A, e Robert J Good. «A theory for the estimation of surface and interfacial energies. I. Derivation and application to interfacial tension.» *Journal of Physical Chemistry* 61, n. 7 (1957): 904-909.
- Good, Robert J., e M. N. Koo. «The effect of drop size on contact angle.» *Journal of Colloid And Interface Science* 71, n. 2 (1979): 283-292.
- Guillen-Burrieza, Elena, Amelia Servi, Boor Lalia, and Hassan A. Arafat. "Membrane structure and surface morfology impact on the wetting of MD membranes." *Journal of Membrane Science* 483 (2015): 94 - 103.
- Hayashi, Tsukasa, Tatsuya Hazuku, Tomoji Takamasa, and Kenrou Takamori. "Contact angle of water droplets in a high-temperature, high-pressure environment." *Proceedings of the International Conference on Nuclear Engineering (ICONE12)* 1 (2004): 797-800.
- Hereijgersa, Jonas , Tom Breugelmans, e Wim De Malschea. «Breakthrough in a flat channel membranemicrocontactor.» *Chemical Engineering Research and Design* 64 (2015): 98-104.
- Jańczuk, Bronisław S, e Tomasz Białopiotrowicz . *Polish Journal of Chemistry* 65 (1991): 487.

- Jiansheng, Li, Wang Lianjun, Hao Yanxia, Liu Xiaodong, and Sun Xiuyun. "Preparation and characterization of Al₂O₃ hollow fiber membranes." *Journal of Membrane Science* 256, no. 1-2 (2005): 1-6.
- Johnson, Rulon E, and Robert H Dettre. "The temperature dependence of wettability: Hexadecane on a fluoropolymer." *Journal of Colloid Science* 20, no. 2 (1965): 173-176.
- Jones, Jamie Bryan, and Arthur W. Adamson. "Temperature dependence of contact angle and of interfacial free energies in the naphthalene-water-air system." *Journal of Physical Chemistry* 72, no. 2 (1968): 646-650.
- Khayet, Mohamed, Armando Velázquez, e Juan I. Mengual. «Modelling mass transport through a porous partition: Effect of pore size distribution.» *Journal of Non-Equilibrium Thermodynamics* 29, n. 3 (2004): 279-299.
- Kong, Jianfeng, e K. Li. «An improved gas permeation method for characterising and predicting the performance of microporous asymmetric hollow fibre membranes used in gas absorption.» *Journal of Membrane Science* 182, n. 1-2 (2001): 271-281.
- Koonaphapdeelert, Sirichai, and K. Li. "Preparation and characterization of hydrophobic ceramic hollow fibre membrane." *Journal of Membrane Science*, no. 291 (2007): 70-76.
- Krajewski, Sebastian R., Wojciech Kujawski, Frédéric Dijoux, Céline Picard, e André Larbot. «Grafting of ZrO₂ powder and ZrO₂ membrane by fluoroalkylsilanes.» *Colloids and Surfaces A: Physicochemical and Engineering Aspects* 243, n. 1-3 (2004): 43-47.
- Kwok, D.Y., e A.W. Neumann. «Contact angle measurement and contact angle interpretation.» *Advances in Colloid and Interface Science* 81, n. 3 (1999): 167-249.
- Kwok, Daniel Y, e August Wilhelm Neumann. «Contact angle measurement and contact angle interpretation.» *Advances in Colloid and Interface Science* 81, n. 3 (1999): 167-249.
- Lee, Y, J Jeong, I J Youn, e W H Lee. «Modified liquid displacement method for determination of the pore size distribution in porous membranes.» *Journal of Membrane Science* 130 (1997): 149-156.
- Lu, Jun, Yun Yu, Jianer Zhou, Lixin Song, Xingfang Hub, e Andre Larbot. «FAS grafted superhydrophobic ceramic membrane.» *Applied Surface Science*, 2009: 9092-9099.
- Lyklema, J. «The surface tension of pure liquids: Thermodynamic components and corresponding states.» *Colloids and Surfaces A: Physicochemical and Engineering Aspects* 153, n. 1-3 (1999): 413-421.
- Mack, G. L. «The determination of contact angles from measurements of the dimensions of small bubbles and drops. I: The spheroidal segment method for acute angles.» *The Journal of Physical Chemistry* 40 (1936): 159-167.

- McGuire, Kenneth S, Kevin W Lawson, e Douglas R Lloyd. «Pore size distribution determination from liquid permeation through microporous membranes.» *Journal of Membrane science* 99 (1995): 127-137.
- Monash , P., and G. Pugazhenthii . "Effect of TiO₂ addition on the fabrication of ceramic membrane supports: A study on the separation of oil droplets and bovine serum albumin (BSA) from its solution." *Desalination* 279, no. 1-3 (2011): 104-114.
- Neumann, August Wilhelm , e R J Good. *Surface and Colloid Science*. A cura di R J Good e R R Stromberg. Vol. 11. New York: Plenum, 1979.
- Neumann, August Wilhelm. "Contact angles and their temperature dependence: thermodynamic status, measurement, interpretation and application." *Advances in Colloid and Interface Science* 4, no. 2-3 (1974): 105-191.
- Neumann, August Wilhelm, G Haage, and Dieter Renzow. "The temperature dependence of contact angles polytetrafluoroethylene/N-alkanes." *Journal of Colloid And Interface Science* 35, no. 3 (1971): 379-385.
- Newmann, A. W., e D Li. «Equation of Staate for Interfacial Tension of Solid-Liquid Systems.» *Adv. Colloid Interf. Sci* 39 (1992): 299-345.
- Petke, F. David, and B. Roger Ray. "Temperature dependence of contact angles of liquids on polymeric solids." *Source of the Document/Journal of Colloid And Interface Science* 31, no. 2 (1969): 216-227.
- Petke, F. David, e B. Roger Ray. «Erratum to temperature dependence of contact angles of liquid on polymeric solids.» *Journal of Colloid And Interface Science*, 1970: 195.
- Phillips, M C, and A C Riddiford. "Temperature dependence of contact angles." *Nature* 205, no. 4975 (1965): 1005-1006.
- Piątkiewicz, W, S Rosiński , D Lewińska, J Bukowski, e W Judyckib. «Determination of pore size distribution in hollow fibre membranes.» *Journal of Membrane Science* 153 (1999): 91-102.
- Picard, C., A. Larbot, E. Tronel-Peyroz, and R. Berjoan. "Characterisation of hydrophilic ceramic membranes modified by fluoroalkylsilanes into hydrophobic membranes." *Solid State Sciences* 6, no. 6 (2004): 605–612.
- Present, R. D. *Kinetic Theory of Gases*. New York: McGraw-Hill, 1958.
- Saffarini, Rasha B, Bilal Mansoor, Rinku Thomas, and Hassan A Arafat. "Effect of temperature-dependent microstructure evolution on pore wetting in PTFE membranes under membrane distillation conditions." *Journal of Membrane Science* 429 (2013): 282–294.

- Schöner, P., P. Plucinski, W. Nitsch, e U. Daiminger. «Mass transfer in the shell side of cross flow hollow fiber modules.» *Chemical Engineering Science* 533, n. 13 (1998): 2319-2326.
- Schonhorn, Harold. «Dependence of Contact Angles on Temperature: Polar liquid on Polyethylene.» *Nature* 210, n. 5039 (1966): 896-897.
- Scott, D. S., and F. A. L. Dullien. "The flow of rarefied gases." *AIChE Journal* 8, no. 3 (1962): 293–297.
- Singh , Dhananjay, e Kamalesh K. Sirkar. «High temperature direct contact membrane distillation based desalination using PTFE hollow fibers.» *Chemical Engineering Science* 116 (2014): 824–833.
- Sun, Xiuyu, Faqiang Xu, Zongmu Li, and Wenhua Zhang. "Photoluminescence properties of anodic alumina membranes with ordered nanopore arrays." *Journal of Luminescence* 121, no. 2 (2006): 588–594.
- Sun, Xiuyu, Faqiang Xu, Zongmu Li, and Wenhua Zhang. "Photoluminescence properties of anodic alumina membranes with ordered nanopore arrays." *Journal of Luminescence* 121, no. 2 (2006): 588–594.
- Tadmor, Rafael. «Line Energy and the Relation between Advancing.» *Langmuir* 20 (2004): 7659-7664.
- Tröger , Jens, Klaus Lunkwitz , e Wolfgang Bürger . «Determination of the Surface Tension of Microporous Membranes Using Contact Angle Measurements.» *Journal of Colloid and Interface Science* 194, n. 2 (1997): 281–286.
- Vesselovsky, W S, e W N Pertzov. *J. Phys. Chem. USSR* 8 (1936): 5.
- Weber, Christian, and Helge Stanjek. "Energetic and entropic contributions to the work of adhesion in two-component, three-phase solid–liquid–vapour systems." *Colloids and Surfaces A: Physicochemical and Engineering Aspects* 441 (2014): 331–339.
- Weyd, Marcus, Hannes Richter, Petra Puhlfürß, Ingolf Voigt, Christof Hamel, e Andreas Seidel-Morgenstern. «Transport of binary water-ethanol mixtures through a multilayer hydrophobic zeolite membrane.» *Journal of Membrane Science* 307 (2008): 239 - 248.
- Yekta-Fard, Mohsen, and Anthony B Ponter. "The influence of vapor enviroment and temperature on the contact angle-drop size relationship." *Journal of colloids and Interface science* 1226, no. 1 (1988): 134-140.
- Zha, Fu Fang, Anthony Gordon Fane, Christopher Josphe D Fell, and R. W. Schofield. "Critical displacement pressure of a supported liquid membrane." *Journal of Membrane Science* 75, no. 1-2 (1992): 69-80.

Design-construction of SGMD pilot plant and test with membrane modules.

Summary

1	Introduction	129
2	Fluid dynamic analysis of hydrophobic membrane modules.....	130
2.1	Module categories selected and its main characteristics for the fluid dynamic analysis. 130	
2.2	Volumetric flow rates	133
2.3	Pressure drops on the membrane module.....	134
2.4	Results.....	139
3	Pilot Plant	144
3.1	Main Equipments.....	146
3.2	Pilot Plant Operative Limits	148
4	Physical-Chemical Equilibrium	150
4.1	Dissolution model for the DAP - ADP- Water system	150
4.1.1	Ideal solution Model	151
4.1.2	ENRTL (Chen & Song, 2004)	153
4.1.3	Experimental results for solution model validation	157
4.2	Henry Constant and Salting-Out Effect (Sechenov, 1889).	161
4.3	Vapor-Liquid equilibrium model at constant volume	164
4.3.1	Mathematical model	165
4.3.2	Model results.....	167
4.3.3	Discussion and conclusions.....	170

5	Pilot Plant Startup and SGMD preliminary test.....	171
5.1	Equilibrium test and pilot plant startup.....	171
5.2	Sweeping gas membrane distillation test (SGMD).....	173
5.2.1	Experimental test.....	173
5.2.2	Results analysis.....	178
6	Conclusions.....	182
7	List of Symbols.....	185
8	Bibliography.....	188

1 Introduction

In order to continue the development of the Membrane Contactors (MC) process, to perform the stripping of the reaction products of an endothermic equilibrium reaction, the membranes previously characterized (see previous chapters of this thesis) should be tested for the use on a Swiping Gas Membrane Distillation process. With this aim experiments were designed and a “bench scale” pilot plant was constructed to perform this sort of tests.

The pilot plant must be flexible and should be able to host a wide range of membrane area; it should be used with different membrane modules configurations using the same instrumentation, tubes and equipment. The size of the main equipment, pipes and instrumentation were defined by the tolerable flow rate, given by a fixed flow velocity and pressure drops on the different modules. For the quantification of the flow rates ranges (for liquid and gas) a fluid dynamics analysis was performed on three different selected modules configurations.

For the understanding of the chemistry of the problem, and start setting up of the main process parameters, it is of great importance to carry out a depth study of the physical-chemical equilibrium. A suitable equilibrium model will allow to understand not only the thermodynamics of the problem but also mass and heat transfer phenomena. This made the equilibrium study of great importance for the description of the problem and finally for the design of the process and the equipment.

With such a plant, it could be possible to evaluate the feasibility of the process for the stripping of a gas, product of the decomposition of salts, on a liquid matrix. The idea is to quantify the fluxes across the membrane, the separation of the volatile components, the effect of the operative conditions, the effect of the membranes and all the different parameters necessary to evaluate the application of the MC technology for a particular process.

2 Fluid dynamic analysis of hydrophobic membrane modules

The quantification of the gas and liquid flow rates and pressure drops were performed through the fluid dynamics analysis of four different selected modules (the modules were selected prior to the analysis of the hydrophobic characterization of the membranes). The selection basis of the modules was the technical characteristics found on literature, considered as the most suitable for the process of interest. Three of the selected modules are prototype modules, the fourth one is commercially produced for industrial purposes, nevertheless the configuration of the prototype modules is pretty standard for a proper sizing of a pilot plant.

2.1 Module categories selected and its main characteristics for the fluid dynamic analysis.

The following modules will be considered for the analysis.

- Single channel membrane module.
- Shell and tubes modules supporting Polymeric or ceramic membranes.
- Shell and tubes cross flow module; Liqui-Cel® module.

Single channel membrane module: a tubular membrane is set in the middle of a tubular housing, (which inner diameter is larger than the outer diameter of the membrane tube) as the one shown in Figure 2.1, very similar to the tube in tube configuration of heat exchangers. The fluids paths are parallel one to the other, regardless the chosen configuration (cocurrent, countercurrent, Liquid on lumen or Gas on lumen). The Geometric characteristics for this configuration are reported on Table 2.1 and Table 2.2.



Figure 2.1 Single Channel module configuration scheme.

Shell and tubes modules: in this configuration the membranes are set in a bundle of capillary tubes inside of a housing shell represented on Figure 2.2. One of the fluids (liquid or gas) pass through the lumen of the capillary fibers whereas the second one is distributed across the external part of the bundle (on the housing shell) and flows parallel to the fibers before being collected on the opposite part of the module. Two prototype modules were selected, for the pilot plant sizing. The first one has polymeric membranes, produced by Markel Corporation®, potted together on a bundle; the characteristics of this prototype module were taken from publication by Khaisri et al, 2011. only for sizing purposes. The latter comprises modules

developed in collaboration with the Fraunhofer Institute for Ceramic Technologies and Systems.

The characteristics of the modules are not completely defined, so two hypothetical configurations (coded as CMB A and CMB B) will be taken for the analysis. For both the prototype modules parallel flow will be considered as well as the possibility of gas and liquid to flow on the lumen or the shell side.



Figure 2.2 Shell and tubes configuration scheme

Shell and tubes, cross flow module: from the wide range of the membranes produce by the **3M Membranes Business Unit** the module **2.5 x 8 EXTRA-FLOW** from the Liquid-Cel® series has been selected for sizing and for experimental applications. The “Extra-Flow” modules are cross flow apparatuses of large membrane area, due to the very high number of fibers in the bundle. They are typically designed for gas transport application, degassing of liquid streams, absorption of gas on liquid streams, particularly tested with CO₂. The polypropylene structure limits the maximum application temperature to 60 °C.

The Liqui-Cel® module configuration is presented on the Figure 2.3. The flow on the shell side of the module has a cross flow pattern induced by a central collector-distributor and the baffle located in the middle of the module. The liquid stream is suggested to flow on the outside of the fibers and the gas on the lumen side for pressure drop consideration (only this configuration will be take into account).

The characteristics of membrane and module are available on the data sheet of the product (3M Company, 2016) additional information was taken from (Schöner, Plucinski, Nitsch, & Daiminger, 1998) and from direct communication of the producer. The Characteristics are present on Table 2.1and Table 2.2.

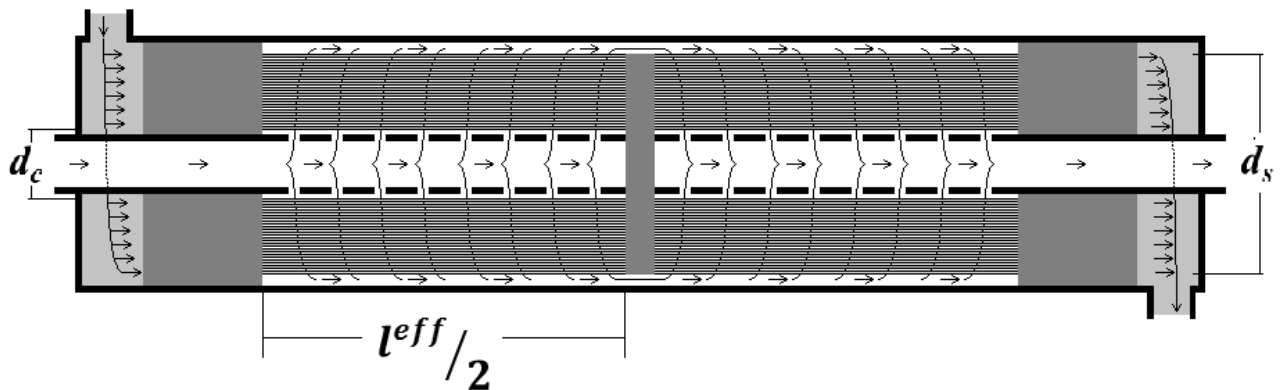


Figure 2.3 Liqui-Cel® cross flow configuration scheme.

Table 2.1 Membranes characteristics.

Membrane	Code	Material	Pore d (μm)	Porosity	d_o (μm)	d_i (μm)	Thickness δ (μm)
Ceramic Single Channel grafted with Polymer	(A)	TiO ₂	0.2	45%	10000	6000	2000
CMB (A)	(A)	TiO ₂	NA	NA	1300	800	250
CMB (B)	(A)	TiO ₂	NA	NA	1300	800	250
Markel (A)	(A)	PTFE	0.161	23%	2007	1626	190.5
Markel (B)	(B)	PTFE	0.161	23%	2007	1626	190.5
Markel (C)	(C)	PTFE	0.313	40%	1971	1600	185.5
2.5 x 8 EXTRA-FLOW	X50	PP	0.04	40%	300	220	40

NA= not available

The Table 2.2 summarizes the geometrical parameters of the modules. Were also calculated the void fraction (θ), the volume capacity of shell and lumen, and the membrane area calculated relatively to the inner diameter, outer diameter and mean diameter (A_i , A_o , A_{av}).

Table 2.2 Modules Specifications (quantity definitions are in Figure 2.1, Figure 2.2 and Figure 2.3).

<i>Module</i>	<i>Fibers Number (N_f)</i>	<i>l^{eff} (cm)</i>	<i>d_s (cm)</i>	<i>d_c (cm)</i>	<i>θ %</i>	<i>V_{lumen} (mL)</i>	<i>V_{Shell} (mL)</i>	<i>A_i (cm²)</i>	<i>A_o (cm²)</i>	<i>A_{Av} (cm²)</i>
Single Channel	1	53	1.7	-	65	15	79	100	167	133
CMB (A)	120	25	2.7	-	72	15	103	754	1225	990
CMB (B)	120	40	2.7	-	72	24	165	1206	1960	1583
Markel (A)	50	14	2.4	-	65	15	41	358	441	399
Markel (B)	50	28	2.4	-	65	29	82	715	883	799
Markel (C)	48	14	2.4	-	68	14	43	338	416	377
2.5 x 8 EXTRA- FLOW	-	18.2	5.5	-	61	150	400	14000	-	-

2.2 Volumetric flow rates

The limit values of volumetric flow rates, calculated for each module configuration are reported on the Table 2.4. The possibility that any fluid could flow on either the lumen or the shell side is considered.

The velocity values in the lumen and in the shell side were set accordingly with the phase flowing on each side. On Table 2.3 are reported the maximum and minimum velocity values admissible for gas and liquid on shell or lumen respectively.

Table 2.3 Limit values for velocities of gas and liquid

	<i>Gas velocity (m/s)</i>	<i>Liquid velocity (m/s)</i>
Shell side	0.5 – 2.0	0.1 – 0.5
Lumen side	1.0 – 10.0	0.1 - 1.0

On the particular case of the Liquid-Cel module the data sheet specifies the values of flow rate for liquid and gas on the shell side and lumen side respectively. For this module the fluid velocity was calculated; for the particular configuration of the shell the following expression proposed (Schöner, Plucinski, Nitsch, & Daiminger, 1998) was used.

$$v_{shellside} = \frac{2Q_{shellside}}{\pi l^{eff}} \frac{\ln(d_s/d_c)}{d_s - d_c} \quad (2.1)$$

Table 2.4 Range of Liquid and gas flow rates for different flow patterns with the corresponding superficial velocity values

Flow rates					
Module	Flow Pattern	Liquid min (L/min)	Liquid max (L/min)	Gas min (L/min)	Gas max (L/min)
Single Channel	<i>Parallel Flow, L-Lumen/G-Shell</i>	0.17 (0.1 m/s)	1.70 (1.0 m/s)	13.6 (1 m/s)	136.2 (10 m/s)
CMB (A) (fibers bundle)	<i>Parallel Flow, L-Lumen/G-Shell</i>	0.36 (0.1 m/s)	13.62 (1.0 m/s)	17.2 (0.5 m/s)	68.7 (2 m/s)
CMB (B) (fibers bundle)	<i>Parallel Flow, L-Lumen/G-Shell</i>	0.36 (0.1 m/s)	3.62 (1.0 m/s)	17.2 (0.5 m/s)	68.7 (2 m/s)
Markel (A) (fibers bundle)	<i>Parallel Flow, L-Lumen/G-Shell</i>	0.62 (0.1 m/s)	6.23 (1.0 m/s)	13.5 (0.5 m/s)	54.28 (2 m/s)
Markel (B) (fibers bundle)	<i>Parallel Flow, L-Lumen/G-Shell</i>	0.62 (0.1 m/s)	6.23 (1.0 m/s)	13.57 (0.5 m/s)	54.28 (2 m/s)
Markel (C) (fibers bundle)	<i>Parallel Flow, L-Lumen/G-Shell</i>	0.17 (0.1 m/s)	1.70 (1.0 m/s)	6.8 (0.5 m/s)	27.24 (2 m/s)
CMB (A) (fibers bundle)	<i>Parallel Flow, L-Shell/G-Lumen</i>	3.44 (0.1 m/s)	17.17 (0.5 m/s)	3.62 (1 m/s)	36.19 (10 m/s)
CMB (B) (fibers bundle)	<i>Parallel Flow, L-Shell/G-Lumen</i>	3.44 (0.1 m/s)	17.17 (0.5 m/s)	3.62 (1 m/s)	36.19 (10 m/s)
Markel (A) (fibers bundle)	<i>Parallel Flow, L-Shell/G-Lumen</i>	2.71 (0.1 m/s)	13.6 (0.5 m/s)	6.23 (1 m/s)	62.29 (10 m/s)
Markel (B) (fibers bundle)	<i>Parallel Flow, L-Shell/G-Lumen</i>	2.71 (0.1 m/s)	13.6 (0.5 m/s)	6.23 (1 m/s)	62.29 (10 m/s)
Markel (C) (fibers bundle)	<i>Parallel Flow, L-Shell/G-Lumen</i>	2.71 (0.1 m/s)	13.6 (0.5 m/s)	5.79 (1 m/s)	57.91 (10 m/s)
2.5 x 8 EXTRA-FLOW (fibers bundle)	<i>Cross Flow, L-Shell/G-Lumen</i>	0.38* (0.06 cm/s)	11.33* (1.83 cm/s)	8.33* (0.33 m/s)	33.33* (1.31 m/s)

L-Lumen = liquid in the tube side; G-Shell= gas in the shell side; * = values reported in the technical sheet

2.3 Pressure drops on the membrane module.

One of the key elements for the sizing of the equipment, especially the pump, is represented by the pressure drops along the membrane module. The quantification of the pressure drop along the modules, assuming low roughness of the wall, allows a conservative sizing of the plant sizing.

Pressure drops along the lumen side.

The pressure drops were calculated according to the well-known Darcy-Weisbach equation (2.2).

$$\Delta P = 4f \frac{l^{eff}}{d_i} \rho \frac{v^2}{2} \tag{2.2}$$

The expression above l_{eff} represents the effective length of the module, d_i is the inner diameter and f is the Fanning friction factor (function of the Reynolds number indicated on Table 2.5). The pressure drops were calculated for each modular configuration, at the limit flow rates (indicated on Table 2.4) and for the inlet pressure of 4 bar at the temperatures of 25 °C and 100 °C

Table 2.5 Fanning factor for different flow regime

$Re < 2300$	$2300 < Re < 5000$	$5000 < Re < 200000$
$f = \frac{16}{Re}$	$f = 0.079 Re^{-1/4}$	$f = 0.046 Re^{-1/5}$

Pressure drops along the Shell side

The shell side, for the modular configuration of shell and tubes, was simulated as a porous bed applying the equivalent ring theory (Gostoli & Gatta, 1980). This model has been found adequate for mass transport analysis, for fibers bundles with high void fraction (θ) and good uniformity of the fibers. It can be supposed that it is also adequate in the quantification of the pressure drops along the Shell side.

The equivalent ring theory states that the flow section, on the shell side, is the sum of the each flow section around each fiber, represented by the concentric area between two adjacent fibers. The flow section area for each fiber is represented by the ring diameter (d_2) as shown in Figure 2.4, the ring diameter and the pressure drops can be calculated with the equations (2.3) to (2.5)

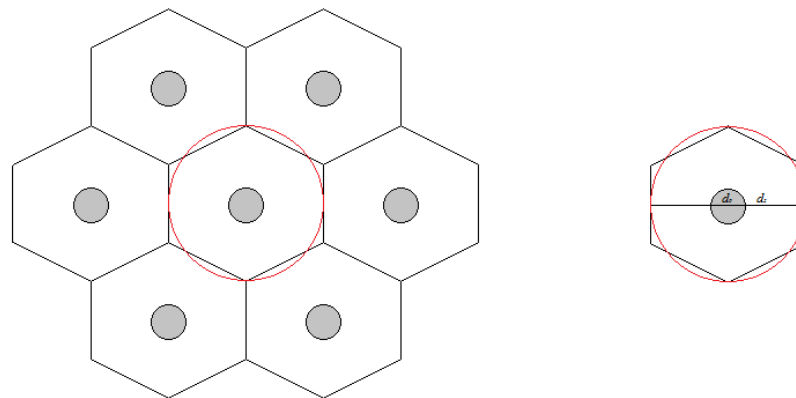


Figure 2.4 Equivalent ring theory model: d_0 fiber Outer diameter, d_2 Equivalent ring diameter.

$$d_2 = \sqrt{\frac{d_s^2}{N_t}} \quad (2.3)$$

$$\Delta P = \frac{8\eta v_0 l_{eff}}{d_2^2 f(\theta)} \quad (2.4)$$

$$f(\theta) = -\frac{1}{2} \left[\frac{\ln(1-\theta)}{\theta} + 1 + \frac{\theta}{2} \right] \quad (2.5)$$

In the expressions above, v_0 represents the characteristic velocity, calculated as a function of the surface velocity (v_∞) and the void fraction by the following expression.

$$v_0 = v_\infty / \theta \quad (2.6)$$

If the flow regime is not completely laminar, the pressure drop might be calculated across the equation (2.2) using the equivalent diameter (2.7) and the friction factor in function of the Reynolds number (Table 2.5)

$$d_h = \frac{4A_{flow}}{wet\ perimeter} = \frac{d_s^2 - N_t d_0^2}{N_t d_0 + d_s} \quad (2.7)$$

$$Re = \frac{\rho v_0 d_h}{\eta} \quad (2.8)$$

Pressure drops along the Shell side crossflow configuration (Liqui-Cel®)

The particular fluid dynamic in the cross flow configuration typical of the Liqui-Cel® modules, made the analysis of the pressure drops a little more difficult. The analogy with the porous bed can be also useful on this case. Schöner et al, (1998) performed this analysis to evaluate the mass transfer on this configuration and the same consideration can be taken for the pressure drop calculation.

The analysis starts from the consideration that there is a collector channel between the fibers bundle and the inner diameter of the shell. This parameters is not listed on the geometrical characteristics of the module, but it can be supposed in the range from 1 to 3 mm. As a consequence the velocity of the liquid v_∞ is expressed as in equation (2.9) in which d_s is the outer diameter of the fibers bundle. The velocity of the liquid will depend on the axial path of the liquid on the cross flow configuration.

$$v_\infty = 2 \frac{\dot{Q}_l}{\pi l_{eff}} \frac{\ln\left(\frac{d_s}{d_c}\right)}{d_s - d_c} \quad (2.9)$$

The void fraction θ is calculated with the outer diameter of the fiber bundle and the outer diameter of the collector.

$$\theta = 1 - \frac{N_t d_o^2}{d_s^2 - d_c^2} \quad (2.10)$$

The void fraction can be represented as channels connecting the collector with the outer part of the bundle with a tortuosity (χ can assume the value of 2) and a diameter (d_m). On this way the velocity across this channel can be represented by the expression below.

$$v_0 = \frac{d_m^2 \Delta P}{K'' \eta l'} \quad (2.11)$$

Where K' is a dimensionless constant representing the channel structure (usually can take a value of 5) and l' is the length of this channel.

Using the equations (2.6) and (2.7) from the porous bed analogy can be possible to obtain an expression to calculate the actual velocity on the "channel".

$$v_\infty = \frac{1}{K''} \frac{\theta^3}{a^2(1-\theta)^2} \frac{1}{\eta} \frac{\Delta P}{\chi l_{eff}} \quad (2.12)$$

The character a represents the specific surface of the hollow fiber of outer diameter d_o .

$$a = \frac{4}{d_o} \quad (2.13)$$

From the equation (2.12) is possible to put the pressure drop along the bundle on an explicit form.

$$\Delta P_{dist} = \chi l_{eff} \eta \left(\frac{\theta^3}{a^2(1-\theta)^2} \right)^{-1} K'' v_\infty \quad (2.14)$$

To the distributed pressure drops should be added the concentrated due to the inlets, outlets, flow restrictions and baffles. This can be calculated in function of the liquid head velocity (kinetic units).

$$\Delta P_{tot} = \Delta P_{in/out} + \Delta P_{baffle} + \Delta P_{distr} \quad (2.15)$$

The baffles restrictions pressure drop (2.17) can be assumed as 2 kinetic units in function of the mean velocity (2.16) across the baffle restriction.

$$v_{baffle} = \frac{\dot{Q}_l}{\frac{\pi}{4} (d_{shell}^2 - (d_s)^2)} \quad (2.16)$$

$$\Delta P_{baffle} = \rho_l v_{baffle}^2 \quad (2.17)$$

The same approach, like in the baffles, will be use for the calculation of the pressure drop across the inlet/outlet of the module. The concentrated pressure drop will be function of the kinetic energy and so of the velocity in the plug caps (d_{pc} is the inside diameter of the plug cap).

The pressure drops due to the inlet outlet will depends on the inlet cap selected to plug the module to the tubes. The producer offer the module with 3 different inlet plugs configurations, two different sizes of the trademark Flaretek® and the third one is the standard NPT.

On the producer data sheet the experimental pressure drop is reported, when using each one of the plug caps. On Figure 2.5 it can be observed that the pressure drops due to the inlet/outlet configuration are a critical point, in that the values can be duplicated, depending on which plug cap is selected.

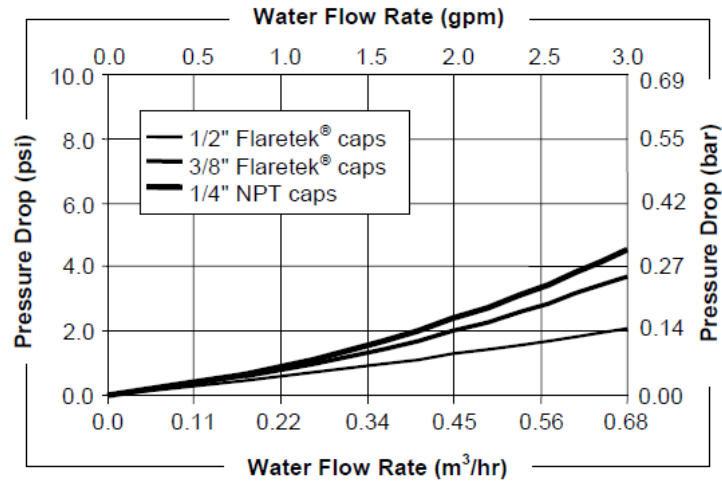


Figure 2.5 Experimental pressure drops for Liqui-Cel module 2.5 X 8 EXTRA FLOW, for the different plug cap

$$v_{in/out} = \frac{\dot{Q}_l}{\frac{\pi}{4} d_{pc}^2} \quad (2.18)$$

$$\Delta P_{in/out} = NKU\rho_l \frac{v_{in/out}^2}{2} \quad (2.19)$$

The unknown geometry of the inlet/outlet of the module made difficult to select the number of kinetics units to perform the calculation and so the experimental data provided by the producer can be fitted in order to obtain this number to be use in for simulations with other fluids. As for sizing analysis the pressure drops with water can be obtain from the experimental data reported on the producer data sheet.

Table 2.6 Fitted Kinematic Units for the different Plug caps

<i>Connections</i>	<i>NKU</i>
<i>1/4" NPT Caps</i>	4
<i>3/8" Flaretek</i>	5
<i>1/2" Flaretek</i>	5

For the sizing analysis the connections with the NPT plug caps were used as are the most conservative.

As in the tubes side the pressure drops were calculated for each modular configuration, at the limit flow rates (indicated on Table 2.4) and for the inlet pressure of 4 bar at the temperatures of 25 °C and 100 °C. The results are reported on Table 2.7 to Table 2.10

2.4 Results

On Table 2.7 to Table 2.10 the pressure drops calculated are reported for the different modules configuration. The flow rates indicated on Table 2.4, used to calculate the pressure drops where obtain from limits values of fluid velocity inside the membrane module for the configuration Liquid on lumen side, liquid on the shell side, gas on the lumen side and gas on the shell side respectively.

The information obtained was useful mainly for the sizing of the pump. Considering the pressure drops along the module and the concentrated pressure drops due to valves, heating coils and fittings in the whole equipment, a pump with a head of 25 m was selected.

Never the less the pressure drop is also important for the definition of the operation mode. It would help to decide which fluid should flow on which side of the module, how many modules could be array in series in order to avoid flooding of the membrane (overcoming the limit differential pressure between gas phase and liquid phase - LEP) and if fluids could be fed on cocurrent mode or countercurrent

From the results reported in the tables below it is easy to observe that when liquid is in the lumen side the pressure drops are always higher than the ones for gas in the shell side. On the same way the pressure drops are higher for the gas phase when it is fed on the tubes.

Table 2.7 Pressure drops in the lumen side, for the cases of liquid and gas at 25°C and 4 bar; liquid velocity = 0.1-1 m/s, gas velocity=1-10 m/s.

Lumen Side 25°C 4 bar							
Module	Flow Pattern Configurations	Re_{min}	ΔP_{min} (mbar)	ΔP_{min} (mbar/m)	Re_{max}	ΔP_{max} (mbar)	ΔP_{max} (mbar/m)
Single Channel	Parallel Flow L-Lumen/G-Shell	657	0.43	0.81	6572	14.00	26.42
CMB (A) (fibers bundle)	Parallel Flow L-Lumen/G-Shell	88	11.41	45.63	876	114.07	456.26
CMB (B) (fibers bundle)	Parallel Flow L-Lumen/G-Shell	88	18.25	45.63	876	182.51	456.26
Markel (A) (fibers bundle)	Parallel Flow L-Lumen/G-Shell	178	1.55	11.04	1781	15.46	110.45
Markel (B) (fibers bundle)	Parallel Flow L-Lumen/G-Shell	178	3.09	11.04	1781	30.93	110.45
Markel (C) (fibers bundle)	Parallel Flow L-Lumen/G-Shell	176	1.60	11.43	1753	15.97	114.07
CMB (A) (fibers bundle)	Parallel Flow L-Shell/G-Lumen	238	2.29	9.15	2380	33.07	132.29
CMB (B) (fibers bundle)	Parallel Flow L-Shell/G-Lumen	238	3.66	9.15	2380	52.91	132.29
Markel (A) (fibers bundle)	Parallel Flow L-Shell/G-Lumen	484	0.31	2.22	4838	7.91	56.48
Markel (B) (fibers bundle)	Parallel Flow L-Shell/G-Lumen	484	0.62	2.22	4838	15.81	56.48
Markel (C) (fibers bundle)	Parallel Flow L-Shell/G-Lumen	476	0.32	2.29	4760	8.06	57.58
2.5 x 8 EXTRA-FLOW (fibers bundle)	Cross Flow, L-Shell/G-Lumen	21	7.23	39.73	86	28.93	158.94

Table 2.8 Pressure drops in the shell side, for the cases of liquid and gas at 25°C and 4 bar; superficial velocity in the liquid = 0.1-0.5 m/s, superficial velocity in the gas =0.5-2 m/s.

<i>Shell Side 25°C 4bar</i>							
<i>Module</i>	<i>Flow Pattern Configurations</i>	<i>Re min</i>	<i>ΔP min (mbar)</i>	<i>ΔP min (mbar/m)</i>	<i>Re max</i>	<i>ΔP max (mbar)</i>	<i>ΔP max (mbar/m)</i>
Single Channel	<i>Parallel Flow L-Lumen/G-Shell</i>	1592	0.05	0.09	6369	0.62	1.16
CMB (A) (fibers bundle)	<i>Parallel Flow L-Lumen/G-Shell</i>	593	0.20	0.81	2370	0.82	3.29
CMB (B) (fibers bundle)	<i>Parallel Flow L-Lumen/G-Shell</i>	593	0.32	0.81	2370	1.32	3.29
Markel (A) (fibers bundle)	<i>Parallel Flow L-Lumen/G-Shell</i>	689	0.09	0.67	2756	0.52	3.73
Markel (B) (fibers bundle)	<i>Parallel Flow L-Lumen/G-Shell</i>	689	0.19	0.67	2756	1.04	3.73
Markel (C) (fibers bundle)	<i>Parallel Flow L-Lumen/G-Shell</i>	722	0.08	0.55	2890	0.44	3.13
CMB (A) (fibers bundle)	<i>Parallel Flow L-Shell/G-Lumen</i>	436	2.02	8.09	2182	10.11	40.44
CMB (B) (fibers bundle)	<i>Parallel Flow L-Shell/G-Lumen</i>	436	3.24	8.09	2182	16.18	40.44
Markel (A) (fibers bundle)	<i>Parallel Flow L-Shell/G-Lumen</i>	507	0.94	6.71	2537	6.11	43.66
Markel (B) (fibers bundle)	<i>Parallel Flow L-Shell/G-Lumen</i>	507	1.88	6.71	2537	12.23	43.66
Markel (C) (fibers bundle)	<i>Parallel Flow L-Shell/G-Lumen</i>	532	0.76	5.46	2660	5.12	36.60
2.5 x 8 EXTRA-FLOW (fibers bundle)	<i>Cross Flow, L-Shell/G-Lumen</i>				15.3*	300*	1600*

*= from technical sheet including contribution of fittings

Table 2.9 Pressure drops in the lumen side, for the cases of liquid and gas at 100°C and 4 bar; liquid velocity = 0.1-1 m/s, gas velocity=1-10 m/s.

<i>Lumen Side 100°C 4 bar</i>							
<i>Module</i>	<i>Flow Pattern Configurations</i>	<i>Re_{min}</i>	<i>ΔP_{min} (mbar)</i>	<i>ΔP_{min} (mbar/m)</i>	<i>Re_{max}</i>	<i>ΔP_{max} (mbar)</i>	<i>ΔP_{max} (mbar/m)</i>
Single Channel	<i>Parallel Flow L-Lumen/G-Shell</i>	2076	0.13	0.25	20758	10.76	20.31
CMB (A) (fibers bundle)	<i>Parallel Flow L-Lumen/G-Shell</i>	277	3.49	13.97	2768	56.97	227.87
CMB (B) (fibers bundle)	<i>Parallel Flow L-Lumen/G-Shell</i>	277	5.59	13.97	2768	91.15	227.87
Markel (A) (fibers bundle)	<i>Parallel Flow L-Lumen/G-Shell</i>	563	0.47	3.38	5625	13.62	97.28
Markel (B) (fibers bundle)	<i>Parallel Flow L-Lumen/G-Shell</i>	563	0.95	3.38	5625	27.24	97.28
Markel (C) (fibers bundle)	<i>Parallel Flow L-Lumen/G-Shell</i>	554	0.49	3.50	5535	13.89	99.18
CMB (A) (fibers bundle)	<i>Parallel Flow L-Shell/G-Lumen</i>	156	2.71	10.83	1564	27.07	108.29
CMB (B) (fibers bundle)	<i>Parallel Flow L-Shell/G-Lumen</i>	156	4.33	10.83	1564	43.31	108.29
Markel (A) (fibers bundle)	<i>Parallel Flow L-Shell/G-Lumen</i>	318	0.37	2.62	3180	6.69	47.76
Markel (B) (fibers bundle)	<i>Parallel Flow L-Shell/G-Lumen</i>	318	0.73	2.62	3180	13.37	47.76
Markel (C) (fibers bundle)	<i>Parallel Flow L-Shell/G-Lumen</i>	313	0.38	2.71	3129	6.82	48.69
2.5 x 8 EXTRA-FLOW (fibers bundle)	<i>Cross Flow, L-Shell/G-Lumen</i>						

Table 2.10 Pressure drops in the shell side, for the cases of liquid and gas at 100°C and 4 bar; superficial velocity in the liquid = 0.1-0.5 m/s, superficial velocity in the gas =0.5-2 m/s

<i>Shell Side 100°C 4bar</i>							
<i>Module</i>	<i>Flow Pattern Configurations</i>	<i>Re_{min}</i>	<i>ΔP_{min} (mbar)</i>	<i>ΔP_{min} (mbar/m)</i>	<i>Re_{max}</i>	<i>ΔP_{max} (mbar)</i>	<i>ΔP_{max} (mbar/m)</i>
<i>Single Channel</i>	<i>Parallel Flow L-Lumen/G-Shell</i>	1047	0.06	0.11	4186	0.52	0.98
<i>CMB (A) (fibers bundle)</i>	<i>Parallel Flow L-Lumen/G-Shell</i>	390	0.24	0.96	1558	0.96	3.84
<i>CMB (B) (fibers bundle)</i>	<i>Parallel Flow L-Lumen/G-Shell</i>	390	0.38	0.96	1558	1.54	3.84
<i>Markel (A) (fibers bundle)</i>	<i>Parallel Flow L-Lumen/G-Shell</i>	453	0.11	0.80	1812	0.45	3.18
<i>Markel (B) (fibers bundle)</i>	<i>Parallel Flow L-Lumen/G-Shell</i>	453	0.22	0.80	1812	0.89	3.18
<i>Markel (C) (fibers bundle)</i>	<i>Parallel Flow L-Lumen/G-Shell</i>	475	0.09	0.65	1899	0.38	2.70
<i>CMB (A) (fibers bundle)</i>	<i>Parallel Flow L-Shell/G-Lumen</i>	1378	0.62	2.48	6891	7.00	27.98
<i>CMB (B) (fibers bundle)</i>	<i>Parallel Flow L-Shell/G-Lumen</i>	1378	0.99	2.48	6891	11.19	27.98
<i>Markel (A) (fibers bundle)</i>	<i>Parallel Flow L-Shell/G-Lumen</i>	1603	0.29	2.05	8013	4.44	31.69
<i>Markel (B) (fibers bundle)</i>	<i>Parallel Flow L-Shell/G-Lumen</i>	1603	0.58	2.05	8013	8.87	31.69
<i>Markel (C) (fibers bundle)</i>	<i>Parallel Flow L-Shell/G-Lumen</i>	1680	0.23	1.67	8401	3.72	26.56
<i>inst2.5 x 8 EXTRA-FLOW (fibers bundle)</i>	<i>Cross Flow, L-Shell/G-Lumen</i>						

3 Pilot Plant

In Figure 3.1 a flow sheet of the pilot plant is reported, which was designed and developed to performed characterization of membrane modules in Sweeping Gas Membrane Distillation (SGMD), it was also used to test the physical chemical models of phosphoric salt solutions.

The pilot plant elements were selected following some operative requirements. In order to perform tests at high temperatures with the phosphoric salt solutions it was mandatory that each element in the pilot plant could stand a maximum temperature of 150 °C and a maximum pressure of 10 barg; furthermore, materials and gaskets should resist to the corrosion of the high concentrated phosphoric salt solutions at such Temperatures. The Table 3.1 summarized all the elements of the pilot plant.

Table 3.1 Equipment and instrumentation on the pilot plant reported on Figure 3.1

<i>Equipment</i>	<i>Description</i>	<i>Instruments</i>	<i>Description</i>
<i>S1</i>	Pressure Tank AISI 316L	<i>AP-1, AP-2</i>	Differential pressure gauges
<i>S2</i>	Pressurized Gas Cylinder	<i>PI-1 - PI-6</i>	Pressure gauges
<i>S3</i>	Condensate Tank	<i>TI-1 - TI-5</i>	Thermometers
<i>S4</i>	Liquid Sampling	<i>FI-1, FI-2</i>	Flowmeters
<i>G1</i>	Centrifugal Pump	<i>V1 - V3; V6 - V9, V11 -V14</i>	Plug Valves on/off
<i>C1</i>	Condenser	<i>V16-V19, V23, V24</i>	Plug Valves on/off
<i>MC1</i>	Membrane Contactor	<i>V4, V5, V10, V15, V20</i>	Regulation Valves
<i>BT1</i>	Thermostatic Oil Bath	<i>V22</i>	Relief Valve
<i>F1</i>	Filter	<i>V21</i>	Check Valve

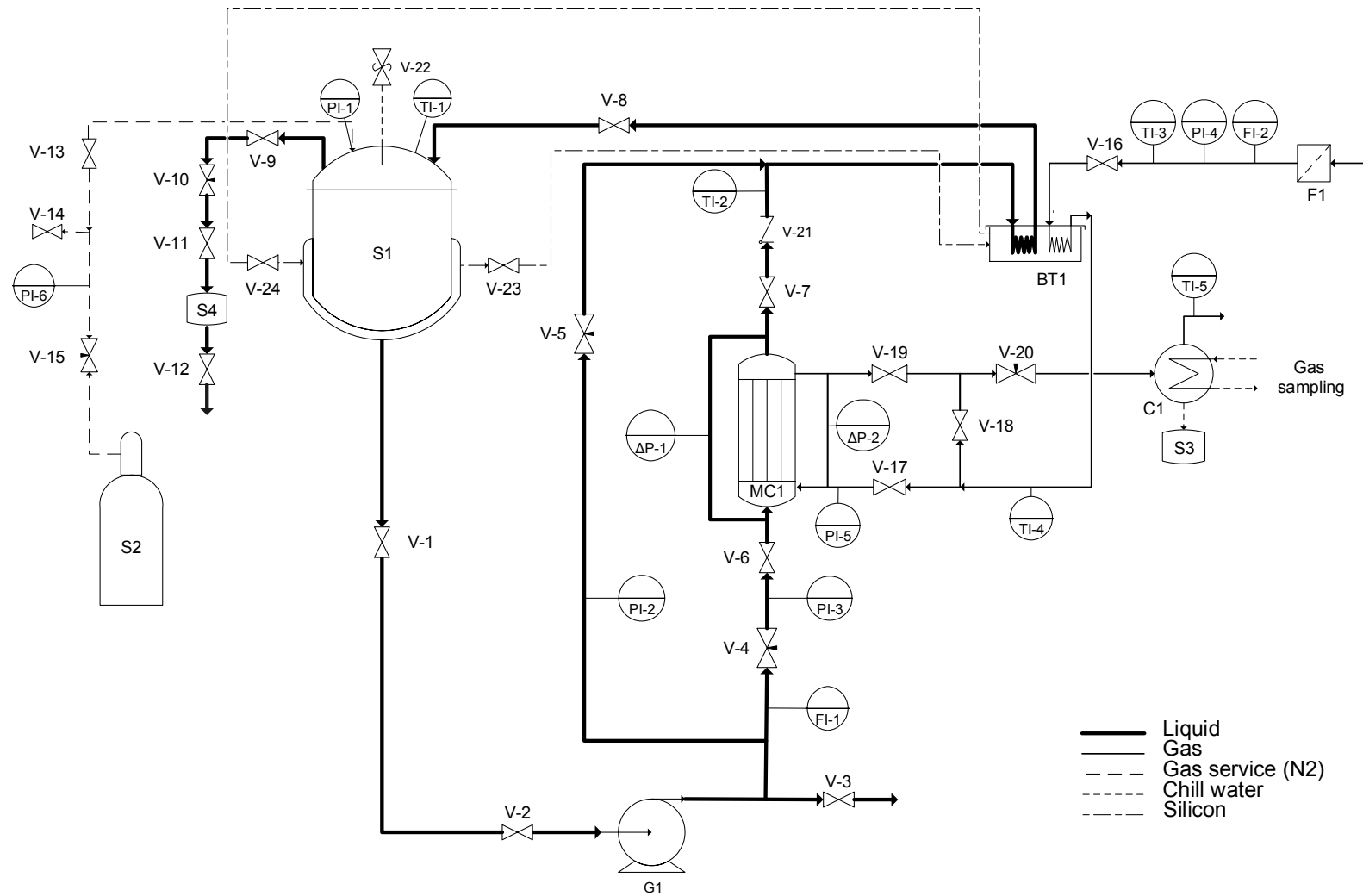


Figure 3.1 Pilot Plant Flow sheet

3.1 Main Equipment

Pressure Tank (S1)

The pressure tank is entirely design and constructed in stainless steel AISI 316L (Table 3.2). The top cover is flanged and sealed with a PTFE gasket, six holes are present, used for the following purposes:

- Relief Valve automatically activated at 10 barg.
- Temperature probe, with Temperature sensor PT 100.
- Inlet for inert pressure Gas (connected to S2)
- Analogical pressure gauge probe
- Sampling pipe.
- Inlet for the liquid circuit

Table 3.2 Technical characteristics of Pressure Tank S1

Material	AISI 316L/PTFE
Tank inner volume (L)	5
Tank Pmax (barg)	10
Tank Tmax (°C)	180
Jacket inner volume (L)	3
Jacket Pmax (barg)	0.5
Jacket Tmax jacket (°C)	190
Standard	I PED

Pressurized Gas Cylinder (S2).

The liquid circuit is kept at a constant pressure, higher than the liquid vapor pressure, with pressurized Nitrogen (N₂).

Centrifugal Pump (G1)

The pump purchased to Lowara ® is from the series 1SV04, the version NH, pumps for design for high temperature operation. The main technical characteristics as rating, construction materials, power, operational characteristics and more are reported on Table 3.3.

Table 3.3 Technical characteristics of centrifugal pump G1

Model	ISV04
Material	AISI 316L
T max (°C)	150
Circuit Pmax (bar)	19 bar
H (m)*	24
Flow min (l/min)*	12
Flow max (l/min)*	40
Power (kW)	0.37
Supply (Hz)	50
Weight (kg)	23.6

liquid density $\rho = 1.0 \text{ kg/dm}^3$
kinematic viscosity $\nu = 1 \text{ mm}^2/\text{s}$

Heat exchanger Thermostatic Oil Bath (BT1) and coils

The thermostatic oil bath, was selected to perform the heating activities in the circuit, was sized considering the necessity to achieve 150 °C with a reduced area exchange coil and the option of pumping the heating fluid through the jacket of the pressure tank S1. For this purpose was selected a silicone oil that can stand a maximum temperature of 240 °C. The technical characteristics of the Heating Circulator, the bath tank and the silicone Oil are reported on Table 3.4.

Table 3.4 Technical characteristics of Thermostatic Bath BT1

	Material	Stainless Steel
Bath tank	Inner dimension WxLxD (mm)	500x300x300
	Outer dimension WxLxD (mm)	540x330x350
	Volume (l)	39
	T min (°C)	20
Bridge mounted circulator	T max (°C)	300
	Heat Capacity (kW)	3
	Dimension WxLxH (mm)	320x170x400
Bath cover	Material	Stainless Steel
Fluid	Silicon oil	
	N° CAS	68083-14-7

On the Thermostatic oil bath might be placed two **exchange coils** in stainless steel AISI 316 designed and constructed for the project. One of the coils is for the gas circuit and the second one, with three times the area of the first one is for the liquid circuit. The stainless steel AISI 316 was the material considered for the coils as it has a greater malleability than other steel alloys.

Table 3.5 Technical characteristics of heat exchanger coils

	<i>Liquid</i>	<i>Gas</i>
<i>n° of coils</i>	3	1
<i>Inner/Outer Diameter</i>	9/12	9/12
<i>Effective length (mm)</i>	7650	2550
<i>Exchange Area (m²)</i>	0.288	0.096
<i>Material</i>	AISI 316	AISI 316

3.2 Pilot Plant Operative Limits

On Table 3.6 the operative limits are listed for each element on the pilot plant particularly the maximum operational pressure and temperature. It can be seen that: operative limits are ruled by the Pressure Tank (S1) maximum pressure and the Centrifugal Pump (G1) maximum temperature. On Figure 3.2 is summarized the reliable working areas ruled by the limits imposed by the Pressure Tank and the Centrifugal Pump

Table 3.6 Operative limits for each element of pilot plant

<i>Equipment</i>	<i>T max (°C)</i>	<i>P max (barg)</i>	<i>Material</i>
<i>Pressure Tank S1</i>	180	10	AISI 316L/PTFE
<i>Centrifugal Pump G1</i>	150	18	AISI 316L/PTFE
<i>Thermostatic Oil Bath BT1</i>	250	0	ASTM 304
<i>Liquid Pipeline</i>	–	352.6 (at 37°C)	316/316L SS*
<i>Liquid Flexible Pipeline</i>	454	46.3 (at 454°C)	316L SS
<i>Needle Valve (liquid side)</i>	232	235	316 SS
<i>Plug Valve (liquid side)</i>	204	68.9 (at 204°C)	316 SS/PTFE

Gas Pipeline	–	179.2 (at 37°C)	316/316L SS*
Gas Flexible Pipeline	454	57.8 (at 454°C)	316L SS
Needle Valve (gas side)	232	235	316 SS
Plug Valve (gas side)	204	68.9 (at 204°C)	316 SS /PTFE
Gas Service Flexible Pipeline	232	99.2 (at 232°C)	PTFE/SS

* Carbon < 0.03 max wt % (Data Sheet)

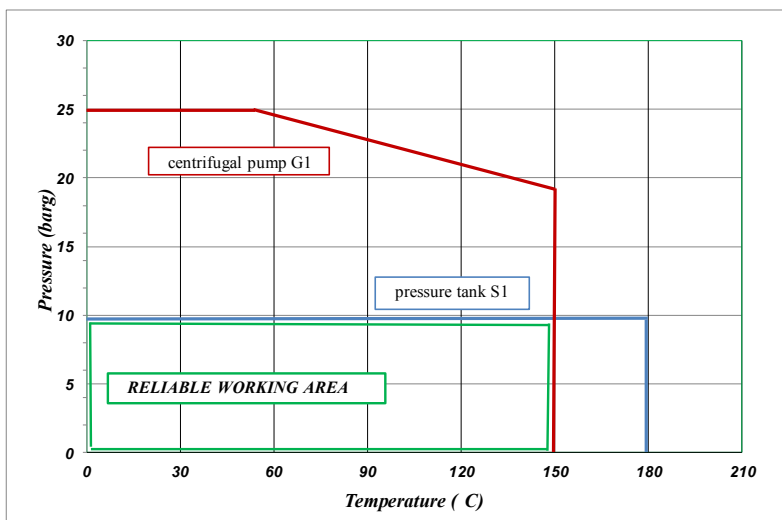
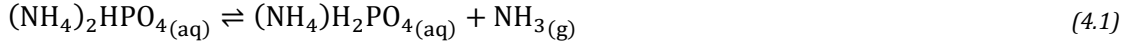


Figure 3.2 Operative condition area for a reliable operation.

4 Physical-Chemical Equilibrium

For the understanding of the chemistry of the problem, and start setting up of the main process parameters, it is of great importance to carry out a deep study of the physical-chemical equilibrium. The chemistry to be studied is multi-phase reaction for the regeneration of Di Ammonium Phosphate ($DAP_{(aq)}$) for the production of Ammonium Di hydrogen Phosphate ($ADP_{(aq)}$) and ammonia in gas phase illustrated on equation (4.1) and (4.2)



A suitable equilibrium model will allow to understand not only the thermodynamics of the problem but also mass and heat transfer phenomena. This made the equilibrium study of great importance for the description of the problem and finally for the design of the process and the equipment.

A dissolution-electrolyte and a phase equilibrium model have been developed for a closed system (Temperature-Volume constant). Some hypothesis have been taken into consideration to develop the models as simple as possible but robust enough to describe with accuracy the system.

4.1 Dissolution model for the DAP - ADP- Water system.

The set of reactions (4.1) and (4.2) can be considered stoichiometrically equivalent to the ionic equilibrium below reported, in the case when at room temperature, it might be supposed ammonia and water volatility as negligible.



For each reaction the corresponding equilibrium constant can be written by using the activity of each component.

$$K_{c1} = \frac{\{H^+\}\{H_2PO_4^-\}}{\{H_3PO_4\}} \quad (4.3)$$

$$K_{c2} = \frac{\{H^+\}\{HPO_4^{2-}\}}{\{H_2PO_4^-\}} \quad (4.4)$$

$$K_{c3} = \frac{\{H^+\}\{PO_4^{3-}\}}{\{HPO_4^{2-}\}} \quad (4.5)$$

$$K_b = \frac{\{NH_4^+\}\{OH^-\}}{\{NH_3\}\{H_2O\}} \quad (4.6)$$

$$K_w = \frac{\{H^+\}\{OH^-\}}{\{H_2O\}} \quad (4.7)$$

In wich

$$\{A\} = x_A \gamma_A \quad (4.8)$$

Represents the activity of each component, and γ_A is the corresponding activity coefficient. Specific models and equations have been develop for γ_i calculation. The Debye-Hückel theory, the Davies (an extension of the previous one) and the Pitzer equations are suitable model. Before performing advance calculations, the ideal solution model was assumed.

4.1.1 Ideal solution Model

The Ideal Model is based on the hypothesis, of extremely diluted solutions, so that, the activity coefficients of ions can be assumed to be unity. For the same reason, also water activity is assumed as unity.

So doing, activities in equation (4.3) to (4.7) can be represented by molar concentrations.

The Table 4.1 collects the literature data of equilibrium constant, free Gibbs energy and activation enthalpy for each reaction in the stoichiometric system.

Table 4.1 Equilibrium constant, free Gibbs energy and activation enthalpy for the stoichiometric system (Lide, 2006)

Reaction	$\Delta G_R^{25^\circ C}$ (J/mol)	$\Delta H_R^{25^\circ C}$ (J/mol)	K_{eq} (25 °C)
[c1]	12255,65	-7650	7,12e-03
[c2]	41000	4200	6,56e-08
[c3]	70400	14700	4,64e-13
[b]	-27531,8	-4437,79	1,51e-5
[w]	80160,61	-7650	9,03e-15

The molar balance for phosphorous and ammonia and the charge balance in equations (4.9) to (4.11) are used to define the complete set of equations:

$$C_{TOT} = [H_3PO_4] + [H_2PO_4^-] + [HPO_4^{2-}] + [PO_4^{3-}] \quad (4.9)$$

$$C_{0,N} = [NH_3] + [NH_4^+] \quad (4.10)$$

$$[H^+] + [NH_4^+] = [OH^-] + [H_2PO_4^-] + 2[HPO_4^{2-}] + 3[PO_4^{3-}] \quad (4.11)$$

The problem can be solved rearranging equations by using parameters α_0 , α_1 , α_2 and α_3 as indicated in equation (4.12); the resulting relationships are reported in equations (4.13) to (4.16).

$$\alpha_0 = \frac{[PO_4^{3-}]}{C_{TOT}}, \alpha_1 = \frac{[HPO_4^{2-}]}{C_{TOT}}, \alpha_2 = \frac{[H_2PO_4^-]}{C_{TOT}}, \alpha_3 = \frac{[H_3PO_4]}{C_{TOT}} \quad (4.12)$$

$$\alpha_0 = \frac{1}{\frac{[H^+]^3}{K_{C1}K_{C2}K_{C3}} + \frac{[H^+]^2}{K_{C2}K_{C3}} + \frac{[H^+]}{K_{C3}} + 1} \quad (4.13)$$

$$\alpha_1 = \frac{1}{\frac{[H^+]^2}{K_{C1}K_{C2}} + \frac{[H^+]}{K_{C2}} + 1 + \frac{K_{C3}}{[H^+]}} \quad (4.14)$$

$$\alpha_2 = \frac{1}{\frac{[H^+]}{K_{C1}} + 1 + \frac{K_{C2}}{[H^+]} + \frac{K_{C2}K_{C3}}{[H^+]^2}} \quad (4.15)$$

$$\alpha_3 = \frac{1}{1 + \frac{K_{C1}}{[H^+]} + \frac{K_{C1}K_{C2}}{[H^+]^2} + \frac{K_{C1}K_{C2}K_{C3}}{[H^+]^3}} \quad (4.16)$$

Finally, the ammonium and the ammonia concentration can be given by.

$$[NH_4^+] = \frac{C_{0,N}}{\left(\frac{K_w}{K_b[H^+]} + 1\right)} \quad (4.17)$$

$$[NH_3] = \frac{C_{0,N}}{\left(1 + \frac{K_b[H^+]}{K_w}\right)} \quad (4.18)$$

Rearranging, we can obtain the following equation, which can be used to get $[H^+]$ and the pH.

$$[H^+] = \frac{K_w}{[H^+]} + C_{TOT}(\alpha_2 + 2\alpha_1 + 3\alpha_0) - \frac{C_{0,N}}{\left(\frac{K_w}{K_b[H^+]} + 1\right)} \quad (4.19)$$

4.1.2 ENRTL (Chen & Song, 2004)

A summary of the model is reported in the following.

The model is developed using the unsymmetrical convention: reference is at infinity dilution for electrolytes, whereas it is pure component for solvent.

The model is developed based on the generalization of segment interaction concept. Such concept permits to model each component of the system (solvent and solute) as an oligomer made of different segment species. The segment species can be anionic, cationic, and molecular (without electric charge). (Chen & Song, 2004).

The model has been further improved during the years, nonetheless the main concepts are the same reported here. It take into account two contributions for the excess Gibbs free energy. The first one is due to the short-range local interactions in the neighborhood; the second is due to the long-range interaction.

The basic equation of the ENRTL model for the excess Gibbs energy of electrolyte systems is:

$$G_m^{*ex} = G_m^{*ex,lc} + G_m^{*ex.PDH} \quad (4.20)$$

* denotes the unsymmetrical state, m the system.

The first term on the right is the short-range term, it is calculated with the NRTL model; the second term on the right is the long-range term due to the ion-ion interaction and is evaluated with the Pitzer-Debye-Hückel (PDH) model.

Consequently, the activity coefficient of the component I results:

$$\ln \gamma_I^* = \ln \gamma_I^{*,lc} + \ln \gamma_I^{*,PDH} \quad (4.21)$$

The local activity coefficient ($\ln \gamma_I^{*,lc}$) is evaluated considering each species divided in three different types of segments: anionic, cationic, and molecular (interaction segment concept).

The local interactions are evaluated using the NRTL model. This model uses the symmetric reference state. Therefore the system has to be “normalized”, the activity coefficient expression becomes:

$$\ln \gamma_I^{*,lc} = \ln \gamma_I^{lc} - \ln \gamma_I^{\infty,lc} \quad (4.22)$$

γ_I^{∞} is the activity coefficient at infinity dilution of ionic compound I, this can be calculated with the following equation:

$$\ln \gamma_I^{lc} = \frac{1}{RT} \left(\frac{\partial G_m^{ex,lc}}{\partial n_I} \right)_{T,P,n_{j \neq I}} \quad (4.23)$$

The expression of the local excess Gibbs energy assumes three types of interactions: the first type considers a central neutral species surrounded by ions, the other two types considers respectively a central cation and a central anion. In each contribution, the local electro neutrality is maintained.

$$\begin{aligned} \frac{G_m^{ex,lc}}{RT} = & \sum_I \sum_m r_{m,I} n_I \left(\frac{\sum_j X_j G_{jm} \tau_{jm}}{\sum_k X_k G_{km}} \right) + \sum_I \sum_c z_c r_{c,I} n_I \left(\sum_c Y_c \frac{\sum_j X_j G_{jc,ac} \tau_{jc,ac}}{\sum_k X_k G_{kc,ac}} \right) \\ & + \sum_I \sum_a z_a r_{a,I} n_I \left(\sum_a Y_a \frac{\sum_j X_j G_{ja,ca} \tau_{ja,ca}}{\sum_k X_k G_{ka,ca}} \right) \end{aligned} \quad (4.24)$$

$$X_j = C_j x_j \quad (4.25)$$

$$x_j = \frac{\sum_j x_j r_{j,J}}{\sum_I \sum_i x_i r_{j,I}} \quad (4.26)$$

$$G = \exp(-\alpha \tau) \quad (4.27)$$

i, j and k means the segment-based species index, I e J denote the component. C_j is the charge for the ionic and is 1 for the neutral species. x_j and x_i are the molar fraction of segments and the molar fraction of the component j and J. $r_{m,I}$, $r_{c,I}$, $r_{a,I}$ are the number of molecular segment species m, cationic species c and anionic species a in the component I, respectively.

The system present two adjustable parameters for each species: τ the asymmetric binary interaction parameters and α , the symmetric nonrandom factor parameters.

The authors assert that, typically, the parameter α is set constant and equal to 0.2 or 0.3. Practically only the τ parameter is adjusted.

Both the parameters are divided in three groups: between two molecular species, between an electrolyte and a neutral species and between two electrolyte species. Here electrolyte is meant to represent an ion pair composed of a cationic species and an anionic species

Finally the local activity coefficient expression is:

$$\ln \gamma_i^{lc} = \sum_m r_{m,I} \gamma_m^{lc} + \sum_c r_{c,I} \gamma_c^{lc} + \sum_a r_{a,I} \gamma_a^{lc} \quad (4.28)$$

The Long-range interaction PDH contribution to the activity coefficient ($\ln \gamma_i^{*PDH}$) is evaluated as follows:

$$\begin{aligned} \ln \gamma_i^{*PDH} &= \frac{1}{RT} \left(\frac{\partial G^{*ex,PDH}}{\partial n_i} \right)_{T,P,n_{j \neq i}} \\ &= - \left(\frac{100}{MW_s} \right)^{1/2} A_\phi \left[\left(\frac{2z_i^2}{\rho} \right) \ln \left(1 + \rho I_x^{1/2} \right) + \frac{z_i^2 I_x^{1/2} - 2I_x^{1/2}}{1 + \rho I_x^{1/2}} \right] \end{aligned} \quad (4.29)$$

$$I_x = \frac{1}{2} \sum_i x_i z_i^2 \quad (4.30)$$

$$A_\phi = \frac{1}{3} \left(\frac{2\pi N_A d_s}{1000} \right)^{1/2} \left(\frac{Q_e^2}{\epsilon_s k_b T} \right)^{3/2} \quad (4.31)$$

A_ϕ is the Debye-Hückel parameter; I_x is the ionic strength (calculated on the segment mole fraction scale); MW_s is the molecular weight of the solvent; ρ is the closest approach parameter ($\rho=14.9$); N_A is the Avogadro's number; d_s is the density of the solvent; Q_e is the electron charge; ϵ_s is the dielectric constant of the solvent; k_b is the Boltzmann constant; z_i is the charge of the based-segment species i .

For an oligomer ionic component I the logarithm activity coefficient expression is the sum of the contribution of each segment:

$$\ln \gamma_I^{*PDH} = \sum_m r_{m,I} \ln \gamma_m^{*PDH} + \sum_c r_{c,I} \ln \gamma_c^{*PDH} + \sum_a r_{a,I} \ln \gamma_a^{*PDH} \quad (4.32)$$

The model is available implemented in the software ASPEN PLUS.

4.1.2.1 Application on Aspen plus simulator

To fit the same hypothesis state in the 4.1 the vapor phase of the mixtures should be set to zero. On the simulator the pressure will be compensated in order to achieve the value of composition of the vapor phase.

Components Selection reaction set.

To describe a particular electrolyte system all the species involve in the equilibriums (Complete dissociation of strong electrolytes, Partial dissociation of weak electrolytes, Ionic reactions among ionic species, Complex ion formation and Salt precipitation and dissolution) have to be listed. In order to guarantee all the component to be listed and all the reactions to be describe, the software offers an electrolyte wizard, available when an electrolyte fluid package is chosen. The main condition to use the wizard is to have selected in the components list the Water and

the non-dissociated form of the species (for example water, Diammonium Phosphate (DAP) and Ammonium dihydrogen Phosphate). Should be selected the desired reactions and the hydrogen ion type. After the wizard have run, it is generated in addition to the components the equation reaction set.

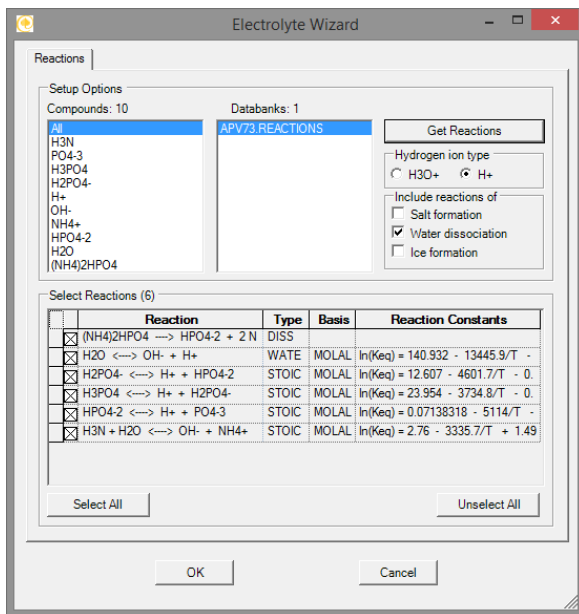


Figure 4.1 Aspen plus Electrolyte Wizard

Simulation Scheme.

The problem was simulated as the mixture two saturate solutions of DAP and ADP with a second stream of pure Water. After each mixture the temperature of the streams was re set to the desired temperature to avoid heating or cooling due to mixing effects.

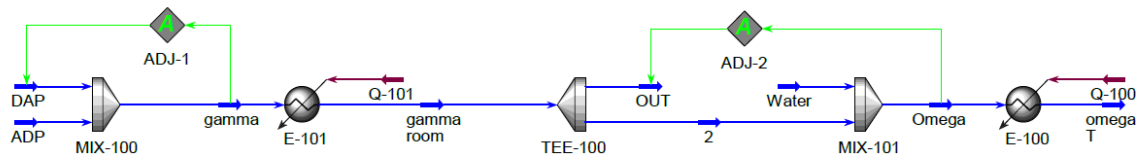


Figure 4.2 Aspen plus Mixture Scheme

4.1.3 Experimental results for solution model validation

The theoretical models proposed to simulate the dissolution of the triprotic acid (phosphate) with a soft base (ammonium) are rather difficult to validate. The analysis of any sample (ex situ) implies the alteration of the equilibrium and the results will give us a complete different state of the mixture composition. However the concentration of each single species on the complex mixture is characterized by a single value of pH as described by the ideal model, possible to measure in situ. Has been decided to follow the behavior of the pH as can be a pretty sensitive value, especially in some range of the mixture, and can describe accurately the composition of the mixture.

To simulate the different mixtures compositions were performed measurements of pH for different mixtures of DAP and ADP in water. Experiments were performed on an open air system at room T up to 70 °C. The effect of composition was investigated; owing to the complexity of the solution two parameters were defined (ω_0 and Γ).

ω_0 is the equivalent mass fraction of DAP. It is defined by the equation:

$$\omega_0 = \frac{m_{DAP}^{equiv}}{m_{TOT}} = \frac{m_{DAP}^0 + m_{ADP}^0 * \left(\frac{MW_{DAP}}{MW_{ADP}} \right)}{m_{TOT}} \quad (4.33)$$

The notation “0” means the initial value in the solution, indeed m_{DAP}^{equiv} is the hypothetical initial mass of DAP in the system in the case in which each mole of ADP is converted to DAP.

Γ (the solution loading) is has the meaning of the ratio between the initial of moles of ADP and the sum of initial moles of DAP and ADP:

$$\Gamma = \frac{c_{0,ADP}}{c_{0,DAP} + c_{0,ADP}} \quad (4.34)$$

The meaning of these two parameters becomes obvious if we set ω_0 and try to change Γ . Setting ω_0 means to set the molar fraction of phosphate that is equivalent to keep the total moles of phosphorus as constant. While, changing Γ value at the same time, means to perform a simulation of the progress of the reaction of conversion from DAP into ADP (4.1).

The experiments have been performed for three values of $\omega_0 = 5.03\%$, 10.05% , 25.13% and different values of T and Γ . The results are reported Figure 4.3 and Figure 4.4

In the same figures, a comparison between the experimental results with the ones provided by the models allows to check its accuracy. Both in the case of “ideal solution model” and in the case of ENRTL model.

Even though the experimental procedure did not fit all the hypothesis made for the models, like the non-volatility of the components. The working temperatures and measurement times were reduced to avoid changes, once the solution has reached the setting temperature.

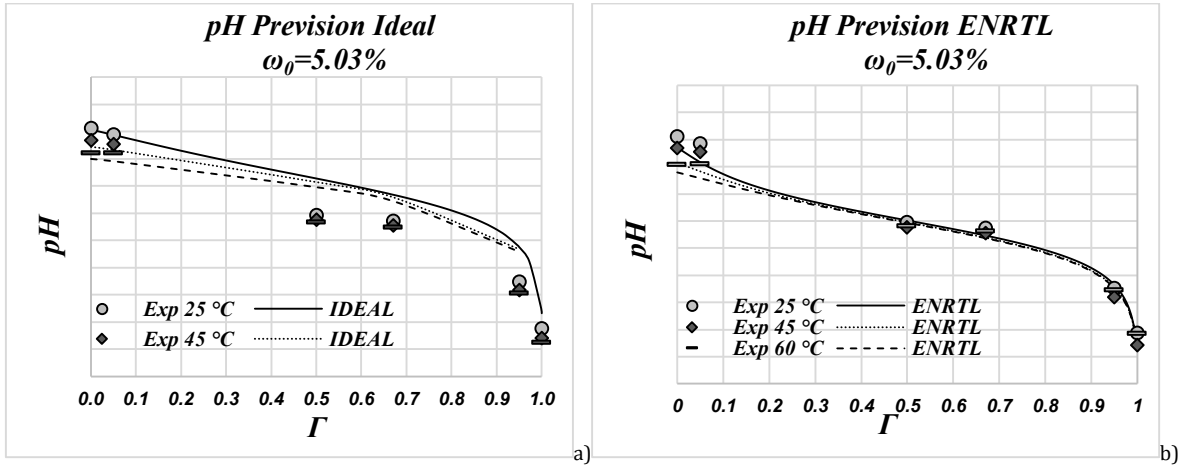


Figure 4.3 pH experimental data and pH model previsions for Ideal model a) and ENRTL model b) for total phosphate molar concentration 5.03 %.

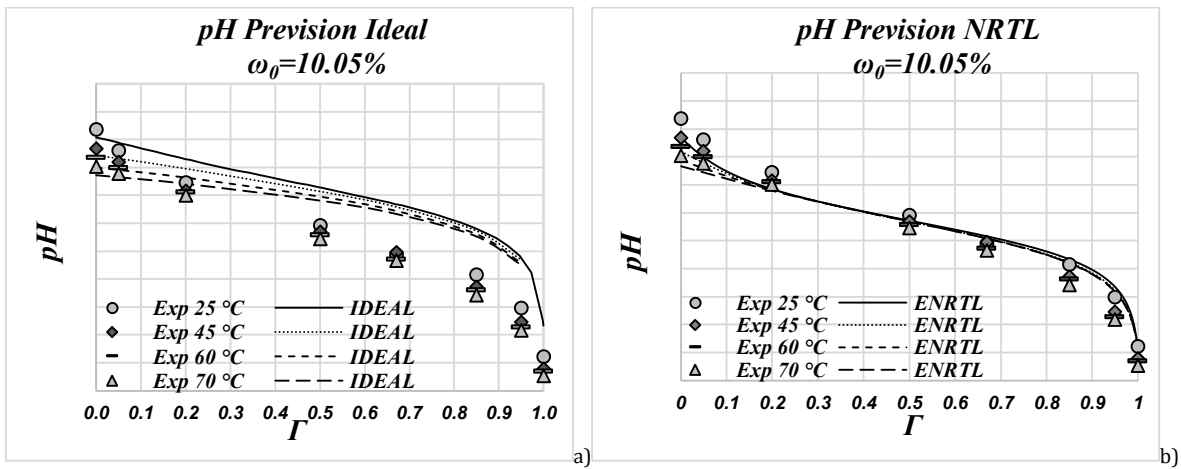


Figure 4.4 pH experimental data and pH model previsions for Ideal model a) and ENRTL model b) for total phosphate molar concentration 10.05 %.

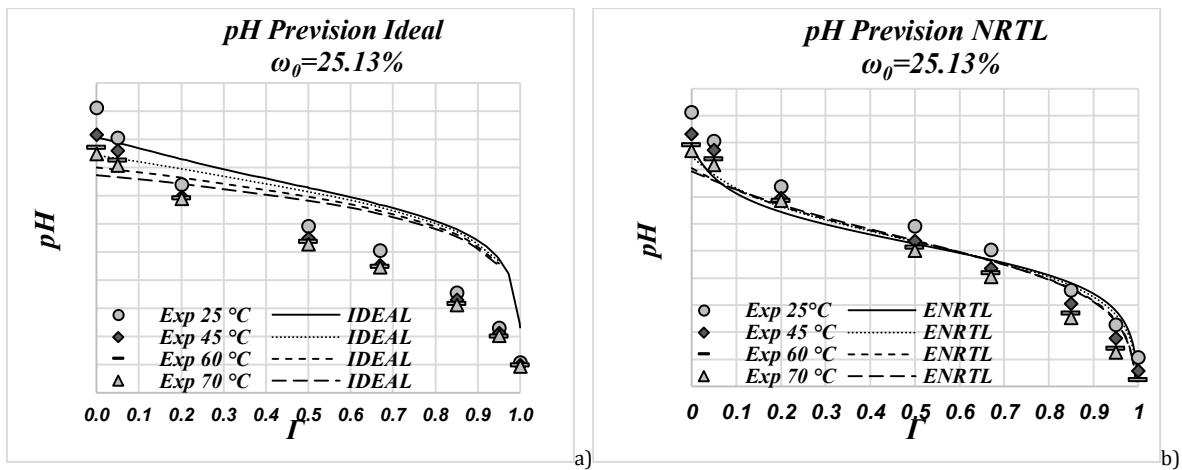


Figure 4.5 pH experimental data and pH model previsions for Ideal model a) and ENRTL model b) for total phosphate molar concentration 25.13 %.

Apparently, it is self-evident that the predictions by ideal solution model greatly overestimated the pH respect experimental trend. Discrepancies are higher as the phosphate concentration (ω_0) increases. On the contrary ENRTL model gives a more accurate prediction, at least in the range of composition investigated.

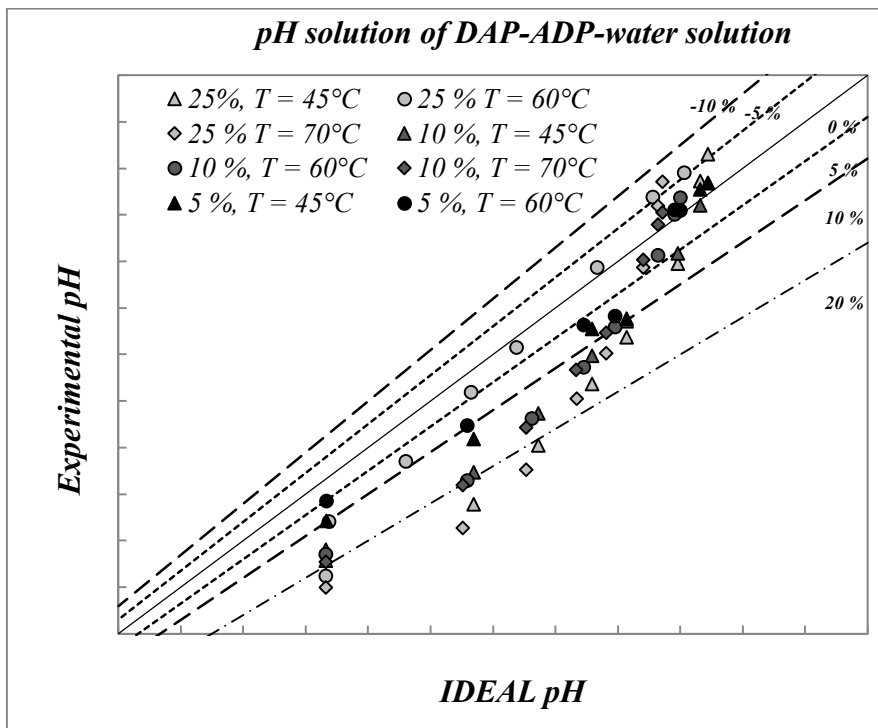


Figure 4.6 Parity plot for Ideal model vs Experimental data

An overall view, of the quality of the predictions is reported in the parity plots, both for, the ideal model (Figure 4.6) and the ENRTL model (Figure 4.7). With regards to the ideal model it can be seen that as the ω_0 value increases the deviation between the model and the experimental data approaches to errors close to 30 % at $\omega_0=25.13$ %.

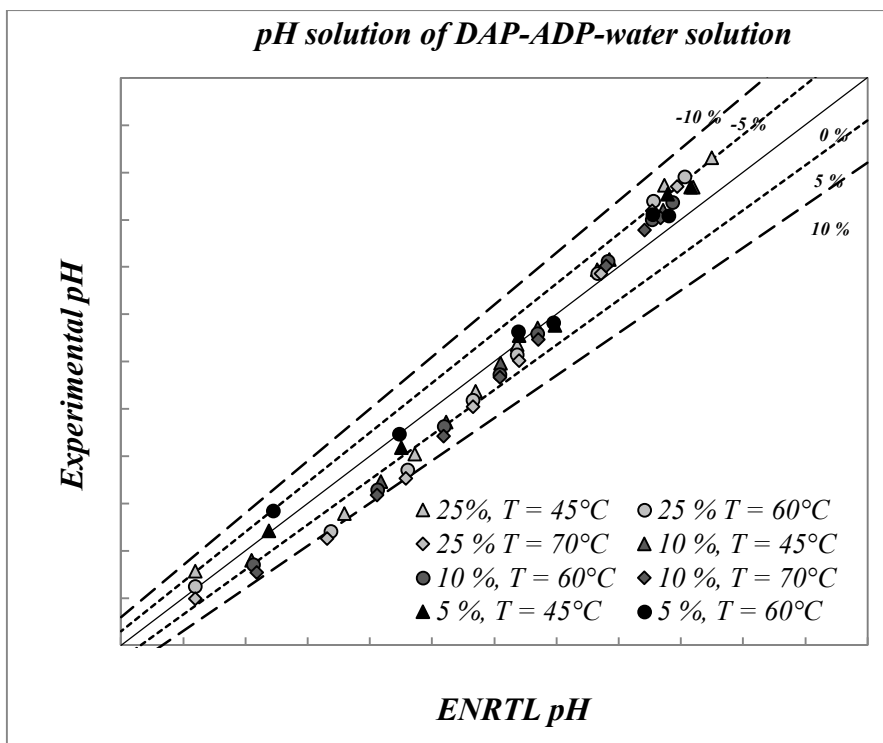


Figure 4.7 Parity plot for ENRTL model vs Experimental data

In the case of ENRTL prediction, errors are lower. At the highest phosphate concentration the error increase as the temperature increases reaching a maximum of 10 %. In addition it can be seen that at room temperature the model copies the experimental data. It is possible that the hypothesis of non-volatility was overtaken during the experimental procedure and at higher temperatures the evaporation of the solvent generates errors even if these are not of great magnitude.

ENRTL model, applied on the process simulator Aspen Plus, is considered an accurate tool to predict concentrations of all the species in the solution, since it is very complicated to perform measurements of them. This is the case of the aqueous ammonia for instance. A case of calculation was performed for the ADP-DAP mixture of $\omega_0=5.03$ % and $\Gamma=0.5$, in the temperature range between 25 and 150 °C. Results are reported on Figure 4.8. With reference to the main ionic species it can be observed that the molar fraction of HPO_4^{2-} and H_2PO_4^- is, in almost all the temperature range 4 – 5 magnitude orders higher than the molar fraction of H_3PO_4 and PO_4^{3-} . The phosphoric acid starts to be relevant only after 125 °C, although it remains 2 magnitude order lower than HPO_4^{2-} .

As a conclusion, the results of this simulation (confirmed by the experimental results) allow us to account only the electrolyte equilibrium between HPO_4^{2-} and H_2PO_4^- in the equilibrium phase model. Thus giving a remarkable simplification of the reaction system.

Finally the model can be used to evaluate mixture properties such as density, viscosity, heat capacity and other parameters important for the heat, mass and momentum transport.

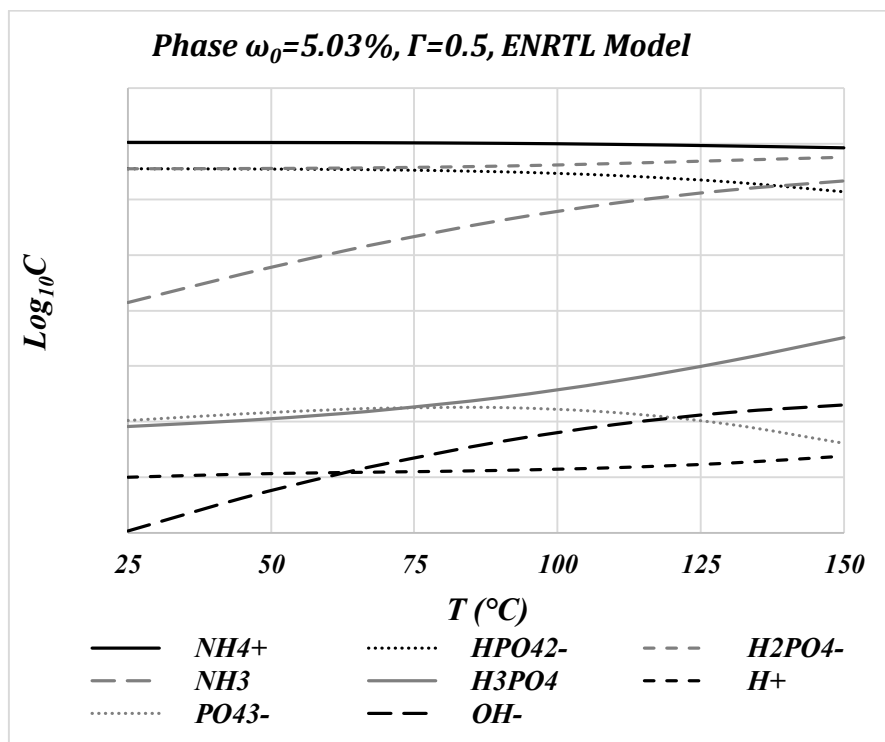


Figure 4.8 Electrolyte concentration vs. Temperature for the system ADP-DAP $\omega_0=5.03\%$, $\Gamma=0.5$: ENRTL model

4.2 Henry Constant and Salting-Out Effect (Sechenov, 1889).

The vapor-liquid equilibrium of aqueous ammonia is usually described by using the Henry constant, this constant and its dependence with the temperature is well reported on literature (Perry & Green, 2007).

In this study, we are faced with the problem of aqueous ammonia solutions containing phosphate at high concentrations and salting-out effect cannot be neglected. The salting-out can be seen as a sort of increasing of the Henry constant, with respect to the case of water-ammonia solutions. This phenomenon and its entity was reported by different authors, among them (Danckwerts, 1970) and (Sechenov, 1889) can be reported.

Those authors proposed to describe this effect according to the equation (4.35).

$$\log_{10} \left(\frac{H_{sol}}{H_w} \right) = hI \quad (4.35)$$

This equation relates the increment of the volatility with the ionic force I and some particular parameters for each ion and gas, indicated as “ h ”.

$$h = h_+ + h_- + h_G \quad (4.36)$$

The parameter h is composed by different contributions, frequently tabulated at room temperature.

(Hermann, Dewes, & Schumpe, 1995) revised the experimental data reported on bibliography and reported optimized values for h and simplified the model for solutions with a single electrolyte according to equation(4.37) parameters are reported on Figure 4.9

$$h = \sum_i (h_+ + h_G) \nu_i \quad (4.37)$$

In which ν_i is the stoichiometric coefficient of dissociated ion

The modified Sechenov equation, reported by Hermann and colleges is:

$$\log_{10} \left(\frac{H_{sol}}{H_w} \right) = hC_{sate} \quad (4.38)$$

For solutions containing mixtures of electrolytes the original model by Sechenov should be used. This should be the right model to apply on the particular case of DAP-ADP solution for the vapor liquid equilibrium of ammonia. Yet experimental measurements are necessary to validate the model predictions in order to be used on a mass transport model.

1674

Shorter Communications

Table 1. Ion-specific parameters h_i and gas-specific parameters h_G for the suggested model [eq. (2)] at 298.2 K

Cation	h_i ($m^3 kmol^{-1}$)	Data [†]	Anion	h_i ($m^3 kmol^{-1}$)	Data [†]	Gas	h_G ($m^3 kmol^{-1}$)	Data [†]
H ⁺	0.0000 [‡]	(22)	OH ⁻	0.0918	(13)	H ₂	-0.0176	(16)
Li ⁺	0.0687	(19)	F ⁻	0.1058	(6)	He	-0.0368	(9)
Na ⁺	0.1079	(77)	Cl ⁻	0.0381	(104)	Ne	-0.0147	(7)
K ⁺	0.0929	(86)	Br ⁻	0.0266	(30)	Ar	-0.0026	(8)
Rb ⁺	0.0749	(10)	I ⁻	0.0233	(24)	Kr	-0.0085	(11)
Cs ⁺	0.0582	(11)	NO ₂ ⁻	0.0726	(1)	Xe	0.0094	(2)
NH ₄ ⁺	0.0555	(28)	NO ₃ ⁻	0.0136	(45)	Rn	0.0170	(1)
Mg ²⁺	0.1576	(12)	ClO ₃ ⁻	0.1390	(1)	CH ₄	0.0028	(8)
Ca ²⁺	0.1543	(9)	ClO ₄ ⁻	0.0549	(4)	C ₂ H ₂	-0.0174	(30)
Ba ²⁺	0.1710	(9)	BrO ₃ ⁻	0.1158	(1)	C ₂ H ₄	0.0014	(15)
Fe ²⁺	0.1694	(2)	IO ₃ ⁻	0.0956	(1)	C ₂ H ₆	0.0115	(7)
Co ²⁺	0.1582	(3)	IO ₄ ⁻	0.1469	(1)	C ₃ H ₈	0.0461	(5)
Ni ²⁺	0.1556	(3)	HCO ₃ ⁻	0.1019	(2)	C ₄ H ₁₀	0.0552	(2)
Cu ²⁺	0.1490	(4)	H ₂ PO ₃ ⁻	0.0601	(1)	CO ₂	-0.0183	(29)
Mn ²⁺	0.1474	(5)	H ₂ PO ₄ ⁻	0.1009	(3)	N ₂	0.0002	(5)
Zn ²⁺	0.1588	(4)	∅OCH ₂ COO ⁻	-0.0089	(1)	NH ₃	-0.0506	(26)
Cd ²⁺	0.2028	(4)	CN ⁻	0.0722	(1)	NO	0.0060	(1)
Al ³⁺	0.2192	(6)	SCN ⁻	0.0670	(1)	N ₂ O	-0.0110	(44)
Fe ³⁺	0.0957	(3)	HCrO ₄ ⁻	0.0408	(1)	O ₂	0.0000 [‡]	(54)
Cr ³⁺	0.0578	(2)	HPO ₄ ²⁻	0.1559	(3)	H ₂ S	-0.0341	(15)
			CO ₃ ²⁻	0.1558	(7)	SO ₂	-0.0832	(14)
			S ₂ O ₃ ²⁻	0.1268	(2)	SF ₆	0.0108	(10)
			SO ₃ ²⁻	0.1357	(3)			
			SO ₄ ²⁻	0.1164	(60)			
			PO ₄ ³⁻	0.2243	(3)			

[†] Number of systems with ion *i*.

[‡] Number of systems with the respective gas.

[§] Arbitrary choice (Schumpe, 1993).

^{||} Adopted from Schumpe (1993).

Figure 4.9 h parameters for ions and Gas for the evaluation of Salting-out effect.

The results obtained are reported in Figure 4.10 for the case of DAP-ADP solution.

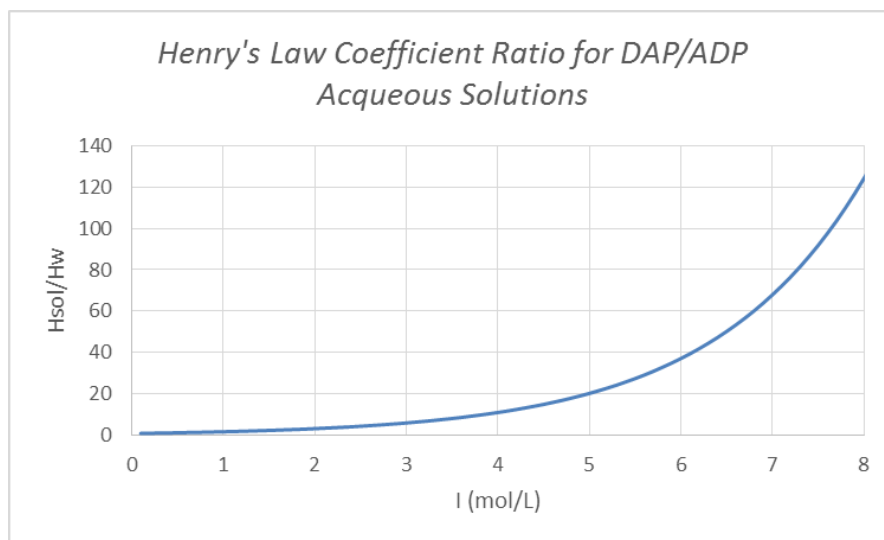


Figure 4.10 Increase of ammonia Henry constant for the DAP-DAP

4.3 Vapor-Liquid equilibrium model at constant volume.

The phase equilibrium (L-V), which involves chemical equilibrium with electrolytic reactions and heterogeneous reactions, will be represented through three equilibrium conditions of the system at constant volume and temperature.

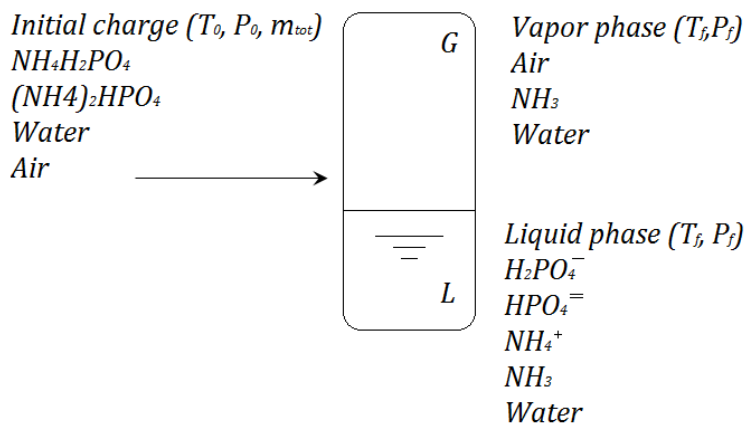


Figure 4.11 Phase equilibrium representation.

Figure 4.11 represents the system where the mixture of aqueous ADP and DAP is loaded on a close tank (with air as inert) and the temperature is raised up to the target temperature. The solution represents the equilibrium of the system at the final temperature. The components from the initial charge separate in two phase accordingly with the physical-chemical equilibrium and the process conditions without considering the kinetics of the reaction.

On the previous section the electrolyte equilibrium system was evaluated deprived of the components volatility. One of the conclusion was that, only the equilibrium between HPO_4^{2-} and H_2PO_4 was relevant on the concentration of the phosphate species and so on the phase equilibrium two of the reaction might be neglected.

The model will only consider the equilibrium between HPO_4^{2-} and H_2PO_4 the ammonia and the water hydrolysis.



The equilibrium model was developed for the case of ideal solution, with the hypothesis proper, of highly diluted solutions.

Notwithstanding the clear deviation of the ideal solution model, it worth performing the phase equilibrium study with the ideal solution hypothesis. The results might be accurate as in the phase equilibrium only volatile components are considered, water and ammonia and the high water concentration should rule the physical conditions.

4.3.1 *Mathematical model*

The physical-chemical equilibrium is represented by the following equation system.

Initial input.

$$n_{NH_4^+}^{IN} = 2n_{DAP}^{IN} + n_{ADP}^{IN} \quad (4.39)$$

$$n_{HPO_4^{2-}}^{IN} = n_{DAP}^{IN} = m_{DAP}^{IN} MW_{DAP} \quad (4.40)$$

$$n_{H_2PO_4^-}^{IN} = m_{ADP}^{IN} MW_{ADP} \quad (4.41)$$

$$n_{H_2O}^{IN} = m_{H_2O}^{IN} MW_{H_2O} \quad (4.42)$$

Chemical and phase equilibriums

$$K_{C2}(T) = \frac{m_{H_2PO_4^-}}{m_H + m_{HPO_4^{2-}}} \quad (4.43)$$

$$K_b(T) = \frac{m_{NH_3} x_{H_2O}}{m_{NH_4^+} + m_{OH^-}} \quad (4.44)$$

$$K_w(T) = \frac{m_H + m_{OH^-}}{x_{H_2O}} \quad (4.45)$$

$$y_{H_2O} P_f = P_{H_2O}^*(T) x_{H_2O} \quad (4.46)$$

$$y_{NH_3} P_f = H_{NH_3}^{(m)}(T) m_{NH_3} \quad (4.47)$$

Phase congruence relations

$$y_{H_2O} + y_{Air} + y_{NH_3} = 1 \quad (4.48)$$

$$x_{H_2O} + x_{NH_3}^{diss} + x_{NH_4^+} + x_{HPO_4^{2-}} + x_{H_2PO_4^-} + x_H + x_{OH^-} = 1 \quad (4.49)$$

$$x_i = \frac{n_i}{n_L} \quad \forall i = 1, \dots, N - 1 \quad (4.50)$$

Molar balance

$$n_{H_2O}^L + Gy_{H_2O} = n_{H_2O}^{IN} + \xi_b - \xi_w \quad (4.51)$$

$$n_{NH_3(aq)} + Gy_{NH_3} = \xi_b \quad (4.52)$$

$$n_{NH_4^+} = n_{NH_4^+}^{IN} - \xi_b \quad (4.53)$$

$$n_{HPO_4^{2-}} = n_{HPO_4^{2-}}^{IN} - \xi_{C2} \quad (4.54)$$

$$n_{H_2PO_4^-} = n_{H_2PO_4^-}^{IN} + \xi_{C2} \quad (4.55)$$

$$n_{H^+} = n_{H^+}^{IN} - \xi_{C2} + \xi_w \quad (4.56)$$

$$n_{OH^-} = n_{OH^-}^{IN} - \xi_b + \xi_w \quad (4.57)$$

$$Gy_{Air} = n_{Air}^{IN} \quad (4.58)$$

$$n_L = n_{H_2O}^L + n_{NH_3(aq)} + n_{NH_4^+} + n_{HPO_4^{2-}} + n_{H_2PO_4^-} + n_{H^+} + n_{OH^-} \quad (4.59)$$

Constant volume constrains

$$V_{TOT} = V_L + V_G \quad (4.60)$$

$$M_L = V_L \rho_L(T) \quad (4.61)$$

$$V_G = G \frac{RT_f}{P_f} \quad (4.62)$$

Molality definition

$$m_i = \frac{n_i}{n_{H_2O}^L MW_{H_2O}} \quad \forall i \neq H_2O \quad (4.63)$$

Additional parameters

$$n_L^{IN} = n_{H_2O}^{IN} + n_{NH_4^+}^{IN} + n_{HPO_4^{2-}}^{IN} + n_{H_2PO_4^-}^{IN} + n_{H^+}^{IN} + n_{OH^-}^{IN} \quad (4.64)$$

$$\chi_{HPO_4^{2-}} = \frac{\xi_{C2}}{n_{HPO_4^{2-}}^{IN}} \quad (4.65)$$

$$pH = -\log_{10} m_{H^+} \quad (4.66)$$

$$\eta_{deso} = \frac{G_{y_{NH_3}}}{n_{HPO_4^{2-}}^{IN}} \quad (4.67)$$

$$n_{NH_4^+,exp} = n_{NH_3(aq)} + n_{NH_4^+} \quad (4.68)$$

In which η refers to the desorption efficiency

4.3.2 Model results

The equation system (4.39)-(4.68) was implemented on TKsolver5.0, to get as results the final equilibrium conditions (P_f), the mass and the composition on each phase and the equilibrium conversion of HPO_4^{2-} into $H_2PO_4^-$ and the ammonia desorption from the liquid phase. The system variables were the final temperature, the initial load (mass and composition) and the initial pressure.

The temperature conditions were variated from 40 °C to 150 °C. At this salt concentration the solution is close to his solubility limit 40 °C is the minimum temperature which avoid the formation of crystals an so a third phase not consider on the simulation.

Results are reported in Figure 4.12 to Figure 4.13. for the specific case of $\omega_0=52.52$ and $\Gamma=0.667$.

Equilibrium conditions vs. Temperature, effect of initial loaded mass.

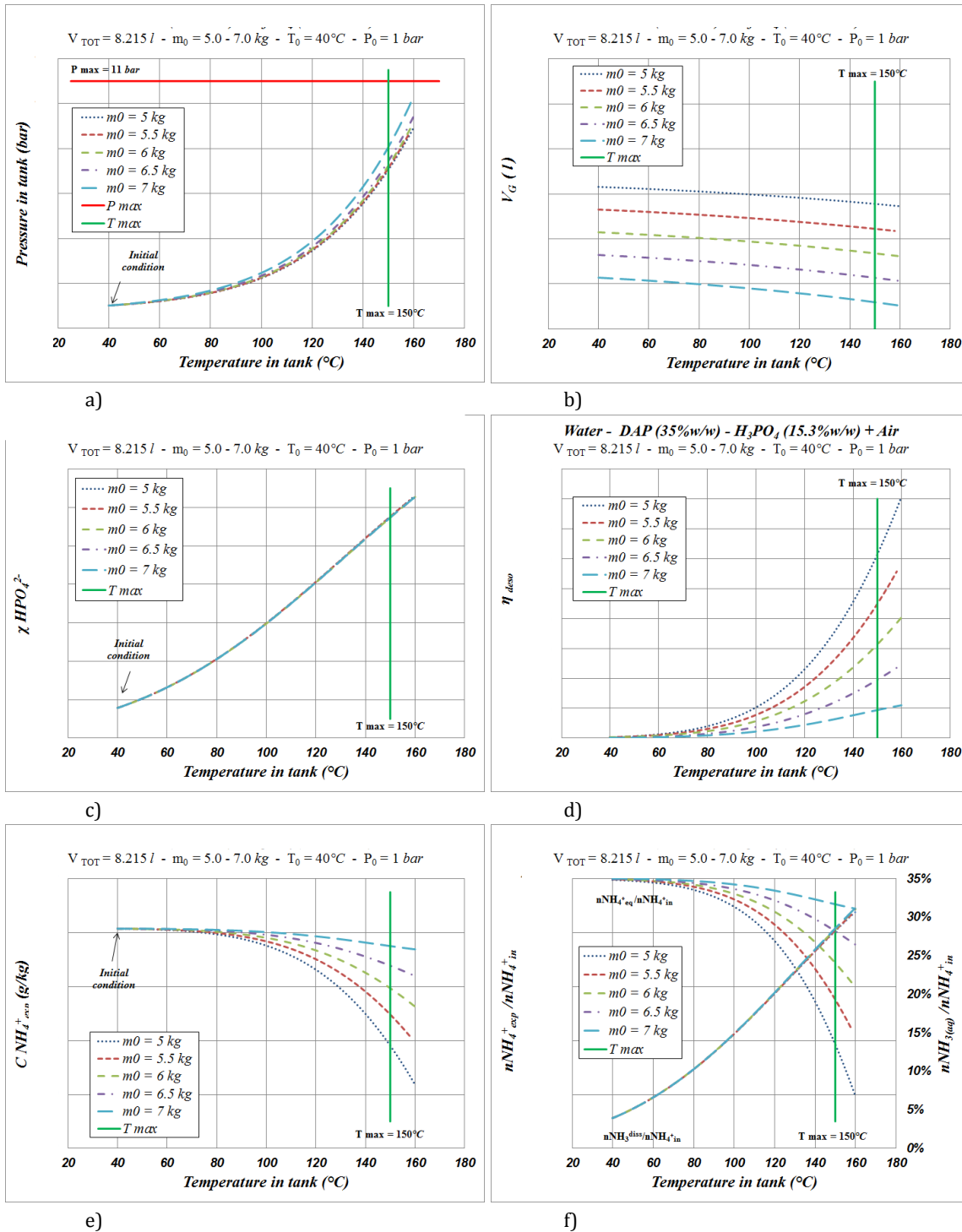


Figure 4.12 Equilibrium conditions vs. Temperature, effect of initial loaded mass: a) final pressure, b) vapor phase volume, c) HPO_4^{2-} conversion, d) desorption efficiency e) experimental ammonium and f) ammonium and ammonia relations.

Results vs. Temperature, effect of initial Pressure.

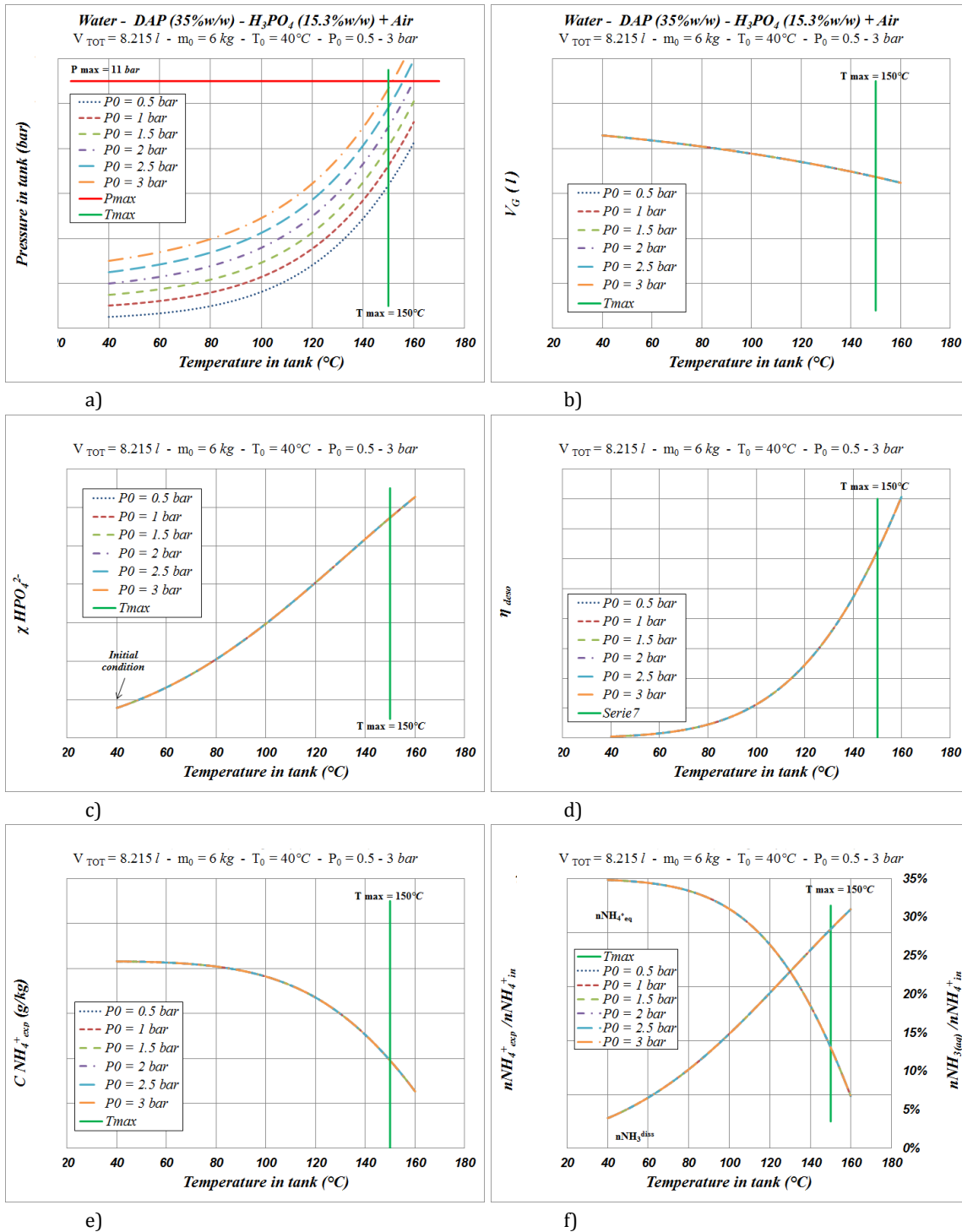


Figure 4.13 Equilibrium conditions vs. Temperature, effect of initial Pressure: a) final pressure, b) vapor phase volume, c) HPO₄²⁻ conversion, d) desorption efficiency e) experimental ammonium and f) ammonium and ammonia relations.

4.3.3 Discussion and conclusions.

From the figures Figure 4.12 and Figure 4.13 is some conclusive remarks can be drawn and some initial considerations of the most relevant operative parameters to perform the conversion of HPO_4^{2-} into H_2PO_4 with the consequent ammonia stripping.

From both the dissolution model and the Vapor-Liquid equilibrium the positive effect of the temperature is evident for the regeneration stripping of ammonia which confirms the basics predictions from the equilibrium constant.

At constant volume and high liquid load, the concentration of the aqueous ammonia increases considerable at higher operative temperatures. Figure 4.12 f) show how the aqueous ammonia increases regardless the initial load (proportion between liquid and gas phase) reaching values of 20 % of the initial ammonia even at 120 °C. This is a direct indication of the DAP regeneration, which reach values of 40 % at 120 °C. Regrettably, the direct measurement of the liquid phase composition will result on the composition of the ammonium plus the aqueous ammonia (the stripped ammonia is too little to be revealed by the analytical methods) and the total phosphate anions present on the solution. The experimental study of the equilibrium state will not show variations in the composition with temperature or with time. The real time, in situ, measurement of the pH could be the only experimental indication of the conversion and the development of aqueous ammonia. Sampling, and sample management (cooling, dilution, analysis...) will restore the equilibrium at room temperature.

A practical experimental observation of the system is the pressure, which follows the water vapor pressure trend. However this can be pretty approximated to the real case due to the high ammonia solubility.

Figure 4.13 shows that the initial pressure of the system does not change the final conditions for the physical chemical equilibrium. The pressure in the system will be only a consequence of the temperature and the mass of water, shifted by the magnitude of the initial pressure. The independence of the chemical equilibrium of the pressure makes possible to set the system pressure accordingly with other operational requirements.

The experimental test for the validation of the physical-chemical equilibrium will be discussed also in the next section.

5 Pilot Plant Startup and SGMD preliminary test.

The pilot plant, whose design was discussed in section 3, was constructed and the tests operative procedures were defined and the analytical methods. Some preliminary tests of SGMD were performed to evaluate the viability of the membrane contactors operation and the effectiveness of the operative procedures and analytical methods.

The Figure 5.1 shows a schematic representation of the pilot plant. On the scheme the liquid circuit and the gas circuit are represented, which can be in contact through the membrane module for the sweeping gas membrane distillation (SGMD) operation. Furthermore, if the membrane module is isolated from the liquid circuit, the equilibrium stage can be studied for a perfect mixed phase at constant volume and temperature.

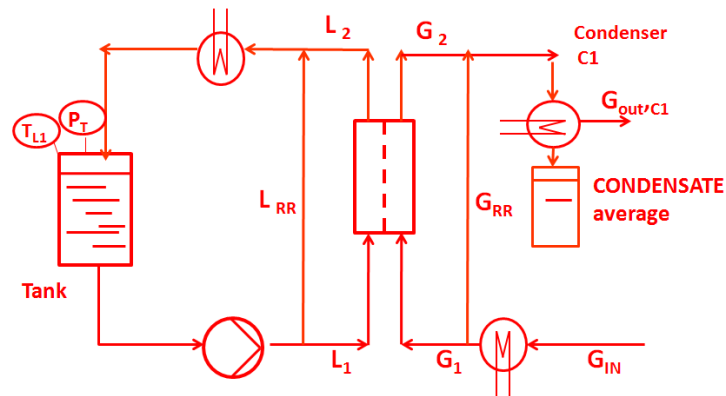


Figure 5.1 schematic representation of the SGMD pilot plant.

Two different tests can be performed with the previous pilot plant configuration: test for the study of the equilibrium stage at defined volume and temperature and the membrane contactors operation known as swapping gas membrane distillation.

5.1 Equilibrium test and pilot plant startup

The phase equilibrium test at defined volume and temperature were performed with three different objectives: perform the startup of the pilot plant and defined the operative procedures, to validate the physical-chemical models developed during this thesis and to evaluate the equilibrium stage of the DAP-ADP mixture, reaction and the kinetics of this reaction.

The objectives were achieved through three different equilibrium systems: the air-water system, the air-sodium chloride solutions and the air-DAP/ADP solutions. With the Air-Water system it was performed the startup of the pilot plant, the operative procedures were defined, the instrumentation was validated, the total volume system was measured and the model described on section 4.3 was validated with the simplification of a pure liquid.

The same way, equilibrium tests were performed for the system air-sodium chloride solutions. The second step on the model validation was achieved. Pressure and phases composition of the system were successfully simulated for a system with one component volatile and one inert. The same model described on section 4.3 was used performing the necessary simplifications.

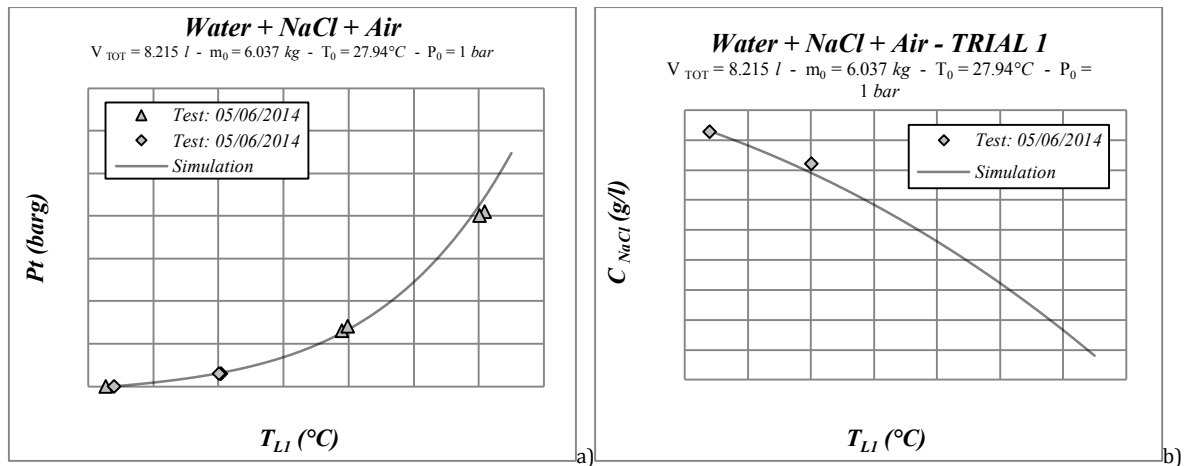


Figure 5.2 Experimental results of the equilibrium stage of the system air aqueous sodium chloride.

The equilibrium test with the aqueous solution of DAP and ADP system, as predicted by the model is a little more complex to validate. Tests with a DAP/ADP concentration of $\omega_0 = 52.52\%$, $\Gamma = 0.667$ were performed and the concentration of the main parameters was follow. Nevertheless it is not possible to obtain information of the species concentration apart from the total ammonium (the ionic ammonium plus the aqueous ammonia) and the total phosphate (the complex measurement of the four phosphate species) but the measurement of this two concentrations should remain constant at the different equilibrium conditions along time.. Results are reported in Figure 5.3.

Also in this case the only dependent physical parameter that can be predicted by equilibrium system is the pressure inside the tank. Apparently, the experimental measurements are close to the predicted values which depends almost exclusively on the water vapor pressure value. Is not really possible to validate the equilibrium model of the DAP/ADP system, major uncertainties remain present. Even if the pressure and the concentration are close to the ones predicted by the model, the results should be the same for an inert salt with non-volatile components like ammonia.

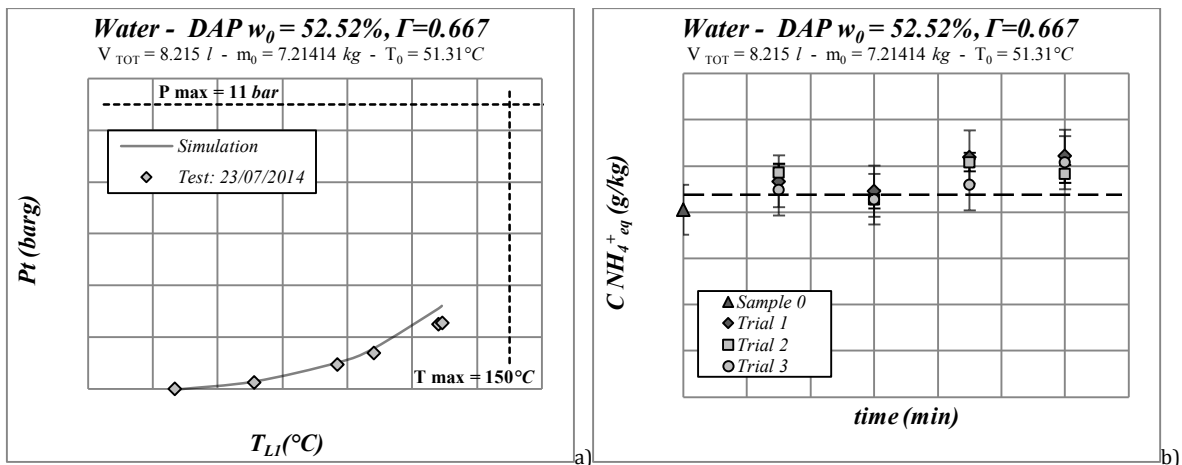


Figure 5.3 Experimental results of the equilibrium stage of the system air aqueous DAP/ADP ($w_0 = 52.52\%$, $\Gamma = 0.667$)

5.2 Sweeping gas membrane distillation test (SGMD).

The SGMD tests were performed with the polymeric module Liqui-Cel[®] - Extra-Flow 2.5 x 8 (described in section 2.1). The Liqui-Cel module is a commercial polypropylene module, used in the academic sector as in the industry and so it is well studied and described. This has a reduce temperature limitation, the operative conditions with the Liqui-Cel should not overcome the 60 °C, in order to avoid that membranes, potting and housing materials could be compromised.

In spite of the temperature limitations, the use of this module was interesting to start evaluating the main parameters involved on the SGMD process. Test with the system Air-aqueous sodium chloride and Air-aqueous ADP/DAP were performed to evaluate fluxes and their dependence on the operative conditions. The same way the test with sodium chloride solutions were used as blank test, to evaluate the integrity of the membrane after the used of DAP/ADP solution.

The characteristics of membranes and module were previously reported in detail in section 2.1.

5.2.1 Experimental test.

In Table 5.1 the whole experimental investigation is summarized, performed with the Liqui-Cel module. All the test are performed at 60 °C on the liquid phase and at the maximum temperature reach by the gas phase on its single pass through the heat exchanger (close to 50 °C). During the blank test were changed the operative parameters like gas and liquid flow rate and the test with DAP/ADP solutions were performed with a salt composition of $\omega_0 = 15.0\%$ $\Gamma = 0$ in order to avoid crystallization and maximizing the initial ammonium concentration to be stripped.

The tests with the Liqui-Cel module were performed in the following sequence:

- Blank test (variable liquid flow rate)
- Rinsing
- Blank test (variable sweeping gas flow rate)
- Rinsing
- DAP/ADP stripping test
- Rinsing
- Blank test (variable sweeping gas flow rate)
- rinsing
- Washing procedure
- Blank test

Blank test have shown some qualitative observations relative to the flux. The test were performed with the double purpose to evaluate the membrane performance before and after a test with DAP and quantify the effect of the process parameters like liquid and gas flow rates on the flux. Blank test are perfect to do so, as the only volatile component to be transported is water.

Table 5.1 SGMD test performed on the pilot plant with the commercial module Liqui-Cel

	(1) NaCl_W 5 g/kg Before test (3)		(2) NaCl_W 5 g/kg before test (3)		(3) DAP_W $\omega_0=15.0\%$ $\Gamma=0$		(4) NaCl_W 4 g/kg After test (3)	
	Gas	Liquid	Gas	Liquid	Gas	Liquid	Gas	Liquid
Time (min)	300-390		240-360-480		360		240-360-480	
Temperature (°C)	54	60	54 - 50 - 46	60	54	60	54 - 50 - 46	60
Press. in Tank (barg)	3		3		3		3	
Pressure L1/G1 (barg)	3.0	3.4	3.0 - 3.0 - 3.1	3.37	3.0	3.2	3.0 - 3.0 - 3.0	3.2
Flow rate (L/h)	2010	100 ($t < 300$) 150 ($t > 300$)	2000 ($t < 240$) 1325 854 ($t > 360$)	100	1972	100	1975 ($t < 240$) 1300 856 ($t > 360$)	100
Total flux (kg/(m² h))	5.14E-02 – 1.74E-01 ($Q_L=100$) 7.79E-02 – 2.11E-01 ($Q_L=150$)		7.60E-01 – 1.23E-01 ($Q_G=2000$) 1.03E-01 – 1.28E-01 ($Q_G=1325$) 5.22E-02 – 1.41E-01 ($Q_G=854$)		H ₂ O: 7.12E-02 – 1.25 E-01 NH ₃ : 1.69E-04 – 5.65 E-03		6.82E-02 – 9.76E-02 ($Q_G=1975$) 6.24E-02 – 9.71E-02 ($Q_G=1300$) 5.54E-02 – 7.63E-02 ($Q_G=856$)	
ΔNH_4^+ (g/kg)	-----		-----		From 39.560 – 41.535		-----	
$\Delta NaCl$ (g/kg)	From 4.317 to 4.755		From 4.274 to 4.706		-----		From 3.624 to 3.915	

ΔNH_4^+ = ammonia concentration difference $t_0 - t_f$ $\Delta NaCl$ = sodium chloride concentration difference $t_0 - t_f$

	(6) NaCl_W 5 g/kg		(7) NaCl_W 5 g/kg		(8) NaCl_W 5 g/kg		(9) NaCl_W 5 g/kg	
	Gas	Liquid	Gas	Liquid	Gas	Liquid	Gas	Liquid
Time (min)	240-360		420		300		300	
Temperature (°C)	50 - 46	60	48	60	47	60	53	60
Press. in Tank (barg)	3		3		3		3	
Pressure L1/G1 (barg)	3.3 - 2.9	4.2	2.9	4.4	3.0	4.5	3	4
Flow rate (L/h)	2014 ($t < 240$) 860 ($t > 240$)	100	2020	100	2010	100	2020	100
Total flux (kg/(m² h))	6.72E-02 - 1.11E-01 ($Q_G=2014$) 6.01E-02 - 1.03E-01 ($Q_G=860$)		5.62E-02 - 1.38E-01		6.29E-02 - 9.11E-02		1.02E-01 - 1.82E-01	
ΔNH_4^+ (g/kg)	-----							
$\Delta NaCl$ (g/kg)	From 4.819 to 5.117		From 4.645 to 5.032		From 4.657 to 4.910		From 4.983 to 5.351	

ΔNH_4^+ = ammonia concentration difference $t_0 - t_f$ $\Delta NaCl$ = sodium chloride concentration difference $t_0 - t_f$

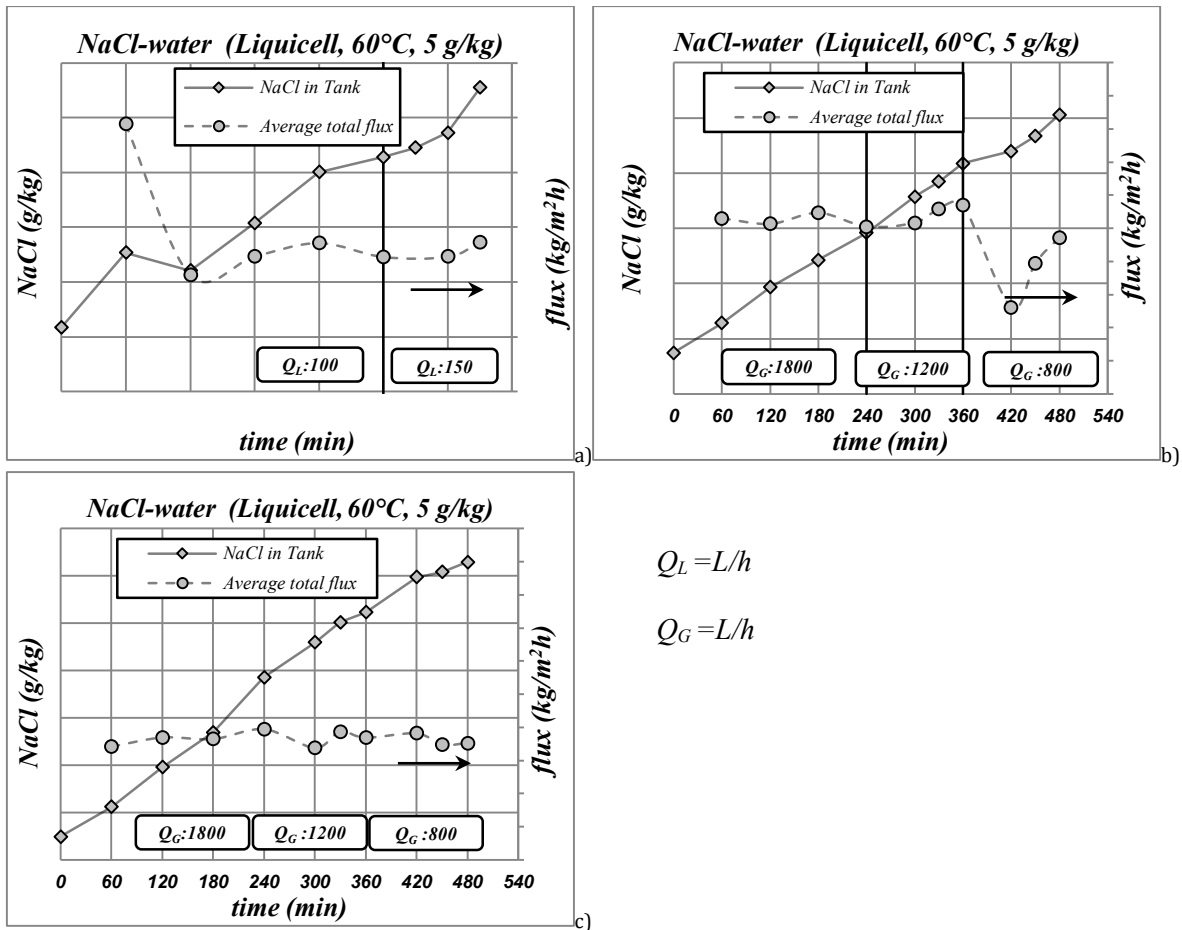


Figure 5.4 SGMD blank test: modification of operative conditions. a) water flow rate b) sweeping air flow rate c) sweeping air flow rate after DAP test (3). Test (1), (2) and (4) of Table 5.1

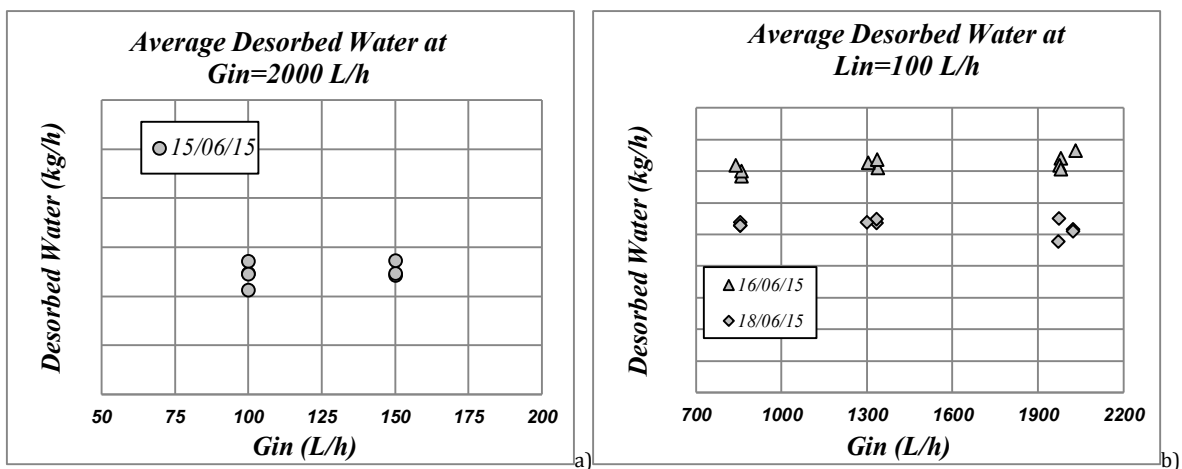


Figure 5.5 effect of flow rate on the water flux a) liquid flow rate b) Sweeping gas flow rate.

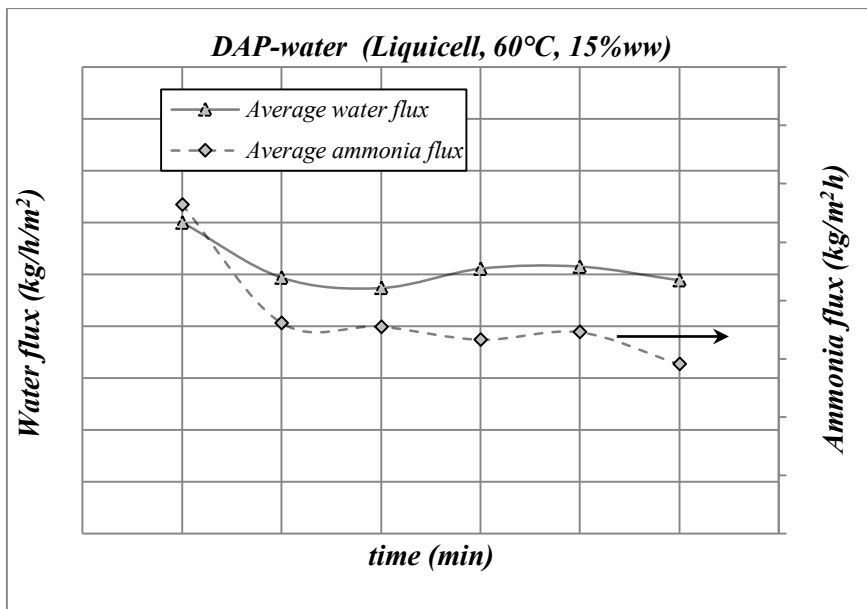


Figure 5.6 test (3) SGMD with $\omega_0=15.0\%$ $\Gamma=0$, 60 °C 4 bar and air.

5.2.2 Results analysis

The qualitative observations have revealed a particularly low effect of liquid flow rate on the water flux (Figure 5.5-a) which might be the consequence of a negligible liquid boundary layer resistance. The effect of the sweeping gas flow rate seems to be also of minor relevance (minor changes respect the increasing of the flow rate) inferring that the dominant resistance might be the mass transfer through the membrane.

The test with DAP has shown very interesting results for such a low temperature (60 °C). Both the water and the ammonia flux are quite constant during the length of the test. The ammonia desorption achieved 9.4 % of the initial ammonium in the solution, which is equivalent to a conversion of DAP into ADP equal to 18.4 %. The time length of the test and the height membrane area of the module are the main reasons of the conversion rate. However the amount of water desorbed is much higher than ammonia one, even though the initial concentration of water on the liquid solution is much higher than the one of ammonia.

The initial concentration of the aqueous species was calculated using the ENRTL model present on "Aspen Plus". On section 4.1 was concluded that the equilibrium model ENRTL was the best one to describe the chemical equilibrium for the ammonium phosphates solution. The bulk concentration of each species, for the solution used on the test (3), is reported in Table 5.2.

Table 5.2 Bulk molar fraction of electrolyte species from the simulation on aspen plus $\omega_0=15.0\%$ $\Gamma=0$, 60 °C 4 bar

<i>Species</i>	<i>Bulk Molar Fraction (60 °C)</i>
H_2O	0.932612
H^+	3.92e-09
NH_4^+	0.042383
NH_3	0.002543
H_3PO_4	1.16E-08
$H_2PO_4^-$	0.002572
OH^-	8.33E-08
HPO_4^{2-}	0.019862
PO_4^{3-}	2.89E-05

The blank tests showed that, in the water (solvent) mass transport, the liquid and gas boundary layer might be neglected. Assuming that this is also valid for the ammonia mass transport, the vapor at the interface could be at the equilibrium with the liquid bulk phase. Calculating the water and ammonia partial pressure at the equilibrium from the bulk concentration. The water molar fraction value is $y_{water} = 0.0442$ and the ammonia molar fraction value is $y_{ammonia} = 0.0024$.

Typically in SGMD the prevailing transport mechanism is the diffusive; it is described by the following equations describing the Knudsen and the molecular diffusion contribution.

$$k_{i,m}^D = \frac{D_{i,g} \varepsilon}{\delta \chi} \quad (5.1)$$

$$D_{i,g} = \left(\frac{1}{D_{i,g}^{Kn}} + \frac{1}{D_{i,mol}} \right)^{-1} \quad (5.2)$$

$$D_{i,g}^{Kn} = \frac{2}{3} r_p \sqrt{\frac{8RT}{\pi M}} \quad (5.3)$$

Where $D_{i,mol}$ is the ordinary diffusion coefficient.

Table 5.3 calculated mass transport coefficient for the membrane

<i>Species</i>	$k_{i,m}^{kn} (m/s)$	$k_{i,m}^{mol} (m/s)$	$k_{i,m} (m/s)$
H_2O	8.34×10^{-2}	2.75×10^{-2}	2.47×10^{-2}
NH_3	8.85×10^{-2}	3.51×10^{-2}	2.08×10^{-2}

The membrane mass transport coefficient are very similar for both components, this were calculated through the geometrical parameters, provided by the producer at the process conditions of 60 °C and 4 barg.

Never the less the water mass transport is close to 30 times the one of ammonia when the driving force is only 18 times higher (if the equilibrium is calculated with the bulk concentration). This indicates that the liquid boundary layer should not be neglected for ammonia. Further test should be performed to confirm the observations.

Is difficult to made flux predictions, some phenomena as the salting out and the desorption enhancement by the chemical reaction are not account for the transport model (further studies must be done to complete the transport model but is preferable to completed with the ceramic prototype module).

Fouling effect and cleaning procedure.

After the series of test involving the DAP solution (blank – DAP – Blank) were performed the cleaning procedure suggested by the producer (3M, 2016), to eliminate chemical and biological fouling besides flooding and restore the membrane integrity and performance.

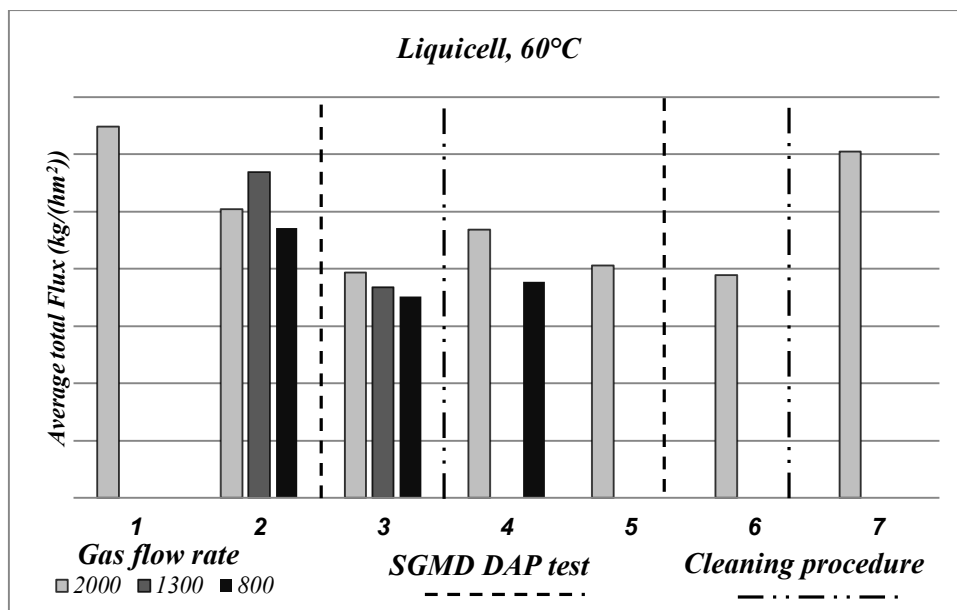


Figure 5.7 Comparative water flux of blank test desorption. Before and after DAP test and cleaning procedure.

The comparative chart illustrates the fouling effect of the phosphoric salts test, and the reduction on the flux when the gas flow rate is reduced. It can be seen that the fouling effect is present also when blank test are performed, despite of the low salt concentration.

Only after the cleaning procedure was performed 2 times, the membrane flux were reestablished to the originals before the test with DAP. It can be observe that the DAP solution, even at lower concentrations than the ones suggested to the process, reduces the potentialities of the membrane and that strong washing procedure is needed to restore these.

After the cleaning procedure the fluxes are reestablished whit out compromising the membrane hydrophobicity and the barrier effect.

6 Conclusions

In order to evaluate the feasibility of the regeneration of ammonium hydrogen phosphate (ADP) from diammonium phosphate (DAP), throughout a membrane contactors (MC) process, was designed, sized and constructed a bench scale pilot plant.

Moreover the experimental tests along with the operative procedures, the analytical methods and the result analysis were designed. Parallel to the pilot plant construction the physical-chemical equilibrium of the problem solution was studied, on this way the main operative parameters that might improve the regeneration were identified.

The regeneration of ADP from DAP passes through the endothermic equilibrium reaction with the production of gaseous ammonia. The MC operation known as sweeping gas membrane distillation (SGMD) is proposed as the most suitable to perform ADP regeneration, avoiding high temperatures. This might be possible after the stripping of the volatile reaction products, avoiding the system to reach the chemical equilibrium, and promoting the formation of further ammonia.

The equipment and the instrumentation sizing was performed after the fluid dynamic analysis of three prototype membrane modules, a single channel, two capillary membrane modules (one polymeric and one ceramic) and one well known polymeric commercial module (Liqui-Cel Extra-Flow).

From two limit values of fluid velocity, there were calculated the fluid flow rates and the pressure drops for each membrane module. With this information it was performed the sizing of pump, valves, pressure probes, tubes diameter, flow meters and heat exchange units to perform the SGMD activity at a maximum temperature of 150 °C and a maximum pressure of 10 barg.

On section 3 the plant designs and the technical characteristics of each component along with the operative limits are registered. The pressure pump temperature limit (150 °C) and the maximum admissible pressure in the tank (10 barg) are the limiting conditions for the MC operation.

The physical-chemical equilibrium was approached starting from the electrolyte reaction equilibrium of the species deriving from the dissolution of ADP and DAP in water. To simplify the analysis it was neglected the components volatility (water and ammonia) as the liquid solution is a complex mixture.

From the equilibrium analysis it was identified the dependence of the composition to only three parameters: the system Temperature, the total phosphate molar concentration and the ratio of the initial moles of DAP to the sum of the initial moles of DAP and ADP (defined by the parameter Γ). These three parameters defined the composition of all the species, among them

there is only one component which composition is easily measured, this is the proton (H^+) quantified throughout the pH.

To model the mixture composition in function of the parameters listed before were developed/used two electrolyte equilibrium models: the first one is an ideal model where the water activity is assumed to be unitary so as the other components activity coefficients. The second is based on the non-random two-liquid model (NRTL) applied to electrolyte solutions (described by Chen & Song, 2004 and detailed on section 4.1.2), it was implemented on the commercial process simulator Aspen plus.

To validate the models there were performed experimental mixtures varying the independent parameters. The only possible analysis that does not modify the equilibrium state is the measurement of the pH, and so this was selected as the only parameter to validate the electrolyte equilibrium models.

The ideal model showed an important diversion degree from the experimental values, especially for higher phosphate concentration. The ENRTL model is much more accurate, the predictions diverged the experimental value only at high temperature, which might be related with evaporation during experiments.

The results of this simulation, confirmed by the experimental results, allowed to consider only the electrolyte equilibrium between HPO_4^{2-} and $H_2PO_4^-$ on the equilibrium phase model and demonstrated the positive effect of the temperature on the ammonia stripping. Furthermore, the composition results in function of the temperature show the possibility of performing a successful stripping operation at temperatures well below the temperature when the equilibrium constant take positive values ($\approx 130^\circ C$). This is evident through the aqueous ammonia concentration that at $100^\circ C$ has increased 100 times.

The physical-chemical equilibrium was completed through a phase equilibrium model of the constant volume system. Notwithstanding the clear deviation of the ideal solution model, it worth performing the phase equilibrium study with the ideal solution hypothesis. The results were accurate as in the phase equilibrium only volatile components are considered, water and ammonia and the high water concentration ruled the physical conditions.

The equilibrium model might be useful to predict the physical conditions like the trend of pressure vs T, though predictions regarding the chemical equilibrium are more trustworthy simulated by the ENRTL model.

The preliminary SGMD tests were performed with the polymeric module Liqui-Cel, as the prototype modules, made of coated ceramic membranes, are yet under development. Two kind of preliminary tests were performed with the Liqui-Cel, blank tests with sodium chloride solutions and secondly with ammonium phosphate salts solutions.

Blank tests indicated a particularly low effect of liquid flow rate on the water flux, it can be assumed a low boundary layer resistance for the solvent mass transport. The effect of the sweeping gas flow rate seemed to be also reduce (minor changes respect the increasing of the flow rate) inferring that the dominant resistance was the membrane.

The test with DAP has shown very interesting results for such a low temperature (60 °C). Both the water and the ammonia flux were quite constant during the length of the test. The ammonia desorption reached 9.4 % of the initial ammonium in the solution, which is equivalent to a conversion of DAP into ADP equal to 18.4 %. However the amount of water desorbed is much bigger than ammonia one. This is imputable to the lower concentration of ammonia in the bulk phase but is also possible that the ammonia mass transport on the liquid as a consequence of the liquid boundary layer.

Nonetheless to complete an effective mass transport model and analysis of the results is necessary account the enhancement effect of the reaction and the salting out effect, which might increase the availability of the ammonia at the equilibrium. To account these effects, further studies should be performed, but is preferable to do so with the ceramic membrane, and their module configuration.

7 List of Symbols

Symbol	Meaning
l^{eff}	Effective length
d_i	Inner diameter
d_o	Outer diameter
d_s	Shell inside diameter
d_c	Collector outer diameter
d_p	Pore diameter
ε	Membrane porosity
δ	Membrane thickness
N_t	Tubes number
θ	Module void fraction
A_i	Inner membrane area
A_o	Outer membrane area
A_{av}	Mean membrane area
v	Velocity
$Q=\dot{V}$	Volumetric flow rate
ΔP	Pressure drop
f	Fanning factor
Re	Reynolds number
η	Cinematic viscosity
d_2	Equivalent ring diameter
d_h	Hydraulic diameter
ρ	Density
χ	Tortuosity
d_{pc}	Plug cap inner diameter
NKU	Kinetic unit number
T	Temperature
P	Pressure
H	Pump head
W	Wide
L	Length
D	Deep
K_i	Equilibrium constant of reaction i

$\{i\}=a_i$	Activity of i
ΔG_R^0	Standard free Gibbs energy
R	Gas constant
γ_i	Activity coefficient of i
$[i]$	Molar concentration of i
ΔH_R^0	Standard reaction enthalpy
C_{TOT}	Total molar concentration
$C_{0,i}$	Initial molar concentration
α_i	Dimensionless phosphate species concentration
Γ	Parameter defined by equation (4.34) Error! Reference source not found.
n_i	i moles number
$G_m^{*,ex}$	Excess Gibbs free energy
$G_m^{*,lc}$	Short-range term
$G_m^{*,PDH}$	Pitzer Debye Huckel term
$\gamma_i^{*,lc}$	Local contribute to activity coefficient
$\gamma_i^{*,lc}$	Long range contribute to activity coefficient
X_j	Parameter defined by equation (4.25)
$\gamma_I^{\infty,lc}$	Infinite dilution activity coefficient
$r_{j,J}$	segment J , species j molar fraction
α	Non-random symmetric parameter
A_ϕ	Debye Huckel parameter
MW_s	Solvent molecular weight
N_A	Avogadro's number
Q_e	Electron charge
k_b	Boltzmann constant
ϵ_s	Solvent dielectric constant
z_i	Charge of the based-segment species i
I_x	Ionic strength
ρ	Closest approach parameter
ω_0	The equivalent mass fraction of DAP defined on equation (4.33)
H_i	i Henry constant
h	Ionic salting out parameter
v_i	Electrolyte stoichiometric coefficient
m_i	i molal concentration.

$P_{H_2O}^*$	<i>Water vapor pressure</i>
ξ_i	<i>Extent of reaction i</i>
G	<i>Gas moles</i>
y_i	<i>i vapor molar fraction</i>
x_i	<i>i liquid molar fraction</i>
V	<i>Volume</i>
χ_i	<i>Conversion of i</i>
η	<i>Efficiency</i>
J_i	<i>I molar flux</i>
$k_{i,j}$	<i>Mass transfer coefficient of I on phase j</i>
$C_{i,j}$	<i>Molar concentration of I on phase j</i>
P_i	<i>Partial pressure of i</i>
P_i^0	<i>I vapor pressure</i>
H	<i>Enhancement factor</i>
d_e	<i>Particles diameter</i>
$\mathcal{D}_{i,g}$	<i>Diffusive coefficient</i>
r_p	<i>Pore radius</i>
Sh	<i>Sherwood number</i>
Gz	<i>Graetz number</i>
Sc	<i>Schmidt number</i>

8 Bibliography

- 3M. (2016). *3M Industrial Group | Membranes Business Unit*. Retrieved February 28, 2016, from <http://www.liquicel.com/technical-resources/startup-operating-guides.cfm>
- 3M Company. (2016, January). *Liqui-Cel*. Retrieved from [www.liquicel.com/:
http://www.liquicel.com/uploads/documents/2%205x8ExtraFlow-D59Rev16%204-15.pdf](http://www.liquicel.com/:http://www.liquicel.com/uploads/documents/2%205x8ExtraFlow-D59Rev16%204-15.pdf)
- Chen, C.-C., & Song, Y. (2004). Generalized Electrolyte-NRTL Model for Mixed-Solvent Electrolyte Systems. *AIChE Journal*, 50(8), 1928-1941.
- Danckwerts, P. (1970). *Gas - Liquid Reactions*. New York: McGraw - Hill.
- Gostoli, C., & Gatta, A. (1980). Mass transfer in a hollow fiber dialyzer. *Journal of Membrane Science*, 6(C), 133-148.
- Hermann, Dewes, I., & Schumpe, A. (1995). *Chem. Eng. Sci.*, 1673.
- Lide, D. R. (Ed.). (2006). *CRC Handbook of Chemistry and Physics* (87 ed.). Boca Raton, Florida: CRC Press.
- Mason, E., & Malinauskas, A. (1983). *Gas transport in porous media: the dusty-Gas model*. New York: Elsevier.
- Perry, R. H., & Green, D. W. (2007). *Perry's Chemical Engineers' Handbook* (8 ed.). McGraw-Hill.
- Prasad, R., & Sirkar, K. (1988). Dispersion-free solvent extraction with microporous hollow-fiber modules. *AIChE Journal*, 34(2), 177-188.
- Schöner, P., Plucinski, P., Nitsch, W., & Daiminger, U. (1998). Mass transfer in the shell side of cross flow hollow fiber modules. *Chemical Engineering Science*, 533(13), 2319-2326.
- Sechenov, I. (1889). *Nouv. Mem. Soc. Imp. Nat. Moscow*, 203-74.

CONCLUSIONS AND PERSPECTIVES

The main objective of this thesis is to evaluate the feasibility in the regeneration of ammonium hydrogen phosphate (ADP) from diammonium phosphate (DAP), throughout the Membrane Contactors (MC) operation known as Sweeping Gas Membrane Distillation (SGMD).

The regeneration of ADP from DAP passes through the endothermic equilibrium reaction with the production of gaseous ammonia. SGMD is proposed as the most suitable operation to perform ADP regeneration, avoiding high temperatures. This might be possible after the stripping of the volatile reaction products, avoiding the system to reach the chemical equilibrium and promoting the formation of further ammonia.

The top requirement to implement the MC technology to this process is the availability of membranes and membrane modules able to work at the process conditions. The membranes must withstand the high temperature when the reaction products start to be available for an effective stripping process, keeping its barrier effect. The selection of the most suitable membranes to the process was performed after the definition of the membranes characteristics and the characterization method to identify them. The membrane characterization concerns a vast section of this thesis particularly as regards to the study of the hydrophobic character of macroporous membranes (Section A).

Parallel to section A, it was taken forward an experimental study to develop the regeneration process on a bench scale MC pilot plant. In this context it was designed, sized and constructed an experimental apparatus along with the definition of the experimental test, the operative procedures, the analytical methodologies and the analysis of the experimental results. Besides the pilot plant construction it was studied the physical-chemical equilibrium of the solution problem, which made possible to identify the main operative parameters that could improve the regeneration operation (Section B).

Membranes characterization.

The central objective of section A was to identify the main characteristics that made the membrane suitable to be used on a particular application, particularly the hydrophobic character of the macroporous membranes and its dependency with the temperature.

The studied application involves the mass exchange operation between a liquid phase and a gas. The membrane defines the barrier between the two phases in contact and avoids the phase mixing or dispersion. The barrier effect is generally performed by the low affinity of the membrane to one or both of the phases in contact, hydrophobic membranes are used to hold aqueous phases and hydrophilic membranes are used to hold organic phases. The barrier effect must be permanent in order to have a successful operation.

It was selected to work with hydrophobic membranes and higher pressure on the aqueous phase in order to keep the phases separated. The hydrophobic membranes are preferable as

the diffusive mass transport through a gas (phase inside the membrane pores) is much more effective than through a liquid matrix, furthermore, phenomena like fouling by crystallization of the salt solution is avoid inside the pores.

The membrane's hydrophobic character is a matter of great importance for the process reliability. If liquid phase floods the membrane, partially or completely, the whole operation might be compromised. After the flooding we can verify the transport of non-volatile components, phases mixing, the membrane fouling and the decrease of mass transport.

A deep study of the hydrophobic character has been performed, the theoretical bases, the key parameters that modify the hydrophobic behavior and the experimental methods to evaluate it, were the focus of the state of the art study. The study of the state of the art allows to identify the necessity of deeper studies on the matter of hydrophobic character dependence with temperature, especially with water at temperatures above the bubble point.

The most diffused methodologies for the measurement of the hydrophobic character are the liquid contact angle over flat surfaces and the break through pressure of a non-wetting phase. Both methodologies provide information about the affinity of the membrane with a liquid and allow to obtain practical information for the selection of a membrane and the operative limits during the MC operation. Both methodologies have their pros and cons, but there is an evident lack, on both procedures, on the measurement of the hydrophobic character at high temperatures. These have shown some contradictory results on the study of the hydrophobic character vs temperature.

Some measurement of water contact angle over different surfaces, including polymeric and metallic surfaces, have left the doubt, that water contact angle at higher temperatures change the linear trend in function of Temperature, many times reported. The results of these experiments have shown that at a certain value of temperature, water contact angle decreases rapidly, approaching to zero at values of temperature well below the critical temperature.

The measurements of contact angle might be the most representative parameter of the hydrophobic character. However the wide hysteresis phenomena (present in most of the samples), the difficulties to measure it on samples of different shapes than flat surfaces and the very sophisticate apparatus to perform measurements at temperature above the boiling point, make the contact angle hard to be measured and a parameter with many uncertainties. On the other hand the liquid entry pressure is a parameter that can adequately evaluate the hydrophobic character of a membrane, and even more, is a direct parameter of the MC operation.

On the study of the state of the art of characterization method for membrane contactors at high temperature, it was evident the lack of a suitable method to evaluate on a simple and economic way the hydrophobic character. Especially there are no references for the measurement of the break through pressure or liquid entry pressure (LEP) at temperatures above 70 °C (Saffarini, et al. 2013). Even more, the method used to perform these measurements is not suitable to be

used at higher temperatures because evaporation phenomena across the membrane starts to be relevant.

With this aim the liquid permeation technique was modified to perform tests at higher temperatures and, in an innovative way, in function of temperature at constant differential pressure.

In order to perform these tests, the regular equipment used to perform the flooding curves was modified and the complete procedure was redefined. With this configuration and procedure we were able to perform for the first time ever the flooding curve at temperatures above the fluid normal bubble point and obtain the value of the break through pressure-Liquid entry pressure. With the same equipment configuration and changing the procedure, it was proposed to perform the flooding curve in function of the temperature, at constant transmembrane pressure and was defined a new operative parameter of breakthrough, the LIQUID ENTRY TEMPERATURE (LET).

With the purpose of comparing the results at different temperatures and obtain correlations of LEP vs T it was defined a successful new way to elaborate the flooding curve data, and the concept itself of breakthrough was redefined, taking into account the experimental results and avoiding an arbitrary definition like the one proposed by Garcia-Payo and colleagues.

The hydrophobic character was studied on commercial polymeric membranes and on prototype ceramic membranes, throughout the contact angle measurement and the flooding curve for the determination of LEP and LET.

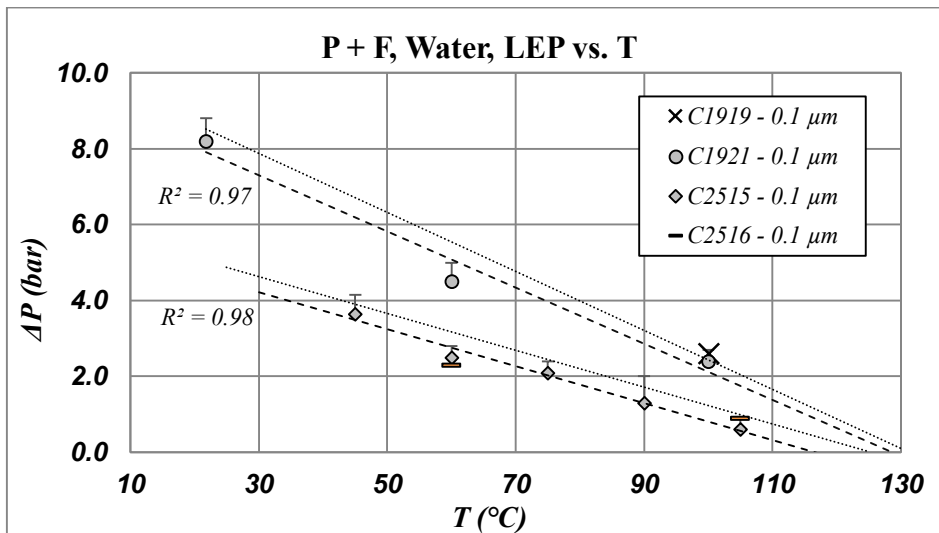
The LEP and LET results with polymeric membranes were less trustworthy. The small membrane area generates a great dispersion in the experimental results and the temperature modifies the polymeric matrix (on a unique way for each membrane) and the pores morphological configuration. This last parameter was not considered on the data elaboration, focusing only on the hydrophobic character of the membranes. Nevertheless the tests were useful to set up the experimental procedure comparing the results with the ones reported in the literature.

Titania membranes coated with four different polymers were tested in order to characterize its hydrophobicity. Throughout the flooding curve, were evaluated the breakthrough conditions of four coating material for two membrane pores sizes. The tests were performed at constant room temperature.

The membranes with coating material P+F presented remarkably high values of LEP. The membranes of this category were furtherly tested at higher temperatures. A complete study of the breaking through conditions, dependence with temperature was performed.

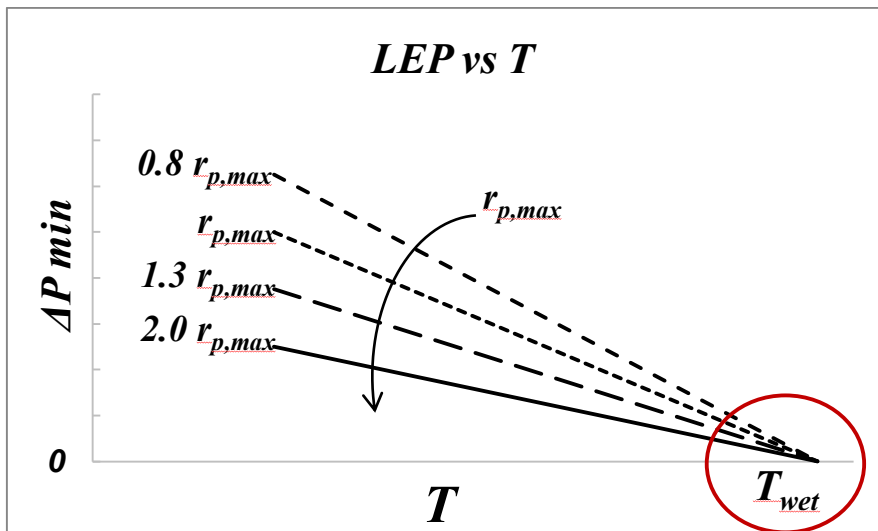
For two membranes it was possible to obtain a set of data of transmembrane pressure of breakthrough (LEP) vs. the operative temperature. A second couple of membranes gave few

data that can be plotted alongside the membrane of the same category (batch). The experimental data and the fitting lines are reported on the figure below.



The experimental data of each sample was fitted with a linear regression line with a good coefficient of determination (R^2). Particularly the sample with the biggest set of data. Both the fitting lines seem to go towards a common point, between 120 and 130 °C.

The experimental results were analyzed through the theoretical background, defining a linear dependence of the pressure of breakthrough (LEP) with the operative temperature, when the maximum pore radius of the membrane is constant (ceramic membranes).



It was defined a new operative parameter, the **wetting temperature**, a unique value for the couple liquid - solid material. The wetting temperature indicates the value of temperature when all the membrane pores get flooded, regardless the pore size. This is a clear operative limit for the membrane material independently of the pore size.

After the ceramic membranes results analysis, the results with polymeric membranes were reevaluated. These revalidate the observation of the wetting temperature when a permanent temperature deformation was assumed.

The search for a suitable membrane to be used in the stripping of the reaction product of an endothermic equilibrium reaction, give as a result that: titania membranes coated with a particular hydrophobic layer (P+F) are the most performant membranes to work at high temperatures keeping its hydrophobicity even at temperatures above normal boiling point. Furthermore the search reveals a general trends of the hydrophobic character behavior in function of the temperature and identifies a temperature limitation for each couple of membrane material and liquid; in the case of the ceramic membranes this value is around 120 - 130 °C.

Design-construction of SGMD pilot plant and test with membrane modules.

The equipment and the instrumentation sizing was performed after the fluid dynamic analysis of three prototype membrane modules, a ceramic membrane single channel module, two capillary membrane modules (one polymeric and one ceramic) and one well known polymeric commercial module (Liqui-Cel Extra-Flow®).

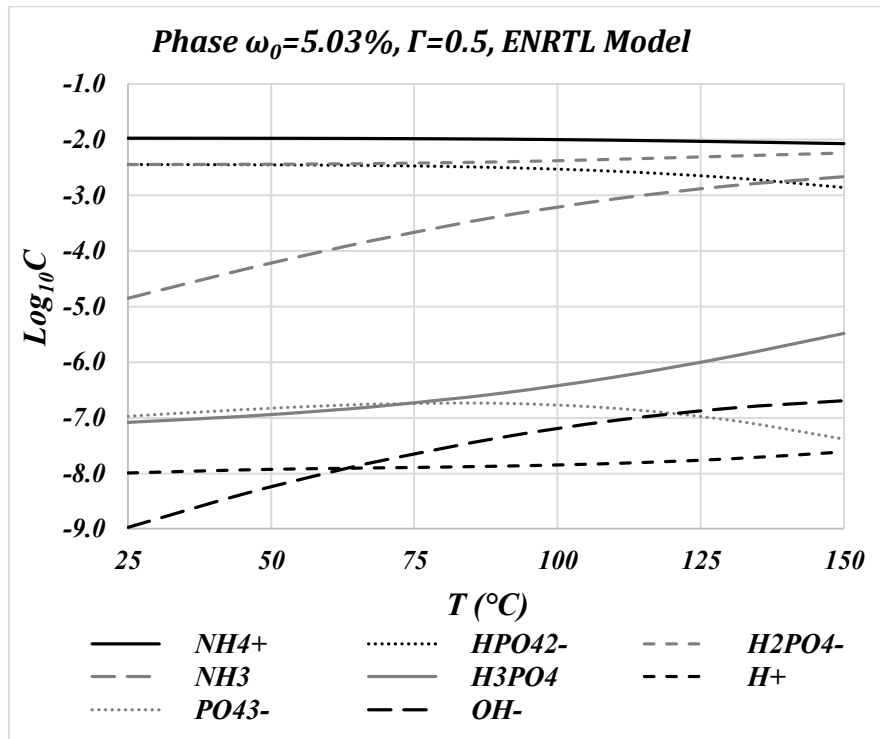
From two limit values of fluid velocity, there were calculated the fluid flow rates and the pressure drops for each membrane module. With this information it was performed the sizing of pump, valves, pressure probes, tubes diameter, flow meters and heat exchange units to perform the SGMD activity at a maximum temperature of 150 °C and a maximum pressure of 10 barg.

The physical-chemical equilibrium was approached starting from the electrolyte reaction equilibrium of the species deriving from the dissolution of ADP and DAP in water. To simplify the analysis it was neglected the components volatility (water and ammonia) as the liquid solution is a complex mixture. From the equilibrium analysis it was identified the dependence of the composition to only three parameters: the system Temperature, the total phosphate molar concentration and the ratio of the initial moles of DAP to the sum of the initial moles of DAP and ADP (defined by the parameter Γ). These three parameters defined the composition of all the species, among them there is only one component which composition is easily measured, this is the proton (H^+) quantified through the pH.

To model the mixture composition in function of the parameters listed before there were developed/used two electrolyte equilibrium models: the first one is an ideal model where the water activity is assumed to be unitary so as the other components activity coefficients. The second is based on the non-random two-liquid model (NRTL) applied to electrolyte solutions (described by Chen & Song, 2004), this model was implemented on the commercial process simulator Aspen plus. To validate the models there were performed experimental mixtures varying the independent parameters. The only possible analysis that does not modify the

equilibrium state is the measurement of the pH, and so this was selected as the only parameter to validate the electrolyte equilibrium models.

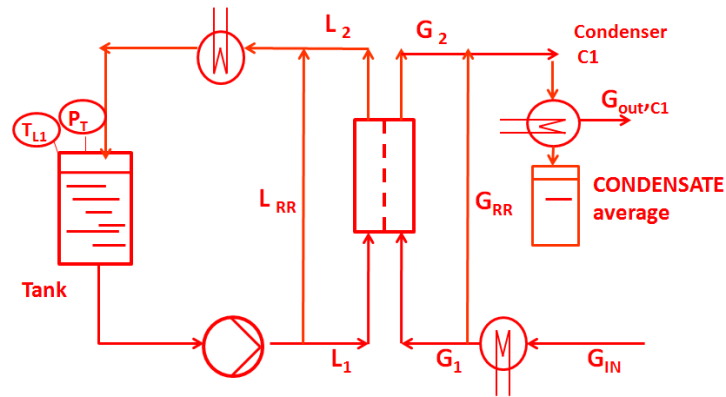
The ideal model showed an important diversion degree from the experimental values, especially for higher phosphate concentration. The ENRTL model is much more accurate, the predictions diverged the experimental value only at high temperature, which might be related with evaporation during experiments.



The results of this simulation, confirmed by the experimental results, allowed to consider only the electrolyte equilibrium between HPO₄²⁻ and H₂PO₄⁻ on the equilibrium phase model and demonstrated the positive effect of the temperature on the ammonia stripping. Furthermore, the composition results in function of the temperature show the possibility of performing a successful stripping operation at temperatures well below the temperature when the equilibrium constant take positive values (≈ 130 °C). This is evident through the aqueous ammonia concentration that at 100 °C has increased 100 times.

The physical-chemical equilibrium was completed through a phase equilibrium model of the constant volume system. Notwithstanding the clear deviation of the ideal solution model, it worth performing the phase equilibrium study with the ideal solution hypothesis. The results were accurate as in the phase equilibrium only volatile components are considered, water and ammonia and the high water concentration ruled the physical conditions.

The equilibrium model was useful to predict the physical conditions like the trend of pressure vs T, though predictions regarding the chemical equilibrium are more trustworthy simulated by the ENRTL model.



The pilot plant, was constructed and the tests operative procedures were defined along with the analytical methods. Some preliminary tests of SGMD were performed to evaluate the viability of the membrane contactors operation and the effectiveness of the operative procedures and analytical methods.

With the Air-Water and air-sodium chloride solutions systems were performed the startup of the pilot plant, were defined the operative procedures, the instrumentation was validated, the total volume system was measured and the phase equilibrium model started to be validated with the simplification of a pure liquid and pure liquid plus nonvolatile component.

The equilibrium test with the aqueous solution of DAP and ADP system, as predicted by the model is a little more complex to validate. It was not possible to obtain information of the species concentration apart from the total ammonium (the ionic ammonium plus the aqueous ammonia) and the total phosphate (the complex measurement of the four phosphate species) but the measurement of this two concentrations remained constant at the different equilibrium conditions along time. To obtain information of the species concentration in situ measurements must be performed and the analytical procedures and equipment available cannot do so.

The preliminary SGMD tests were performed with the polymeric module Liqui-Cel, as the prototype modules, made of coated ceramic membranes are yet under development. Two kind of preliminary tests were performed with the Liqui-Cel, blank tests with sodium chloride solutions and secondly with ammonium phosphate salts solutions.

Blank tests indicated a particularly low effect of liquid flow rate on the water flux, it can be assumed a low boundary layer resistance for the solvent mass transport. The effect of the sweeping gas flow rate seems to be also reduce (minor changes respect the increasing of the flow rate) inferring that the dominant resistance might be the membrane.

The test with DAP has shown very interesting results for such a low temperature (60 °C). Both the water and the ammonia flux are quite constant during the length of the test. The ammonia desorption have reach 9.4 % of the initial ammonium in the solution, which is equivalent to a conversion of DAP into ADP equal to 18.4 %. However the amount of water desorbed is much bigger than ammonia one. This is imputable to the lower concentration of ammonia in the bulk phase but is also possible that the ammonia mass transport on the liquid as a consequence of the liquid boundary layer.

Nonetheless to complete an effective mass transport model and analysis of the results is necessary account the enhancement effect of the reaction and the salting out effect, which might increase the availability of the ammonia at the equilibrium. To account these effects, further studies should be performed, but is preferable to do so with the ceramic membrane, and their module configuration.

General process feasibility.

It is possible to perform the regeneration of ammonium hydrogen phosphate from diammonium phosphate throughout sweeping gas membrane distillation.

In the section A of this thesis it was identified a suitable membrane to perform the stripping of the regeneration process avoiding the reaction to reach the chemical equilibrium. Throughout the study of the hydrophobic character vs Temperature, the coated ceramic membranes (P+F) of 100 nm (pore diameter) were identified as the most suitable for the process. The ceramic structure made the membrane thermally stable and chemically inert, neither the temperature nor the salt solutions, modifying the membrane matrix or the surface coating.

Even more, the study allowed to identify the dependence of the hydrophobic membrane character with the temperature and the identification of an upper temperature limit, beyond this temperature the complete membrane will flood at the minimum differential pressure. For the ceramic membranes off 100 nm with the coating P+F this upper limit is close to 120-130 °C. Though the upper limit is fixed around 120 °C, during the operation the transmembrane pressure is fixed to be 1 bar and so the upper operative temperature is about 100 -110 °C.

This value of temperature should be enough to make the aqueous ammonia concentration sufficiently high for an effective stripping operation. On the physical chemical study was evaluated different models to predict the electrolyte species concentration. The ENRTL model, has shown a good reliability validated with the experimental results. From model data it is illustrated how the aqueous ammonia increases its concentration one hundred times when the temperature reach values of 110 °C, increasing the stripping driving force as many times.

The model shows the clear positive effect of the temperature on the DAP conversion, however it is evident that the temperature does not need to reach higher values, turning the equilibrium constant to the ADP production. The aqueous ammonia concentration will not increase much furtherly at higher temperatures than 110 °C.

The test with the polymeric module Liqui-Cel gives clear evidence of the process feasibility. The operative temperature at which were performed the test with the Liqui-Cel was 60 °C, which is the maximum temperature that supports the module. Though this low operative temperature, the DAP conversion was close to 18 %. These results are encouraging for the process, higher temperature up to 110°C might only increase the ammonia desorption and so de DAP conversion.

The ceramic membranes have the potentialities to achieve higher temperatures and perform the regeneration operation with a reduced membrane area. The increase of 40 °C will increase the ammonia bulk concentration on one magnitude order and so the mass transport might be improved.

Yet there are many aspects of the operation that should be evaluated and solved. The module configuration (under development) must withstand the temperature and the transmembrane pressure as good as the membranes. The flow pattern configuration should enhance the mass transport and reduce the pressure drops. The high amount of water desorption is an important matter to take care of. It does not only reduce the ammonia concentration on the gas phase but increases the salt concentration on the liquid phase and the probability of crystallization and fouling. A proper transport model should be developed to evaluate the relevance of the operative parameters (flow rates, temperatures, pressure). It is necessary to account the enhancement effect of the reaction and the salting out effect, which might increase the availability of the ammonia at the equilibrium.